Report No. 181 / UILU ENG-98-4012

Mechanical Behavior of Metals Under Triaxial Stress: Apparatus and Experiments

by

Mark Anthony Balzer

B.Engr., Stevens Institute of Technology, 1987
M.S., State University of New York at Buffalo, 1991

THESIS

Submitted in partial fulfillment of the requirements
for the degree of Doctor of Philosophy in Mechanical Engineering
in the Graduate College of the
University of Illinois at Urbana-Champaign, 1998

Urbana, Illinois

ABSTRACT

A novel materials testing system has been designed and constructed to conduct monotonic and cyclic triaxial stress-controlled tests on solid, cylindrical specimens. The system can simultaneously generate any combination of tensile/compressive axial load and lateral pressure up to 750 MPa. Details of the test chamber design, high pressure fluid production and sealing, load and strain measurement under high pressure, computer control and data acquisition are described.

Under combined axial-stress/external-pressure loadings, a solid specimen experiences a truly three-dimensional, homogenous stress state comprised of a uniform axial stress in conjunction with radial and circumferential stresses equal to the negative of the pressure, -P. Through independent computer control of the pressure and axial stress, material behavior under a variety of multiaxial stress states is investigated. Experimental results obtained from conventional uniaxial and from triaxial monotonic and cyclic tests conducted using this unique apparatus are presented for carburized 4320 steel, hardened 4340 steel, nickel-titanium shape memory alloy and normalized 1070 steel. For the first three materials, stress state is shown to have a dramatic effect on the yield strength, the shape of the stress-strain curves and the phase transformation behavior. Pressure raised the fatigue strength of the 1070 steel, but did not affect the flow stress.

ACKNOWLEDGMENTS

The research presented in this dissertation was funded by grants from the Department of Energy, Basic Energy Sciences, Germantown, Maryland and the National Science Foundation, Mechanics and Materials Program, Arlington, Virginia. Early funding for this research was given by the Association of American Railroads, Pueblo, Colorado.

I would like to thank my advisor, Professor Huseyin Sehitoglu for his valuable insight and guidance during my extended tenure at UIUC. He has my gratitude for the original idea to explore materials testing under pressure and the considerable time and effort he spent supporting this investigation and providing all the means necessary to develop this capability.

I would also like to thank Professor Norman Miller for helping to make this pressure test machine a working device. It was in his graduate electromechanical devices course that I learned most of what was required to code the test machine program and how to connect all the electronic devices described herein. He was always willing to lend equipment and/or lend a hand to help solve my numerous test control and instrumentation problems, even telling me to call him at home.

I must of course thank my parents for letting me take over the garage, basement and driveway as I grew up and filled them alternately with bicycles, mini-bikes, mopeds, automobiles, tools, and piles of parts. My passion for fixing, designing and building mechanical devices stems from those early experiences. I especially wish to thank my mother who encouraged me to study engineering.

Finally, I wish to dedicate this work in memory of an incredible woman and a dear friend who I both met and then tragically lost at UIUC: Maria Pia Gratton. You are welcome to browse the web site that her family created in her memory:

http://www.hereforever.com/memorials/gratton_pia/

http://www.hereforever.com/memorials/gratton_pia/balzer.html

TABLE OF CONTENTS

1. INTRODUCTION

1.1: Motivation

Knowledge of the stress-strain behavior of engineering materials is a prerequisite for safe, economic design, yet stresses in structures and components are rarely as simple as in the conventional tension tests that are widely used to characterize material properties. Since the mechanical properties of engineering materials can be dramatically influenced by the prevailing stress system, it is important to be able to measure a material's behavior under appropriately simulated multi-axial loading conditions. To meet this need, a materials testing system has been developed to conduct multi-axial tension, compression and fatigue tests on cylindrical metal specimens using a combination of axial mechanical loading and lateral fluid pressure loading.

Uniaxial stress-strain data is commonplace and documented widely. A meager amount of stress-strain behavior under biaxial stress states is available. However, triaxial stress-strain test results are rare. The following two quotations summarize the ongoing high pressure materials testing around the globe rather succinctly. "The aim of investigations carried out in recent years in a relatively small number of laboratories has been to obtain information on such questions as the initiation of flow under combined stresses, the development of strain hardening in metals and changes in the strength characteristics of materials under combined stresses. Work has also been done on the phenomenon of fracture and on the determination of certain mechanical properties that cannot be determined in the normal way, such as the yield stress of brittle materials and the brittle fracture strength of ductile materials" [1]. "The number of published experimental investigations devoted to the study of the mechanical properties of metals under conditions of high hydrostatic pressure is very limited. This is no doubt partly due to the serious difficulties associated with the performance of mechanical tests in a pressurized fluid and with the associated measurements" [2].

Since these were written, there has been very little activity in the field of high pressure material stress-strain testing. This is unfortunate because there are research issues in fatigue and fracture that cannot be resolved without these techniques. For example, knowledge of the stress-strain response of materials under pressure could be used to assess the validity of plasticity

theories. Once found, knowledge of the pressure induced changes in strength and ductility can be applied to manufacturing processes such as drawing, forging and hydrostatic extrusion. Monotonic stress-strain tests under pressure allow exploration of compressive axial mean stress effects at stress levels that are unattainable in conventional uniaxial testing where the material fails by gross yielding. Once determined, the effect of triaxial stress on the onset, rate and extent of stress-induced phase transformations can provide a key for unlocking the transformation behavior in materials from steels to shape-memory alloys. Fatigue tests under pressure can be used to evaluate multiaxial fatigue life prediction models which are useful in design and failure analysis, and to propose new ones for handling stress states applicable to, for instance, rolling contact.

1.2: Objectives

The purpose of this work is:

(1) to develop an apparatus that can simultaneously apply variable axial loads and lateral pressure to a test specimen, under computer control.

(2) to develop a robust internal load cell that can measure axial forces without the effects of seal friction, and a reliable method of calibrating it.

(3) to develop methods of axial and circumferential strain measurement in a pressure environment and verify accuracy of these results.

(4) to utilize this unique apparatus to measure the monotonic and cyclic response of metallic materials (carburized 4320 steel, nickel-titanium shape memory alloy, and 4340VAR steel), under multiaxial stress states that are not otherwise achievable, with special emphasis on determining the *macroscopic* effects of hydrostatic stress, triaxial stress state and triaxiality on phase transformation evolution.

1.3: Significance

Towards these ends, we have assembled a novel, computer controlled apparatus which simultaneously subjects a solid, cylindrical, monotonic or fatigue test specimen to time-varying external pressures and axial loads, for the purpose of measuring its triaxial stress-strain behavior and/or determining its fatigue life. Under combined axial-stress/external-pressure loadings, a solid specimen experiences a truly three-dimensional, homogenous stress state where the axial stress equals σ_z and the pressure creates radial and circumferential stresses equal to -P. The extremely high pressures used are comparable to working stress levels and material strengths. With this capability, a wide range of hydrostatic and non-hydrostatic triaxial stress states can be investigated.

In all previously published work, testing under pressure has either been performed at constant, manually set pressures or at pressures which varied uncontrollably throughout the tests. No studies have been reported where axial stress and pressure were independently varied in a continuous manner. Our apparatus, under computer control, is the first to permit application of mutually independent, repeatable axial stress *and pressure* amplitudes, phase relationships, and wave forms. Additionally, our apparatus can conduct tests at constant "triaxiality" ratios.

Many load measurement techniques have been employed in the published literature, but not all the methods described feature rigorous load calibrations. Calibration of an internal load cell in a pressurized environment is a complicated endeavor: consequently many investigators have avoided this aspect entirely. As Pugh wrote in 1965, serious difficulties remain regarding the accuracy of load measurements. Since then there have been no new developments. In the present work we will demonstrate a unique load cell design and a unique, accurate calibration method which circumvents the previously encountered problems and seal friction effects.

Using strain gages for strain measurement in a pressurized environment also presents certain difficulties: one must account for curvature effects, temperature effects, and pressure effects. In the present work we describe a more sophisticated approach employing dummy gages *within* the pressure vessel for automatic curvature, temperature and pressure sensitivity compensation. Utilizing dummy gages within the pressure vessel allows the choice of gages based upon their fatigue performance and zero shift stability, without concern for their pressure sensitivity. An external extensometer and an algorithm developed herein provides a second measure of strain.

Studying the published papers on testing under high pressure, one finds that most authors describe their equipment, present a few preliminary test results, and then never publish again in the field. The reasons for this are manifold; pressure testing requires innovative techniques for reliably measuring load and strain under pressure, and expensive equipment with many highly stressed components that are time consuming to rebuild when they fail. However, the few successful researchers in the field have developed test equipment embodying several key features that assure the reliability of their test data. These are: (i) use of an internal load cell, or an external load cell used in conjunction with a frictionless "controlled clearance" seal gland, (ii) a method of calibrating their load cells under pressure, and (iii) provision for measuring deformation during the test. Our apparatus provides these key features, using new designs and methods that permit application of mutually independent, repeatable axial stress *and pressure* amplitudes, phase relationships, and wave forms. This equipment offers fine resolution of load and pressure through computer control and permits application of pre-selected multiaxial stress trajectories: in previous reported studies the pressure was varied manually. The equipment permits simultaneous application of pressure and load beginning at a zero stress state: previous systems apply the pressure first, then apply the load as a secondary operation.

Data generated with this apparatus will set the stage for macroscopic stress-strain modeling employing the evolution of phases at the micro-level. This will provide better understanding of how to utilize phase transformations for improved processing and mechanical behavior of materials. Pressure loadings produce a homogenous stress state and enable unambiguous interpretation of stresses and strains on the specimen. Other multiaxial loadings, such as axial/torsion combinations, result in stress gradients, even for thin walled cylinders, and the interpretation of results are difficult. Pressure loadings will permit the isolation of hydrostatic stress, effective stress and principal stress as the thermodynamic driving force for phase transformation.

The models proposed for the evolution of the martensite volume fraction due to plastic straining of austenite are based on uniaxial data; experiments exploring the effect of hydrostatic stress are missing for metallic systems. Pressure loadings permit generation of controlled hydrostatic stress levels. The shift in martensite start temperature with stress state reported in early studies does not provide information concerning the evolution of macroscopic transformation strains with stress state.

In the modelling of contact stresses experienced by an element of material beneath the contact surface, a problem arises: the service stresses are often high enough to cause transformation. Since the element experiences non-proportional loadings with a significant hydrostatic component, it is important to employ models which predict the transformation strain accurately. Our work will have an accelerating impact on the analytical and numerical treatment of such contact stress simulations and may eventually allow a new class of models to be developed relying on fewer assumptions about the material behavior under complex stress states.

Finally, under a compressive hydrostatic stress state ductility is enhanced through suppression of fracture; even brittle high-strength steels and ceramics exhibit ductile behavior when strained under pressure. This enables the study of materials over a much wider range of strain than is possible with uniaxial tests only, permitting a higher degree of transformation before specimen fracture than in studies conducted at atmospheric pressure. Strain-induced and stress-assisted modes of transformation could occur simultaneously especially if compressive hydrostatic stresses suppress early fracture of the specimen.

List of References

1. Brandes, Marek. Mechanical properties of materials under hydrostatic pressure. In H.Ll.D. Pugh (Ed.), Mechanical Behavior of Materials Under Pressure, London: Elsevier, 1970.

2. Pugh, H. Ll. D. The mechanical properties and deformation characteristic of metals and alloys under pressure. ASTM STP 374 Irreversible Effects of High Pressure and Temperature on Materials, 1965, 68-139.

2. BACKGROUND

2.1 Overview

The field of materials testing under high pressure can be generally subdivided into two categories: the testing of *internally* pressurized specimens and *externally* pressurized specimens. Internally pressurized specimens must be hollow, whereas externally pressurized specimens are typically solid. Though simultaneous internal-external pressurization has been tried [1], internally pressurized specimens are typically used for biaxial stress studies at relatively low pressures. Furthermore, they produce non-uniform radial stress distributions characteristic of pressure vessels, and so will not be considered here.

The testing of externally pressurized solid specimens can be further subdivided based on the stress application strategy. A test in which a specimen is triaxially stressed a single time, (without regard to the order or rates of stress application) is termed a "monotonic" triaxial stress-controlled test. An example of such a test would be an axial tension test conducted under constant pressure. A test in which a specimen is triaxially stressed, where at least one stress component is repeatedly varied with time, is termed a "cyclic" triaxial stress-controlled test. An example of such a test would be an axial fatigue test conducted under constant pressure.

Utilizing the monotonic and cyclic delineation described above, this chapter discusses the major advances in the evolution of apparatus used for conducting externally pressurized triaxial tests on solid metal specimens. Representative results and significant findings are presented to illustrate the often dramatic effect of triaxial stress on the mechanical behavior of test specimens.

2.2 Seminal Works in the History of Monotonic Testing Under Pressure

2.2.1 In the Beginning...

There exists a 100+ year history of materials testing under pressure. One of the earliest investigations into the deformation behavior of materials under pressure was conducted by Professor Kick in 1892. His results showed that pressure dramatically increased the degree of ductility exhibited by a normally brittle material during deformation processing. In 1901, Adams

and Nicholson [2] described his pioneering work on marble as follows:

> "Kick, in his experiments on deformation, made use of different materials, the only rock investigated being marble... A stout casting was bored out to receive a piston, the hole being closed at the lower end. In the bottom of the hole a steel die, having some device standing out from its surface, was placed face upwards. On this was placed a circular disk of marble. Oil was then poured in to fill up all vacant spaces. The piston was then inserted, and by it pressure was brought to bear upon the marble, which pressure was gradually increased to 13,000 atmospheres. The oil, which could escape only through the very narrow space between the piston and the casting, served to maintain a considerable pressure on all parts of the apparatus and the marble to which it had access, while the raised portions of the die coming in contact with the marble were pressed against it with great force. It was found that a well marked, although not very perfect, reproduction of the device upon the die was impressed upon the marble. *[thus Kick was able to coin a normally brittle material under high pressure... the first hydrostatic coining].*
>
> He also placed a small marble sphere in a stout copper box, filling the space between the marble and the sides of the box with alum or sulphur, poured in while molten. A heavy cover was placed upon the box, and the whole was squeezed down to a fraction of its former height by means of a powerful press. After compression the alum or sulphur was dissolved away, setting free the enclosed marble, which was found to have been considerably flattened in a direction at right angles to the pressure. *[thus Kick was able to upset a normally brittle material under high pressure... the first hydrostatic forging].*
>
> In another experiment he enclosed a marble cylinder in an iron tube, and having filled the intervening space with water, bent the whole transversely by the application of a high pressure. When the tube was sawn open, the marble was found to have acted `like a plastic body,' without having `altered its original characters'. *[thus Kick was able to bend a normally brittle material under high pressure... the first hydrostatic flexure test].*

The next researcher to enter this field was Voigt in 1893. His experiments showed that the fracture strength of sodium chloride was not influenced by pressures up to 850 psi, though his findings would have been more beneficial had his pressure range been higher [3]. Nevertheless, these early studies launched what was to become a continuous stream of research on this topic.

Between 1901 and 1917, Adams and his coworkers conducted a series of experiments in which they placed a right, circular, cylindrical specimen in a tightly fitting but longer, hollow steel tube [4]. Closely fitting steel pistons were inserted into each end of the steel tube, and brought to bear on the ends of the specimen. As the pistons were forced together, the specimen was upset. The confining pressure was developed by the steel tube's resistance to a "bulging" type of deformation encountered as the tube deformed with the enclosed specimen. Tests were conducted on lead, copper, and various minerals where the bulging of the steel tubes was recorded as a function of the axial load on the pistons (raw data). Next, the *pressure* required to bring about diametral bulging of the steel tubes was determined from separate experiments conducted on specimens made of tallow (the axial load exerted on the tallow created a pressure equal to the force on the pistons divided by their area). Finally, the "contribution of the steel tubes" was removed from the final plots by subtracting the pressure/tube bulging relationship (and neglecting friction) from the raw data. While Adam's experiments demonstrated that normally brittle minerals can

indeed be plastically deformed (upset and barreled) under pressure, his apparatus had inherent defects which made only qualitative measurements possible. These are quite clearly described by Griggs [5];

> 1. it is impossible to measure exactly the confining pressure because of the friction between the jacket and the specimen.
> 2. since the confining pressure depends on the amount of bulging of the tube, it increases as the deformation of the specimen increases, hence the confining pressure is sensibly zero at the moment of beginning the deformation.
> 3. by this method of confining the specimen is not free to fracture by major shear or tension fractures, since a fracture would have to tear through the walls of the steel tube.

From these humble beginnings it was clear that triaxial stress had a dramatic effect of on the mechanical behavior of materials. These findings piqued the interest of researchers around the globe and a handful entered this new field. However, careful examination of the numerous, subsequent investigations into monotonic axial tension/compression behavior of materials under high pressure listed in Table 2.1 reveals that the much of the work conducted was seriously flawed in one or more respects. While a great deal can be learned from studying the body of pressure-test literature, only the work of five noteworthy researchers will be presented here: In Germany, von Karman [6] was the first to develop what would become the basis for many future test machines used for pressure testing investigations. In the USA, Bridgman spent his entire life working in the high pressure field, examined a wide variety of metallic and non-metallic materials, and won the Nobel prize for his myriad accomplishments [3,7,8]. In the UK, the brilliant experimentalist Pugh refined many existing techniques and developed several novel high pressure test machines like his vessel with optical windows which allowed continuous true stress/true-strain testing under pressure [9-11]. Griggs, a student of Bridgman's, led the development of high pressure/high temperature testing of rocks and minerals with innovative test equipment incorporating electric furnaces operating under high pressure [12]. Finally Spitzig et al., working for US Steel, conducted numerous exacting experiments into the pressure effects on the behavior of single- and polycrystalline metals [13-17]. The shaded rows in Table 2.1 and the following discussion covers this in greater detail.

2.2.2 von Kármán

Great strides were made in experimental technique by Theodore von Kármán when he developed the apparatus shown in Figure 2.1. The lower half was a pressure intensifier and the upper half was an axial test machine. Low pressure fluid introduced into chamber "a" forced piston "b" upwards, raising the pressure of the fluid in chamber "c" to much higher values. This high pressure fluid was conveyed to the specimen chamber through tube "e." Load could be applied to specimen "d" through ram "f."

Investigator	Year	Type of Test[1]	Maximum Pressure in psi	Pressure Variation	Test Method	Loads Measured	Strains Measured	Materials Tested
Kick [2]	1892	C, B	unknown	variable	coined, upset and bent using various methods	none	after deformation	marble
Voigt [3]	1893	T	850	unknown	unknown	unknown	unknown	NaCl
Adams [2,4]	1901-1917	C	43,100	variable	plungers compressed cylindrical specimen	measured externally	bulge of support tube measured externally	marble, Cu, Pb
Von Kármán [6]	1911	C (II)	48,000	constant	plunger compressed cylindrical specimen	measured externally	measured externally	sandstone, marble
Böker [18]	1914	T (II)	80,500	constant	plunger compressed cylindrical specimen	measured externally	measured externally	sandstone, marble, cast Zn
Böker [18]	1914	C/TR	80,500	constant	externally applied torque/twist-angle through a packed gland	torque derived from an external load cell	strains derived from counting revolutions to find over-all twist angle	Carrara marble
Polyani and Schmid [19]	1923	T	600	constant	unknown	unknown	unknown	Sn, Zn
Richart, Brandtzaeg, and Brown [20]	1928	C (II)	4,300	constant	plunger compressed cylindrical specimen	measured externally with a weighing scale	dial indicator externally measured over-all extension.	concrete
Ros and Eichinger [21]	1929	C	28,000	unknown	unknown	unknown	unknown	annealed cast steel
Cook [22]	1934	TR	37,000	constant	axially loaded helically coiled wire	specimen loaded by weight inside vessel	axial deflection of helix was measured	annealed mild steel, annealed Cu
Griggs [5]	1936	TR	147,000	constant	externally applied torque/twist-angle through a packed gland	none	none	Solenhofen limestone
Griggs [5]	1936	T C (I)	194,000	constant	plunger compressed cylindrical specimen, tension yoke arrangement	measured externally	dial indicator externally measured over-all extension.	Solenhofen limestone, marble, single crystal quartz
Bridgman [7]	begun 1941 publ. 1952 1953	T C (I)	430,000	variable	tension yoke arrangement, plunger compressed cylindrical specimen	electrically from internal grid load cell	1. dial indicator externally measured over-all extension. 2. Neck diameters measured during interrupted tests.	Al, Cu, Ni, Ta, Nb, Mo, W, Sb, brass, bronze, steels
Ratner [23]	1949	T	32,000	constant	unspecified	measured externally using a proving ring	unspecified	Al, Al-alloy, Be-bronze, Cu, Mg, Mg-alloy

Table 2.1: Monotonic tests under pressure. "T" = Tension, "C" = Compression, "B" = Bending, "T" = Torsion, "I" = Type I, "II" = Type II.

Investigator	Year	Type of Test[1]	Maximum Pressure in psi	Pressure Variation	Test Method	Loads Measured	Strains Measured	Materials Tested
Handin [24]	1953	T C (II)	83,800	constant	plunger operating through frictionless control led clearance glands	electrically from external strain gaged proving ring	dial indicator externally measured over-all extension.	hard brass, Yule marble, rock salt, anhydrite
Wiseman and Marin [25]	1954	T (II)	23,750	variable	tension plunger operating under a differential pressure	electrically from internal strain gaged load cell, though not used in published test results	dial indicator externally measured over-all extension	Al alloy 14S-T6
Pugh and Green [10]	1954 1956	T (I)	220,000	constant	tension plunger operating under a differential pressure	electrically from internal strain gaged load cell	diameters measured before and after tests	Al alloy, ERHC Cu, Mg, Zn, Zn-Al alloy, cast iron
Crossland [26,27]	1954 1956	TR (I)	44,800	constant	externally applied torque/twist-angle through a Morrison seal	torque derived from optically measured angle of twist of an internal elastic tube	strains derived from optically measured relative angle of over-all twist	Al-Si alloy, cold rolled Cu, annealed Cu, Zn, Mazak, annealed 1020 steel, En25 Ni-Cr-Mo steel
Haasen and Lawson [28]	1955	T (I)	73,500	constant	externally rotated, screw driven crosshead inside vessel	electrically from internal strain gaged proving ring	over-all extension determined from the lead of screw driving the crosshead	single crystal Al, Cu, Ni, Zn, α-brass, polycrystalline Ni
Gladkovskii and Olejnik [29]	1957	T (I)	45,000	constant	tension plunger arrangement trans-mitting externally applied load	electrically from internal strain gaged load cell	strain gaged beam extensometer externally measured over-all extension	hardened Be-bronze
Crossland and Dearden [30]	1958	TR (I)	78,400	constant	externally applied torque/twist-angle through a Morrison seal	torque derived from optically measured angle of twist of an internal elastic tube	strains derived from optically measured relative angle of over-all twist	grey cast iron, quenched and tempered En25 steel
Hu [31]	1958 1966	T (I)	53,200	constant	tension yoke arrangement	calculated from pressure times area of plungers and external load measurement	diameters at points on tapered specimen measured before and after tests (McGregor's two-load method).	Nittany No. 2 brass
Ryabinin, Vereshchagin, Balashov, and Livshits [32]	1958	T (I)	450,000	variable	tension yoke arrangement	electrically from internal grid load cell	dial indicator externally measured over-all extension.	steels, Duralumin, Fe, brass

Table 2.1: Monotonic tests under pressure, continued. "T" = Tension, "C" = Compression, "B" = Bending, "T" = Torsion, "I," "II" = Type.

Investigator	Year	Type of Test[1]	Maximum Pressure in psi	Pressure Variation	Test Method	Loads Measured	Strains Measured	Materials Tested
Beresnev, Vereshchagin, Ryabinin, and Livshits [33]	1960	T (I)	450,000	variable	tension yoke arrangement	electrically from internal grid load cell	dial indicator externally measured over-all extension.	Al, Cu, Ni, Ta, Nb, Mo, W, Sb, steels, brass, bronze, steels
Griggs, Turner, and Heard. [12] Heard [34]	1960	T C (I)	73,500	constant	plunger compressed cylindrical specimen, tension yoke arrangement operating through frictionless control-led clearance glands	measured externally	dial indicator externally measured over-all extension.	basalt, dolomite, granite, peridotite, marble, pyroxenite, quartz crystals, and aggregates. Solenhofen limestone
Handin, Higgs, and O'Brien [35]	1960	TR T/TR C/TR (I)	39,105	constant	externally applied torque/twist-angle through a Johnson-Newhall seal	torque derived from an external, strain gaged load cell	strains derived from electrically counting revolutions to find over-all twist angle	Yule marble, single crystal calcite
Pelczynski [36]	1962	T (I)	75,000	constant	tension yoke arrangement	none	externally measured over-all extension.	mild steel, Al, Cu, brass
Brandes [37]	1962 1967	T (I)	450,000	variable	tension yoke arrangement	electrically from internal strain gaged load cell	dial indicator externally measured over-all extension	steels, Armco iron, cast iron, Cu
Davidson and Homan [38]	1963 1966	T (I)	450,000	variable	tension yoke arrangement	none	externally measured over-all extension	quenched carbon steel, Co, Mg, W, Zn
Pugh, Hodgson, and Gunn [9]	1963	T (I)	156,800	constant	tension plunger arrangement trans-mitting externally applied load	electrically from internal strain gaged load cell	dial indicator externally measured over-all extension	steels, Armco iron, cast iron, Cu
Paterson [39]	1964	T C (I)	150,000	constant	tension/compression plunger arrangement	electrically from external load cell	LVDT externally measured over-all extension	granite, limestone, marble, sandstone, serpentinite, Cu, grey cast iron
Nishihara, Tanaka, and Muramatsu [40]	1964	T C (I)	60,000	constant	1. plunger acted through hollow tension specimen 2. plunger acted on solid compression specimen	electrically from external load cell	dial indicator or LVDT externally measured over-all extension	granite, marble, sandstone, Al, Ti, Zr, Zn, Mg-Al alloy
Pugh and Gunn [41]	1964	TR (I)	134,000	constant	internally generated torque/twist-angle from a motor and reduction gearset	torque derived from an internal, strain gaged elastic tube load cell	strains derived from electrically counting revolutions to find over-all twist angle	Mg, Al-Mg alloy, cast iron

Table 2.1: Monotonic tests under pressure, continued. "T" = Tension, "C" = Compression, "B" = Bending, "T" = Torsion, "I," "II" = Type.

Investigator	Year	Type of Test[1]	Maximum Pressure in psi	Pressure Variation	Test Method	Loads Measured	Strains Measured	Materials Tested
Nishihara, Tanaka, and Hamada [42]	1965	T C (I)	51,200	constant	1. plunger acted through hollow tension specimen 2. plunger acted on solid compression specimen	electrically from internal strain gaged load cell	Neck development photographed during tests.	carbon steel, Al, Ti, Zr, Zn, Mg-Al alloy
Erbel [43]	1966	TR (I)	57,000	constant	externally applied torque/twist-angle through a packed gland	torque derived from an external, strain gaged load cell	strains derived from electrically counting revolutions to find over-all twist angle	Al, Cu, steel
Gordon and Mike [44]	1967	T,C (I)	147,000	constant	internally generated loads; motor and reduction gearset driving crosshead	electrically from internal strain gaged load cell	over-all extension determined from the lead of screw driving the crosshead	granite, halite, Zn
Tanaka and Nakashima [45]	1967	T (I)	28,500	constant	externally rotated, screw driven crosshead inside vessel	electrically from LVDT measurement of spring deflection	LVDT internally measured specimen extension	annealed and drawn Al alloy
Oguchi and Yoshida [46, 47, 48]	1968 1970 1971 1972	T (I)	213,500	constant	tension plunger/ tension yoke arrangement	electrically from internal magnetostrictive load cell	externally measured over-all extension.	Al, Cu, Fe, Mo, Zn, Zr 18-8 stainless steel and a series of Fe-Mn alloys
Carpentier and Contre [49]	1969	T C (I)	220,500	constant	tension plunger/ tension yoke arrangement	electrically from LVDT measurement of diaphragm deflection	LVDT externally measured specimen extension	Be, Cu, Zn, Zr
Ohmori, Yoshinaga, Kawahata and Sanemasu [50]	1970	T C TR (I)	44,100	constant	externally applied torque/twist-angle through a packed gland	torque derived from an internal, strain gaged elastic tube load cell	unspecified	annealed 1014 steel, annealed 70Cu30Zn brass
Sakata, Aoki and Tsujimoto [51]	1971	TR (I)	56,900	constant	externally applied torque/twist-angle through a Morrison seal	torque derived from an internal, strain gaged elastic tube load cell	specimen was strain gaged	annealed and extruded Al, annealed low carbon steel, Zn-Al alloy
Fung [52]; Fung, Burns and Ling [53]	1972 1973	T (I)	60,000	constant	tension plunger/ tension yoke arrangement	electrically from internal strain gaged load cell	Extensometer internally measured specimen extension	Cu, ASTM B-16 leaded brass
Hoeg and Davis [54]	1972	T C	80,000	constant	unspecified	unspecified	unspecified	AISI 304 stainless steel
Motoie, Yamakage, and Ohnami [55]	1972	TR (I)	28,450	constant	externally applied torque/twist-angle through a packed gland	torque derived from an internal, strain gaged elastic tube load cell	strains derived from counting revolutions to find over-all twist angle	Pure Al, Fe, Zn

Table 2.1: Monotonic tests under pressure, continued. "T" = Tension, "C" = Compression, "B" = Bending, "T" = Torsion, "I," "II" = Type.

Investigator	Year	Type of Test[1]	Maximum Pressure in psi	Pressure Variation	Test Method	Loads Measured	Strains Measured	Materials Tested
Hawley and Drucker [56]	1973	T (I)	9,200	constant	tension plunger arrangement	external load cell	externally measured crosshead displacement	AISI 1020 hot rolled steel precompressed to a strain of -0.65
Sakata and Aoki [57]	1973	TR (I)	14,200	constant	externally applied torque/twist-angle through a Morrison seal	torque derived from an internal, strain gaged elastic tube load cell	specimen was strain gaged	Pyrex glass
Ohji, Ogura, Sugimoto, Yaji [58]	1973	T (I)	56,880	constant	tension plunger arrangement	electrically from internal strain gaged load cell	LVDT externally measured over-all extension	S35C steel, OFHC Cu, 5005 Al alloy
Crossland and Mitra [59]	1974	TR (I)	160,000	constant	externally applied torque/twist-angle through a Morrison seal	torque derived from optically measured angle of twist of an internal elastic tube	strains derived from optically measured relative angle of over-all twist	annealed 1020 steel, white cast iron
Spitzig, Sober, Richmond, Spitzig 1979 [14, 15]	1975 1976	T C (I)	160,000	constant	tension plunger arrangement	electrically from internal strain gaged load cell	LVDT externally measured over-all extension	steels, single crystal iron
Kolpashnikov, Fedorov, Kucheryaev, Bespalov [60]	1984	T (II)	290,000	constant	hydrostatic extru-sion of a billet from the vessel stressed the attached specimen in tension	none	axial and tangential strains measured after test from the deformation of a photographically applied grid	Nb, high-Sn-bronze
Kolpashnikov, Fedorov, Kucheryaev, Bespalov [61]	1986	T (I)	290,000	constant	hydrostatic extru-sion of a billet from the vessel advanced a screw, twisting the specimen in torsion	none	shear strains measured after test from the deformation of a line parallel to the specimen axis	Nb, high-Sn-bronze
Liu, Manoharan, Lewandowski [62,63]	1989 1990 1992 1993	T (I)	43,500	constant	tension plunger operating under a differential pressure	electrically from internal strain gaged load cell	Strain gages on specimen, or LVDT externally measured over-all extension	2XXX, 6061 and 7XXX Al alloys and Al matrix composites

Table 2.1: Monotonic tests under pressure, continued. "T" = Tension, "C" = Compression, "B" = Bending, "T" = Torsion, "I," "II" = Type.

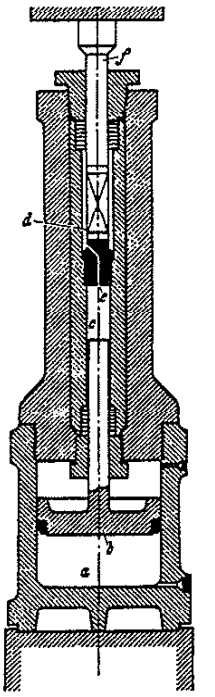

Figur 3. Versuchseinrichtung

Figure 2.1: von Kármán's pressure test apparatus [6].

In 1911 von Kármán reported on constant pressure tests in which he axially compressed marble and sandstone cylinders (he wrapped them in 0.1 mm thick annealed brass sheet to prevent penetration of the pressurized fluid into the porous specimens) at pressures up to 48,000 psi [6]. Since the pressure was generated in a fluid, it could be maintained constant during the deformation of the specimen. Additionally, since the specimen was surrounded by fluid only, it was free to fracture in a manner that could be directly compared with atmospheric pressure laboratory tests. His load and pressure measurements were not exact: pressures were not measured, but rather were calculated by measuring the pressure on the low side of the intensifier, multiplying by its area ratio and correcting for seal friction. Likewise, axial loads were determined by measuring load external to their high-pressure vessel and correcting for seal friction. Nevertheless, von Kármán's results in Figure 2.2 demonstrate a dramatic raising of the stress-strain curve (plotted as (axial stress - pressure) vs. strain) and improvements in ductility with increasing fluid pressure.

Using the same equipment in 1914, Böker, a student of von Kármán's, conducted constant tension, monotonically increasing pressure tests of marble, sandstone and for the first time a metal; cast zinc [18]. Though their measurements were corrupted by seal friction, they nevertheless were the first to show that these materials became many times more ductile as the pressure was increased up to 80,500 psi, and that increasing the pressure raised the entire stress-strain curve, with the rate of increase flagging at higher pressures.

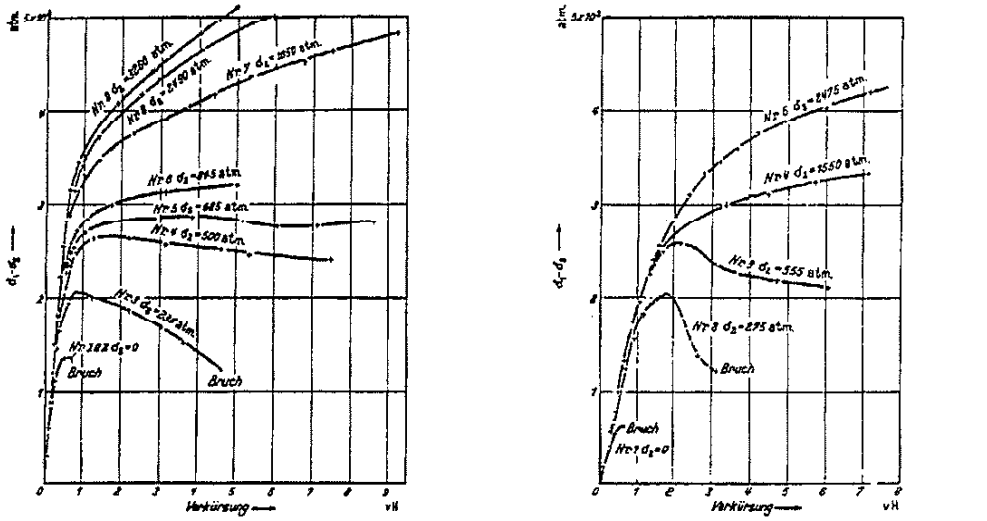

Figur 5. Formänderungskurve des Marmors beim Versuch unter allseitigem Druck *Figur 6. Formänderungskurven des Sandsteines beim Versuch unter allseitigem Druck*

Figure 2.2: Results from von Kármán's pressure tests on marble (left) and sandstone (right) [6].

At this point, it is necessary to make a distinction between the two major types of pressure test apparatus. If we placed a right circular cylinder of test material inside a pressurized vessel, the pressure acting on the cylindrical surface would cause radial and tangential stresses equal to the negative of the absolute pressure, and the pressure acting on the circular ends would cause axial stresses equal to the negative of the absolute pressure. We would declare the specimen to be in a state of hydrostatic stress. If this vessel surrounded not only the specimen, but an entire test machine as well, we could alter this hydrostatic stress state by, for instance, pushing or pulling on the pressurized circular ends with a force **F**. Then in our "pressurized laboratory" a simple free-body-diagram reveals that cracking (or any area change such as necking or barreling) of the specimen would *not* change the magnitude of the force acting through the remaining ligament. In this case, **pressure and applied load are truly independent variables and the apparatus is termed a "Type I" apparatus.**

By preventing the ends of their right circular cylindrical specimen from being pressurized, Von Kármán and Böker constructed their apparatus such that pressurizing the vessel produced a non-hydrostatic state of stress in their specimen. To generate a hydrostatic state of stress in the specimen they had to apply a compressive axial stress equal to the pressure. Of course, by varying the magnitude of the axial stress, other stress states could be generated. Then in Von Kármán and Böker's "pressurized laboratory" a simple free-body-diagram reveals that cracking (or any area change such as necking or barreling) *would* change the magnitude of the force acting through the remaining ligament. Because of the pressure and area products which appear, **pressure and applied load are not independent variables and the apparatus is termed a "Type II" apparatus.** These Type I and Type II designations will be used throughout this thesis.

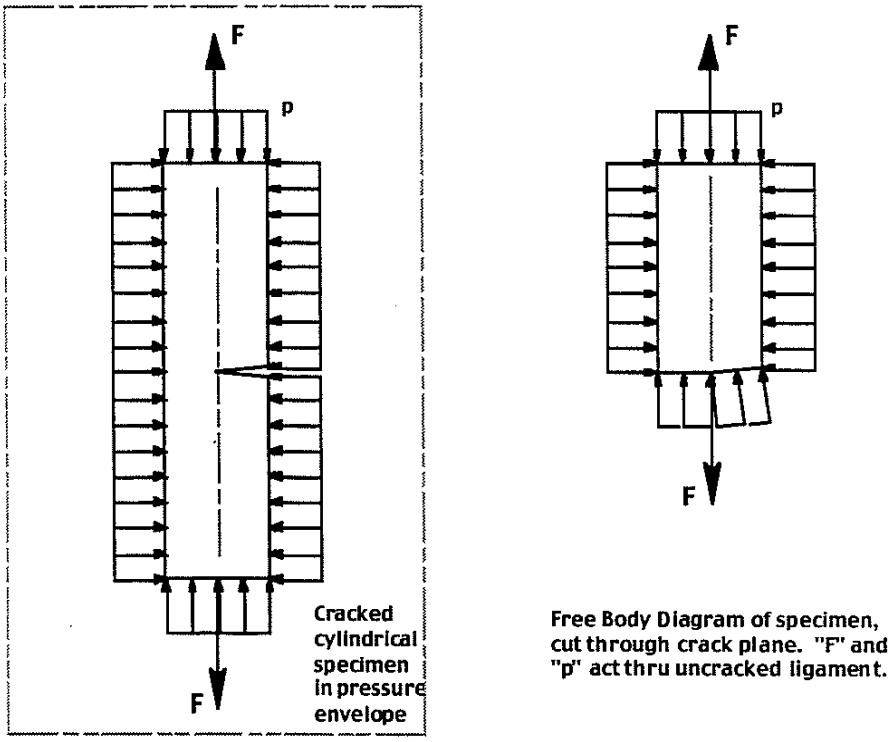

Figure 2.3: Free body diagram of a tension specimen in a "Type I" pressure test apparatus. Cracking, necking or barreling under pressure do not affect the load F.

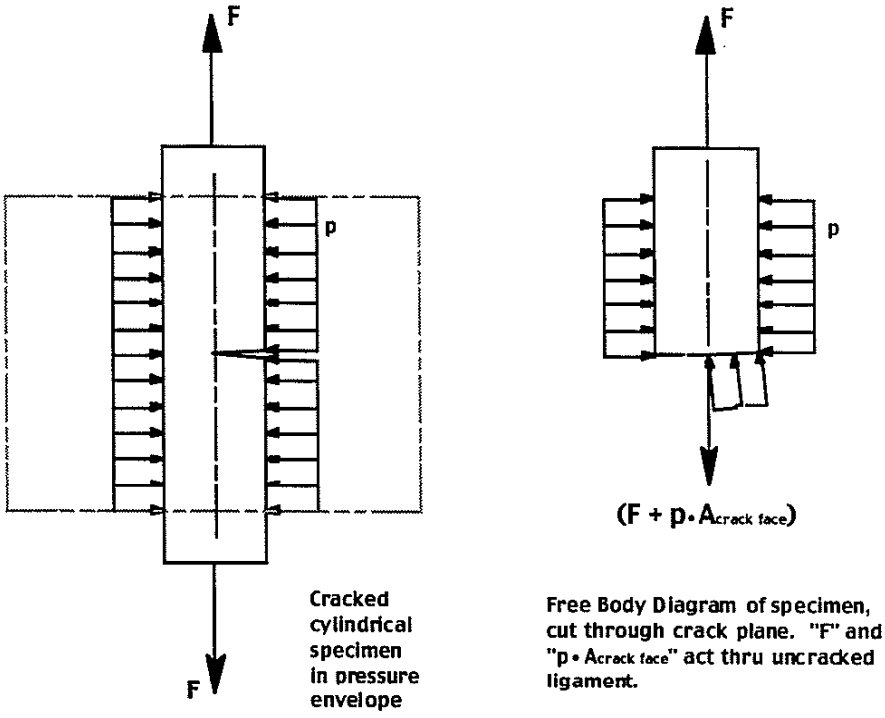

Figure 2.4: Free body diagram of the specimen in a "Type II" pressure test apparatus. Cracking, necking or barreling under pressure affect the load F.

2.2.3 Bridgman

After having spent many years in the field of hydrostatic high pressure testing, Percy W. Bridgman designed and operated a successful Type I apparatus for determining the mechanical properties of materials under high pressure in 1941 [7,8]. He conducted tensile tests inside a fluid-filled vessel that was plugged at one end and fitted with a ram at the other. Forcing the ram into the vessel both pressurized and loaded the dumb-bell specimen through a double-yoke mechanism.

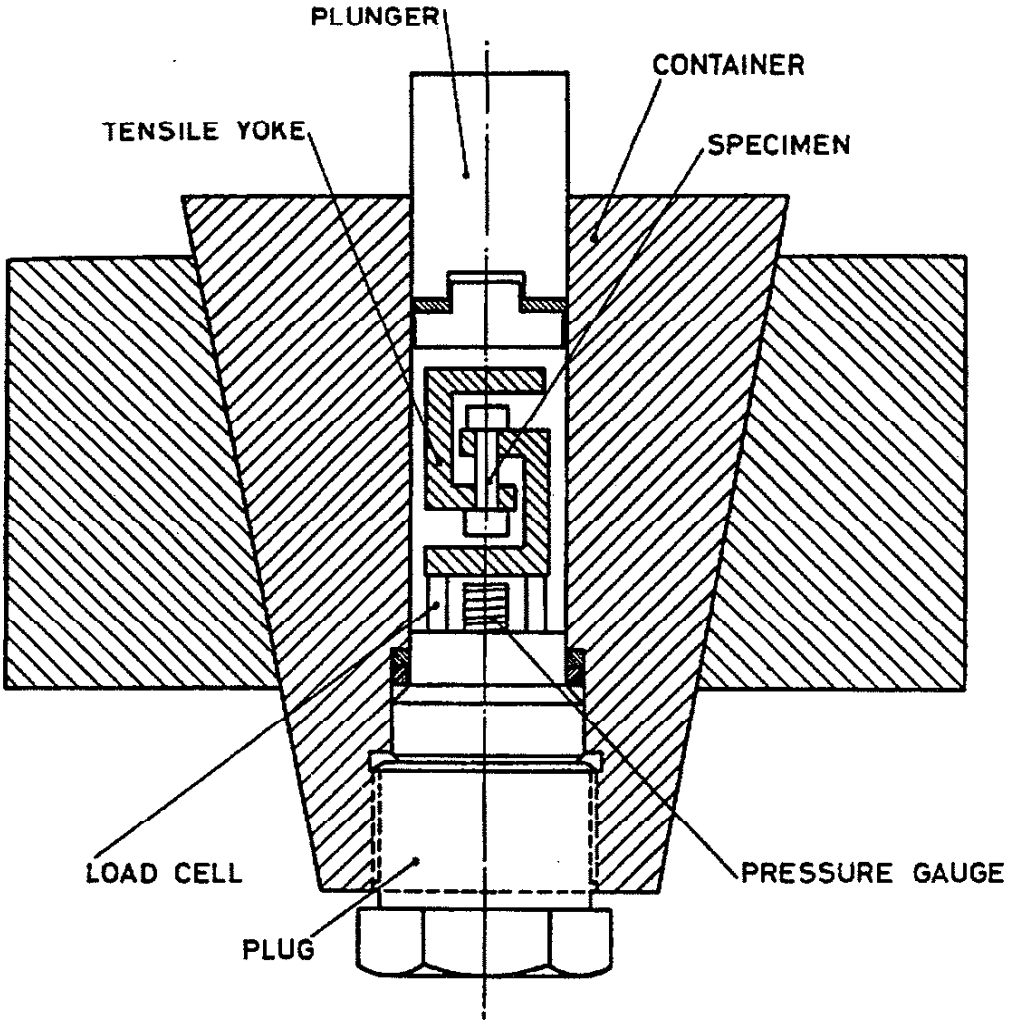

Figure 2.5: Bridgman's pressure test apparatus [64]

To avoid the uncertainties introduced by seal friction, Bridgman measured the load applied to the specimen with a special 3300 pound capacity load cell that he termed the "grid", located inside his vessel. The design of Bridgman's apparatus [7] did not permit the tests to be conducted at constant, predetermined hydrostatic pressures; instead the pressure generated rose by as much as 45,000 psi during each test, with the test usually characterized by the pressure of the final reading.

Bridgman measured the displacement of his loading/pressurizing ram externally with a dial indicator to determine the extension of the specimen. To determine the extent of the necking deformation he repeatedly interrupted each experiment and tore down the apparatus to take measurements. Experimental difficulties aside, he was able to conduct tensile tests on copper, aluminum, brass, glass, beryllium, phosphor-bronze, cast iron, nickel, tantalum, columbium, molybdenum, niobium, tungsten, antimony and a wide range of steels, at pressures up to 430,000 psi. For comparison, the pressure at the bottom of the Mariana Trench, the deepest spot of the world's oceans at 38,500 feet below sea level, is only 16,000 psi.

Under the higher pressures, Bridgman obtained ideal plastic tensile failures; "reductions of area so great as to be no longer measurable... the tensile specimen being pulled out practically to a point before fracture." [7]. Whereas atmospheric tension testing rarely provides true strain values of 1.0, Bridgman was able to conduct tests to true strains of over 5.0 under pressure. His apparatus thus opened up regions of ductility that had not previously been explored, and allowed him to investigate certain intriguing aspects of material behavior. He found that the strain hardening *curve* (the plot resulting when flow stress is graphed against true strain) is linear to true strains between 3.0 and 4.0. Beyond these strains, grain size related effects began to dominate the material behavior in the necked region, and the load readings lost accuracy as the applied loads became increasingly small due to the decrease in section size. *Curve* is italicized because Bridgman addresses the fact that the data points which comprise the graph correspond to different and haphazardly arrived at pressures; "It is only when all the measurements are made at a single pressure that one has the right to expect a strain hardening *curve*" [8]. Nevertheless, he does state for the steels he tested that *roughly,* the flow stress at fracture increases 7/10ths as fast as the corresponding increase in pressure.

In most of his experiments Bridgman found that while pressure permitted testing to high strains, no correlation existed between pressure and the stress-strain data points. However, by the last series of measurements, he claimed that his experimental skill had developed to the point where he was able to establish that (1) the strain hardening for a given strain increases with increasing pressure, and that (2) the strain hardening curve deviates to the low side of linearity by a few percent at the upper end. Expanding on (1) for tempered pearlite and tempered martensite, Bridgman found that the flow stress at true strains near 0.2 where necking starts is nearly independent of pressure, but that the flow stress at a true strain of 3.0 increases approximately 20% above its atmospheric value when tested at 400,000 psi. For points between these extremes, the flow stress increase was linear in both pressure and strain. Result (2) is sensible because otherwise an indefinitely high strength would be obtainable at high enough strains. Bridgman also found that steels exhibited a strain at final fracture which increased linearly with pressure, sensibly without bound! The pressure dependence of strain hardening and of ductility were found to be independent of each other [8]. From a continuum mechanics model, these results can be

interpreted as a displacement of the intrinsic (Mohr) curve of the material, whereas from a structure and morphology standpoint, they indicate that external pressure closes any internal microcracks and microvoids as they form [65].

Bridgman cited experimental difficulties associated with measuring small deflections (and thus the inability to determine small strains or an elastic modulus) using his apparatus. However he stated that he could usually detect when the elastic limit was exceeded and that the elastic limit stress was raised by an amount "roughly proportional to the pressure", though he gave nothing quantitative in that regard. Bridgman did state that it was possible to determine the effect of pressure on the maximum load (corresponding to the onset of necking, i.e. the UTS) "with greater accuracy" than at the elastic limit. For steels he found that the maximum load increased by 10,000 psi for every 150,000 psi increase in pressure, with the data displaying less scatter than for any other tensile quantity. Once a neck formed, Bridgman noted that for any given material the relationship between the axial strain, the neck diameter and the radius of curvature of the neck profile was independent of pressure.

With gray cast iron, Bridgman found that specimens exposed to the pressurized fluid remained completely brittle when tested under pressure, but exhibited considerable strength and ductility when sheathed in copper to prevent fluid contact. By sheathing the specimen, the fluid was prevented from pressurizing incipient cracks in the material. He also conducted compression tests under pressure. In 1946, Bridgman was awarded the Nobel prize in physics "for the invention of an apparatus to produce extremely high pressures, and for the discoveries he made therewith in the field of high pressure physics."

2.2.4 Pugh

In 1954, Pugh and Green developed a Type I apparatus for conducting tensile tests under constant, internally generated fluid pressure [10,11]. As in Bridgman's case, forcing the upper ram into the vessel pressurized it; however the more advanced design of Pugh and Green's apparatus allowed tests to be conducted at constant, predetermined pressures. One end of a cylindrical specimen with button ends was affixed to the pressure vessel while the other end was attached to a "tension plunger"; a sliding piston driven by the differential pressure across it and fit so closely to its bore that it required no seals. After pressurizing the vessel with the top plunger, axial loads were applied to the specimen by withdrawing the lower plunger, thus creating the differential pressure across the tension plunger. Load measurement was accomplished via a strain gage load cell inside the vessel whose Wheatstone bridge was manually balanced after the vessel was pressurized. No provisions were incorporated for measuring strains during their tests, as they were interested primarily in ductility's and fracture stresses. Strain at fracture was taken to be $\ln(A_o/A)$ where A_o and A are the cross sectional areas of the specimen, initially and at the point of fracture, respectively.

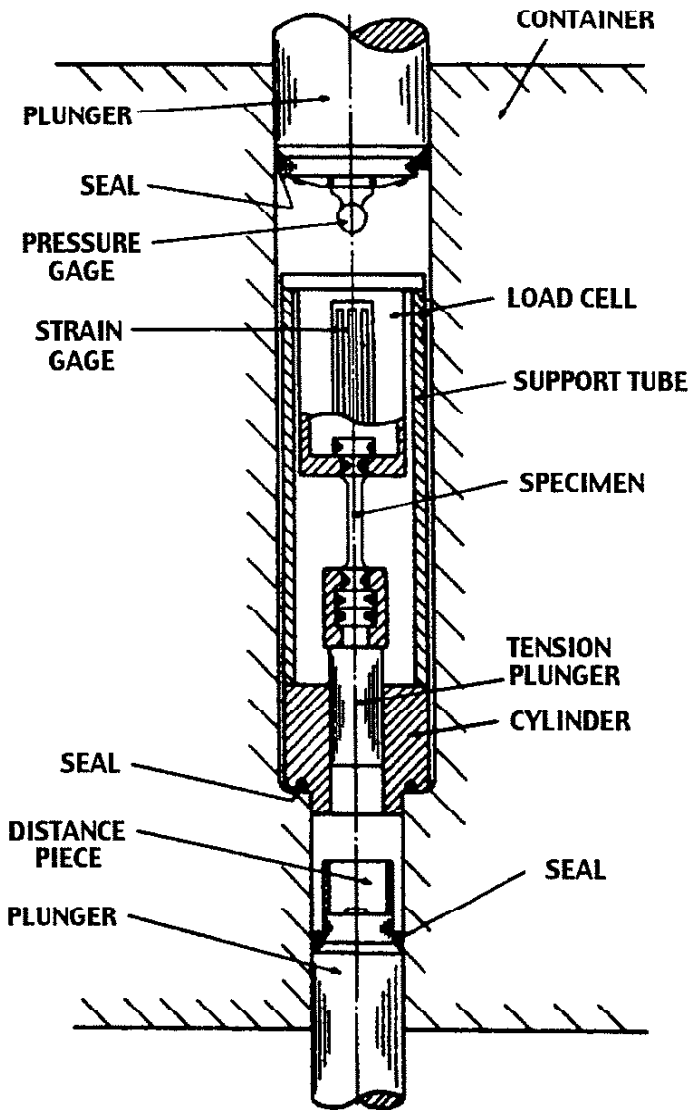

Figure 2.6: Pugh's 1954 pressure test apparatus [64]

Pugh and Green conducted tests on ERHC copper, aluminum alloy, cast iron, zinc, Mazak (a Zn-Al alloy) and magnesium at pressures up to 134,400psi. (Their original results were only released in an internal report at the National Engineering Laboratory in Glasgow. It was ten years before they were first published in a journal!) By 67,000 psi, they found that the ductility of the Zinc and the Mazak increased so much that they simply necked down to a point at failure. By 90,000 psi, copper and the aluminum alloy did the same. By 134,000 psi rubber-sheathed cast iron displayed a reduction of area of 80 percent whereas its atmospheric pressure value was zero. As was noted by Bridgman with gray cast iron, Pugh found decreased scatter in the results from his cast materials (the magnesium, the Mazak and the cast iron) and found improved rate of

increase of ductility with pressure when the specimens were sheathed in rubber to prevent fluid contact. By sheathing such specimens, the fluid was prevented from pressurizing incipient cracks in the material.

For the fcc aluminum alloy and the copper, Pugh and Green observed that as the test pressure was raised, the mode of fracture changed to a cup and cone type, the tensile fracture area decreased and the shear fracture area increased. Since hydrostatic pressure decreases the tensile stresses in the neck of a specimen, they proposed that the formation and growth of voids from the specimen axis was suppressed. As Bridgman found, with a high enough pressure the tensile fracture area becomes essentially zero.

The normally brittle bcc cast iron required pressures of 45,000 to 65000 psi before any ductility increases were shown.

The hcp metals zinc, Mazak and magnesium initially displayed very slight changes in ductility with pressure. Though the magnesium continued to display its initial rate of ductility increase up to the 90,000 psi maximum pressure at which tests were conducted on it, a pressure was reached for which the zinc and the Mazak displayed a veritable step-increase in ductility. To explain this behavior, Pugh and Green in 1964 borrowed some concepts from Galli and Gibbs's 1963 work on molybdenum and hypothesized that a brittle-ductile transition *pressure* exists. If this is true, then the explanation for the meager ductility increase seen in the magnesium specimens is that its transition pressure was never reached.

Pugh and Green related that: a) fracture strength is generally dependent on the maximum value of the tensile stress, and b) Bridgman's analysis showed that the hydrostatic pressure decreases the tensile stresses in the neck of the specimen. Therefore material under hydrostatic pressure requires a larger superimposed tensile stress to initiate brittle fracture, and we see this experimentally as increased ductility. Since the flow stress is generally unaffected by hydrostatic pressure, a graph of the failure envelope will show a pressure where the brittle fracture and the flow stress curves intersect. That point is the brittle/ductile transition pressure. Furthermore, it is related to the brittle/ductile transition temperature because both the fracture strength and flow stress are functions of temperature and so the higher the hydrostatic pressure, the lower the brittle/ductile transition temperature becomes.

Pugh and Green next added to their model a way to determine the abruptness of the transition from brittle to ductile behavior. They proposed that it is related to the rate of work-hardening of the material, with gradual transitions being displayed by materials possessing steeply rising stress-strain curves, and abrupt transitions displayed by materials possessing flat-topped stress-strain curves. They assumed that the stress-stress strain curve is a characteristic of a material, and that testing under pressure simply allowed one to travel further along it, to higher stress/strain values, before fracture occurs. Therefore, a material with a steeply rising stress/strain curve requires a greater increase in pressure to realize a given strain (ductility) increase than does a

material with a flat-topped curve. This translates, respectively, into a gradual or abrupt brittle to ductile transition when plotted on pressure coordinates.

In 1963, Pugh et al developed a very sophisticated Type I apparatus (see Figure 2.7) which enabled the first true stress-strain curves to be obtained beyond necking at constant pressure [9].

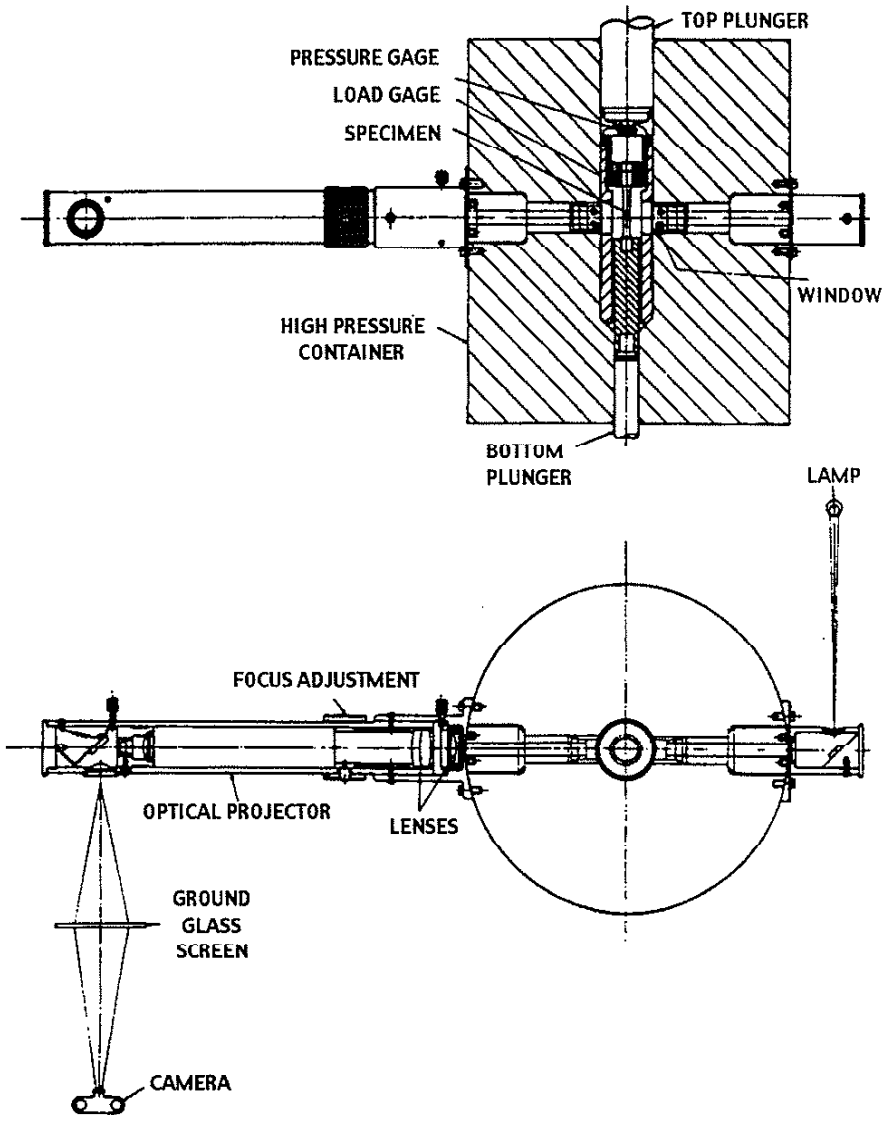

Figure 2.7: Pugh's 1963 pressure test apparatus [64]

Like in Bridgman's case, forcing the upper ram into the vessel pressurized it; however the more advanced design of Pugh's apparatus allowed tests to be conducted at constant, predetermined pressures.

One end of a cylindrical specimen with threaded ends was affixed to the pressure vessel while the other end was attached to a lower ram. Axial loads were applied to the specimen by

moving the lower rams. Load measurement was accomplished via a strain gage load cell inside the vessel (later they added pressure and temperature compensating dummy gages in its circuit), and they continuously photographed the silhouetted specimen through sapphire windows mounted in the walls of their pressure vessel. The photos revealed the neck diameter and radius of curvature of the neck profile while the specimen was under test conditions. This allowed calculation of true stresses and strains, corrected for the non-uniformity of stress at the neck (Bridgman correction factor). Overall elongation could be measured from displacement of the lower ram.

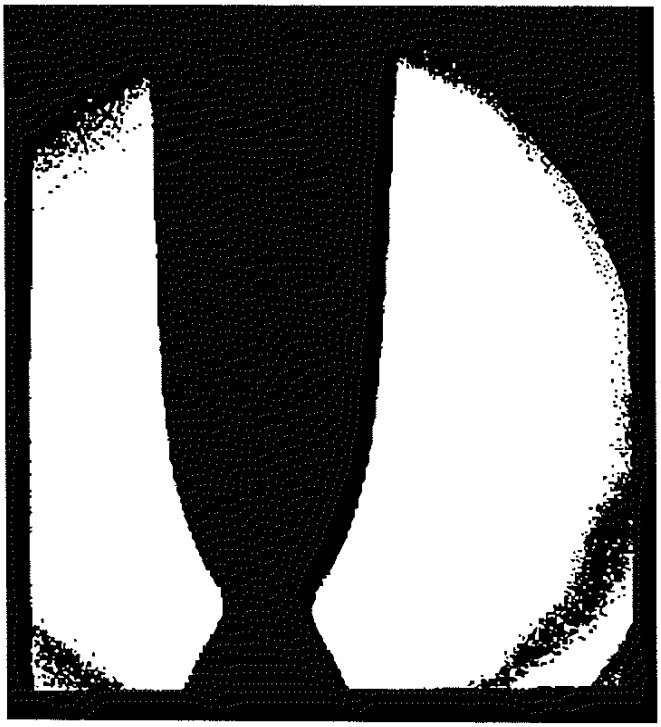

Figure 2.8: Photo of necking during a tension test under high pressure [64]

Pugh conducted tests on ERHC and OFHC copper, aluminum alloy, pearlitic gray cast iron, hot rolled En2A steel (SAE 1010), zinc, Mazak, magnesium and a bismuth alloy. As was noted by Bridgman with gray cast iron, Pugh found that cast materials, liable to having surface cracks or to being otherwise porous, obtained no increase in ductility when tested under pressure while exposed to the fluid, but exhibited considerable strength and ductility when sheathed in rubber to prevent fluid contact. By sheathing such specimens, the fluid was prevented from pressurizing incipient cracks in the material, and the scatter in the results was greatly reduced. Sheathing had no effect on materials free of surface cracks and porosity.

Pugh's results for the En2A (SAE 1010) steel confirmed Bridgman's findings that steels exhibited a strain at final fracture which increased linearly with pressure. However, contrary to the results of many others, Pugh found the ductility's of the other metals he tested were not linear

functions of pressure at all; rather he obtained a variety of curve shapes which all deviated from linearity. Additionally, these curves displayed certain features unique to the crystal structures of the materials tested.

Pugh's successive photographs of necking behavior during his tensile tests show that each material possesses characteristic relations between the axial strain, the neck diameter and the radius of curvature of the neck profile, as found by Bridgman. Further, they confirm Bridgman's observation that for any given material, the relationship between the axial strain, the neck diameter and the radius of curvature of the neck profile is independent of pressure.

Citing his carefully conducted testing, wherein he performed several repeat tests for each set of conditions using sophisticated equipment, Pugh strongly states that for the materials he tested and over the pressure ranges he explored, pressure has *no* effect on the maximum load (corresponding to the onset of necking, i.e. the UTS) reached. In his experiments on En2A and En26 steel at pressures up to 110,000 psi, Pugh found *no* correlation between pressure and the stress-strain points, other than that the pressures permitted achieving high strains. The strain hardening curves he measured were linear to fracture, yet the strain hardening for a given strain followed *no* trend with increasing pressure. These conclusions are very definitely contrary to the findings of previous workers. Pugh hypothesizes that this may be due to the fact that in general, no other researchers appear to have made comparisons of the reproducibility of results obtainable with their apparatus! Thus the pressure effects on the stress-strain curves reported by other researchers could be based on nothing more than statistical errors. Pugh notes that most researchers agree that the true stress at fracture increases as a linear function of pressure, as he found with steel and copper. Pugh found further that the net axial stress at fracture, determined by subtracting the pressure from the applied tensile stress at fracture, remains constant for steels and copper.

2.2.5 Griggs

In 1936, David T. Griggs, a student of Bridgman's, assembled a Type I apparatus for conducting compression, tension and torsion tests under constant, internally generated fluid pressure [5]. Pressures were measured by the change of resistance of a coil of manganin wire and loads were measured externally. Griggs measured the displacement of his loading/pressurizing ram externally with a dial indicator to determine the extension of the specimen. In compression tests, the loading piston bore down directly on the cylindrical specimen, and tension tests were done with the aid of a "double-yoke" mechanism which converted an externally applied compressive force into a tensile force. Frictional forces were measured on the pressurized but unloaded piston, and subtracted from the measured total load recordings. Descendants of this design would later be used by Bridgman in his tests on metals. Griggs tested Solenhofen limestone, marble and single crystal quartz at pressures up to 194,000 psi. In compression tests of

the limestone and marble they found that pressure induced a brittle to ductile transition, dramatically increasing not only the strain at final fracture, but also the compressive fracture strength. Tests with copper jacketed specimens displayed up to an additional 40% increase in compressive fracture strength. Paradoxically, in tension and torsion tests, these materials behaved the same under high pressure as at atmospheric pressure.

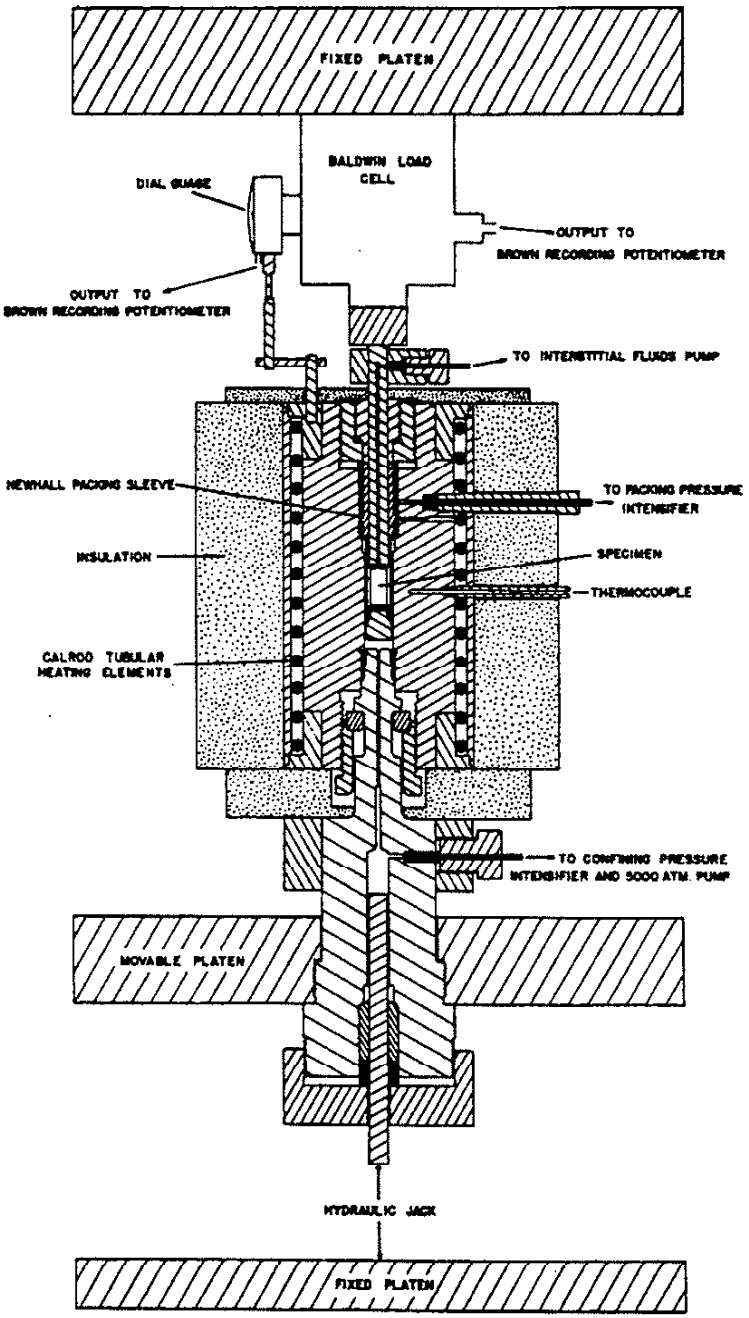

Figure 2.8: Griggs' 1960 pressure test apparatus [12]

Griggs continued to push the state of the art in pressure test apparatus. In 1960, Griggs, Turner and Heard assembled a Type I apparatus for conducting high-temperature compression and tension tests under constant pressure, externally pressurized CO_2 gas [12]. A gas was chosen because liquids could not withstand the high temperatures of up to 800°C that Griggs et al were interested in testing to. Pressures were measured by the change of resistance of a coil of manganin wire and loads were measured externally. One end of a solid specimen was fixed to the pressure vessel, while axial loads were applied to the other end of the specimen through a ram which exited the vessel through a Johnson and Newhall "controlled clearance" gland [13]. This sealing device allowed the precise control of the clearance between a plunger and its gland by externally pressurizing the gland. In this way, clearances too tight to machine could be achieved, thus limiting fluid leakage past the gland to acceptable levels without incurring any frictional penalty. The gland pressure was adjusted during the test to maintain a constant CO_2 leakage rate. Typical frictional loads were reported as being 1 percent of the force exerted by the CO_2 pressure on the plunger, with the variation in friction load being less than half a percent. Because of the frictionless controlled clearance glands, Griggs *et al* were able to apply loads to the specimen and accurately measure them external to the vessel. Griggs measured the displacement of his loading ram externally with a dial indicator, then corrected it for ram deflection to determine the extension of the specimen. This apparatus in shown in Figure 2.8.

In compression tests, the loading ram bore down directly on the cylindrical specimen, and tension tests were done with the aid of a double-yoke. This apparatus also had the capability to internally pressurize hollow or porous specimens. Griggs *et al* tested a variety of rocks, crystals and minerals at pressures up to 73,500 psi and identified their deformation mechanisms. Heating elements within the vessel could raise the temperature of the specimen to 800°C. Griggs *et al* reported that the elevated temperature tests displayed specimen ductility so enhanced compared to tests done under pressure alone, that fracture was often suppressed. Heard (1960) used this same apparatus to test Solenhofen limestone, interstitially pressurized with water and CO_2.

2.2.6 Spitzig

Spitzig was not a designer of *equipment* like the others in this list; he used a updated version of Pugh and Green's 1954 Type I apparatus to conduct his tests. He is included here because he was such a noteworthy designer of *experiments*. One simply cannot find fault with this experimentalist's high caliber work! All his research was conducted on quality equipment, displayed thorough planning and great attention to detail, and produced fabulous results. In the field of high pressure testing, this is a rarity that deserves mention.

In 1975, Spitzig *et al.* conducted monotonic axial load tests [14]. They measured the displacement of their bottom ram externally with an LVDT to determine the extension of the specimen. Tests were conducted on quenched and tempered SAE 4310 and 4330 steel specimens

heat treated to eliminate retained austenite, at pressures up to 160,000 psi. No mention is made of any protective sheathing to prevent fluid contact, thus it is assumed that all testing was conducted with bare specimens.

Spitzig subjected several specimens to hydrostatic pressure soaking at 200,000 psi, and then tested them in tension and compression at atmospheric pressure to true strains of 0.04 (4.0%). The absence of variation in the results, when compared with specimens that were not pressure soaked, proved that pressurization itself did not change the specimen structure. Tension and compression tests were then conducted at 20,000, 40,000, 80,000, 120,000, and 160,000 psi. Both steels responded similarly, with the pressure raising the stress-strain curve (through a linear increase in the yield strength equal to 7.5% of the pressure increase) but not significantly affecting the strain hardening characteristics. Spitzig *et al.* stated that the pressure dependence of the yield strength of these steels appears to be larger than observed in mild steels by Pugh, Bridgman and Brandes, and derived a specific yield condition which accounts for it.

In 1976, Spitzig *et al.* conducted an identical series of tests on a maraging steel in both the unaged and aged condition, and on HY-80 submarine hull steel [15]. Again, pressure raised the stress-strain curve (through a linear increase in the yield strength), but did not significantly affect the strain hardening characteristics. The unaged maraging steel responded with an increase in the yield strength equal to 4.6% of the pressure increase. The aged maraging steel responded with an increase in the yield strength equal to 10.0% of the pressure increase. The HY-80 submarine hull steel responded with an increase in the yield strength equal to 2.5% of the pressure increase. Spitzig *et al.* again derived a specific yield condition which accounts for the pressure dependence of the yield strength of these steels.

In 1979, because the literature was so contradictory, Spitzig conducted an series of tests to determine what effect normal stress on slip planes had on the flow stress of single crystal iron specimens [16]. Spitzig subjected one specimen to hydrostatic pressure soaking at 160,000 psi, and then tested it in tension at atmospheric pressure. The absence of variation in the results, when compared with a specimen that was not pressure soaked, proved that pressurization itself did not change the mechanical properties of the specimen. Then tension tests were conducted at 40,000, 80,000, 120,000, and 160,000 psi. Subsequent analysis demonstrated that the slip systems operating, the types of dislocations produced and the dislocation distributions observed were the same or similar under pressure as at atmospheric pressure. During testing the specimens were oriented so that they would shear on the same crystallographic slip plane but in different directions. Under pressure, a linear increase in the proportional limit equal to approximately 0.13% of the pressure increase was observed on the shear stress-shear strain curve, but the predominant effect was an increase in the strain hardening characteristics - an increased rate of hardening in the early stages of deformation. The single crystal iron samples responded with a yield strength increase of approximately 0.13% of the pressure increase; a much lower figure than for the polycrystalline

samples Spitzig reports in other papers. From these experiments, Spitzig concluded that normal stress on the slip plane has a larger influence on work-hardening than on the Critical Resolved Shear Stress. This suggests that dislocation generation is decreased under pressure (the pressure dependency stemming from the fact that there is a volume increase associated with the generation of dislocations) which accelerates dislocation tangling.

In 1984, Spitzig and Richmond conducted a series of tests on grade 1100 aluminum plate specimens [17]. Spitzig subjected a pair of specimens to hydrostatic pressure soaking at 120,000 psi, and then tested them in tension and compression at atmospheric pressure. The absence of variation in the results, when compared with specimens that were not pressure soaked, proved that pressurization itself did not change the mechanical properties of the specimen. Then tension and compression tests were conducted at 20,000, 60,000 and 120,000 psi. Pressure raised the stress-strain curve, through a linear increase in the yield strength three times greater than for iron-based materials. Spitzig and Richmond critically examined several dislocation models put forward to explain the pressure dependence of the yield strength; Shmatov, 1973; Ashby and Verall, 1971; and Jung, 1981. The experimental results matched most closely with the predictions of the Jung model. The Jung model is thermodynamics-based and takes into account the work of the pressure resisting the volume change associated with dislocation generation and motion.

2.3 Major Effects of Pressure on Monotonic Behavior

In general, ductility is enhanced under pressure via the suppression of fracture by microvoid nucleation, growth and/or coalescence. The degree of ductility exhibited by both brittle and ductile materials during tension and compression tests (and during deformation processing) is very definitely related to the pressure acting upon them, with increases in pressure promoting increased strain to fracture. Of course, the levels of pressure necessary to increase ductility (and the magnitude of the resulting increase) are dependent on the deformation and fracture mechanisms operating in the material, but true strains greater than 5.0 are often achievable. Most frequently, pressure suppresses void growth and coalescence, and retards cleavage fracture. The behavior of normally brittle materials is often so greatly affected by application of pressure that one can either speak of the existence of a brittle to ductile transition pressure, or say that pressure lowers a material's brittle-to-ductile transition temperature.

In general, pressure changes the shape of the stress strain curve. As a minimum, pressure extends the strain to fracture, and frequently it raises the entire curve, increasing the flow stress, ultimate strength and affecting the strain hardening rates via pressure induced decreases in the density and mobility of dislocations. However, unlike the tremendous pressure-induced increases in ductility, observed pressure-induced increases in strength are usually less than 10%. Though often debated, it was eventually proven that pressure does not affect the strain at which tension instability (necking) occurs in tension tests [67].

When *ideal* single crystal samples of any of the seven crystal systems are subjected to external hydrostatic pressure, no shear stresses are developed within the samples. Examination of the elastic compliance (or stiffness) tensors for these crystals verifies this. However, *real* single crystals contain defects such as voids, dislocations, inclusions, etc., which act as elastic inhomogeneities. When subjected to hydrostatic pressure, shear stresses of substantial magnitudes are generated at these internal defects, and these shear stresses can cause substructure changes; i.e., the production of dislocations. Such pressure-induced changes can impact the structure-sensitive material behavior (i.e., producing changes in flow stress and ductility), both under pressure and after a hydrostatic pressurization cycle [68-78].

2.4 Seminal Works in the History of Cyclic Testing Under Pressure

2.4.1 60 Years Later...

Because of the technical hurdles involved, more than 60 years passed between Professor Kick's initial experiments on marble under pressure and the first reported cyclic test under pressure. Due to the numerous experimental difficulties encountered, the few reliable fatigue test results under pressure are noteworthy: of fourteen published reports listed in Table 2.2, only four investigators present reliable results. Professor Crossland spent his entire life in the high pressure field, and with his students (i.e., White) contributed greatly to advancing the state of the art with his numerous robust test machine designs [26,27,30,79,80,81,82,83,59]. Ohji et al. published only one paper, but described many tests on a variety of materials, all conducted on a well-designed apparatus [84]. Gustafson took a brute force approach and put an entire rotating-four-point-bending test machine in a large pressure vessel (designed for HIP work) to generate his data [85]. The shaded rows in Table 2.2 and the following discussion covers this in greater detail. Note that of the nine who tried axial fatigue testing, only two appear here. The high rate of failure is due to the increased level of sophistication required to make an axial testing apparatus work.

2.4.2 Crossland

In 1956 Crossland constructed a Type I apparatus for conducting torsional fatigue tests inside an externally pressurized, fluid-filled cylindrical vessel [27]. The vessel was mounted to the fixed end of a torsional fatigue testing machine. The rotating chuck of the machine was attached to Crossland's input shaft which entered his vessel through a Morrison gland. One end of a cylindrical torsion specimen was keyed to this input shaft and the other end was keyed to a hollow elastic tube. The opposite end of the tube was fixed to the vessel, allowing the tube to act as a torsional load cell. Mirrors mounted at each end of the hollow tube permitted optical monitoring of its angle of twist, from which the torque on the specimen was determined. The over-all angle of twist of the keyed specimen was determined from the difference between the angle of rotation of the input shaft and the torsional load cell tube.

Investigator	Year	Type of Test[1]	Maximum Pressure in psi	Pressure Variation	Test Method	Loads Measured	Strains Measured	Materials Tested
Crossland [27]	1956	TR (I)	44,800	constant	externally applied torque/twist-angle through a Morrison seal (torque control)	torque derived from optically measured angle of twist of an elastic tube	strains derived from optically measured relative angle of over-all twist	quenched and tempered En25 steel
White, Crossland, Morrison [78]	1959	AF (I)	45,000	constant	yoke arrangement operating through frictionless Morrison glands (load controlled)	electrically from external load cell	neck diameters and fracture surfaces measured after tests	quenched and tempered En25 steel
Burns and Parry [85]	1964	TR (I)	56,000	constant	externally applied torque/twist-angle through a Morrison seal (strain control)	torque derived from optically measured angle of twist of an elastic tube	strains derived from optically measured relative angle of over-all twist	quenched and tempered En25 and En40B steel
Rowland, DeVries, Gibbs [86]	1967	RF (I)	100,000	constant	rotating cantilever tests (constant total strain range)	none	fixed deflection was imposed upon the specimen	Al, Fe, Ni
Libertiny [87, 88, 89, 90]	1967 1968, 1968, 1970	AF (I)	45,000	constant	yoke arrangement operating through frictionless Morrison glands (strain controlled)	electrically from external load cell	neck diameters measured optically during tests	soft, and quenched and tempered En25 steel
Nakazawa, Koizuma, Kobayashi, Maruyama [91]	1971	AF	43,000	constant	(load controlled)	unspecified	unspecified	Al alloy 17S, ASTM A302B steel
Ohji, Ogura, Sugimoto, Yaji [92]	1972	AF	55,500	constant	(strain controlled)	unspecified	unspecified	5005 Al alloy
Ohji, Ogura, Sugimoto, Yaji [83]	1973	AF (I)	57,000	constant	tension plunger arrangement (load controlled)	electrically from internal strain gaged load cell	LVDT externally measured over-all extension	S35C steel, OFHC Cu, 5005 Al alloy
Lunsford, Pense, Venkatesan, McIntosh [93]	1973	AF (I)	100,000	constant	tension plunger arrangement (load controlled)	electrically from external load cell	none	Vascomax 300 maraging steel

Table 2.2: Cyclic tests under pressure. "AF" = Axial Fatigue, "RF" = Rotating Fatigue, "TF" = Torsional Fatigue, "I," "II" = Type.

Investigator	Year	Type of Test[1]	Maximum Pressure in psi.	Pressure Variation	Test Method	Loads Measured	Strains Measured	Materials Tested
Gustafson [84]	1975	RF (I)	159,500	constant	rotating four-point-bending tests (constant total strain range)	none	fixed deflection was imposed upon the specimen	tool steel
Nakazawa, Kobayashi, Homma [94]	1977	AF (I)	43,500	constant	tension plunger operating under a differential pressure	calculated from differential pressure across plunger	none	2017 Al alloy, ASTM A302B steel, NiCrMo steel and CrMo steel
Plumbridge, Ross and Parry [95, 96]	1981 1985	AF (I)	5,000	constant	tension plunger arrangement (load controlled)	electrically from internal strain gaged load cell	crack length monitored via COD gages and potential drop technique	Hiduminium RR58 Al alloy, BS 4360 grade 50D steel
Davis, Ellison and Plumbridge [97]	1986	AF (I)	5,000	constant	tension plunger arrangement (load controlled)	electrically from internal strain gaged load cell	crack length monitored via COD gages and potential drop technique	Hiduminium RR58 Al alloy, BS 4360 grade 50D steel

Table 2.2: Cyclic tests under pressure, continued. "AF" = Axial Fatigue, "RF" = Rotating Fatigue, "TF" = Torsional Fatigue, "I," "II" = Type.

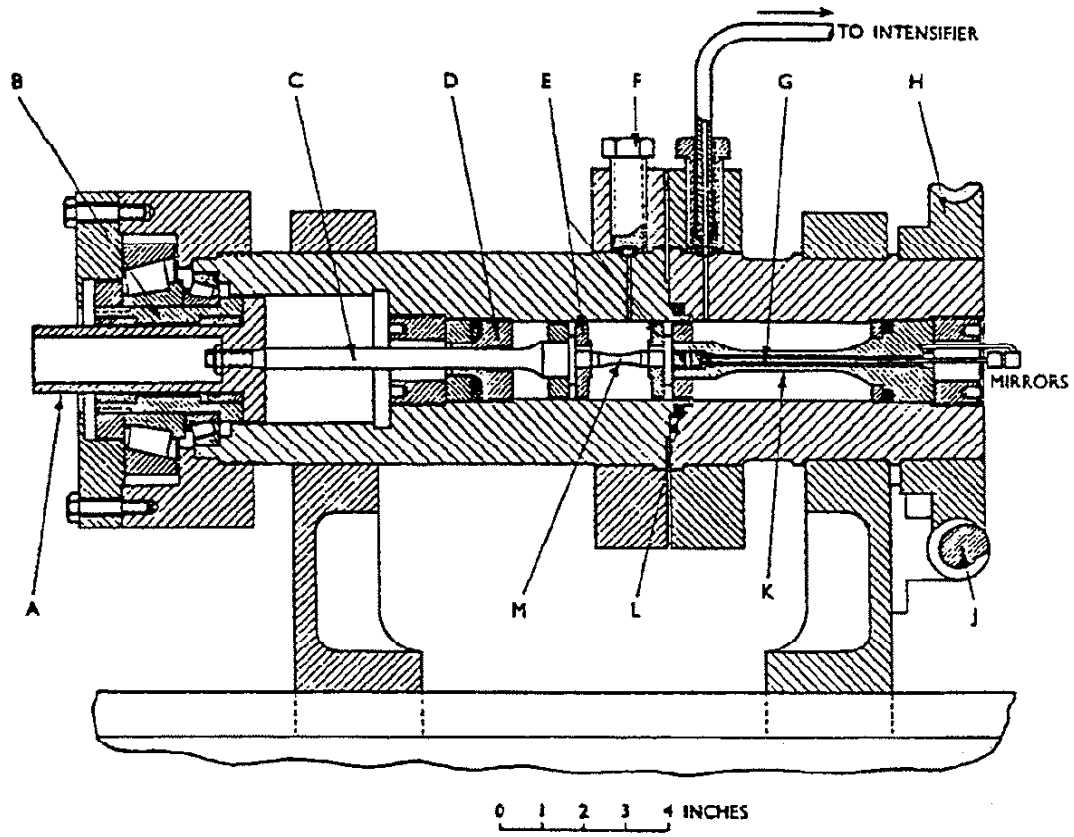

Fig. 2.75. Section of High-pressure Assembly

A	Coupling shaft.	E	Torsion grips.	J	Worm gear.
B	Bearing shaft.	F	Air bleed.	K	Torque bar.
C	Torque shaft.	G	Mirror shaft.	L	High-pressure joint.
D	Morrison seal.	H	Worm wheel.	M	Specimen.

Figure 2.9: Crossland's 1956 torsional fatigue test apparatus [27]

The Morrison seal gland [99] was one of two major advances in high-pressure/low-friction fluid sealing technology which occurred almost simultaneously (see the previous description of Johnson and Newhall's "controlled clearance" principle, as used by Griggs). The Morrison gland uses Bridgman's "unsupported area" principle to increase the unit loading of a deformable rubber element. This rubber element transmits the elevated unit loading to a close fitting section of the seal body, compressing it so as to decrease the clearance between the seal body and the shaft. Bridgman employed a similar concept in his free-piston gages, except that in his embodiment, fluid pressure provided the unit loading on the external surface of a reentrant cylindrical extension of the seal body. The advantages of the Morrison gland are as follows:

1. the unit loading is proportional to the pressure of the fluid to be sealed (it must be controlled separately in the Johnson and Newhall seal),

2. the seal body dimensions may be varied to achieve any desired constant of proportionality of unit loading to fluid pressure (it is always equal to the fluid pressure in the Bridgman embodiment), and

3. the rubber element can serve double duty by simultaneously sealing the outer diameter of the seal body (as an "unsupported area" seal). In this way, clearances too tight to machine could be achieved, thus preventing fluid leakage past the gland without incurring any frictional penalty.

The torsional fatigue machine was designed to oscillate its chuck through a set angle, ie, under shear strain control. Crossland, however, wished to conduct constant shear stress range tests. To accomplish this, he had to continuously monitor the shear stress range being applied to his specimen, and adjust the oscillation angle on the torsion machine to account for cyclic changes in the material being tested. Tests were conducted on cylindrical torsion specimens of a quenched and tempered Ni-Cr-Mo steel, at pressures from atmospheric to 44,800 psi. Tests conducted on bare specimens proved that contact with the high pressure fluid had a deleterious effect on fatigue life. Tests done with protective rubber coatings applied to the specimens showed that at 44,800 psi, the torsional fatigue life increased 32% over that measured at atmospheric pressure. Crossland graphed the fatigue limit (as Von Mises stress amplitude) for a number of cyclic axial, torsion, and rotating bending tests conducted at both atmospheric and high pressure, vs. the maximum hydrostatic stress in each test. (Hydrostatic stress being defined as $\sigma_H = \frac{\sigma_{zz} + \sigma_{rr} + \sigma_{\theta\theta}}{3}$). Crossland's figure, redrawn in Figure 2.10, shows the fatigue limit to be a function of hydrostatic stress.

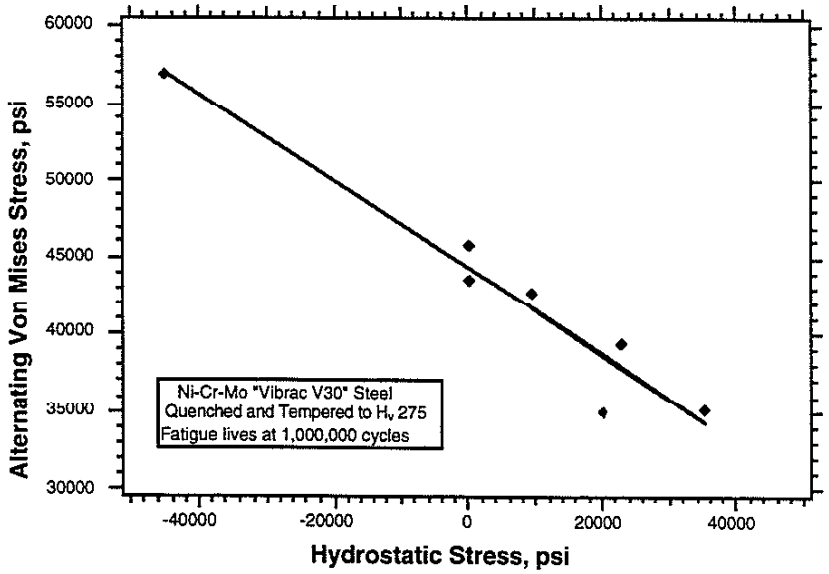

Figure 2.10: Von Mises stress amplitude vs. maximum hydrostatic stress for a number of axial and torsion tests conducted at atmospheric and high pressure [27]

The early multiaxial fatigue theories popular in the 1950's assumed that failure would occur after N_f cycles when the Tresca or von Mises effective stress equaled the uniaxial fatigue strength of the material measured experimentally at N_f cycles.

$$\sigma_e = A(N_f)$$

where: σ_e = equivalent stress amplitude
A = function of fatigue life obtained experimentally

However, because they are modifications of the failure criteria used to predict the onset of yield, these early "equivalent stress" theories neglect the mean and hydrostatic stress components of the multiaxial stress state. Obviously, this is a problem for someone who wants to use equivalent stress theories to describe failure under pressure. Crossland's plot in Figure 2.10 modified the equivalent stress concept by adding a hydrostatic stress term as follows:

$$\sigma_e + \alpha\sigma_H = A(N_f)$$

where: σ_e = equivalent stress amplitude
σ_H = maximum hydrostatic stress
α = material constant obtained experimentally
A = function of fatigue life obtained experimentally

Crossland found that this model correlated the results of all his fatigue tests very well. Sines' model follows a similar approach.

Even with the addition of a hydrostatic stress term, equivalent stress approaches to fatigue failure such as this do not recognize that fatigue initiates on certain material planes. They provide an average of the stresses and strains in the body without regard to the resolved stresses and strains on specific planes. Libertiny [91] briefly mentions the "critical plane" theories first put forth by Gough and Pollard and by Findley which hypothesize that fatigue failure depends on a function of the alternating shear stress (or strain), modified by the magnitude and sign of the normal stress on the "critical" plane of maximum shear stress (or strain). Burns and Parry [86] conducted torsional fatigue tests of quenched and tempered En25 and En40 steels under pressure, and observed a significant increase in fatigue lives with pressure. They attributed this to the pressure-induced compressive normal stress on the planes of maximum alternating shear stress in the material. Fatigue failure is predicted to occur when:

$$\tau_c + B\sigma_n = A(N_f)$$

where: τ_c = shear stress (strain) amplitude on the critical plane
σ_n = maximum normal stress (strain) amplitude on the critical plane
B = material constant obtained experimentally
A = function of fatigue life obtained experimentally

The major advantage of the critical plane approaches in multiaxial fatigue is that they not only predict fatigue life, but correlate it to the experimentally observed cracking behavior. Morrow presents an excellent treatment of this topic in his Ph.D. thesis [1].

2.4.2 White, *et al.*

The very first group to report axial fatigue data under pressure - White, Crossland and Morrison in 1959 - constructed a Type I apparatus to conduct cyclic axial load tests inside an externally pressurized, fluid-filled cylindrical vessel [79]. One end of an hourglass specimen was fixed to the pressure vessel, while the other end was attached to a yoke. Mean and cyclic axial loads were applied to the yoke via rams which exited each end of the vessel through Morrison glands. Because of the frictionless Morrison glands, White *et al.* were able to apply loads to the specimen and accurately measure them external to the vessel. Tests were conducted under both atmospheric and 45,000 psi pressure; cyclic loads were applied at 50 Hertz. No provisions were made to determine the extension of the specimen during the test, but elongations were measured afterwards. A simplified schematic of this apparatus is shown in Figure 2.11.

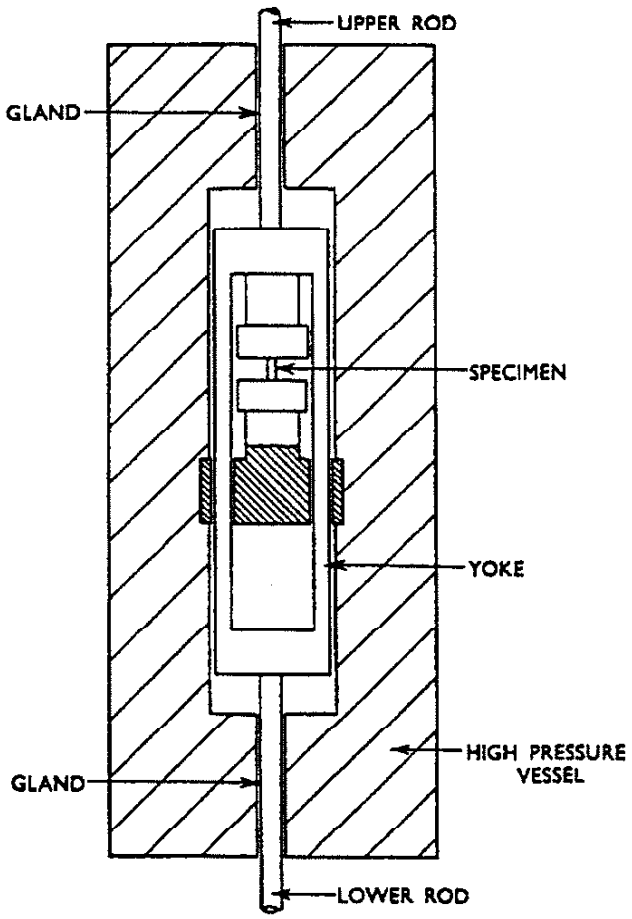

Figure 2.11: White's *et al* pressure test apparatus [79]

Tests were conducted on an oil quenched and tempered En25 (similar to 4340) steel. In initial tests under pressure, White *et al.* measured lower cyclic strengths when specimens were exposed to the fluid than when sheathed in rubber to prevent fluid contact. All testing, even at atmospheric pressure, was then done with rubber sheathed specimens.

Before the results of White *et al.* can be discussed, it is important to discuss the various failure modes which may operate during cyclic testing. If a smooth specimen of a ductile material is subjected to a symmetrical inelastic stress cycle (zero mean stress) below its UTS, it will respond with an inelastic strain cycle that depends on the material, its processing and the test conditions. The material may;

1. Cyclically strain harden (typical for soft materials)
2. Cyclically strain soften (typical for hard materials)
3. Be cyclically stable
4. Exhibit mixed behavior depending on the strain range.

The inelastic stress-strain response will trace out a hysteresis loop when plotted on stress-strain coordinates. Specimens typically exhibit some transient behavior of 1 or 2 above, and then become cyclically stable. When in condition 3, the beginning and end points of the hysteresis loop will be coincident, and the loop is termed "closed". Continued stress cycling of a material which remains in this condition typically results in the localization of plastic strain at sites termed "persistent slip bands" and the formation of intrusions and extrusions at a free surface. Cracks often initiate at these sites and propagate across the specimen to cause failure by either fast fracture or overload of the uncracked ligament. Collectively, this process of the initiation and propagation of a crack is termed a fatigue failure.

If a smooth specimen of a ductile material is subjected to an asymmetrical inelastic stress cycle (non-zero mean stress) below its UTS, it may respond with an inelastic strain cycle that, when plotted on stress-strain coordinates, does not exhibit coincident beginning and end points. Such a hysteresis loop is termed "open", and the material will accumulate unidirectional plastic strain with each stress cycle. This accumulation of plastic strain is termed "ratchetting" and typically occurs in the mean stress direction. Compressive ratchetting under cyclic load continues until the specimen diameter increases to the point where the stress is reduced to elastic levels. Tensile ratchetting under cyclic load continues until the specimen necks and fails as in a monotonic tension test by exhausting its ductility. Collectively, this process of accumulating unidirectional plastic strain is termed a ratchetting failure.

However, if a smooth specimen of a ductile material is subjected to an asymmetrical inelastic stress cycle (non-zero mean stress) below its UTS, it may alternately respond by ratchetting with a rate that decreases to zero (shakedown); resulting in a cyclically stable, closed hysteresis loop and a final fatigue failure.

It is worth noting that if a smooth specimen of a ductile material is subjected to a symmetrical inelastic *load* cycle (zero mean *load*) causing stresses below its UTS, there will theoretically be a small bias of the *true stress* in the tensile direction. This mean stress bias may cause tensile ratchetting.

A Haigh diagram is typically used to show cyclic test results as a function of the mean stress levels. On a set of alternating stress vs. mean stress axes, we can plot lines of constant life, "fatigue curves", bounded by competing failure modes such as gross yielding. After normalizing by the UTS of his En25 steel, White chose to plot his fatigue curves for failure at 1,000,000 cycles on such a diagram.

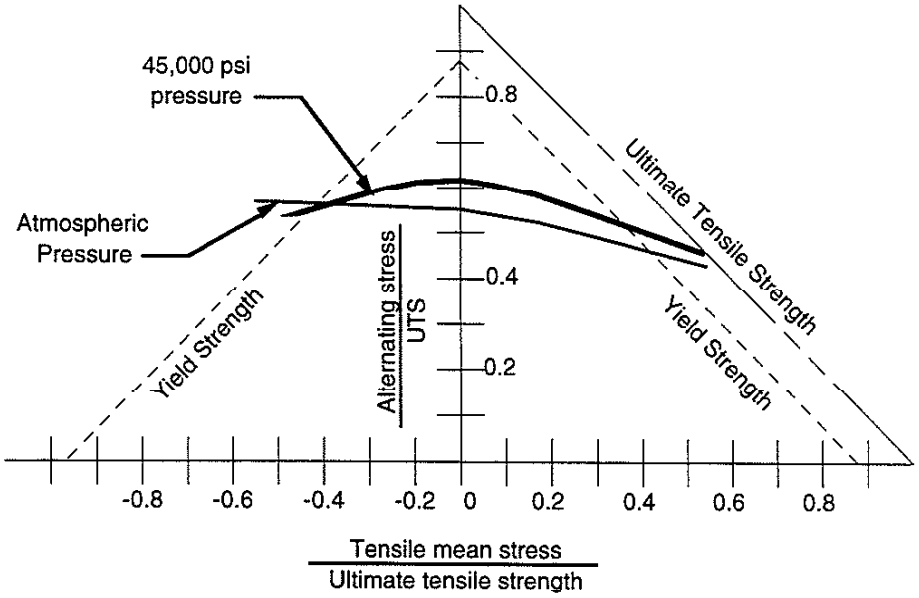

Figure 2.12: White's *et al* fatigue test results on En25 steel [79]

For tests conducted at atmospheric pressure, White *et al.* found:

1. failure by compressive yielding (barreling) at compressive mean stress levels plotting to the left of -0.5. Fatigue failures could not be induced, even for alternating stress levels of 0.64.
2. failure by transverse fatigue cracking at compressive mean stress levels plotting to the right of -0.5. All specimens tested to failure displayed barreling due to compressive ratchetting.
3. failure by transverse fatigue cracking at tensile mean stress levels. All specimens tested to failure displayed a reduction in area due to tensile ratchetting, the reduction increasing slightly with the mean stress level.
4. no measurable plastic deformation exhibited by specimens tested in the region below both the fatigue curve and the primitive yield lines.
5. failure by transverse fatigue cracking for specimens tested in a narrow region of alternating stress just above the fatigue curve.
6. failure by "gross yielding" (ratchetting) for specimens tested above the narrow region just described in 5. For specimens tested under tensile mean stresses, fracture took place with a reduction of area comparable to that observed in a monotonic tension test.

For tests conducted at 45,000 psi pressure, White *et al.* found that failure by fatigue was almost completely suppressed. Specifically they observed:

1. no effect on the yield point due to the application of pressure.
2. failure by barreling due to compressive ratchetting at all compressive mean stress levels. Fatigue failures could not be induced. The absence of fatigue failure indicates that pressure raised the fatigue curve above the alternating stress value that causes ratchetting failures, at compressive mean stress levels.
3. failure by transverse fatigue cracking at zero mean stress levels. All specimens tested to failure below fatigue ratios of 0.643 displayed no measurable plastic deformation.
4. failure by tensile ratchetting predominated at tensile mean stress levels. A reduction in area greater than observed in atmospheric pressure tensile tests was noted in specimens tested to ratchetting failure. The few failures due to transverse fatigue cracking also exhibited plastic deformation due to tensile ratchetting. If it is assumed that these few fatigue failures were not attributable to a damaged protective rubber sheathing on the specimen, then the presence of both modes of failure indicates that pressure raised the fatigue curve to the same alternating stress value that causes ratchetting failures, at tensile mean stress levels.

White *et al.* state that if the yield and plastic flow of ductile materials in monotonic tests is determined almost entirely by the shear stresses acting on them, then the mechanism of slip must be unaffected by pressure. They could find no sensible reason to suppose otherwise for cyclic stress, and so concluded that the formation of persistent slip bands, intrusions and extrusions should not be affected by pressure. If this is so, then they conclude that the increases they found in the fatigue limit must be due to pressure effects retarding the process of fatigue crack initiation and growth, not slip.

2.4.3 Ohji *et al.*

In 1973, Ohji *et al.* constructed an apparatus to conduct cyclic axial load tests inside an externally pressurized, fluid-filled cylindrical vessel [84]. Ohji *et al.* used a Type I test machine that was basically an inversion of the one used by White *et al.*, but incorporating internal load measurement via a strain gage load cell inside the vessel. Its full Wheatstone bridge strain gage circuit did not include any dummy gages, thus pressure effects on the gages had to be measured ahead of time and compensated for manually. Ohji *et al.* measured the displacement of their loading ram externally with an LVDT to determine the extension of the specimen. These tests were run using axial load control, under constant pressures up to 57,000 psi; loads were applied via a hydraulic actuator at 1 Hertz.

Tests were conducted on 5005 aluminum alloy, cold worked OFHC copper and S35C (similar to SAE 1035) steel hourglass specimens. In initial tests under pressure, Ohji et al. measured no change in cyclic strengths when specimens were exposed to the fluid and when sheathed in silicone rubber to prevent fluid contact. All testing, even at atmospheric pressure, was then done with uncoated specimens.

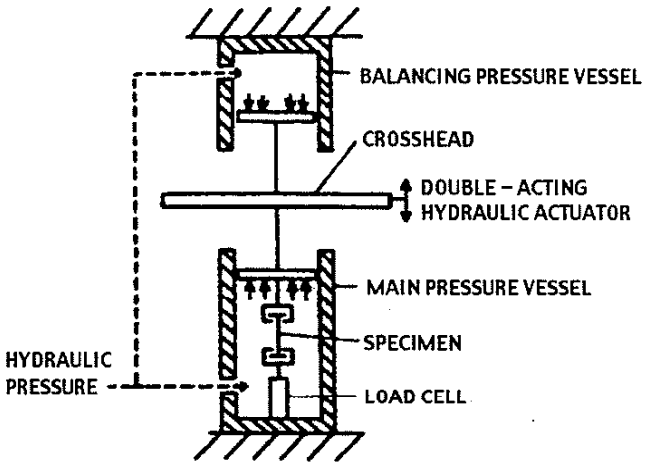

Figure 2.13: Ohji's *et al* pressure test apparatus [84]

Ohji et al subjected the specimens to fully reversed cyclic loads high enough to cause failure in 5,000 cycles or less. For tests conducted at all pressures, Ohji et al found:

1. failure by tensile ratchetting at all stress amplitudes
2. failure by tensile ratchetting at lives below 100 cycles for the cold worked OFHC copper and S35C (~SAE 1035) steel specimens.
3. failure by transverse fatigue cracking at lives above 100 cycles for the cold worked OFHC copper and S35C (~SAE 1035) steel specimens.

Ohji et al found that the fatigue strength under completely reversed stress cycling definitely increased with increasing pressure. The failure mode for each specimen was not described, so

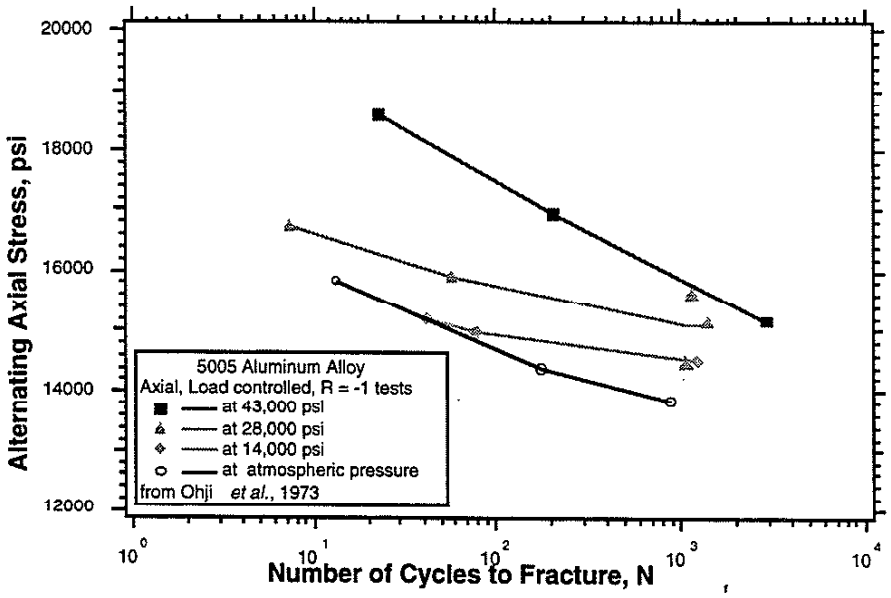

Figure 2.14: Results of low cycle tests conducted on 5005 aluminum alloy under various pressures [84]. Note that increasing pressures raise the fatigue curve.

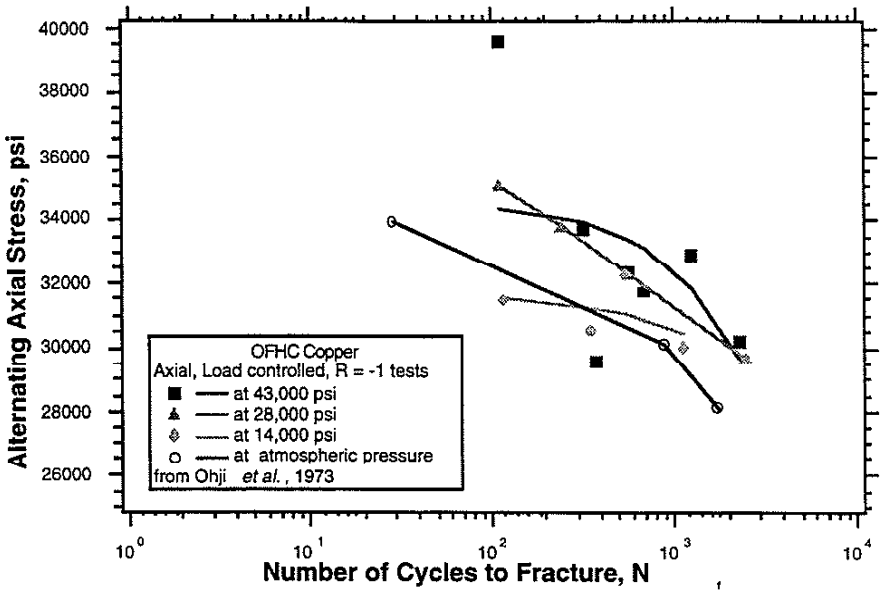

Figure 2.15: Results of low cycle tests conducted on OFHC copper under various pressures [84]. Note that increasing pressures raise the fatigue curve.

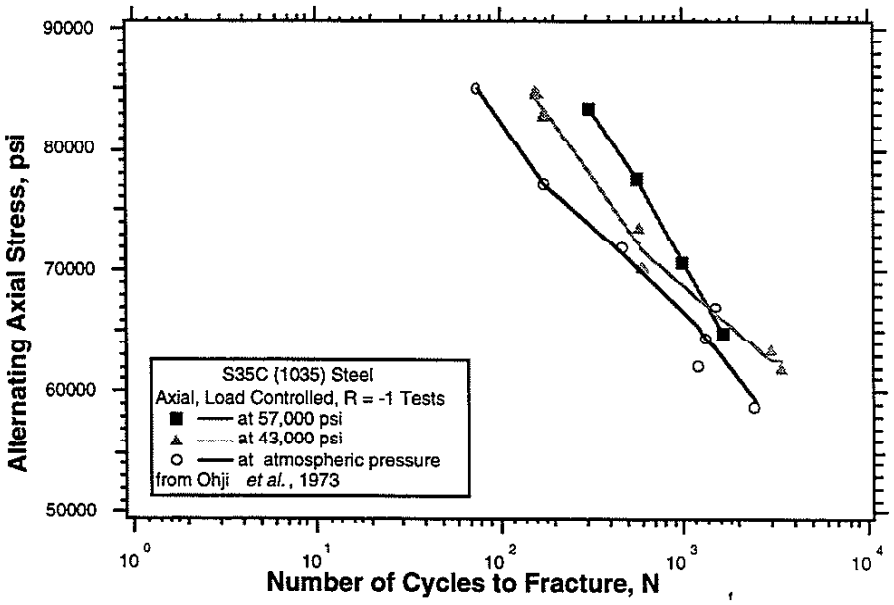

Figure 2.16: Results of low cycle tests conducted on S35C steel under various pressures [84]. Note that increasing pressures raise the fatigue curve.

it is impossible to attribute any change in failure mode to pressure, as was done by White et al. No information as to strain at fracture was given for specimens failing by ratchetting. Figures 2.14-2.16 present his fatigue test results.

Next, Ohji et al subjected notched, cold worked OFHC copper specimens to fully reversed cyclic loads high enough to cause failure in 5,000 cycles or less. In general, fatigue investigators

use notched specimens because the high stress at the notch root greatly reduces the life to crack initiation. As expected then, failure was by transverse fatigue cracking at all stress amplitudes for all the notched, cold worked OFHC copper specimens. Interestingly, Ohji et al found that the fatigue strength under completely reversed stress cycling was *not* affected by pressure. SEM micrographs of the fracture surface areas corresponding to fatigue crack propagation reveal similar fatigue striations at all pressures. *Though it is difficult to corroborate with the general understanding that the effect of normal stress is small on the crack initiation process but large on the crack propagation process*, they state that these findings, in conjunction with the smooth specimen results, indicate that pressure affects the crack initiation process rather than the crack propagation process.

2.4.4 Gustafsen

In 1975, Gustafsen constructed a Type I apparatus to conduct rotating bar fatigue tests inside an externally pressurized, fluid-filled cylindrical vessel [85]. A waisted specimen, loaded in four point bending and held at a preset deflection by an adjustable bearing, was axially coupled to an electric motor, and placed inside the pressure vessel. A deflection vs. gage section strain calibration curve was determined for the bending rig at atmospheric pressure. Since the bending rig was designed to be much stiffer than the specimen, Gustafsen says that the machine is therefore "very nearly a constant-strain (range) machine". The number of cycles to failure was determined using a Hall effect sensor coupled to the specimen and read via an electronic counter. Because of the waisted design of the rotating bar specimens, all failures occurred in the gage section. A nickel foil resistance thermometer placed inside the vessel revealed that the temperature in the vessel never rose more than 40°C above room temperature. This apparatus is shown in Figure 2.17.

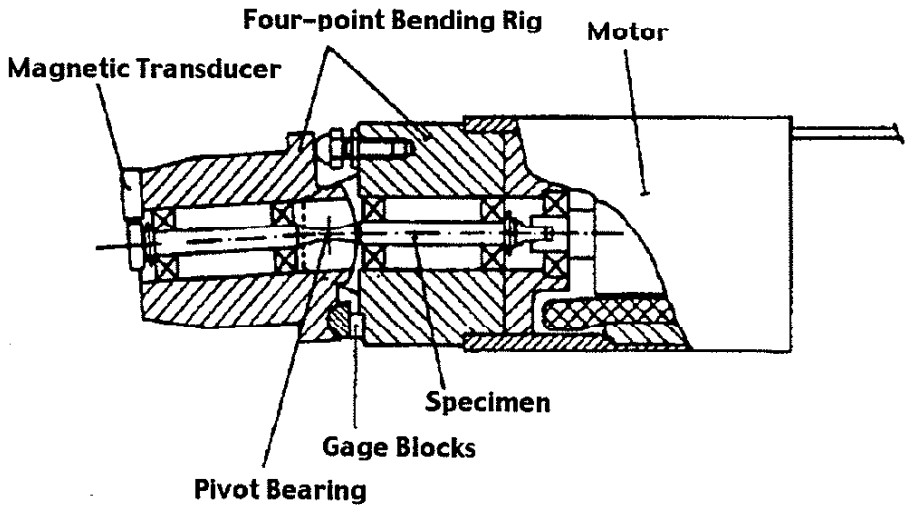

Figure 2.17: Gustafsen's pressure test apparatus which was placed inside a pressure vessel designed for HIP [85].

Before a seal blew and damaged the equipment, four series of constant pressure fatigue tests were run on oil quenched and triple tempered high-strength tool steel specimens;

I. bare specimens under atmospheric conditions,
II. bare specimens pressurized at 100,000 psi,
III bare specimens pressurized at 160,000 psi, and
IV. epoxy-polysulphide coated specimens pressurized at 100,000 psi.

The results of the first three series of tests reveal a definite improvement in fatigue life due to pressure, with the rate of life extension decreasing with further increases in pressure. Examination of the failed specimens shows that the area of the fracture surface corresponding to final fracture decreased when tested under increasing pressure; or stated in other terms, the area of the fracture surface corresponding to fatigue crack propagation increased with pressure. In the longer life tests, the cracks did not propagate in a direction perpendicular to the specimen axis.

The results of the first and last series of tests shown in Figure 2.18 reveal a significant improvement in fatigue life due to pressure, again with the rate of life extension decreasing with further increases in pressure. The area of the fracture surface corresponding to fatigue crack propagation was very large for series IV. In the longer life tests, the variation of the fracture surface from a direction perpendicular to the specimen axis was more pronounced than seen in the bare specimen tests.

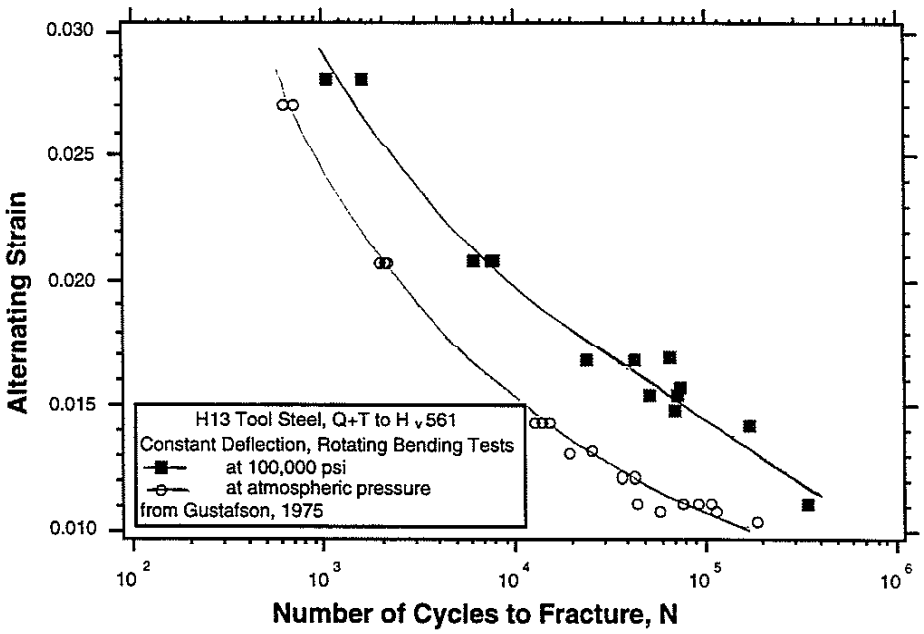

Figure 2.18: Results of cyclic tests conducted on coated tool steel specimens under atmospheric and high pressure [85]. Note that increasing pressures raise the fatigue curve.

Gustafson notes further that under pressure the fracture surface topography at the crack origin changes, and attributes it to a pressure induced extension of the stage I crack propagation phase. He interprets the increase in the fracture surface area corresponding to fatigue crack

propagation as a pressure induced extension of the stage II crack propagation phase, though he states that it is difficult to determine which phase is affected more by the superimposed pressure. No counting of crack striations was presented.

Other investigators have surmised that the additional fatigue life extension seen in tests of coated specimens results from the prevention of the ingress of pressurized fluid into developing cracks. Gustafson points out that this mechanism can only be valid when the cracks are of microscopic dimensions, for most coatings would themselves fail in the presence of a substantial crack size. For a Type I apparatus like his own rotating bar tests where the entire specimen is immersed in the hydrostatic pressure field, a cracked specimen with an intact coating will have its effective stress intensity factor range, ΔK_e, decreased by the presence of pressure, P, according to:

$$\Delta K_e = f\,(\sigma - P)\,\sqrt{(\pi a)}$$

where: f = geometry factor,
σ = far field tensile stress neglecting pressure, and
a = crack depth.

Then the Paris equation:

$$da/dN = C\,(\Delta K_e)^n$$

where: N = number of applications of crack opening stress,
C,n = empirical constants,

predicts a decreased crack propagation rate whenever ΔK_e is reduced. In the absence of a coating or once a coating fails and the crack faces become pressurized, the effective stress intensity factor range, ΔK_e, is given by:

$$\Delta K_e = f\,\sigma\,\sqrt{(\pi a)}\,.$$

Thus in a Type I apparatus, the Paris equation predicts no pressure effect on the crack propagation rate. Therefore any decrease in the crack propagation rate must be due to C and n being functions of pressure, rather than constants.

Ewalds and Wanhill [100] present a proof based on the theory of elasticity and LEFM, showing that uniform pressure applied to the faces of a crack in a center cracked plate is equivalent to an increase in the applied far-field stress of magnitude equal to the numerical value of the pressure. Part of the problem with this is that some investigators do not realize the difference

between Type I and Type II test machines, and they further confuse the issue by reporting stress values referenced to their pressure, rather than referenced to atmospheric pressure as zero stress.

2.5 Major Effects of Pressure on Cyclic Behavior

Due to the experimental difficulties of cyclic testing under pressure, very little cyclic triaxial test data exists. In general however, pressure raises the stress-life and strain life curves for metals. The first cyclic experiments under pressure demonstrated that the fatigue limit increased as the magnitude of the hydrostatic stress decreased. This spawned early multiaxial fatigue theories which predicted failure after N_f cycles when the Tresca or Von Mises effective stress, modified by a hydrostatic stress term, equaled the uniaxial fatigue strength of the material measured experimentally at N_f cycles. Modern "critical plane" approaches in multiaxial fatigue predict fatigue life and correlate it to the experimentally observed cracking behavior [1].

No matter how they were cyclically tested under pressure -- rotating bending, torsion, axial, etc. -- similar increases in fatigue performance are seen in a wide variety of steels, aluminum alloys and copper. However, there is no universally accepted reason which explains the observed increases. Various contradictory theories have been proposed, including

> The formation of persistent slip bands, intrusions and extrusions are not affected by pressure - increases in the fatigue limit must be due to pressure effects retarding the process of fatigue crack initiation *and* propagation [79].
>
> Pressure retards the crack initiation process rather than the crack propagation process [93, 87].
>
> Fatigue crack propagation is faster in high pressure oil than in unpressurized oil [91].
>
> Fatigue crack propagation is slower in unpressurized oil than in air, with the difference increasing with decreasing R. This is attributed to a squeeze-film lubrication effect that occurs when a closing crack tries to pump out the fluid trapped between its faces. The pressures so generated (which increase with loading frequency and fluid viscosity) delay crack closure and decrease the effective ΔK [97].
>
> Hydrostatic pressure delays or prevents the initiation of fatigue cracks, with the advantageous effect being higher in short-life than in long life fatigue [88].
>
> Pressure can change the fatigue failure mode, for example, from transverse fatigue cracking to one showing plastic deformation due to tensile ratchetting. Due to the pressure-induced increases in ductility, greater reductions in area are seen for ratchetting failures under pressure [79].
>
> The area of the fracture surface corresponding to final fracture decreased when tested under increasing pressure; or stated in other terms, the area of the fracture surface corresponding to fatigue crack propagation increased with pressure [85].
>
> There is no connection between pressure-induced increases in fatigue strength and the well known pressure-induced increases in ductility. The beneficial effect of

hydrostatic pressure is due to the compressive normal stress that it induces on the planes of maximum alternating shear stress, which reduces the rate of crack initiation (a critical plane approach) [86].

Cyclic life under pressure often depends on whether or not the specimens are in direct contact with the pressurizing fluid. Porous materials or materials with a large number of voids or inclusions typically show a significant life extension when coated, while high purity, non-porous materials usually show no change.

2.6 Seminal Works in the History of Phase Transformation Testing Under Pressure

2.6.1 Phase Transformations Under Purely Hydrostatic Stress

Metallurgists are familiar with alloy phase diagrams plotted on temperature vs. composition coordinates. In reality, these diagrams are but a slice taken out of the pressure, temperature, composition phase *surfaces* for the alloy at atmospheric pressure. The Clausius-Clapeyron equation is used to predict the hydrostatic pressure sensitivity of the phase transition temperatures:

$$\frac{dP}{dT} \approx \frac{\Delta H}{T_0 \Delta V}$$

where
- P = pressure
- T_0 = equilibrium phase change temperature
- ΔH = enthalpy of the transformation
- ΔV = volume change caused by the transformation

In particular, it predicts that equilibrium phase transition temperature should decrease with pure hydrostatic pressure for materials which exhibit a positive volume change upon transformation. Conversely, it predicts increases for materials which exhibit a negative volume change.

A large number of investigations into athermal and isothermal phase transformation behavior at high hydrostatic pressures have been conducted by researchers who have hydrostatically pressurized, heated and cooled specimens using a wide variety of test equipment, while monitoring for evidence of phase transformation in an equally wide variety of ways. Bridgman was a pioneer in this field, and the phase transition pressures that he determined for different materials became the standards used for calibrating high pressure equipment in laboratories around the world.

However, hydrostatic pressure is just a special case of a multiaxial stress state. Documented material behavior under biaxial stress states is still not commonplace, and of the even more rare non-hydrostatic triaxial stress tests, only the investigations contained in this thesis specifically examine the effect of stress state on phase transformation behavior.

2.6.2 Effects of Triaxial Stress on Phase Transformations

Before one can discuss the effects of triaxial stress on phase transformation, it is necessary to provide some background on the basic martensitic phase transformation process using carbon steel as an example. Though "martensite" was initially used to describe the fine, needlelike microstructure first observed in quenched steels by Adolph Martens, its current definition is much more encompassing. Today, a martensitic transformation is defined as a solid-state diffusionless phase transformation in any alloy system, brought about by cooperative atomic movements, that results in shear deformation of the parent (austenite) phase. The term martensite is applied to the product phase of any such transformation. A complete discussion of martensite and the classification of martensitic transformations can be found in the text of Nishiyama [101]. In addition, the text of Meyers and Chawla [102] may be consulted for more introductory material.

At temperatures above Tc, low carbon steels are "austenitic" (FCC crystal structure). If they are slowly cooled below Tc they transform to a stable pearlite (BCC iron + Fe_3C) structure. If they are cooled below Tc quickly enough to bypass the "pearlitic knee," they remain austenitic for a time, until they are cooled to the M_s (martensite start) temperature. As they are cooled through the M_s temperature the austenite begins to spontaneously transform to metastable "martensite" (BCT). Transformation to martensite is complete upon cooling to the M_f (martensite finish) temperature. For many steels, M_f is well below room temperature, and so it may never be reached unless special low-temperature quenches are imposed. Remaining austenite that does not transform is termed "retained austenite." Figure 2.19 illustrates this graphically, plus introduces the M_{50} line which refers to a temperature at which 50% martensite and 50% austenite exist.

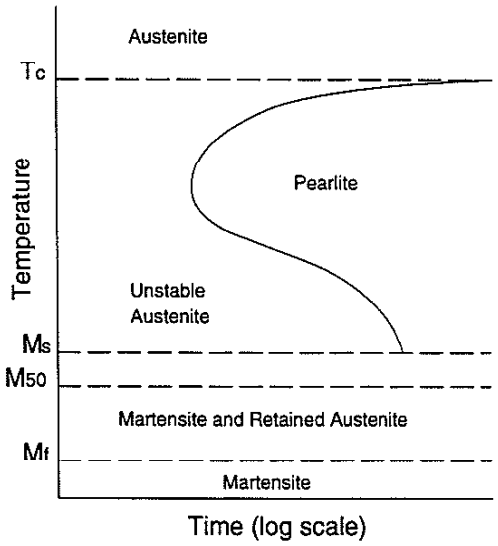

Figure 2.19: Schematic TTT diagram for a carbon steel, showing the relations between temperature, time and the existence of the various solid phases.

An empirical equation exists for calculating the Ms temperature from the elemental composition of a low alloy steel (expressed in weight percent). It is:

$$M_s\ (°C) = 500° - 333\ C - 34\ Mn - 35\ V - 20\ Cr - 17\ Ni - 11\ Mo - 10\ Cu - 5\ W + 15\ Co + 30\ Al$$

The M_s temperature of thru-carburized (1.1% carbon potential) bearing 4320 steel per ASTM A535 calculates to be:

$$\begin{aligned} M_s\ (°C) &= 500° - 333\ (1.10) - 34\ (.55) - 35\ (0) - 20\ (.50) - 17\ (1.83) - \\ &\quad 11\ (.25) - 10\ (0) - 5\ (0) + 15\ (0) + 30\ (0) + 0\ (.25) \\ &= 71.1\ °C \end{aligned}$$

Thus this steel would be expected to be at least partially martensitic after quenching from the austenitic phase to room temperature.

The laws of thermodynamics permit phase transformations to occur only when the chemical free energy change of the transformation is favorable; i.e., when the free energy of the product phase is less than that of the parent phase. Figure 2.20 is a schematic chemical free energy vs. temperature diagram for a steel. It shows the temperature T_0 where thermodynamics predicts the austenite to phase to transform to martensite upon cooling. However, when the phase transformation temperature is actually measured, it is found to occur at the M_s temperature described earlier - where *kinetics* permits it to occur. The difference between this temperature and the T_0 temperature represents the energy barrier which must be overcome for the new phase to nucleate. The ΔG is this supercooling or superheating activation energy. Upon heating, the reverse transformation from martensite phase to the austenite parent phase occurs in an analogous fashion. For this reverse transformation, the austenite start temperature, A_s, is defined in similar fashion to the M_s temperature.

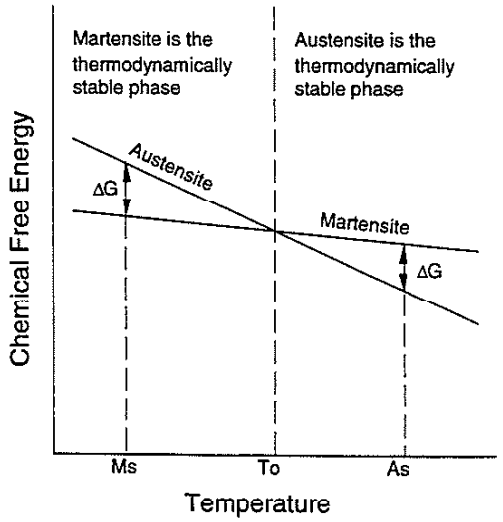

Figure 2.20: Schematic chemical free energy vs. temperature diagram for a steel.

In the absence of external stresses, substantial shear strains and a volume increase are observed for the transformation of austenite to martensite. If the transforming material is placed under stress, mechanical work is done when the external stress acts through the transformation strains. Thermodynamics requires that we then include a work term (applied stress * transformation strain) in the free energy calculations. Including this term means that the temperature at which transformation begins is not a constant, but rather a function of stress-state. Therefore, formulations that specifically include externally applied stress are necessary.

The M_s temperature is specified to be the temperature at which the first transformation from austenite to martensite spontaneously occurs upon cooling with no externally applied stress imposed. On a graph of uniaxial stress vs. temperature like the one shown in Figure 2.21, one can plot the variation of tensile yield strength of austenitic steel. On such a plot, the M_s temperature is a point on the abscissa.

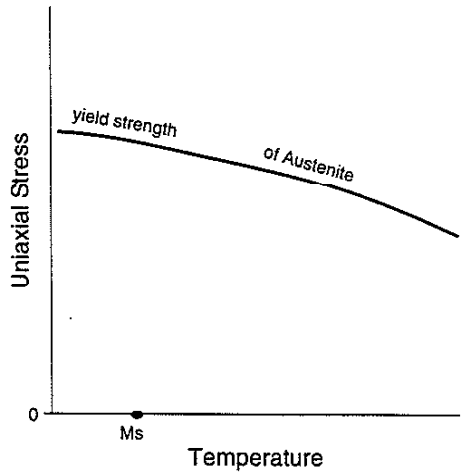

Figure 2.21: Schematic austenite yield strength vs. temperature diagram for a steel. The M_s temperature is the temperature at which spontaneous transformation occurs at zero applied stress.

Experiments show that within a specific temperature range above M_s a tensile stress (below the austenite yield strength) applied to an austenitic sample will bring about the onset of transformation. In this regime, Stringfellow says that transformation occurs through "stress-assisted" nucleation on the same sites which are responsible when transformation occurs without any applied stress [103]. The upper bound to this transformation behavior occurs at stress levels equal to the yield strength, at a temperature called the M_s^{σ} temperature. This is plotted in Figure 2.22.

In stress-assisted martensitic transformation, only elastic deformation occurs in the parent phase prior to transformation. Elastic strain energy represents the principal driving force. The transformation and flow behavior in this regime have been modeled by incorporating the thermodynamic effects of the mechanical work done during transformation (by the applied stress

acting through the transformation strains) into the kinetics model used for spontaneous transformations (those free from externally applied stress). The slope of the "stress-assisted Xfn" line in Figure 2.22 is given by the Clausius-Clapeyron Equation, recast in uniaxial stress form:

$$\frac{d\sigma}{dT} \approx \frac{\Delta H}{T_0 \Delta V}$$

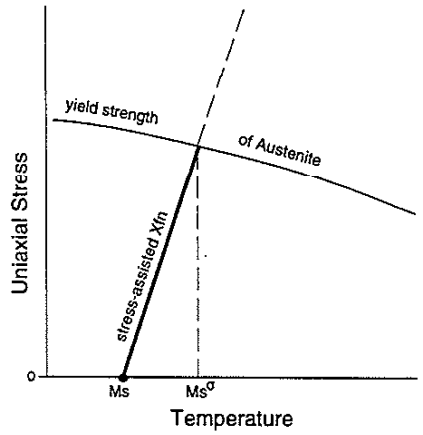

Figure 2.22: Schematic austenite yield strength vs. temperature diagram for a steel with the stress-assisted transformation line ending at M_s^{σ} included.

When a large enough tensile stress is applied to the transforming sample, the yield strength is reached. New, potent nucleation sites are then formed by plastic deformation, and within a specific temperature range above M_s^{σ}, these sites trigger "strain-induced" transformation.

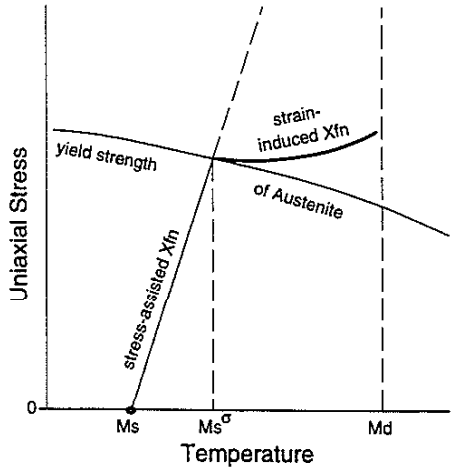

Figure 2.23: Schematic austenite yield strength vs. temperature diagram for a steel with the strain-induced transformation line starting at M_s^{σ} and ending at M_d.

As shown in figure 2.23, the upper bound to this type of transformation occurs at a temperature called the M_d temperature. Above M_d, no further transformation can by brought about by mechanical means. Further deformation will be due to slip processes

The transformation behavior in this regime has been modeled in terms of a distribution of defect potency used for transformations and the flow behavior as a complex interaction of slip and transformation [103]. Both stress-assisted and strain-induced transformation processes occur simultaneously around M_s^{σ} .

From Figure 2.19, the microstructure of a steel quenched to room temperature is expected to be a combination of martensite and retained austenite. Immediately after quenching, application of a tensile stress or cooling below room temperature will induce further transformation of the retained austenite.

However if one ignores the prior heat treatment history of the material and views it only in terms of what is currently present in the microstructure at room temperature, a second way to define all these temperatures and transformation regimes emerges. At room temperature the retained austenite becomes stabilized with time or after tempering. Around room temperature this stabilized retained austenite then displays analogous behavior to the original retained austenite described above, but with the temperature values all shifted down: subcooling below room temp is required before further transformation occurs (a "new, relative" M_s temperature), tensile stress is required to initiate transformation at temperatures above this new M_s, and a change in the slope of the uniaxial stress vs. temperature plot signals the change from stress-assisted to strain-induced transformation (a new, relative M_s^{σ} temp). These new, relative temperatures can all be determined through the proper experiments, where their impact on the transformation kinetics can be seen [104].

In 1975, Olson and Cohen presented a model for austenite-martensite transformation kinetics in steels under uniaxial tensile loading, which depended on temperature and plastic strain [105]. They proposed that in the strain induced temperature range the intersecting slip bands in the austenite generated a number of martensite nucleation sites, each with a different potency. Because of the distribution of these potencies, only some sites were sufficiently potent to trigger transformation. Building upon Olson and Cohen's model, Stringfellow [103] and Stringfellow, Parks and Olson [106] added stress state dependence into the potency distribution. They proposed that the thermodynamic driving force for transformation was dependent on stress state through a parameter they call the "triaxiality," Σ, where:

$$\Sigma = \frac{\sigma_H}{\sigma_{eff}}$$

or, the ratio of the hydrostatic stress to the deviatoric (von Mises effective) stress. In general, this equals:

$$\Sigma = \frac{\frac{\sigma_{zz} + \sigma_{rr} + \sigma_{\theta\theta}}{3}}{\sqrt{\frac{(\sigma_{zz} - \sigma_{rr})^2 + (\sigma_{rr} - \sigma_{\theta\theta})^2 + (\sigma_{\theta\theta} - \sigma_{zz})^2}{2}}}$$

where: σ_z = principal stress in the specimen axial direction, and

P = denotes the pressure.

However, simplified for tests conducted in the apparatus described in chapter 3, it reduces to:

$$\Sigma = \frac{\frac{\sigma_{zz} - 2P}{3}}{|\sigma_{zz} + P|}$$

Note that if σ_z is set proportional to P during a test, the pressure terms cancel and the triaxiality becomes a constant. For example, in stress-controlled experiments, the axial stress and pressure may varied in such a way that the hydrostatic stress is maintained zero (σ_z = +2P which gives Σ = 0), or say, -P/3 (σ_z = +P which gives Σ = -1/6), throughout the test. The principal stress states can be described as (2P, -P, -P) and (P, -P, -P) respectively. Figure 2.24 illustrates these two examples in axial stress-pressure space.

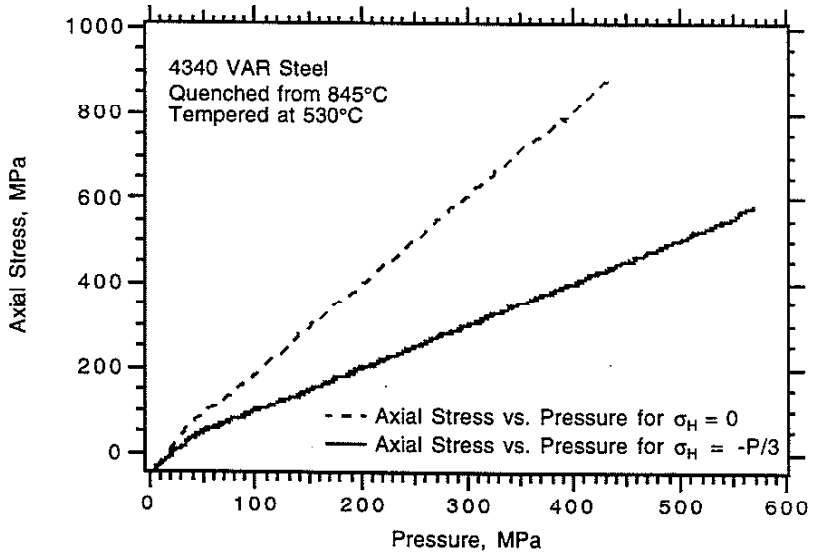

Figure 2.24: Two monotonic axial stress-pressure histories where hydrostatic stress equals zero and -P/3 respectively (from this study).

The transformation model predicts that as the triaxiality increases, so does the probability that martensite will form at a potential site. Stringfellow writes that the variation of the probability with stress-state is seen as one of the most important features of the transformation [103]. Our data supports this and shows a definite dependence on hydrostatic stress level.

As important as stress state is, all the equations proposed by Stringfellow for the thermodynamic driving force are currently based on uniaxial experimental data. The role of hydrostatic stress, effective stress and principal stress has not been explored over a wide range of triaxiality. A main purpose of this research is then to experimentally determine the evolution of the macroscopic transformation strains under multiaxial stress states (generated using externally applied pressures) in order to isolate the effects of hydrostatic stress, effective stress and principal stress on the rate and extent of the transformation. As our equipment makes it easy to conduct tests at constant σ_z / P ratios, it is instructive to plot the loci of achievable triaxiality values shown in Figure 2.25.

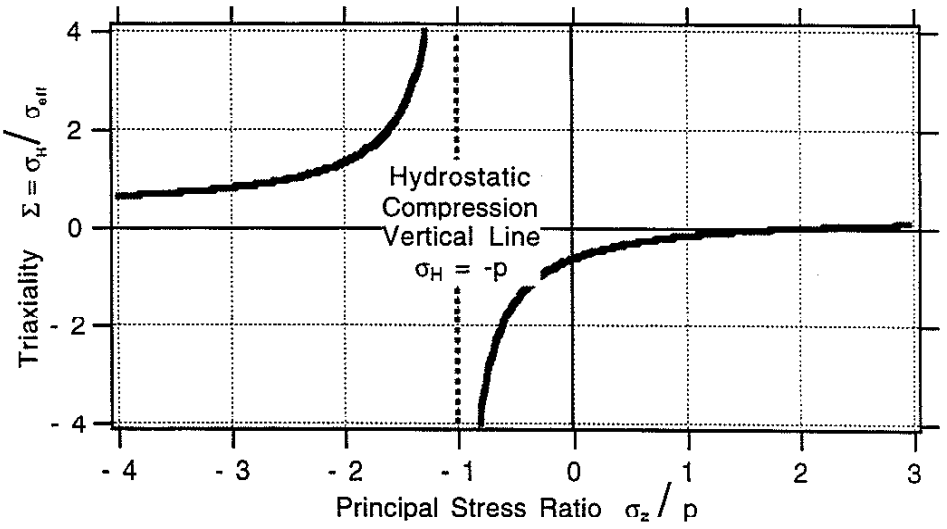

Figure 2.25: Triaxiality vs. Principal Stress Ratio diagram displaying the range of tests possible.

Two sets of experiments can then be conducted to shed light into the rate and extent of the transformation:

(a) deform the specimens while maintaining Σ constant to establish the evolution of transformation strains as a function of the tensile principal stress, σ_z.

(b) change σ_z under constant pressure to establish the evolution of transformation strains as a function of Σ.

From such tests we will be able to experimentally determine how the transformation strains evolve for monotonic (unidirectional) loading under multiaxial stress trajectories. This has a first order

effect on the flow rule because it is the stress-assisted/strain-induced volumetric transformation strain associated with the phase transformations that provides the bulk of the permanent strain which defines the flow and yield strengths.

List of References

1. Morrow, D. L. Biaxial Tension Fatigue of Inconel 718. Ph.D. Thesis, UIUC, Urbana, IL 1988

2. Adams, Frank D., & Nicolson, John Thomas. An experimental investigation into the flow of marble. Royal Society of London Philosophical Transactions, series A, 1901, 195, 363-401.

3. Bridgman, P. W. The Physics of High Pressure. New York: The Macmillan Company, 1931.

4. Adams, Frank D., & Bancroft, J. Austen. On the amount of internal friction developed in rocks during deformation and on the relative plasticity of different types of rocks. The Journal of Geology, 1917, 25(7), 597-637.

5. Griggs, David T. Deformation of rocks under high confining pressures. The Journal of Geology, 1936, 44(5), 541-577.

6. von Karman Th. Collected Works of Theodore von Karman. London: Butterworth's Scientific Publications, 1956. Originally appeared as von Kármán, Th., Strength Investigations Under Hydrostatic Pressure, Zeitschrift des Vereines Deutscher Ingenieure, 1911, vol 55, p. 1749-1757 : Forsch. Arb. ing. Wes., 1912, p37.

7. Bridgman, P. W. The effect of pressure on the tensile properties of several metals and other materials. Journal of Applied Physics, 1953, 24(5), 560-570.

8. Bridgman, P. W. Studies in Large Flow and Fracture. Cambridge, MA: Harvard University Press, 1964.

9. Pugh, H. Ll. D., Hodgson, G., & Gunn, D. A. Tensile strain measurement under high hydrostatic pressure using an optical method. Journal of Scientific Instrumentation, 1963, 40(5), 221-224.

10. Pugh, J. Ll. D., & Green, D. The effect of hydrostatic pressure on the plastic flow and fracture of metals. Proceedings of the Institution of Mechanical Engineers, 1964, 179(12), 415-437.

11. Pugh, H. Ll. D. The mechanical properties and deformation characteristic of metals and alloys under pressure. ASTM STP 374 Irreversible Effects of High Pressure and Temperature on Materials, 1965, 68-139.

12. Griggs, D. T., Turner, F. J., & Heard, H. C. Deformation of rocks at 500° C to 800° C. In David Griggs & John Handin (Ed.), Rock Deformation. U. S. A.: Waverly Press, Inc., 1960, 39-49.

13. Spitzig, W. A., Sober, R. J., & Richmond, O. Pressure dependece of yielding and associated volume expansion in tempered martensite. Acta Metallurgica, 1975, 23, 885-893.

14. Spitzig, W. A., Sober, R. J., & Richmond, O. The effect of hydrostatic pressure on the deformation behavior of maraging and HY-80 steels and its implications for plasticity theory. Metallurgical Transactions A, 1976, 7A, 1703-1710.

15. Spitzig, W. A. Effect of hydrostatic pressure on plastic-flow properties of iron single crystals. Acta Metallurgica, 1979, 27, 523-534.

16. Spitzig, W. A., & Richmond, O. The effect of pressure on the flow stress of metals. Acta Metallurgica, 1984, 32(3), 457-463.

17. Spitzig, W. A. Effect of hydrostatic pressure on deformation, damage evolution, and fracture of iron with various inital porosities. Acta Metallurgica Et Materialia, 1990, 38(8), 1445-1453.

18. Böker, Robert. Die mechanik der bleibenden formaenderung in kristallinisch aufgebauten koerpern (The Mechanism of Plastic Deformation in Crystalline Bodies). Dissertation Technischen Hochschule Zeitung, Rheinische West Fälische Hochschule, Aachen, 1914 : also in Forschungsarbeiten Auf Dem Gebiete Des Ingenieurwesens (Ver. Deutsch. Ingenieure. Mitt. Forschungsarbeiten), 1915, 175-176, 1-51.

19. Polyani and Schmid paper.

20. Richart, Frank E., Brandtzaeg, Anton, & Brown, Rex L. A Study of the Failure of Concrete Under Combined Compressive Stresses. University of Illinois Engineering Experimental Station. 1928, 185, 3-69.

21. M. Ros and Eighinger, "Researches to Explain the Problem of the Danger of Fracture. III. Metals" (in German), Eidgenoss. Material prufungs-Versuchanstalt Inus. Bauw. Gewerbe, Ber. No. 34, pp.1-20, Schweizerisches Polytechnikum, Zurich, 1929. English translation: NEL 449, National Engineering Laboratory, East Kilbride, Glasgow.

22. Cook, Gilbert. The effect of fluid-pressure on the permanent deformation of metals by shear. Selected Engineering Papers, 1934, 170, 1-17.

23. Ratner, S.I. Change of mechanical properties of metals under hydrostatic pressure (in Russian). Zh. Tekn. Fiz., 1949, 19(3), 408.

24. Handin, John. An application of high pressure in geophysics: Experimental rock deformation. Transactions of the ASME, April 1953, vol 75, 315-324.

25. Wiseman, H. A. B., & Marin, Joseph. A new triaxial stress testing machine for determining plastic stress-strain relations. American Society for Testing Materials. Proceedings, 1954, 54, 1365-1381.

26. Crossland, B. The effect of fluid pressure on the shear properties of metals. Proceeding of the Institution of Mechanical Engineers, 1954, 168(40), 935-946.

27. Crossland, B. Effect of large hydrostatic pressures on the torsional fatigue strength of an alloy steel. Proceeding of the Institution of Mechanical Engineers: International Conference on the Fatigue of Metals, 1956, 138-149.

28. Haasen, Peter, & Lawson, Andrew W. Jr. Der Einfluss hydrostatischen Druckes aur die Zugverformung von Einkristallen. Zeitschrift fuer Metallkunde, 1958, 49(6), 280-291.

29. Gladkovskii, V. A., & Oleinik, M. I. Apparatus for investigating the mechanical qualities of metals under high hydrostatic pressure. Physics of Metals and Metallography, 1957, 4(3), 118-121.

30. Crossland, B., & Dearden, W. H. The plastic flow and fracture of a 'brittle' material (grey cast iron) with particular reference to the effect of fluid pressure. Proceeding of the Institution of Mechanical Engineers, 1958, 172(26), 805-820.

31. Hu, L. W. Determination of the plastic stress-strain relations in tension of nittany no. 2 brass under hydrostatic pressure. Proceedings of the Third U. S. National Congress of Applied Mechanics. New York: The American Society of Mechanical Engineers, 1958.

32. Ryabinin, Yu. N., Vereschagin, L. F., Balashov, D. B., and Livshitz, L.D., Pribory I Tekhn. Eksperm., 1958, 2, 79. English translation: Instr. Exp. Tech., 1959, 2, 265.

33. Beresnev, B.I., Vereschagin, L. F., Ryabinin, Yu. N., and Livshitz, L.D., 'Some Problems of Large Plastics Deformation in Metals under High Pressure', Akad. Nauk, SSSR, Moscow, 1960. English translation: ASTIA Doc. AD-259 251, Washington D. C. Office of Technical Services, U.S. Dept of Commerce, 1961.

34. Heard, Hugh C. Transition from brittle fracture to ductile flow in solenhofen limestone as a function of temperature, confining pressure, and interstitial fluid pressure. In David Griggs & John Handin (Ed.), Rock Deformation. U. S. A.: Waverly Press, Inc., 1960, 193-199.

35. Handin, John, Higgs, Donald V., & O'Brien, Joseph K. Torsion of yule marble under confining pressure. In David Griggs & John Handin (Ed.), Rock Deformation. U. S. A.: Waverly Press, Inc., 1960, 245-274.

36. T. Pelczynski, "the Influence of Hydrostatic Pressure on the Plastic Deformation Properties of Metals" (in Polish-summary in English), Arch. Hutnictwa, Vol. 7, No. 1, 1962, pp. 3-13.

37. Brandes, Marek. Studies in large plastic flow of cast iron specimens stretched under hydrostatic pressures of up to 17,500 kg/cm^2. International Journal of Fracture Mechanics, 1967, 3, 175-182.

38. Davidson, T. E. & Homan, C. G. Some observations on the effects of hydrostatic pressures to 20,000 atm on the structure of polycrystalline bismuth. Transactions of the Metallurgical Society of AIME, 1963, 227, 167-176.

39. Paterson, M. S. Triaxial testing of materials at pressures up to 10,000 kg./sq. cm. (150,000 lb./sq. in.) Journal of the Institution of Engineers, 1964, 36(1-2), 23-29.

40. Nishihara, Masao, Tanaka, Kichinosuke, & Muramatsu, Takao. Effect of hydrostatic pressure on mechanical behaviour of materials. In The Editorial Committee of Japan Congress on Testing Materials (Eds.), Proceedings of the Seventh Japan Congress on Testing Materials. Kyoto: The Society of Materials Science, Japan, 1964.

41. Pugh H.L1. D. and Gunn D. An apparatus for torsion tests under high hydrostatic pressures. NEL Report No. 159. East Kilbride, Glasgow: National Engineering Laboratory, 1964.

42. Nishihara, Masao, Tanaka, Kichinosuke, & Hamada, Hiroyoshi. Effect of hydrostatic pressure on mechanical behaviour of materials (the second report). In The Editorial Committee of Japan Congress on Testing Materials (Eds.), Proceedings of The Eight Japan Congress on Testing Materials. Kyoto: The Society of Materials Science, 1965.

43. Erbel S. Behavior of materials twisted under hydrostatic pressure. Presented at conference organized by Department of Metallurgy, Polish Academy of Science, April 1966.

44. Gordon, Robert B., & Mike, Leslie F. Measurement of the mechanical properties of solids at high pressure. Review of Scientific Instruments, 1967, 38(4), 541-546.

45. Tanaka, Kichinosuke, & Nakashima, Minoru. Plastic deformation of aluminum under high pressure. In The Editorial Committee of Japan Congress on Testing Materials (Eds.), Proceedings of the Tenth Japan Congress on Testing Materials. Kyoto: The Society of Materials Science, Japan, 1967.

46. Oguchi, Atsushi, & Yoshida, Susumu. A magnetostrictive load cell for use under high hydrostatic pressures. Japanese Journal of Applied Physics, 1968, 7(6), 672-678.

47. Yoshida, Susumu, Oguchi, Atsushi. Influence of high hydrostatic pressure on the flow stress of aluminum polycrystals. Transactions of the Japan Institute of Metals, 1970, 11(6), 424-430.

48. Yoshida, Susumu, Oguchi, Atsushi, & Nobuki, Minoru. Influence of high hydrostatic pressure on the flow stress of copper polycrystals. Transactions of the Japan Institute of Metals, 1971, 12(4), 238-242.

49. Carpentier, D., & Contre, M. Description of an apparatus allowing mechanical tests under hydrostatic pressure up to 15 kilobars. The Review of Scientific Instruments, 1970, 41(2), 189-192.

50. Ohmori, Masanobu, Yoshinaga, Yoshitoyo, Kawahata, Takeshi, & Sanemasu, Yoshihiko. Plastic deformation of metals under high hydrostatic pressure. Proceedings of the Sixteenth Japan Congress on Materials Research, 1970, 13, 139-142.

51. Sakata, Masaru, Aoki, Sigeru, & Tsujimoto, Takashi. An experimental study on the deformation of materials under high hydrostatic pressures. Bulletin of the JSME, 1971, 14(74), 737-744.

52. Fung, P. K. Instrumentation for measuring load and deformation under high pressure. Experimental Mechanics, February 1975, 61-66.

53. Fung, P. K., Burns, D. J., & Lind, N. C. Yield under high hydrostatic pressure. In A. Sawczuk (Ed.), Foundations of Plasticity. Leyden: Noordhoff International Publishing, 1973.

54. Hoeg, J. G., & Davis, R. L. Effects of cold working under pressure on subsequent yield. American Society of Mechanical Engineers, 1971.

55. Motoie, Katsuhiko, Yamakage, Tetsuro, & Ohnami, Masateru. Torsional creep of polycrystalline metallic materials under hydrostatic pressure at room temperature. Journal of the Society of Materials Science, Japan, 1972, 21(227), 74-82.

56. Hawley, R. H., & Drucker, D. C. Brittle fracture of precompressed steel as affected by hydrostatic pressure, temperature and strain concentration. Experimental Mechanics, Jan. 1973, 1-6.

57. Sakata, M., & Aoki, S. Torsional strength of glass under hydrostatic pressure. Journal of Engineering Materials and Technology, 1973, 95(2), 83-86. (SUBJECT: TORSION TESTS)

58. Ohji, Kiotsugu, Ogura, Keiji, Sugimoto, Kazuo, & Yaji, Keiichi. Some experiments on push-pull low-cycle fatigue strength of metals under very high pressures. Proceedings of the Sixteenth Japan Congress on Materials Research, 1973, 16, 104-110.

59. Crossland, B., & Mitra, A. K. Torsion machine for use under superimposed pressures of 1 GPa, and preliminary results. High Temperatures - High Pressures, 1974, 6, 165-172.

60. Kolpashnikov, A. I., Fedorov, A. A., Kucheryaev, B. V., & Bespalov, A. V. Equipment for tensile testing of materials at high hydrostatic pressures. Industrial Laboratory, 1983, 49(7), 1190-1192.

61. Kolpashnikov, A. I., Fedorov, A. A., Kucheryaev, B. V., & Bespalov, A. V. Device for torsion testing of materials at high hydrostatic pressures. Industrial Laboratory, 1986, 52(6), 563-565

62. Liu, D. S., & Lewandowski, J. J. The effects of superimposed hydrostatic pressure on deformation and fracture: Part I. Monolithic 6061 aluminum. Metallurgical Transactions A, 1993, 24A, 601-608.

63. Liu, D. S., & Lewandowski, J. J. The effects of superimposed hydrostatic pressure on deformation and fracture: Part II. Particulate-reinforced 6061 composites. Metallurgical Transactions A, 1993, 24A, 609-615.

64. Pugh, H. Ll. D., Chandler, E. F. Review of methods and equipments for material testing under pressure. In H. Ll. D. Pugh (Ed.) High Pressure Engineering: the Second International Conference (proceedings of the Second International Conference on High Pressure Engineering, held at the U. of Sussex, 1975), London: Mechanical Engineering Publications Ltd., 1977, 41-52.

65. Vodar, Boris and Jean Kieffer. Historical Introduction. In H.Ll.D. Pugh (Ed.), Mechanical Behavior of Materials Under Pressure, London: Elsevier, 1970

66. Johnson, D. P., & Newhall, D. H. The piston gage as a precise pressure-measuring instrument. Transactions of the ASME, 1953, 75, 301-310.

67. Alexander, J. M. The effect of pressure on tensile plastic instability- a fallacious argument. Journal of the Institute of Metals, 1965, 93, 366-367.

68. Davidson, T. E., & Lee, A. P. The study of the structural and transformation characteristics of the pressure-induced polymorphs in bismuth. Transactions of the Metallurgical Society of AIME, 1964, 230, 1035-1042.

69. Davidson, T. E., Uy, J. C., & Lee, A. P. Hydrostatic pressure-induced plastic flow in polycrystalline metals. Transactions of the Metallurgical Society of AIME, 1965, 233, 820-826.

70. Vu, Hai, & Johannin, Pierre. Deformations permanentes de solides polycristallins apres action d'une pression hydrostatique elevee. Acadamie Des Science Comptes Rendus, 1955, 241(6), 565-566.

71. Bullen, F. P. Pressurization effects in metals. In H. Ll. D. Pugh (Ed.), Engineering Solids Under Pressure. London: The Institution of Mechanical Engineers, 1971.

72. Bullen, F. P. The effect of hydrostatic pressure on yielding in iron. The Philosophical Magazine, 1964, 9(98), 285-297.

73. Bullen, F. P., & Wain, H. L. Yielding and fracture in some body-centered cubic metals. The Journal of the Australian Institute of Metals, 1967, 12(1), 64-70.

74. Bullen, F. P., Henderson, F., & Wain, H. L. The effect of hydrostatic pressure on brittleness in chromium. Philisophical Magazine, 1964, 9(101), 803-815.

75. Radcliffe, S. V. Effects of high pressure and temperature on the mechanical properties of metals and alloys. ASTM STP 374 Irreversible Effects of High Pressure and Temperature on Materials, 1965, 141-163.

76. Ohnami, Masateru, Ohmura, Masaru, Shiozawa, Kazuaki, & Kamitani, Akira. Effect of hydrostatic pressure soaking on the plastic deformation of polycrystalline aluminum. Proceedings of the Sixteenth Japan Congress on Materials Research, 1972, 16, 115-119.

77. Yajima, M., Ishii, M. Pressure-induced dislocations in pure iron containing oxide inclusions. Transactions ISIJ, 1968, 8, 34-35.

78. Yajima, M., Ishii, M., & Kobayashi, M. The effects of hydrostatic pressure on the ductility of metals and alloys. International Journal of Fracture Mechanics, 1970, 6, 139-150.

79. White, D. J., Crossland, B., & Morrison, J. L. M. Effect of hydrostatic pressure on the direct-stress fatigue strength of an alloy steel. Journal of Mechanical Engineering Science, 1959, 1(1), 39-49.

80. Crossland, B., Skelton, W. J., & Wilson, W. R. D. High pressure intensifiers: development of a unit for pressures of 200 000 lbf/in^2 and possible improvements in design. Proceedings of the Institution of Mechanical Engineers 1967-68 (High Pressure Engineering), 1968, 182(3C), 175-179.

81. Crossland, B., Agnew, R. H., Birks, A. W., Ludlow, C. G., & Logan, J. G. The development of an automatic intensifier system for operation at 200,000 psi. National Conference on Fluid Power, 1971, 117-135.

82. Crossland, B., & Logan, J. G. Review of the design of very high pressure containers. In H. Ll. D. Pugh (Ed.), Hydrostatic Extrusion. London: Mechanical Engineering Publications Ltd., 1973.

83. Crossland, B., & Ludlow, C. Design and development of a machine for compression testing of rock samples under a constant pressure of up to 0.7 GPa (7 kbar). High Temperatures - High Pressures, 1973, 5, 509-514.

84. Ohji, Kiotsugu, Ogura, Keiji, Sugimoto, Kazuo, & Yaji, Keiichi. Some experiments on push-pull low-cycle fatigue strength of metals under very high pressures. Proceedings of the Sixteenth Japan Congress on Materials Research, 1973, 16, 104-110.

85. Gustafson, C. G. A rotating-bar fatigue machine for use in high-pressyure environment. High Temperatures-High Pressures, 1975, 7, 467-476.

86. Burns, D. J., & Parry, J. S. C. Effect of large hydrostatic pressures on the torsional fatigue strength of two steels. Journal of Mechanical Engineering Science, 1964, 6(3), 293-305.

87. Rowland, S. C., DeVries, K. L., & Gibbs, P. The effect of pressure on fatigue. International Journal of Fracture Mechanics, 1967, 3, 131-144.

88. Libertiny, G. Z. Short life fatigue under combined stresses. Journal of Strain Analysis, 1967, 2(1), 91-95.

89. Libertiny, G. Z. High pressure low speed push-pull fatigue machine. Proceedings of the Institution of Mechanical Engineers 1967-68 (High Pressure Engineering), 1968, 182(3C), 115-121.

90. Libertiny, G. Z. Effect of hydrostatic pressure on the short life fatigue property of an alloy steel. Proceedings of the Institution of Mechanical Engineers 1967-68 (High Pressure Engineering), 1968, 182(3C), 58-64.

91. Libertiny, G. Z. Cyclical strain softening of a heat treated steel at various hydrostatic pressures. In H. Ll. D. Pugh (Ed.), Engineering Solids Under Pressure. London: The Institution of Mechanical Engineers, 1971.

92. H. Nakazawa, T. Koizumi, H. Koyayshi, and M. Mruyama: Preprint of Papers, Japan Soc. Mech. Engrs. 714-2, 68 (1971).

93. Ohji, Kiyotsugu, Ogura, Keiji, Sugimoto, Kazuo, & Yaji, Keiichi. Development of a push-pull fatigue testing machine under high pressure, and the results of preliminary fatigue tests. Journal of the Society of Materials Science, Japan, 1972, 21(227), 64-69.

94. Lunsford, G., Pense, A. W., Venkatesan, P. S., & McIntosh, M. J. The effect of hydrostatic pressure environment on the low cycle fatigue properties of a maraging steel. Journal of Engineering Materials and Technology: Transactions of the ASME, 1973, 195(3), 157-160.

95. Nakazawa, H., Kobayashi, H., & Homma, H. Effect of hydrostatic pressure on fatigue crack propagation. In the American Society of Mechanical Engineers (Eds.), Third International Conference on Pressure Vessel Technology. New York: ASME, 1977.

96. Ross, P. J., Plumbridge, W. J., & Parry, J. S. C. A system for carrying out fatigue crack propagation tests under superimposed hydrostatic pressure. In F. Sherratt & J. B. Sturgeon (Eds.), Materials, Experimentation and Design in Fatigue. United Kingdom: Westbury House, 1981.

97. Plumbridge, W. J., Ross, P. J., & Parry, J. S. C. Fatigue crack growth in liquids under pressure. Materials Science and Engineering, 1985, 68(2), 219-232.

98. Davis, F. H., & Ellison, E. G., & Plumbridge, W. J. Effects of hydrostatic pressure on the rate of fatigue crack growth. Fatigue Fracture Engineering & Materials Structure, 1989, 12(6), 511-525.

99. Morrison, W. M. A new approach to hydraulic seal design. Compressed Air And Hydraulics, 1962, 27(316), 277-279.

100. Ewalds, H. L. & R.J.H. Wanhill, Fracture Mechanics, pub. by Edward Arnold, London, 1989.

101. Z. Nishiyama, Martensitic Transformation, Academic Press, 1978

102. Meyers, M. A. & K. K. Chawla, Mechanical Metallurgy, Prentice Hall, 1984.

103. Stringfellow, R. G., Mechanics of Strain-Induced Transformation Toughening in Metastable Austenitic Steels, PhD Thesis, MIT, Cambridge, MA, 1990.

104. Haidemenopolous, G. N., M. Grujicic, M., G.B. Olson & M. Cohen, Transformation Microyielding of Retained Austenite, Acta Metall., vol. 37, No. 6, pp 1677-1682, 1989

105. Olson, G. B., and M. Cohen, Kinetics of Strain Induced Martensitic Nucleation, Met Trans A, Vol. 6A, April 1975, pp 791-795.

106. Stringfellow, Parks and Olson A Constitutive Model for Transformation Plasticity Accompanying Strain-Induced Martensitic Transformations in Metastable Austenitic Steels, Acta Metallurgica, 40, 1703-1716

3. EXPERIMENTAL EQUIPMENT AND TECHNIQUES:

3.1 Overview of the Apparatus

To measure triaxial stress-strain response and/or fatigue life data, a novel, computer controlled apparatus which simultaneously subjects a solid, cylindrical, monotonic or fatigue test specimen to time-varying external pressures and axial loads has been assembled. It can be thought of as a compression test machine where the specimen is enclosed inside a fluid-filled pressure vessel test chamber. Figure 3.1 shows a cross-section of the assembled apparatus.

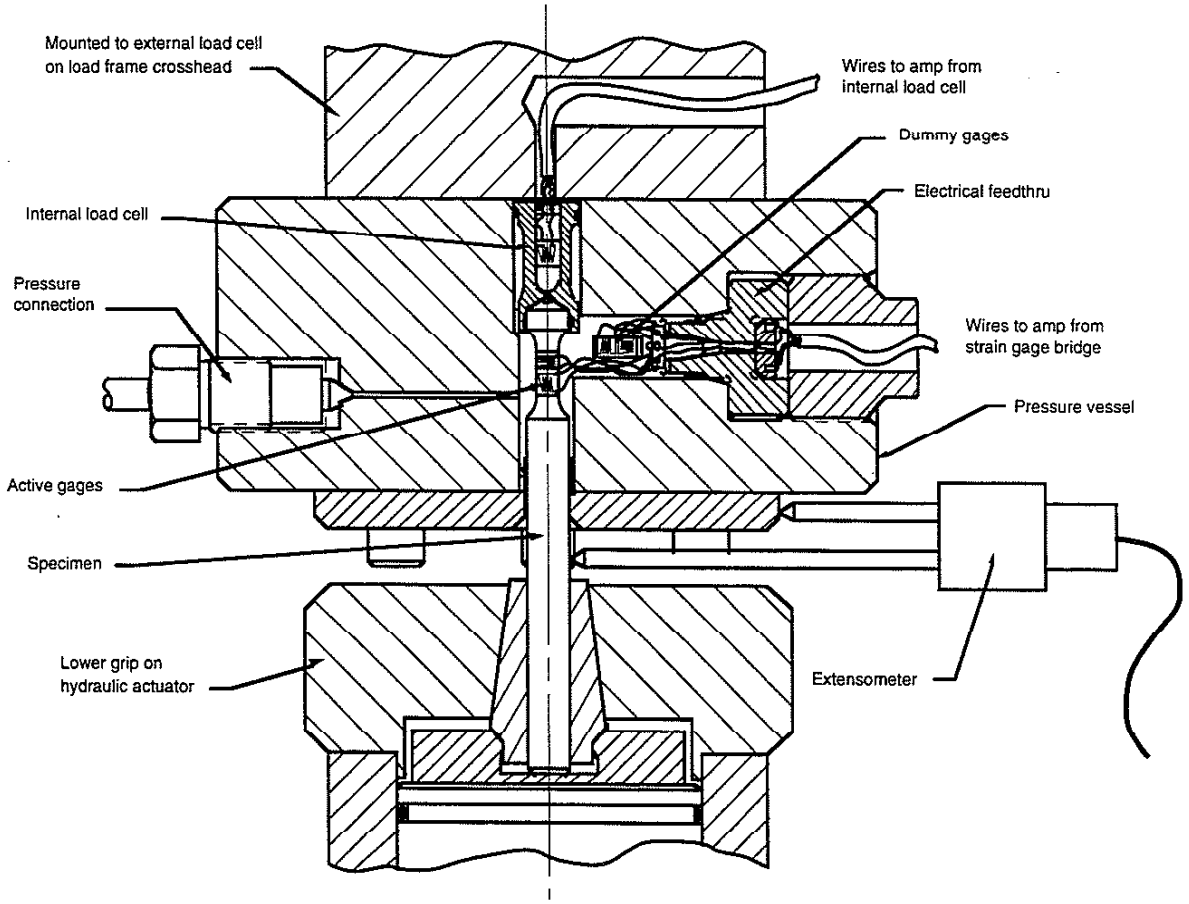

Figure 3.1: Sectional view of pressure test chamber, specimen, pressure transducer, electrical feed-thrus and lower grip, assembled for testing.

In the apparatus, a pressure vessel takes the place of the upper grip on an MTS servohydraulic universal test machine. From the vessel's bore protrudes the shoulder of the test specimen which mounts into the collet-type lower grip attached to the hydraulic actuator. Fluid is pressurized externally by a servohydraulic pressure intensifier. The pressurized fluid is conveyed to the vessel through high pressure tubing and fittings. A pressure transducer plumbed into this tubing permits accurate pressure measurement and provides a feedback signal for the pressure control loop. A seal on the specimen shoulder prevents fluid from escaping where the specimen exits the vessel. Signals to and from electrical resistance strain gages mounted on the specimen are conducted across the vessel wall via a high pressure electrical feed-through, and amplified externally; axial strain is also determined from extensometer measurements of overall specimen deflection (made outside the vessel) using a modification of a method described by Arora and Raghavan [1].

3.2 How Pressure is Used to Generate Tensile Axial Loads

Our cylindrical specimen geometry is shown in Figure 3.2 with cross sectional areas "A" for the shoulder and "a_o" for the gage section. The annular area located between the shoulder and gage section, and exposed to pressure, P, is A-a_o.

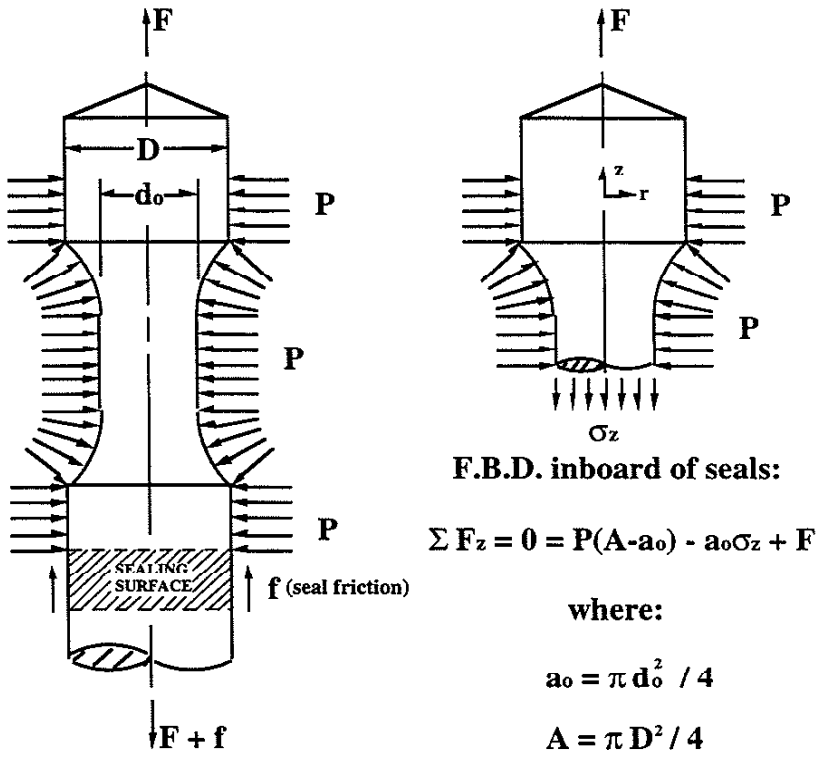

Figure 3.2: Pressure, P, acts normal to specimen surface; force, F, acts on specimen ends, and seal friction, f, acts at the sealing surface as shown.

In our test apparatus, pressure, P, applied externally to the lateral surfaces of a solid cylindrical specimen creates radial and circumferential stresses equal to -P. The ends of the specimen are maintained at atmospheric pressure. With this design, fluid pressure acting over the annular area generates a tensile axial stress in the gage section $\sigma_z = \frac{P(A - a_0)}{a_0}$. Thus the specimen geometry complicates the control scheme because the area difference between the specimen's shoulder and gage section couples the magnitude of the surrounding pressure into its load/deflection relationship. The axial load control system has to compensate for this interaction so that the desired axial stress magnitude is not altered as the pressure is varied. In our apparatus, a computer maintains the total axial stress in the gage section at its desired value by adjusting the magnitude of the (always compressive, always negative) axial load applied externally to the lower specimen shoulder.

By choosing this approach for generating tensile stress in the gage section, we knowingly gave up a portion of the tensile axial stress/pressure regime in which we could test. However we will now show that through the use of different gage section diameters, most any desirable tensile stress/pressure ratio can in fact be generated. The governing equation in terms of stress comes from the force balance inboard of the seals: $\sigma_z = \frac{P(A - a_0)}{a_0} + \frac{F}{a_0}$. Specimen shoulder area "A" was fixed when the shoulder diameter "D" was chosen during the design stage of the the apparatus, however "a_0" can by varied by changing the gage section diameter "d_0". The limiting stress states achievable using this apparatus occur when F = 0, and F = -89kN (the MTS universal test machine capacity). Individually substituting these limiting cases into the overall force balance

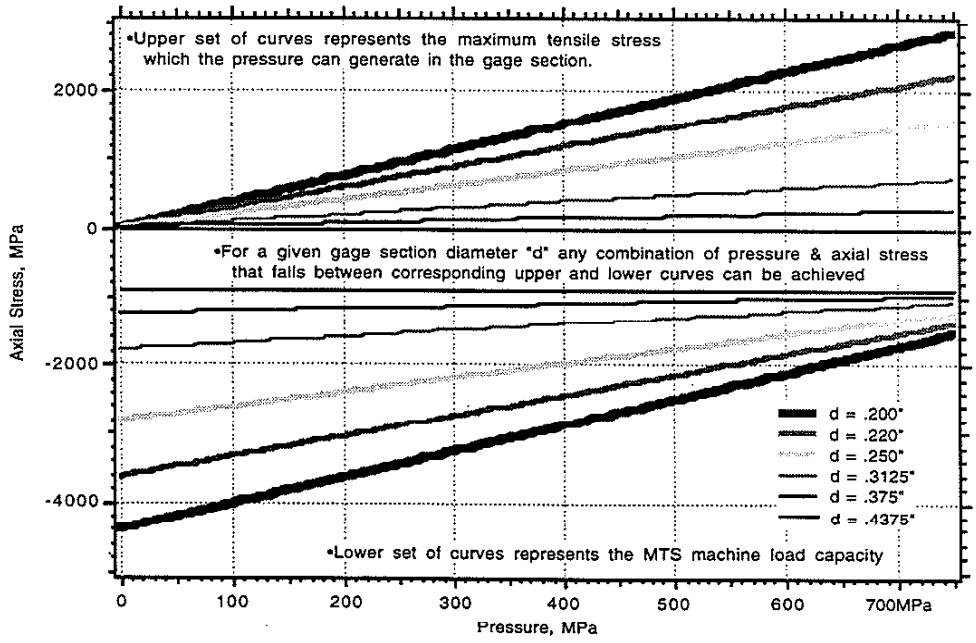

Figure 3.3: Axial Stress vs. Pressure capability as a function of gage section diameter.

equation and plotting σ_1 as a function of pressure P gives us the 2 families of curves shown in Figure 3.3.

The gage section diameter to use for a particular test is chosen as follows: The pressure/axial-stress history for the planned test is mapped out. This history will lie between one or more sets of corresponding upper and lower curves on Figure 3.3. The set of upper and lower curves that most closely brackets the history (leaving some leeway for seal friction effects) determines the gage section diameter to be used. The largest gage section diameter possible is always selected, as this ensures the greatest load cell signal to noise ratio, and the greatest resistance to buckling for $\sigma_z < 0$ tests.

3.3 Specifics Of the Apparatus

In the following section the major components comprising the pressure testing apparatus are described in detail. Some design elements, such as the internal load cell and test control program, will be described in later sections.

The MTS model 812.21 servohydraulic universal test machine used here is composed of a servohydraulic linear actuator which produces forces up to -89kN and a load frame which reacts those forces. The load frame consists of two vertical columns that join a moveable crosshead to the fixed platen on which the actuator is mounted. The crosshead, which mounts the pressure vessel assembly, is vertically adjustable to accommodate specimens of various lengths. An MTS model 661.21A-03 load cell mounted on the crosshead uses a strain gauged sensing element to convert a displacement proportional to the magnitude of the applied axial load, into a resistive change. It is wired to the DC transducer conditioner that is part of the MTS model 406.11 controller. The conditioner features an adjustable transducer excitation supply (for powering the strain gage bridge of the load cell), and its power supply is transformer isolated. Once again, its input measures the change in voltage across the strain gage bridge of the load cell, and its output is calibrated to be ±10 V for ±20,000 lbf (-89kN) load.

A rack mounted MTS model 406 test machine servocontroller is used in conjunction with the ±10 V output from either the MTS load cell or our own internal load cell (described in section 3.4.1) to close the force loop and generate the ±40 mA signal required to drive the parallel-connected servovalve on the actuator. It has its own power supply, and incorporates a summing junction for feedback and command signals, an adjustable gain stage and a current driver stage, as well as other functions which simplify installing the specimen and setting up a test..

A differential area piston-type pressure intensifier, supplied by the Harwood Engineering Company and considerably modified at the University of Illinois, is used to pressurize the fluid which fills the pressure vessel assembly. This intensifier and its associated equipment (which we term a "servohydraulic pressure intensifier") function as a stand-alone unit to produce cyclic fluid pressures of between 7.5 MPa and 750 MPa at speeds of up to 1 Hertz, in response to external

electrical command. The intensifier's power cylinder is plumbed as a "3-way" hydraulic circuit, as shown in Figure 3.4. A small electric motor driven hydraulic pump, hydraulic accumulator and a pressure relief valve maintain hydraulic oil at a constant, low pressure (3.4 MPa) for retracting the intensifier piston. A second electric motor driven hydraulic pump supplies medium pressure hydraulic oil (34 MPa max) to an electrohydraulic servovalve for extending the intensifier piston. Under computer control, the servovalve adjusts the pressure and the flow rates in the power side of the intensifier. This determines the force produced, plus the speed and direction in which the intensifier piston operates, respectively. A compressed air driven feed pump charges the high pressure side of the intensifier with Monoplex® DOS fluid, through a check valve. The small area piston, coupled to the power side piston, delivers the high pressure output desired (750 MPa max).

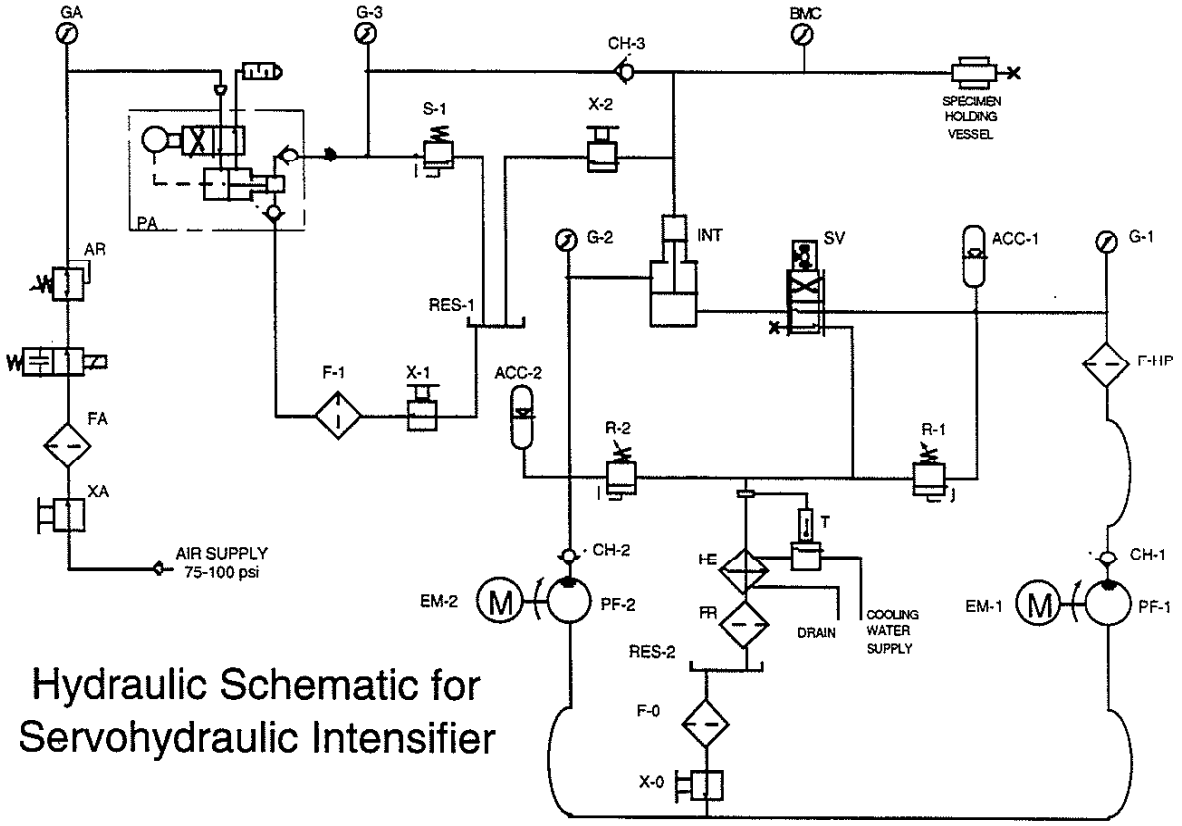

Figure 3.4: Hydraulic schematic for the servohydraulic intensifier, as modified at UIUC.

The ideal fluid for use at high pressures should display instantaneous pressure transmissibility, show no phase transitions, be relatively incompressible, be a dielectric, be chemically inert, and provide good lubricity. Monoplex® DOS fluid, an ester (Di-2-ethylhexyl sebacate) used industrially as a vinyl plasticizer, was chosen as the high pressure fluid because it meets these requirements very well over the range of pressures of interest. Many oils display dramatic increases in viscosity with pressure, becoming tar-like and eventually solid at the highest

pressures. Obviously, this behavior makes pressure transmission and flow impossible and would be unacceptable in an apparatus like ours. Fortunately the pressure transmissibility of Monoplex® DOS in even the smallest 1.6mm bore tubing used in our apparatus is unaffected even at 750MPa, allowing high frequency pressure cycling without time lag. Its high bulk modulus minimizes the work of pressurization. Its dielectric (electrically insulating) qualities allow exposed wire connections to be made within the pressure vessel, and its chemical stability means that no special coatings or materials need be employed in the apparatus. Finally its good lubricity prolongs the life of the seals and bearings in the apparatus.

A Moog model 122A142 Proportional-integral Servoamplifier (with the integral feature removed) closes the pressure control loop. This servoamplifier incorporates a summing junction for ±10 V feedback and command signals, an adjustable gain stage, and a current driver stage which generates the ±40 mA signal required to drive the 80 Ω parallel connected coils in the intensifier's servovalve. An Adtech ±15 VDC, 350 mA power supply powers this servoamplifier.

A Harwood Engineering Company model D2881 Bulk Modulus Cell was chosen as a pressure transducer. Designed for 1500 MPa operation with ±1% accuracy, it measures the pressure with a compressively stressed sensing element that is extremely resistant to fatigue. Internally it uses a strain gauged beam to convert a compressive displacement that is proportional to the magnitude of the pressure, into a resistive change. It is wired to a Ectron model 687 signal conditioning amplifier which incorporates a transformer isolated transducer excitation supply, transformer isolated signal inputs, and transformer isolated ±10 V output.

In our apparatus, elastomeric o-ring seals backed up by metal "chamfer rings" are used for static sealing. The chamfer rings bridge the gaps and prevent the o-ring seals from extruding through the running clearances between the specimen and the components which comprise the seal gland in the vessel. However, the initial clearances are only one consideration in seal design for high pressures; under 750 MPa pressure, the seal gland diameter expands by 0.0635 mm. This pressure-generated expansion alone would create an unacceptable extrusion gap for any elastomeric seal. To counter this, the chamfer rings were made of a soft bearing brass which yields under the force of the applied fluid pressure and thus prevents any gaps from forming.

Very few dynamic seals are commercially available for use at the pressures generated in this research. Conventional wisdom says that dynamic seal friction is great at very high pressures. To counter this, Teflon® is often used as a high pressure seal material because of its friction-reducing and wear-resistant properties. However, the trade-off is that a relatively hard thermoplastic polymer like Teflon® does not seal as well as a softer elastomer rubber. To determine the best seal design our application, machined Teflon® Bal Seals® and molded Buna-N (rubber) o-ring's were evaluated during cyclic tests on actual specimens. Evaluation focused on scaling ability, life, and friction levels. Friction levels were obtained from the difference between the suitably corrected internal and external load cell outputs. To provide a meaningful, test-related unit for comparison,

seal friction forces were expressed in terms of axial stress in the specimen gage section by dividing by a_0.

As expected, the Teflon® seals weeped fluid (especially at low pressures) though their friction levels remained stable during the tests. Also as expected, the Buna-N o-rings sealed very well. Interestingly, their initial friction levels were only slightly higher than observed with the Teflon® seals. More surprisingly however, was the fact that the o-ring friction levels consistently dropped to essentially zero (friction induced "stress" equivalent to only 13.8 MPa of gage section axial stress) after 100 cycles of axial load and remained at near zero for the rest of the test. It is rationalized that the low durometer rubber o-rings creep to a mean position during the initial 100 pressure/load cycles. From there they deflect elastically with the specimen rather than sliding relative to the specimen the way that the high durometer Teflon® seals do. The combination of their lower friction and better sealing made o-rings the obvious choice for all subsequent investigations.

An electrical feedthrough was designed and fabricated to allow electrical signals to pass through the wall of the pressure vessel. After evaluating many different styles, the feedthrough design shown in Figure 3.5 was developed.

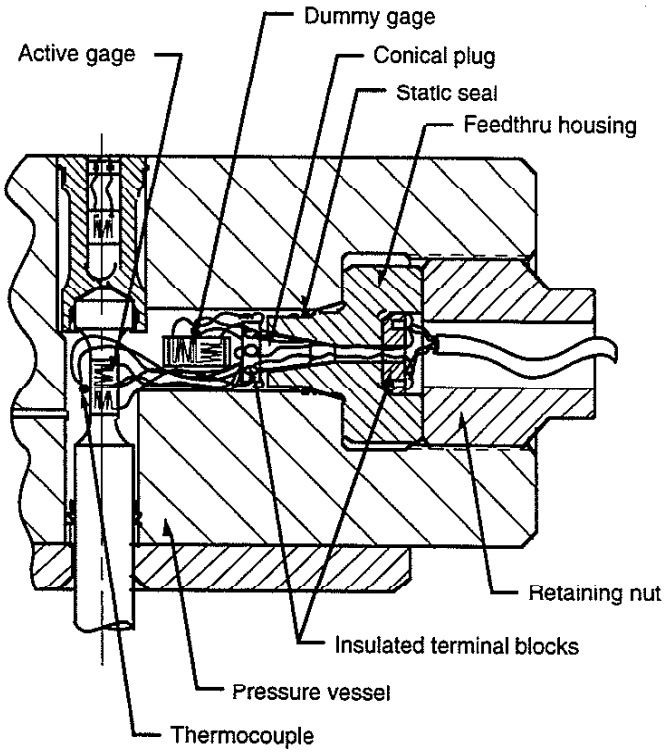

Figure 3.5: Cross section of electrical feedthrough, shown installed in vessel.

It is built around a conical plug that fits inside a mating bore of identical taper angle. A layer of epoxy is spread in the tapered bore and 8 strands of enameled magnet wire are embedded in the

epoxy. After a layer of epoxy is spread over the tapered surface of the conical plug, the plug is inserted into the bore. This traps the wires in a thin layer of epoxy, and the assembly is then cured in a laboratory oven. The epoxy - selected for its chemical inertness, high ductility in the cured condition, and excellent bonding characteristics with steel - forms the fluid seal. Pressure acting on the big end of the conical plug creates a force that attempts to push the conical plug further into the tapered bore. The taper angle effectively multiplies the applied pressure, creating a higher pressure in the epoxy "gasket," precluding fluid leakage.

Two separate strain gage circuits pass into and out of the pressure vessel. For each circuit, one active and one dummy strain gage are wired into "half-bridge" configurations inside the vessel. Precision matched resistors with low temperature coefficients of resistance are used to complete the Wheatstone bridge circuit external to the vessel. Each strain gage bridge is wired to an Ectron model 687 signal conditioning amplifier which incorporates a transformer isolated transducer excitation supply, transformer isolated signal inputs, and transformer isolated ±10 V output.

As on the pressure transducer, the MTS model 632.50B-04 extensometer employs a strain gauged beam for converting a displacement change to a resistive change. It is also wired to an Ectron model 687 signal conditioning amplifier.

A thermocouple was attached to the specimen for several tests. The thermocouple was wired to the feed-through, and an Accufiber Model 100C High Temperature Controller was used to convert its output into a 0-10 V signal proportional to temperature. Pressure corrections were not required because thermocouple output is known to be essentially independent of pressure up through the highest pressures achievable with this apparatus.

Careful attention was paid to shielding and grounding all wiring to minimize electrical noise problems. The Macintosh computer and test control program will be described in detail in section 3.7.

3.4 Internal Load Measurement

It is imperative that the load on the specimen be accurately measured during any test. Ensuring accurate load measurement under high pressure is not a trivial task and several different approaches were evaluated before a workable solution was developed. The next section briefly describes the development that led to the current load cell design.

3.4.1 Load Cell Development

In the original configuration of our apparatus we attempted to measure load externally using the original-equipment load cell on the MTS test machine. In that design, both ends of the cylindrical specimen were maintained at atmospheric pressure by having the shoulders protrude through openings in a specially designed pressure vessel. The upper shoulder was externally fixed to the vessel, and the lower shoulder was free to deflect axially along its high pressure seal gland.

Specimen deflection under the combination of the pressure and axial load caused relative motion to occur between the free specimen shoulder and seal. Frictional forces, **f**, of variable magnitude and sign were transferred at this pressurized seal interface which, if neglected, would create stresses in the specimen gage section with a magnitude easily equal to 20% of the applied pressure. With the pressure vessel attached to the original-equipment load cell on the MTS test machine, the measured load was a combination of the forces exerted by the hydraulic ram to stress the specimen's gage section, react the pressure-induced load (caused by the pressure acting over the annular area formed by the specimen shoulder and gage section), and overcome seal friction. The Mac II computer was programmed to determine the load on the specimen's gage section by subtracting from the measured load:

a) the pressure-induced load, calculated in real time.
b) an estimate of seal friction (as a function of pressure and specimen deflection) in real time.

However, we quickly found this method to be a failure. Seal friction is a combination of break-out and running friction, which depends on variables like seal material and hardness, type of surface, surface finish, initial "squeeze" on the seal, amount and type of lubrication, fluid pressure and temperature. The seal friction levels were too variable and the attempt to measure/model seal friction and have the test machine controller account for it in real time during a test did not provide the desired precision.

To truly obviate the effects of seal friction it became clear that we needed to measure the friction-free load inside the pressure vessel, between (on the gage section side of) the seals rather than the friction-inclusive load outboard the seals. To accomplish this, we tried converting each existing specimen into its own load cell by bonding an electrical resistance strain gage to a section of its pressurized shoulder inside the vessel. A second dummy gage was wired to this "shoulder gage" and the computer was re-programmed to calculate axial load from shoulder strain data. Unfortunately, this method also proved to be a failure when accurate load control was lost during several of the tests due to plastic deformation in the specimen shoulder. The plastic deformation made it clear that this method would only work for specimens with high strength shoulders. Since butt-welding high strength material to each specimen before machining, bonding gages to this new shoulder and then calibrating each individual specimen/load cell was cost and time-prohibitive, we abandoned this approach in favor of designing a reusable internal load-cell/upper-grip that fit in the pressure vessel bore.

Others had successfully used load cells inside pressure vessels before [2-5], but most of the load cells with electrical outputs were either unduplicatable by other researchers or required frequent re-gauging and re-calibration (because they employed strain gages which had a limited life in the high pressure fluid environment). In our application, a successful load cell design would have to meet certain functional requirements. The load cell:

1. must fit within the 16mm diameter pressure vessel bore,
2. must serve double-duty as an upper-grip due to space constraints. It must be able to mount the 11mm diameter specimen shoulder so that the specimen centerline is aligned with that of the seal gland and lower grip. For tension tests the specimen must not pull out of the load cell,
3. must be able to withstand cyclic applications of the full 89 kN capacity of the MTS universal test machine in compression and 750 MPa external pressure without drift,
4. must possess maximum sensitivity and signal/noise ratio while displaying minimal output due to external pressurization (pressure effect),
5. must be reusable and not require frequent rebuilding and/or recalibration.

Meeting these goals required adopting unique methods. Borrowing a conceptual element from Sakata, Aoki and Tsujimoto's 1971 torsion testing apparatus [6] (which was itself an update of Crossland's 1954 apparatus [5]) our load cell was designed to double as a closure for the pressure vessel. However, in practice our design differs substantially; our load cell measures axial, not torsional deflection. Our load cell is not a complete plug in and of itself either; it is designed to vent the upper end of the specimen shoulder to the atmosphere to ensure that end remains unpressurized. The upper specimen shoulder completes the closure and an o-ring seal in the load cell housing prevents any fluid leaks. Specimen mounting and alignment was achieved via a shallow, "female" internally coned surface in the load cell into which the upper specimen shoulder (machined into a mating "male" cone) fit.

To elastically withstand the combination of high cyclic loads and fluid pressure without drift, the load cell was constructed out of O-1 tool steel, heat treated to the maximum hardness possible, R_c 60 - 64. In the design chosen, all principal stresses were compressive. Thus there is no danger of cracking and failure of this relatively brittle material, even at the peak stress levels which an ANSYS finite element analysis predicted to be in excess of -2,070 MPa. A drawing of the load cell appears in Appendix D.

The specimen was prevented from pulling out of the load cell through software control: the test control program was written to always maintain a small, minimum compressive load on the specimen. Ensuring $F < 0$ prevents tension from ever appearing in the specimen shoulder.

To eliminate the need for frequent rebuilding and/or recalibration, sensing elements (strain gages) were mounted in the bore of the load cell. Since this location is outside the pressure envelope, the gages are not exposed to any fluid pressure and the adhesive bonds attaching the metal foil grids and the gage backings won't suffer accelerated degradation. Bending-induced apparent strain is canceled out by mounting two identical strain gages 180° apart in the load cell bore, and wiring them in series.

The strain gage bridge is wired to an Ectron model 687 signal conditioning amplifier which incorporates a transformer isolated transducer excitation supply, transformer isolated signal inputs, and transformer isolated ±10 V output. A shunt calibration method is used to check and maintain accuracy.

3.5 Load Calibration

Many different load measurement techniques have been employed in the published literature on high pressure testing, but not all the methods described feature rigorous load calibrations conducted under pressure.

Calibration of a load cell is done to develop a relation between the force placed on the load cell and its output, usually Volts. In atmospheric pressure applications this is a straightforward process: conventional load cells are loaded using precision dead weights while their electrical output is recorded. However, calibration of an internal load cell under high pressure is more complicated because while pressure often affects load cell output, the typical pressure vessel seldom provides enough room for checking this effect with dead weights. Consequently many investigators have skipped over this calibration-under-pressure aspect entirely. The next sections briefly describe the relatively few calibration methods that were documented in the literature, and then our newly developed technique for load calibration under high pressure.

3.5.1 Historical Load Calibrations

To avoid the uncertainties introduced by seal friction in tests for which load was measured, Bridgman designed and built a 3300 pound capacity electrical-resistance load cell that he termed the "grid" [3]. Located inside his vessel, its output was a function of pressure as well as compressive load. Bridgman described the grid as having "somewhat low sensitivity" which prevented him from testing metals that were softer than steel [2]. In fact, several other noted researchers were unsuccessful in their attempts to construct and employ load cells of the grid type [4]. In 1967, Pugh and Gunn described the grid as "unsuccessful" and "too flimsy to give the required sensitivity." [7] and Gordon and Mike write "Very great sensitivity in the detection of resistance changes is required for the success of this method. This sensitivity is difficult to attain because of the necessarily low resistance of the elastic members of the load cell." [8].

To calibrate his load cell, Bridgman used an atmospheric dead weight method to arrive at a "compression coefficient." For years he accounted for the extra force required to drive his pressure generating piston (as he admits, this includes the pressure sensitivity and uncertainties due to seal friction), with an estimated "pressure coefficient" determined from the average of many external load measurements.

To improve the accuracy of his calibrations, Bridgman later developed the "split-specimen" technique of load calibration; a simple, independent technique which first involves cutting a tensile specimen in two, perpendicular to its tensile axis [3]. The cut faces are then carefully machined flat, placed back into contact and sealed with a soldered-on sheath made of copper foil. The compound specimen is then tested under pressure as a normal tensile specimen, and when the tensile stress equals the hydrostatic pressure (plus a minute resistance offered by the copper sheath), the specimen faces separate and the load immediately drops to zero. Each run from the

split-specimen technique gives a single stress/pressure data point from which a calibration curve may be constructed. Bridgman used this method to show that the pressure coefficient so-obtained agreed "within the sensitiveness of the measurements" with the coefficient he had been using prior to developing the split-specimen method. Brandes[9], and Pugh and Green [10] later used this method, though Pugh considered it ""not an entirely satisfactory nor an unequivocally positive type of calibration... because of large variations that could occur in the results" [4]. This was elucidated in a paper where Pugh presented a plot of his widely scattered calibration results using the split specimen technique and wrote "...if the halves of the specimen were not held concentrically... then the contact area, and hence the load to cause separation, would be smaller than the assumed value. Similarly if the axes were not co-linear, owing to particles or misalignment between the faces, early penetration of the interference gap by the sleeve would occur and a low load value would be obtained." [7]

For their 1963 apparatus, Pugh, Hodgson and Gunn developed a 4000 pound capacity electrical-resistance internal load cell [11]. It was calibrated at atmospheric pressure in a Hounsfield tensometer and with dead weights. Pugh could not calibrate his strain-gauged internal load cell under pressure by the dead weight technique due to insufficient space in his vessel, and so, unsatisfied with the split-specimen technique, Pugh devised his own method[4]. Pugh substituted a solid bar for a specimen in his test machine, and loaded the solid bar using differential pressure across a seal-free piston riding in a bore with only 0.006 to 0.025 mm diametral clearance. In the absence of hydraulic lock, such a "laminar-fit" piston is friction free, so Pugh simply measured the differential pressure across it and multiplied by the piston area to accurately determine load. Pugh reported that during his calibrations under pressure "The hysteresis was of the same order obtained in the atmospheric calibration, indicating little or no friction..."

This effort by Pugh, a brilliant experimentalist, is one of the best, both in design and calibration. The only problem with this load cell is that its strain gages are directly subjected to the fluid pressure. Pugh reports "The gage lives vary considerably, some gages failing at their first pressurization, owing to flaws in the adhesive or foil gages, and others showing only negligible changes in calibration after constant use."

In 1967, Gordon and Mike assembled a unique apparatus, enclosing an electric motor driven screw-type test machine within a pressure vessel [8]. They constructed a strain gauged load cell similar to Pugh and Gunn's, but did not include any compensating gages because they deemed it unnecessary for their constant pressure/temperature tests. In fact, they counted on it showing a pressure dependent output, because they also used the load cell as a pressure transducer (though it is unclear exactly how this was done in practice). To avoid gage debonding under pressure, they mounted their gages with "mechanically deposited alumina."

In a fine example of a thorough load cell calibration, Gordon and Mike replaced their specimen with a calibrated compression spring, and recorded its deflection as a function of load

cell output while running compression tests on it at atmospheric pressure, and under pressure. With such a scheme, the full range of load is truly applied to the load cell while it is held under pressure. Additionally, since the load was generated inside the vessel, seal friction was not an issue (though their error analysis did consider the change in the spring calibration due to the expected pressure effect on the elastic modulus of the spring material.)

Oguchi & Yoshida describe a magnetostrictive internal load cell design with a non-linear, though repeatable output [12]. In addition to an atmospheric calibration, they performed calibrations under pressure using a pre-compressed spring inside their vessel. The spring was calibrated at atmospheric pressure, and was used to apply and maintain a compressive load on their load cell while they pressurized the vessel. In an effort at added accuracy, Oguchi & Yoshida mention that they corrected the spring load for expected pressure effects on the elastic modulus of the spring material.

Birks and Ludlow describe a 20 tonf capacity electrical-resistance strain-gage internal load cell which they constructed and calibrated [13]. They describe it by saying "The basic construction is similar to that used by Pugh and Gunn...." First they loaded it at atmospheric pressure on a universal test machine to obtain an atmospheric pressure calibration curve. Then they assembled the load cell into a pressure vessel and pressurized it to 690 MPa with no axial load on the load cell to obtain a pressure effect calibration curve. Birks and Ludlow write that during a test the true axial load may be determined by measuring both the load cell output and the pressure in the vessel. Then one finds the corresponding (negative) pressure effect from the pressure effect calibration curve, adds it to the measured load cell output, and then uses the atmospheric pressure calibration curve to find the load. This method of calibration places no load on the load cell under pressure and assumes that the atmospheric pressure curve is not affected by pressure. Additionally, they reported that the strain gages often de-bonded during their calibration runs under pressure, requiring re-gauging and recalibration.

In a 1975 paper, Fung describes a well designed pressure test machine with "frictionless" Morrison glands sealing the load-carrying rods that entered his pressure vessel [14]. It contained an internal load cell similar to the Pugh and Gunn type, using electrical resistance strain gages bonded to a thin-walled cylinder and a separate set of internally mounted compensating gages. This load cell was calibrated at atmospheric pressure using a dummy specimen connected to an external load cell, and then calibrated again at unspecified "high" pressure(s?). Fung's loading apparatus incorporated "clearances" which allowed the load carrying rods to move 0.5 inches before stressing the specimen. This feature permitted direct measurement of the frictional force required to move the rods. Though the Morrison seal glands can be constructed to be frictionless, a true frictionless version tends to leak large amounts of fluid. It seems that Fung made his seal glands "tight" to minimize this leakage because his second paper reports friction levels of up to 219 pounds at 20,000 psi test pressure. In a statement that casts further doubt on the calibrations,

Fung writes that during his calibration "The value recorded by the external load cell included the measurement of the seal friction, so that the seal friction has to be measured and deducted from the recorded value."

Fung reported only 2 tests on copper specimens using his internal load cell. As for reliability, in a second paper this internal load cell was not used; all loads were measured exernally and corrected for friction measured at the start of each test. He makes the excuse that "This (internal) load cell is redundant if the Morrison high pressure seals are functioning correctly, i.e., if friction is small or essentially constant during a test." and that "the strain gages were damaged at the start of the tests reported herein, so the aforementioned measurements of seal friction before and after a tension test were very necessary."

Pugh summed it up best in 1965 when he wrote that 'serious difficulties remain regarding the accuracy of load measurements.' [4]. Since then there have no major new developments. Next we will demonstrate a unique load cell design and a unique, accurate calibration method which circumvents the previously encountered problems and seal friction effects.

3.5.2 Frictionless Load Calibration Under Pressure

Our load cell calibration method is noteworthy because we developed a technique to load the load cell under both atmospheric and high pressure *without* friction, as follows. To determine the atmospheric pressure calibration curve, a specimen of constant diameter (D = d = 11.11 mm) is substituted for the normal test specimen and the apparatus is assembled without seals. The MTS universal test machine is placed in load-control using the external load cell as the feedback device, and the load is swept through a range of compressive loads. The voltage output from the internal load cell is recorded and plotted against the force measured by the external load cell divided by the cross sectional area of the specimen shoulder. This provides an atmospheric pressure load calibration curve in terms of Volts vs. "Stress on the shoulder cross sectional area $A = \frac{\pi D^2}{4}$," which is then curve fit.

While our load cell is of course sensitive to changes in axial load, its design causes it to have a pressure dependent component to its output, as most load cells do. To determine this pressure dependence, the set-up is torn down and reassembled with a specially made closure placed in the bottom of the pressure vessel bore to seal the opening where the lower specimen shoulder normally protrudes. A plug made from the top-most or conical-tipped shoulder of a spare specimen is inserted into the specimen side of the load cell.

The vessel is then slowly pressurized and de-pressurized. The voltage output from the internal load cell is recorded and plotted against the negative of the pressure measured by the calibrated pressure transducer. Note that pressure acting on the exposed right circular face of the plug generates a compressive axial load $\left(\text{axial load} = -P\frac{\pi D^2}{4} \right)$ on the load cell. The simplicity

of this method becomes apparent when we realize that since this plug is the same "D" diameter as the specimen shoulder, the compressive load in terms of "stress on the shoulder cross sectional area, A" is just the negative of the pressure, -P. This provides a load-under-pressure calibration curve in terms of Volts vs. "Stress on the shoulder cross sectional area $A = \frac{\pi D^2}{4}$," which is then curve fit. The results are shown in Figure 3.6.

The plug calibration method was verified in the following way: The plug calibration set-up was torn down and reassembled with a specimen of constant diameter (D = d = 11.11 mm) substituted for the normal test specimen. The MTS universal test machine was placed in external-load-cell-load-control and the load and pressure were simultaneously ramped to produce a specific hydrostatic stress level in the constant diameter specimen, while the output of a calibrated pressure transducer, the internal load cell and the external load cell were monitored and stored. As expected,

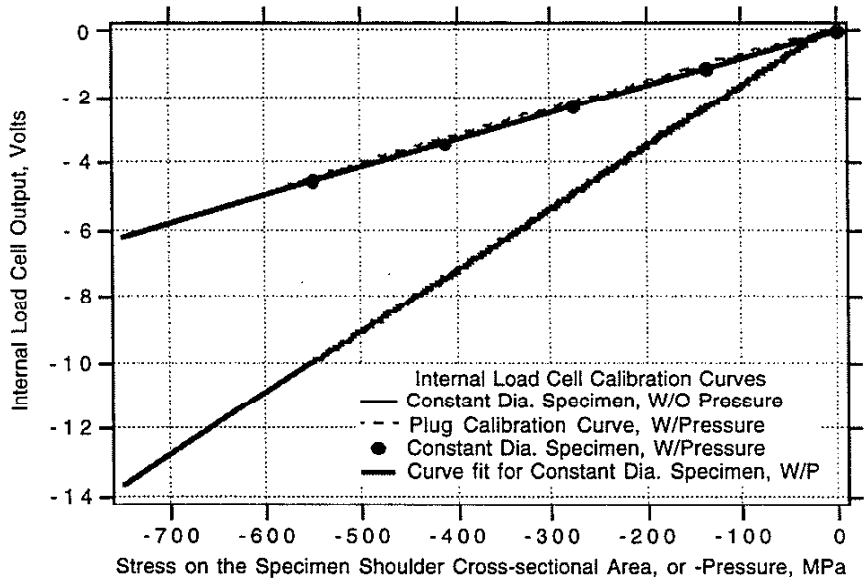

Figure 3.6: Internal load cell calibration curves.

at the end of the ramp there was a discrepancy between the internal and external load cell readouts, due to seal friction. The specimen was then held at this constant pressure and (externally controlled) load while a dither signal was added to the load command. The internal load cell signal was observed to slowly change with "hold" time, until after approximately 2 minutes it remained steady. At this time, all transducer readings were recorded and the load and pressure were then simultaneously ramped back down to zero.

This process was repeated for several different hydrostatic stress levels. Each time we saw the internal load cell signal change with time and then stabilize as the dither signal slowly

"vibrated" the seal friction away. When plotted as points in Figure 3.6, the stabilized readings fell right on top of the plug calibration curve. We interpreted this correspondence as a verification of the novel plug calibration method's friction-free loading of the load cell. At any pressure, P, the pressure effect in volts as a function of "stress on the shoulder cross sectional area, A" is easily found from the voltage difference between the two curves at the same axial load value.

Note that our method differs from that of Birks and Ludlow [13] because here the load cell is simultaneously under axial load and pressure during calibration. The pressure effect here is truly the difference in internal load cell output due to pressure, while axial load is held constant.

This is incorporated into the control program as follows. First the load command representing the load $\sigma_z a_0$ necessary to cause the desired axial stress σ_z in the gage section is computed. Then the tensile load in the gage section created by the fluid pressure is calculated and subtracted from the load command. The difference is the load that must be provided by the test machine's hydraulic ram. If it turns out to be more positive than the user-specified minimum compressive load, an if-then statement sets it equal to a that predetermined minimum compressive load to prevent the specimen shoulder from ever being placed in tension. This load is then converted to a "stress on the shoulder cross sectional area" basis by dividing by A. The magnitude of the internal load cell command in volts is then simply determined from the desired stress/pressure state using the curve-fit calibration functions, and output to the test machine servocontroller. In pseudo-code, it is:

```
previously computed                 load_command
shoulder cross sectional area       A
gage section cross sectional area   a
current pressure transducer reading P
minimum compressive load            min_comp_load


load_in_shoulder            =   load_command - (A - a) * P;

/* Prevent load_in_shoulder from ever going positive by keeping it below min_comp_load */

if ((load_command - (A - a) * P)  >= min_comp_load) load_in_shoulder = min_comp_load;

stress_in_shoulder          =   load_in_shoulder / A;

internal_load_cell_command  =   atmos_curve_fit_function (stress_in_shoulder) +
                                pressure_effect_curve_fit _function (P);
```

3.6 Strain Measurement

It is imperative that the deflection of the specimen be accurately measured during any test. Ensuring accurate strain measurement under high pressure is not a trivial task and two different approaches are employed. The next sections describe the use of strain gages and extensometers.

3.6.1 Strain Gages

Because of their accuracy, size, and simplicity, electrical resistance metal foil strain gages were chosen as the transducer type which could most effectively measure the elasto-plastic axial and circumferential strains on the 5 to 10 mm diameter test specimen gage sections inside the pressure vessel.

An ideal gage type would provide high elongation capability, fatigue life and stability so that it could be used for all types of tests. In reality though, the test conditions and the gage characteristics both provide constraints which make the gage selection process one of finding a best possible compromise. In general, the greatest elongation capability and fatigue life is exhibited by gages whose metal foil grids are 3.175 mm or larger, so for our use the 3.175 mm size was chosen. Having both the axial and circumferential gages mounted on a single piece of backing material greatly simplifies handling and mounting. For this reason a general purpose 2-element 90° "tee" rosette gage (MicroMeasurements "TM" pattern) was selected. The 1/8 inch TM pattern gages fit very nicely on the 12mm long specimen gage sections we used.

Strain gage tests at pressures up to 960MPa [15-17] demonstrated that Constantan alloy gages perform well, however they display a pressure-induced apparent strain. To minimize the apparent strain, MicroMeasurements [18] suggests using Constantan alloy gages for hydrostatic pressure environments due to their low pressure sensitivity (~1.2 microstrain apparent strain per 1MPa pressure). For low pressure measurements the pressure induced apparent strain is usually neglected, though it could be measured, curve fit, and subtracted off of any test data taken. However, to deal with the time-varying high pressures generated by our apparatus we chose to utilize a more sophisticated approach employing dummy gages *within* the pressure vessel for automatic temperature and pressure sensitivity compensation. The dummy gages are bonded to a right circular cylinder of specimen material and placed in the pressure vessel. Strain gages mounted upon this cylinder show an apparent strain reading comprised of the pressure and temperature sensitivity on the gage material plus the theoretically predicted hydrostatic strains. When wired into an active/dummy gage half-bridge circuit, the pressure and temperature effects cancel each other out and we need only subtract off the dummy gage's (known) hydrostatic strain;

$$\varepsilon_{\theta\theta} = \varepsilon_{zz} = \frac{-p\,(1 - 2\nu)}{E}$$

to arrive at the gage section strains. Utilizing dummy gages within the pressure vessel allows the choice of gages based upon their fatigue performance and zero shift stability, without concern for their pressure sensitivity. This will be discussed in more detail shortly.

Strain gages can be used to measure large strains because they remain accurate as they undergo plastic deformation. The following quote and figure 3.7 from Daley and Riley explain why [19].

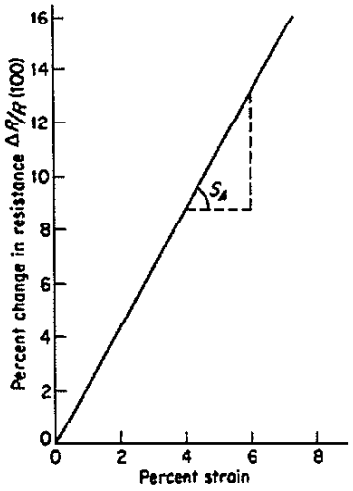

Figure 3.7: Percent change in resistance as a function of percent strain for Advance alloy. [19]

> "Most electrical-resistance strain gages produced today are fabricated from the copper-nickel alloy known as Advance or Constantan. A typical curve showing the percent change in resistance ΔR/R ["R" is the gage resistance] as a function of percent strain for this alloy is given [in Figure 3.7]
>
> This alloy is useful in strain-gage applications for the following reasons:
> 1. The value of the strain sensitivity, S_a, is constant over a wide range of strain, and the hysteresis of bonded filaments is extremely small.
> 2. The value of S_a does not change significantly as the material goes plastic.
> ...
> The first advantage of the Advance-type alloy over other alloys implies that the gage calibration constant will not vary with strain level; therefore, a single calibration constant is adequate for all levels of strain. The wide range of linearity with strain (even into the alloy's plastic region) indicates that it can be employed for measurements of both elastic and plastic strains in most structural materials."

Now the specifics of each test begin to force your hand in the selection process. Monotonic tension tests conducted in a high-pressure field display greatly enhanced elongation. For such tests involving large strains, specially designed gages made of ductile, annealed Constantan alloy with high-elongation cast polyimide backings must be used (MicroMeasurements "EP" series). Additionally, special high-elongation adhesives must also be used to mount the gages, or they will delaminate from the specimen under the large strains. EP gages are not recommended for cyclic loading because they exhibit poor fatigue lives and large zero shifts.

For less severe elongations (under 5%), gages made of specially processed Constantan alloy with cast polyimide backings can be used (MicroMeasurements "EA" series). However, under cyclic loading EA gages exhibit short fatigue lives and large zero shifts.

For longer fatigue lives and smaller zero shifts, gages made of specially processed nickel-chromium "Karma" alloy on a cast polyimide backing (MicroMeasurements "EK" series) can be

used. The elongation capability of EK gages is limited to 1.5%.

Dally and Riley state that foil gages with the thinnest possible carriers (backings) should be employed in applications where the gages are exposed to high pressures [19]. Though no reason was given, their recommendation most likely stems from two concerns: 1) less shear force is required to transmit strains across a thin backing than a thick one, and 2) the modulus of the conventional polyimide backing is much less than that of the typical metal specimen. In the former, less shear force places less shear stress on the adhesive bond line, and should result in less output from nonlinear effects such as creep and hysteresis of the polyimide backing. The latter concern is that under hydrostatic pressure, the low modulus of the polyimide backing makes it want to deflect significantly more than the high modulus specimen it is bonded to. The metal specimen is amply strong enough to restrain the backing, but in so doing it further loads the adhesive bond line in shear which accelerates bond degradation.

Dally and Riley also state that the thinnest possible, bubble-free bond line must be obtained. Since the adhesive is also a polymer, it must be thin for reasons similar to those given above for thin backings. It must be bubble-free to prevent pressure from forcing the gage into the bubble or void, thereby causing an erroneous gage output or breaking the metal foil. To achieve thin, bubble-free bond lines they recommend thinning the adhesive. This was not done because adding volatile solvents would only create gas bubbles during the elevated temperature curing. Instead I have found that a smooth surface finish on the specimen and careful gage installation both go a long way in eliminating void formation under the gage. All of our experiments employed MicroMeasurements M-BOND AE-15, an adhesive recommended for critical transducer applications. MicroMeasurements describes M-BOND AE-15 as a 100% solids, medium viscosity epoxy adhesive which forms extremely thin, hard, void-free glue lines and allows a maximum elongation of 15% [20]. M-BOND AE-15 requires careful heating and an elevated temperature cure. Its temperature must be raised to the curing temperature at a rate of 3 to 11°C per minute: excessively high heating rates will result in gas bubbles trapped in the adhesive, bond lines of uneven thickness and high adhesive film residual stresses. To ensure proper heating, a computer program was written which allows the Mac II to serve double duty; when not running pressure tests the Mac II, connected to a Micristar temperature controller, sets the time/temperature history in a laboratory oven during the adhesive curing cycle.

The Monoplex® DOS fluid surrounding the specimen was chosen in part for its dielectric (electrical insulating) qualities which allow exposed wire connections to be made within the pressure vessel. Testing has shown that it is compatible with the polyimide gage backings, not causing them to swell or become rubbery. No protective coating was applied over the gages because under pressure, low modulus coatings in direct contact with the metal foil grid can cause more problems than protective benefits. Likewise, factory encapsulated gages are never used. With the metal foil grids of the gages in direct contact with the Monoplex® DOS fluid, higher

excitation voltages can be used without fear of overheating the gages. This provides improved noise rejection because it allows smaller gains to be used on the strain gage amplifiers.

Dummy gages within the pressure vessel allow strain gage usage without concern for their pressure sensitivity. A right circular cylinder of identical radius and material as the specimen gage section is machined and strain gauged in the same way as the specimen gage section. This strain gauged cylinder is placed in the pressure field with the specimen and wired so that the gages on the cylinder can be used as temperature, pressure, and curvature compensating dummy gages for the active gages on the specimen (see figure 3.5).

For a right circular cylinder with Young's modulus E and Poisson's ratio ν, Hooke's law in three dimensions gives:

$$\varepsilon_{rr} = \frac{1}{E}(\sigma_{rr} - \nu\ (\sigma_{zz} + \sigma_{\theta\theta}))$$

$$\varepsilon_{\theta\theta} = \frac{1}{E}(\sigma_{\theta\theta} - \nu\ (\sigma_{zz} + \sigma_{rr}))$$

$$\varepsilon_{zz} = \frac{1}{E}(\sigma_{zz} - \nu\ (\sigma_{\theta\theta} + \sigma_{rr}))$$

When the right circular cylinder is placed in a pressure field of magnitude P, we have a hydrostatic strain condition:

$$\varepsilon_{rr} = \varepsilon_{\theta\theta} = \varepsilon_{zz} = \frac{-p\ (1 - 2\nu)}{E}$$

If a strain gage is mounted upon the right circular cylinder, the apparent or indicated strain readings will include the effects of pressure sensitivity on the gage material, transverse sensitivity from the two stress components parallel to the surface of the cylinder and radius of curvature sensitivity since they are bonded to a curved surface [17]. Thus the apparent strain readings will not be the same as the theoretically predicted strains. For a dummy strain gage mounted upon the right circular cylinder in each of the axial and circumferential directions, and used as dummy gages in an active/dummy gage half bridge circuit, we can write [19]:

$$\varepsilon_{\theta\theta\ dummy} = \varepsilon'_{\theta\theta\ dummy}\ [1 - \nu_o\ K_{t\theta\ dummy}]\ - K_{t\theta\ dummy}\ \varepsilon_{zz\ dummy}$$

$$\varepsilon_{zz\ dummy} = \varepsilon'_{zz\ dummy}\ [1 - \nu_o\ K_{tz\ dummy}]\ - K_{tz\ dummy}\ \varepsilon_{\theta\theta\ dummy}$$

where the unprimed strains are the actual hydrostatic strains, the primed strains are the apparent strains, K_t is the transverse sensitivity of each strain gage and ν_o is the Poisson's ratio of a standardized strain gage calibration beam. When the dummy gages mounted on the right circular cylinder are placed in the pressure field,

$$\varepsilon_{\theta\theta\ \text{dummy}} = \varepsilon_{zz\ \text{dummy}} = \frac{-p\,(1 - 2\nu)}{E}$$

In this hydrostatic strain case, $\dfrac{\varepsilon_{\theta\theta\ \text{dummy}}}{\varepsilon_{zz\ \text{dummy}}} = 1$ always, and so we can write:

$$\varepsilon_{\theta\theta\ \text{dummy}} = \varepsilon'_{\theta\theta\ \text{dummy}} \frac{1 - \nu_o K_{t\theta\ \text{dummy}}}{1 + K_{t\theta\ \text{dummy}}} \quad \text{, and}$$

$$\varepsilon_{zz\ \text{dummy}} = \varepsilon'_{zz\ \text{dummy}} \frac{1 - \nu_o K_{tz\ \text{dummy}}}{1 + K_{tz\ \text{dummy}}}$$

Rearranging and substituting the above relation, these become:

$$\varepsilon'_{\theta\theta\ \text{dummy}} = \frac{-p\,(1 - 2\nu)}{E} \frac{1 + K_{t\theta\ \text{dummy}}}{1 - \nu_o K_{t\theta\ \text{dummy}}} \quad \text{, and}$$

$$\varepsilon'_{zz\ \text{dummy}} = \frac{-p\,(1 - 2\nu)}{E} \frac{1 + K_{tz\ \text{dummy}}}{1 - \nu_o K_{tz\ \text{dummy}}} \quad .$$

If the specimen is placed in the pressure field with the right circular cylinder and its gage section is the same diameter as the cylinder and is strain gauged in the same way as the cylinder, then the gages on the cylinder can be wired into the bridge and used as temperature, pressure, and curvature compensating dummy gages for the active gages on the specimen.

Pressure and curvature effects are known to be independent of strain [15]. Assuming the temperature effects are also independent of strain, wiring the active and dummy gages into a half bridge circuit with excitation voltage V_{excit} leads to a voltage output ΔE, proportional to ε_{zz}, of:

$$\Delta E = \frac{(\text{Amp Gain})\, V_{excit}}{4} \left[\frac{\Delta R_{active}}{R_{active}} - \frac{\Delta R_{dummy}}{R_{dummy}} \right]$$

$$= \frac{(\text{Amp Gain})\, V_{excit}}{4} [\, Sg_{\text{active}}\, \varepsilon'_{\text{active}} - Sg_{\text{dummy}}\, \varepsilon'_{\text{dummy}}]$$

where R is the resistance and Sg is the gage factor of a particular strain gage. In the axial direction, this is

$$\Delta E = \frac{(\text{Amp Gain})\, V_{excit}}{4} [\, Sg_{zz\ \text{active}}\, \varepsilon'_{zz\ \text{active}} - Sg_{zz\ \text{dummy}}\, \varepsilon'_{zz\ \text{dummy}}]$$

and substituting the previous relation for $\varepsilon'_{zz\ \text{dummy}}$ gives:

$$\Delta E = \frac{(\text{Amp Gain})V_{excit}}{4}\left[Sg_{zzactive}e'_{zzactive} - Sg_{zzdummy}\left(\frac{-P(1-2\nu)}{E}\right)\left(\frac{1+K_{tzdummy}}{1-n_oK_{tzdummy}}\right)\right]$$

solving this for the apparent axial strain, $\varepsilon'_{zz\ active}$ gives:

$$\varepsilon'_{zz\ active} = \frac{4\Delta E}{Sg_{zzactive}(\text{Amp Gain})V_{excit}} + P\frac{Sg_{zzdummy}}{Sg_{zzactive}}\frac{(2\nu-1)}{E}\left(\frac{1+K_{tzdummy}}{1-\nu_oK_{tzdummy}}\right)$$

and a similar derivation for the apparent circumferential strain, $\varepsilon'_{\theta\theta\ active}$ yields:

$$\varepsilon'_{\theta\theta\ active} = \frac{4\Delta E}{Sg_{zzactive}(\text{Amp Gain})V_{excit}} + P\frac{Sg_{zzdummy}}{Sg_{\theta\theta active}}\frac{(2\nu-1)}{E}\left(\frac{1+K_{tzdummy}}{1-\nu_oK_{tzdummy}}\right)$$

Now we will present a derivation useful for converting these apparent strains to the actual (engineering) strains, ε_θ and ε_z. For a strain gage mounted upon the gage section of the specimen in each of the axial and circumferential directions and used as active gages in an active/dummy gage half bridge circuit, we can write [19]:

$$\varepsilon_{\theta\theta\ active} = \varepsilon'_{\theta\theta\ active}\left[1 - \nu_o\ K_{t\theta\ active}\right] - K_{t\theta\ active}\,\varepsilon_{zz\ active}$$

$$\varepsilon_{zz\ active} = \varepsilon'_{zz\ active}\left[1 - \nu_o\ K_{tz\ active}\right] - K_{tz\ active}\,\varepsilon_{\theta\theta\ active}$$

Substituting the second equation into the first gives:

$$\varepsilon_{\theta\theta\ active} = \varepsilon'_{\theta\theta\ active}\left[1 - \nu_o\ K_{t\theta\ active}\right] - K_{t\theta\ active}\left(\varepsilon'_{zz\ active}\left[1 - \nu_o\ K_{tz\ active}\right] - K_{tz\ active}\,\varepsilon_{\theta\theta\ active}\right) \quad \text{or,}$$

$$= \varepsilon'_{\theta\theta\ active}\left[1 - \nu_o\ K_{t\theta\ active}\right] - \varepsilon'_{zz\ active}\ K_{t\theta\ active}\left[1 - \nu_o\ K_{tz\ active}\right] - K_{t\theta\ active}\,K_{tz\ active}\,\varepsilon_{\theta\theta\ active}$$

Collecting $\varepsilon_{\theta\theta\ active}$ terms gives:

$$\left[1 - K_{t\theta}K_{tz}\right]\varepsilon_{\theta\theta\ active} = \varepsilon'_{\theta\theta\ active}\left[1 - \nu_o\ K_{t\theta}\right] - \varepsilon'_{zz\ active}\ K_{t\theta}\left[1 - \nu_o\ K_{tz}\right]$$

and solving for the actual circumferential strain yields:

$$\varepsilon_{\theta\theta\ active} = \frac{\varepsilon'_{\theta\theta\ active}\left[1 - \nu_o\ K_{t\theta\ active}\right] - \varepsilon'_{zz\ active}\ K_{t\theta\ active}\left[1 - \nu_o\ K_{tz\ active}\right]}{\left[1 - K_{t\theta\ active}\ K_{tz\ active}\right]}$$

and a similar derivation for the actual axial strain, $\varepsilon'_{zz\ active}$ yields:

$$\varepsilon_{\theta\theta\ active} = \frac{\varepsilon'_{zz\ active}\,[\,1 - \nu_o\, K_{tz\ active}] - \varepsilon'_{\theta\theta\ active}\, K_{tz\ active}\,[\,1 - \nu_o\, K_{t\theta\ active}]}{[\,1 - K_{t\theta\ active}\, K_{tz\ active}]}$$

Using both axial and circumferential gages actually provides *three* strain measurements since the radial and circumferential strains are equal for a cylindrical test specimen.

$$\varepsilon_{rr} = \varepsilon_{\theta\theta}$$

Conversion of measured strain data to true strains may then be accomplished using the following equations:

$$\varepsilon_{zz}^{true} = \ln(\varepsilon_{zz} + 1)$$

$$\varepsilon_{rr}^{true} = \varepsilon_{\theta\theta}^{true} = \ln(\varepsilon_{\theta\theta} + 1)$$

3.6.2 Extensometry

A literature search and our own experience uncovered the disappointing fact that strain gages mounted to the specimen gage section fail before the specimen does. Strain gages possess lower ductilities and shorter fatigue lives than the specimens to which they are bonded: therefore to record either large monotonic strains or cyclic strains over the fatigue life of a specimen, another strain measurement scheme must be employed. The method described here is one in which gage section axial strain (inside the vessel) is calculated from external measurement of overall specimen and load cell deflection. An axial extensometer is employed to measure the deflection of a point on the specimen shoulder, relative to the vessel itself. This deflection is the sum of the extensions of the specimen gage section, pressurized shoulder, unpressurized shoulder and load cell. By subtracting off the calculated elastic extensions and taking seal friction into account, the deflection of the gage section alone is determined. Gage section strains calculated in this method agree quite well with those measured with the strain gages. Of course, an extensometer provides more of an average strain over the entire gage section, as compared to the strain gages which give a more local strain over their 1/8" grid. An axial deflection model was developed to identify the variables involved, and to develop the equation needed to calculate the gage section axial strain. This model could also be adapted for running strain-controlled cyclic tests.

3.6.3 Model Development:

The axial deflection model is based on a summation of deflections as depicted in Figure 3.8. Only axial strains are considered. End effects on each element are neglected. The overall

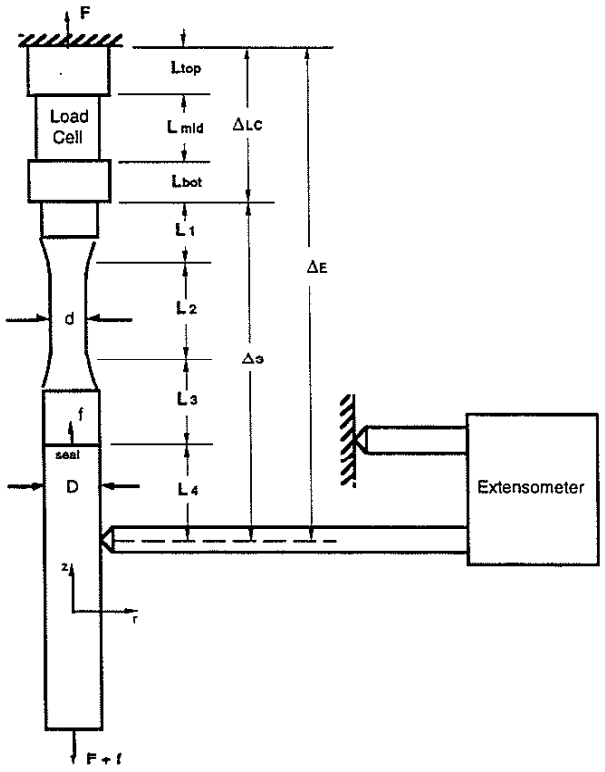

Figure 3.8: Specimen, load cell and extensometer showing dimensions used in axial deflection model.

summation of deflections is given by:

$$\Delta_E = \Delta_{LC} + \Delta_S$$

where Δ_{LC} = deflection of the Load Cell,

Δ_S = deflection of the Specimen, and

Δ_E = deflection of the Load Cell and Specimen, as measured by the Extensometer.

For the first term in this model, the Load Cell was divided into 3 hollow cylinders; top, middle and bottom. Numerical values for the cylinder dimensions are given in Table 3.1.

Load Cell	Top	Middle	Bottom
ID, inches	0.260	0.260	0.062
OD, inches	0.625	0.437	0.437
Effective Length, in	0.250	0.686	0.178

Table 3.1. Parameters for Load Cell Axial Deflection Model

The deflection was found for each cylinder, and then summed according to:

$$\Delta_{LC} = \varepsilon_{top}L_{top} + \varepsilon_{mid}L_{mid} + \varepsilon_{bot}L_{bot}$$

where the ε's are the axial strains in the cylinders and the L's are the effective lengths of the cylinders. The axial strain in each of the externally pressurized, thick-walled, hollow cylinders which comprise the load cell is given by the following expression found in Roark and Young [21]:

$$\varepsilon_{axial} = \frac{2\,P\,\nu\,OD^2}{E_{LC}\,(\,OD^2 - ID^2\,)} \qquad + \frac{4\,(F-f)}{\pi\,E_{LC}\,(\,OD^2 - ID^2\,)}$$

In the Load Cell, axial load = F and pressure = P. Substituting, we find:

$$\varepsilon_{top}\,L_{top} = \frac{L_{top}}{E_{LC}\,(\,OD^2_{top} - ID^2_{top}\,)}\left(\,2\,P\,\nu\,OD^2_{top} + 4\,\frac{F}{\pi}\,\right)$$

$$= \frac{0.250}{29000000\,(\,0.625^2 - 0.260^2\,)}\left(\,2\,P\,0.3 * 0.625^2 + 4\,\frac{F}{\pi}\,\right)$$

$$\varepsilon_{mid}\,L_{mid} = \frac{L_{mid}}{E_{LC}\,(\,OD^2_{mid} - ID^2_{mid}\,)}\left(\,2\,P\,\nu\,OD^2_{mid} + 4\,\frac{F}{\pi}\,\right)$$

$$= \frac{0.686}{29000000\,(\,0.437^2 - 0.260^2\,)}\left(\,2\,P\,0.3 * 0.437^2 + 4\,\frac{F}{\pi}\,\right)$$

$$\varepsilon_{bot}\,L_{bot} = \frac{L_{bot}}{E_{LC}\,(\,OD^2_{bot} - ID^2_{bot}\,)}\left(\,2\,P\,\nu\,OD^2_{bot} + 4\,\frac{F}{\pi}\,\right)$$

$$= \frac{0.178}{29000000\,(\,0.437^2 - 0.062^2\,)}\left(\,2\,P\,0.3 * 0.437^2 + 4\,\frac{F}{\pi}\,\right)$$

$$\Delta_{LC} = \begin{array}{l} 6.255\text{e-}9 * P + 3.398\text{e-}8 * F + \\ 2.197\text{e-}8 * P + 2.441\text{e-}7 * F + \\ 3.758\text{e-}9 * P + 4.176\text{e-}8 * F \end{array}$$

$$\Delta_{LC} = 3.198\text{e-}8 * P + 3.198\text{e-}7 * F$$

For the second term in this model, the specimen was divided into 4 solid cylinders: short-shoulder, gage section, internal long shoulder and external long shoulder (below the seal yet above the centerline of the Extensometer's lower rod). Numerical values for the cylinder dimensions are given in Table 3.2.

Specimen	Short Shoulder (1)	Gage Section (2)	Internal Long Shoulder (3)	External Long Shoulder (4)
OD, inches	0.437	0.250	0.437	0.437
Effective Length, in	0.313	0.993	0.280	0.178

Table 3.2: Parameters for Specimen Axial Deflection Model

The deflection was found for each cylinder, and then summed according to:

$$\Delta_S = \varepsilon_1 L_1 + \varepsilon_2 L_2 + \varepsilon_3 L_3 + \varepsilon_4 L_4$$

where the ε's are the axial strains in the cylinders and the L's are the effective lengths of the cylinders. In pressurized regions of the specimen, $\sigma_{rr} = \sigma_{\theta\theta} = -P$. The axial strain in each of the solid cylinders comprising the Specimen is given by Hooke's law:

$$\varepsilon_{zz}^{el} = \frac{1}{E}(\sigma_{zz} - \nu(\sigma_{rr} + \sigma_{\theta\theta}))$$

In the specimen's short-shoulder, $\sigma_{zz} = \dfrac{F - f}{A}$; $\qquad \sigma_{rr} = \sigma_{\theta\theta} = -P$

$$\varepsilon_1 = \frac{1}{E}\left(\frac{F-f}{A} - \nu(-P - P)\right) = \frac{1}{E}\left(\frac{F-f}{A} + 2P\nu\right)$$

In section 2, $\sigma_{zz} = \dfrac{F + P(A - a)}{a}$; $\qquad \sigma_{rr} = \sigma_{\theta\theta} = -P$

ε_2 = the unknown strain we wish to find

In section 3, $\sigma_{zz} = \dfrac{F - f}{A}$; $\qquad \sigma_{rr} = \sigma_{\theta\theta} = -P$

$$\varepsilon_3 = \frac{1}{E}\left(\frac{F-f}{A} - \nu(-P - P)\right) = \frac{1}{E}\left(\frac{F-f}{A} + 2P\nu\right)$$

In section 4, $\sigma_{zz} = \dfrac{F + f}{A}$; $\qquad \sigma_{rr} = \sigma_{\theta\theta} = 0$

$$\varepsilon_4 = \frac{1}{E}\left(\frac{F}{A} - \nu(0 + 0)\right) = \frac{F}{EA}$$

Summing, $\Delta_S = \dfrac{L_1}{E}\left(\dfrac{F-f}{A} + 2P\nu\right) + L_2\varepsilon_2 + \dfrac{L_3}{E}\left(\dfrac{F-f}{A} + 2P\nu\right) + \dfrac{L_4 F}{EA}$

These relations are then substituted back into the original equation for total displacement:

$$\Delta_E = \Delta_{LC} + \Delta_S$$

$$\Delta_E = 3.198e\text{-}8 * P + 3.198e\text{-}7 * F + \frac{L_1}{E}\left(\frac{F}{A} + 2P\nu\right) + L_2\varepsilon_2 + \frac{L_3}{E}\left(\frac{F}{A} + 2P\nu\right) + \frac{L_4(F + f)}{EA},$$

or

$$\Delta_E = F\left(3.198e-7 + \frac{L_1 + L_3}{EA}\right) + (F+f)\frac{L_4}{EA} + P\left(3.198e-8 + \frac{2\nu(L_1 + L_3)}{E}\right) + L_2\varepsilon_2$$

Solving for ε_2 provides the equation for the strain in the gage section as a function of total deflection, load measured by the external and internal load cells, and pressure:

$$\varepsilon_2 = \Delta_E\left(\frac{1}{L_2}\right) - F\left(\frac{3.198e-7}{L_2} + \frac{L_1 + L_3}{EAL_2}\right) - (F+f)\left(\frac{L_4}{EAL_2}\right) - P\left(\frac{3.198e-8}{L_2} + \frac{2\nu(L_1 + L_3)}{EL_2}\right)$$

During a test, we see that ε_2 is equal to the Axial Strain Gage output in inches/inch. We recognize the leading multiplier in each summand as:

Δ_E = the Extensometer output in inches,

F = the Internal Load Cell output in pounds force,

(F+f) = the External Load Cell output in pounds force, and

P = the Pressure Transducer output in psi.

When Δ_E is determined using an extensometer, L_4 is the effective length of the specimen's external long-shoulder (below the seal yet above the middle of the Extensometer Extension). However, Δ_E can also be determined using the stroke transducer mounted in the hydraulic actuator on the universal test machine. When this is done, L_4 is replaced by S_4, the effective length of the specimen's external long-shoulder (below the seal). S_4 is larger than L_4 because it includes a length contribution which accounts for the deflection of the columns and crosshead of the test machine. This ε_2 relation was then converted to the following form:

$$\varepsilon_2 = \Delta_E C_0 - F C_1 - (F+f) C_2 - P C_3 + C_4$$

A macro was written using IGOR plotting software which allowed this equation to be entered as a "user-defined function." Test data was read into IGOR, and initial guesses for the curve fitting constants C_0 - C_4 were calculated from the following equations and entered:

$$C_0 = \left(\frac{1}{L_2} \right)$$

$$C_1 = \left(\frac{3.198e\text{-}7}{L_2} + \frac{L_1 + L_3}{EAL_2} \right)$$

$$C_2 = \left(\frac{L_4}{EAL_2} \right)$$

$$C_3 = \left(\frac{3.198e\text{-}8}{L_2} + \frac{2\nu(L_1 + L_3)}{EL_2} \right)$$

C_4 = constant representing the aggregate zero-offsets of the experimentally measured Δ_E, P, F, and F-f signals

Correct numerical values for C_0 - C_4 are found by calling IGOR's multivariate curve fitting algorithm. This employs an iterative scheme to find the constants in the user-defined function which best fit the test data. Once the constants are found, they can be inserted into the model, and the axial strain can be determined for large elongations or cycles beyond that at which the gage fails.

Actual Gage Diameter d	Short-Shoulder Length L_1	Gage Length L_2	Int Long-Shoulder Length L_3	Ext Long Shoulder Length L_4	L_4 For Stroke Xdcr S_4
0.200	0.340	1.003	0.275	0.88	1.00
0.220	0.346	1.004	0.274	0.88	1.00
0.250	0.356	0.993	0.280	0.88	1.00
0.290	0.370	0.984	0.284	0.88	1.00

Table 3.2: Values for initial guesses to be used for finding the curve fit constants

Rigorously, this linear elastic model cannot be used when there is plastic deformation in the shoulder of the specimen. Unfortunately, many of the tests which are of interest involve stress levels high enough to cause limited yielding in the shoulder. For monotonic tests with limited yielding in the shoulder, the model cannot be applied; one can only use high-elongation strain gages and adhesive and settle for a maximum recordable deformation of 15%. However, for cyclic tests with limited yielding in the shoulder, the model can still be applied.

Though the magnitudes of the stresses in the shoulder and gage section vary in a cyclic test, the specimen shoulder is always in a state of axial compression. Therefore any plastic flow that occurs in the shoulder will always be in one direction. This serves to work-harden the shoulder and will result in linearly elastic behavior upon subsequent loadings to that same stress level. Once the shoulder is behaving elastically, the model is applicable and the values of the constants in the model become steady. This is evident from the plot of C_0 vs. cycle number shown in Figure 3.9.

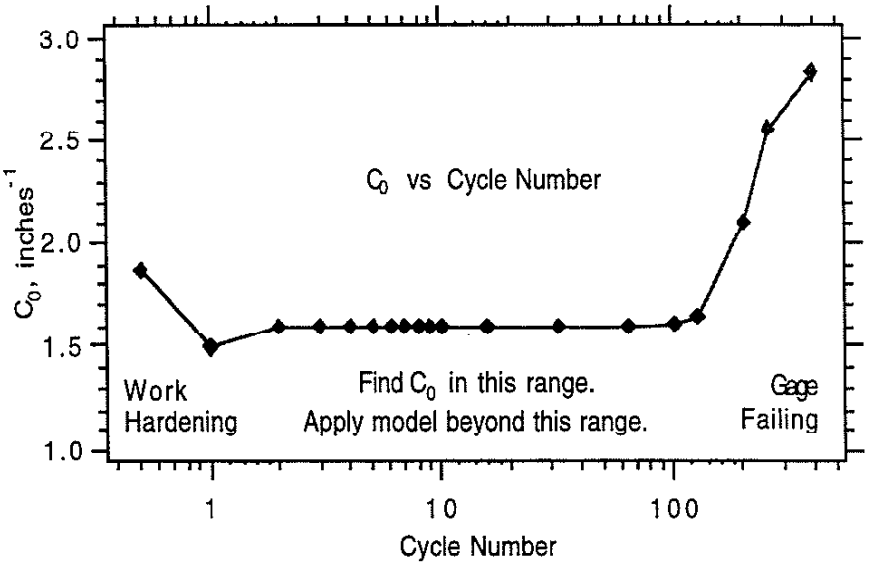

Figure 3.9: Variation of model constant C_0 as a function of cycle number.

Here we see that the value of constant C_0 changed during the initial loading (cycle 0.5) and during the first full cycle (cycle 1), but leveled out for the next 90+ cycles. Under these conditions, the constants will remain steady until the strain gage starts to fail in fatigue and its output becomes unreliable, which is what we observe beyond cycle 100. Constants C_1, C_2, C_3, and C_4 show behavior similar to that of C_0. Once the constants are found, they can be inserted into the model, and the axial strain can be determined for cycles beyond that at which the gage fails.

3.7 Computer Control

In all previously published work, testing has either been done at constant, manually set pressures or at pressures which varied uncontrollably throughout the tests. No studies have been reported where axial stress and pressure were independently varied in a continuous manner. Our apparatus, under computer control, is the first to permit application of mutually independent, repeatable axial stress *and pressure* amplitudes, phase relationships, and wave forms.

3.7.1 System Layout and Block Diagram

The system is configured using two control loops: one for pressure control, and a second for load (stress) control. As can be seen in the block diagram in Figure 3.10, the two loops are coupled by (the pressurized annular area of) the test specimen and the pressure sensitivity of the load cell. One unique aspect of this project is the use of a computer to mathematically uncouple the pressure and load loops. In other words, the test control program corrects the load command signal in real time to compensate for the pressure/load interaction, ensuring that the desired axial stress magnitude in the gage section would not be altered if the pressure was varied.

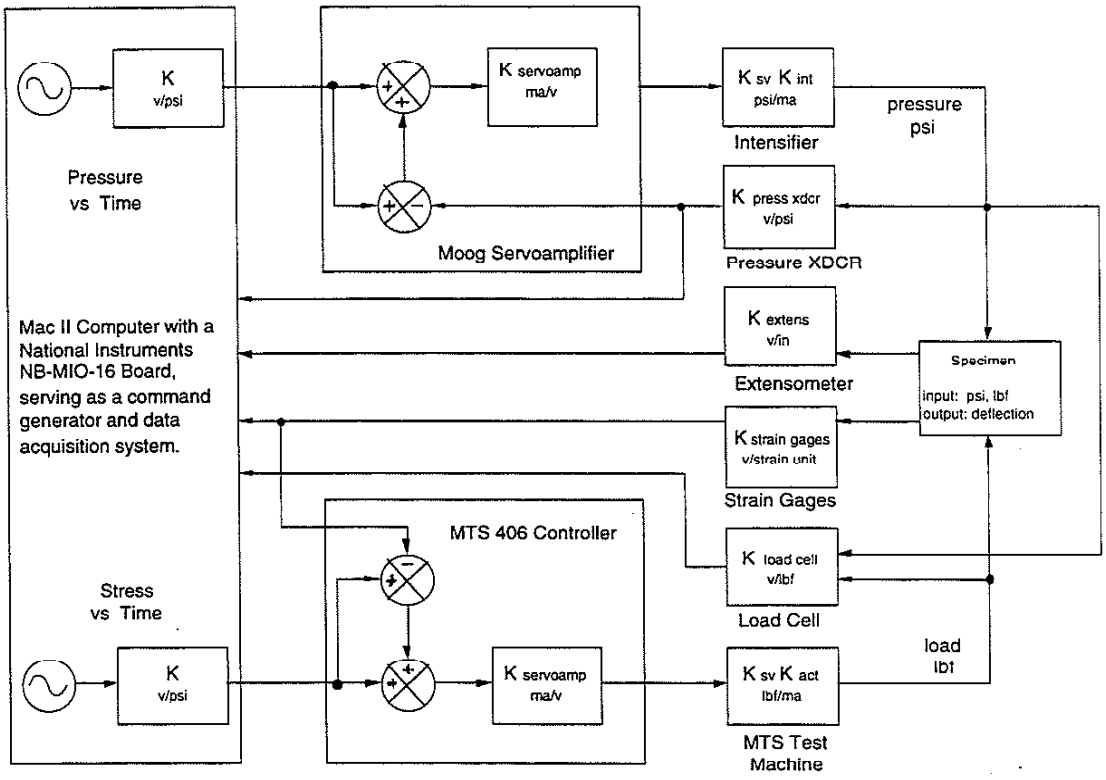

Figure 3.10: Control system block diagram.

The test control program generates the pressure command in a straightforward way as a function of time. However, early on it was found that the response time of the pressure intensifier is greater than that of the MTS machine. This can become a problem at high cyclic frequencies. To keep the pressure in the vessel from lagging behind the pressure command, an algorithm was written into the control program to determine the pressure error in real time, and overdrive the pressure command to minimize the error.

The other variable that we wish to control is the load in the specimen gage section. The test control program generates this load command in a straightforward way as a function of time. However, that form of the load command never makes it out of the computer. Why? Because due to the pressure/load coupling and the load cell design, it is not possible to directly measure the load in the specimen gage section. Instead the load cell measures the load exerted on the conical-tipped shoulder of the specimen, which differs from the load in the specimen gage section due to the pressure acting over the annular area. Since the load cell output is used as the load feedback signal, the load control loop (and thus the load command signal) must also be in terms of load on the shoulder; not load in the gage section. As described in section 3.5 Load Calibration, an algorithm was written that puts the load command in the proper terms using the current pressure transducer reading, the geometry of the test specimen, and the curve-fit calibration functions.

Both these command generating algorithms are processed in real time and the results converted to ±10 V analog signals by the I/O board before being sent to the Moog Servoamplifier or the MTS 406 controller, respectively.

As just mentioned above, the load cell measures the load exerted on the conical-tipped shoulder of the specimen. Because this differs from the load in the specimen gage section due to the pressure acting over the annular area, the gage section diameter is critical. Accurate use of the test control program is limited to strains below necking because it currently does not compensate for any change in the cross sectional area of the gage section which may occur as the test proceeds. As the specimen is strained in tension, the original cross sectional area of the gage section a_o, decreases, causing the annular area subjected to pressure to increase. This applies more tension to the gage section, raising the true axial stress in the gage section above its desired value. Beyond yield, the stress dichotomy grows at an even faster rate than the difference between engineering/true stress as observed in standard tension tests.

It is not possible to compensate for the decrease in gage section cross sectional area which occurs as the test proceeds. Instead we chose to a) correct the axial stress data, and b) convert it to true stress *after* each test was complete. This is done as follows:

$$\text{Nominal axial stress in gage section} = \sigma_{zz} = \frac{F}{a_0}$$

Pressure P is always a "true" stress quantity, so $\sigma_{\theta\theta}^{true} = \sigma_{rr}^{true} = -P$.

$$\text{Engineering axial stress in gage section} = \frac{\text{F increased by P } (a_0\text{-}a)}{a_0} \qquad \text{or}$$

$$\sigma_{zz,engineering} = \frac{F + a_0 P\left(1 - \frac{a}{a_0}\right)}{a_0} = \left(\frac{F}{a_0}\right) + P\left(1 - \frac{a}{a_0}\right) = \sigma_{zz} + P\left(1 - \frac{a}{a_0}\right)$$

$$\text{True axial stress in gage section} = \frac{\text{F increased by P } (a_0\text{-}a)}{a_0 \text{ decreased by } (a_0\text{-}a)} \qquad \text{or}$$

$$\sigma_{zz,true} = \frac{F + a_0 P\left(1 - \frac{a}{a_0}\right)}{a} = \left(\frac{a_0}{a}\right)\sigma_{zz,engineering}$$

In terms of the strains ε_{zz} and $\varepsilon_{\theta\theta}$ (and ε_{rr} equals $\varepsilon_{\theta\theta}$) that we are measuring, the original and instantaneous gage section areas are

$$a_0 = \pi r_0^2 \; ; \qquad a = \pi (r_0 + r_0\varepsilon_{rr})^2$$

Their quotient is

$$\frac{a_0}{a} = \frac{1}{1 + 2\varepsilon_{rr} + \varepsilon_{rr}^2}$$

and substituting this into the equation for true axial stress gives:

$$\sigma_{zz,engineering} = \sigma_{zz} - P\,(2\varepsilon_{rr} + \varepsilon_{rr}^2)$$

$$\sigma_{zz,true} = \frac{\sigma_{zz} + P}{1 + 2\varepsilon_{rr} + \varepsilon_{rr}^2} - P$$

3.7.2 Test Control Program

Using National Instruments' "NB Lab Driver" software, and Symantec's "Think C 5.0" software, a program was written in "C" to enable an Apple Mac II microcomputer fitted with a National Instruments NB-MIO-16X Multi-function I/O Board to conduct triaxial monotonic and cyclic stress tests by simultaneously commanding the MTS universal test machine and the servohydraulic pressure intensifier. The I/O board contains a 16 bit ADC, 8 differential analog inputs with software programmable gain settings of 1, 2, 4, and 8 for each analog input channel, two 12 bit DAC's with voltage outputs, 8 lines of TTL compatible digital I/O and three 16 bit counter/timer channels for timing I/O.

Working through the I/O board the program displays the outputs of seven analog transducers (internal and external load cells, a pressure transducer, an extensometer, a stroke transducer in the hydraulic ram and axial and circumferential strain gages on the specimen gage section) on the Mac II's screen, allowing them to be quickly and easily zeroed before a test. The program then ramps pressure and load to the starting points, generates constant and/or cyclic pressure and load command signals (accounting for the pressure contribution to the gage section stress and providing a modified load command signal in real time), displays the current cycle number, and ends tests at an operator defined maximum cycle number by ramping down the pressure and load. It even provides the capability to pause, resume and prematurely stop tests. Figure 3.11 graphically illustrates the variables which control command generation for stress-controlled monotonic tests, while Figure 3.12 is for stress-controlled cyclic tests. Figure 3.13 presents a generalized flow chart for the test control programs.

At 125 Hertz the program continuously samples the digital state of a limit switch on the intensifier as well as all seven analog transducers. Every analog input channel is differentially connected for improved noise and common mode signal rejection. After their conversion to 12 bit digital form, where 1 LSB = 4.88 mV for 0.05% precision on a ±10 V scale, their values are put on the Mac II's data bus. The program monitors critical test machine functions by evaluating this incoming data stream. For instance, the program can recharge the intensifier when limit switches

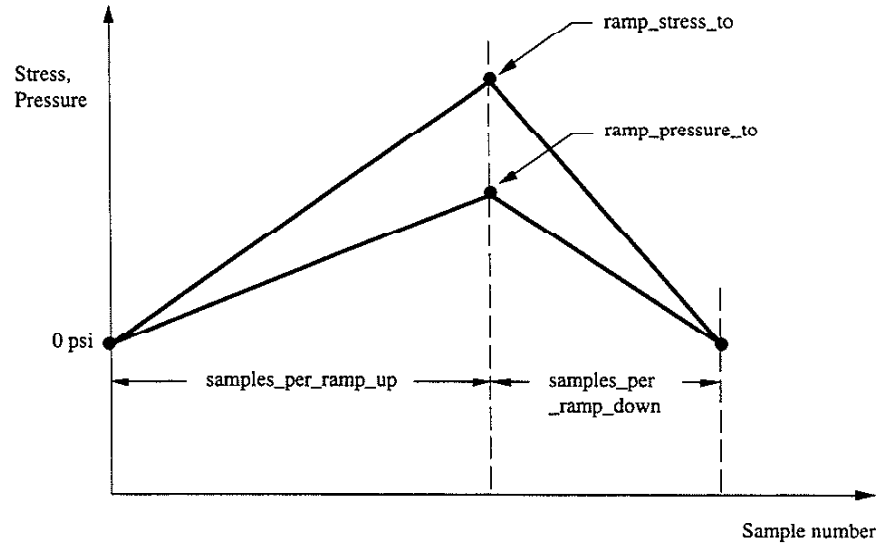

Figure 3.11: Graphical illustration of the variables which control command generation for stress-controlled monotonic tests.

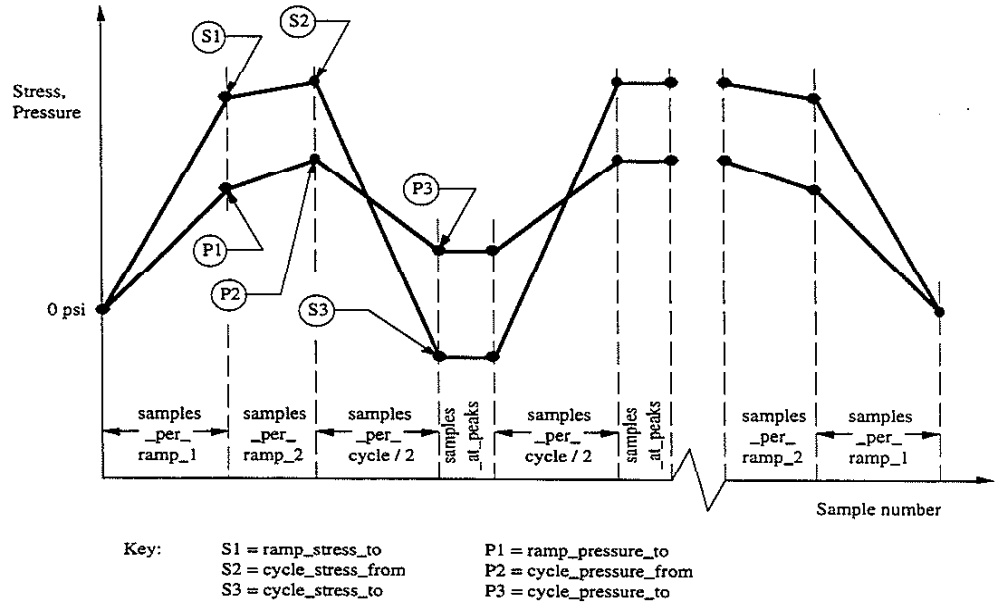

Figure 3.12: Graphical illustration of the variables which control command generation for stress-controlled cyclic tests.

are tripped, or execute a controlled shut down of the test machines when the stroke transducer output exceeds specified values due to fracture of a specimen. The values of the variables are also available for use or modification by the test control program. For instance, the strain gage readings are corrected for transverse sensitivity effects. All transducer readings are then stored in a linked list and when the test is complete they are written to a file in a format compatible with WaveMetrics' "IGOR" graphing and data analysis software, for subsequent analysis and plotting.

Figure 3.13: A flow chart for the test control program.

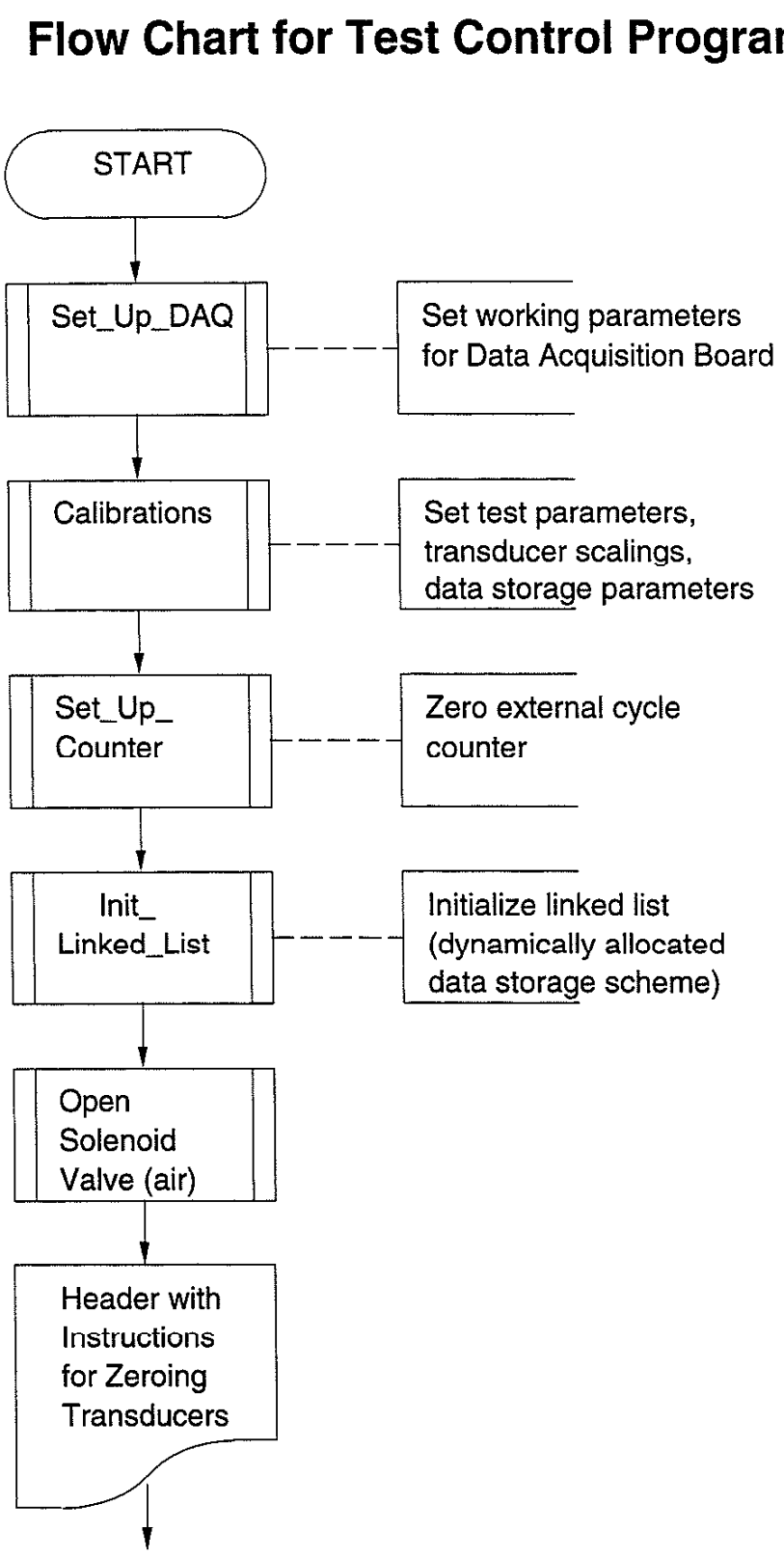

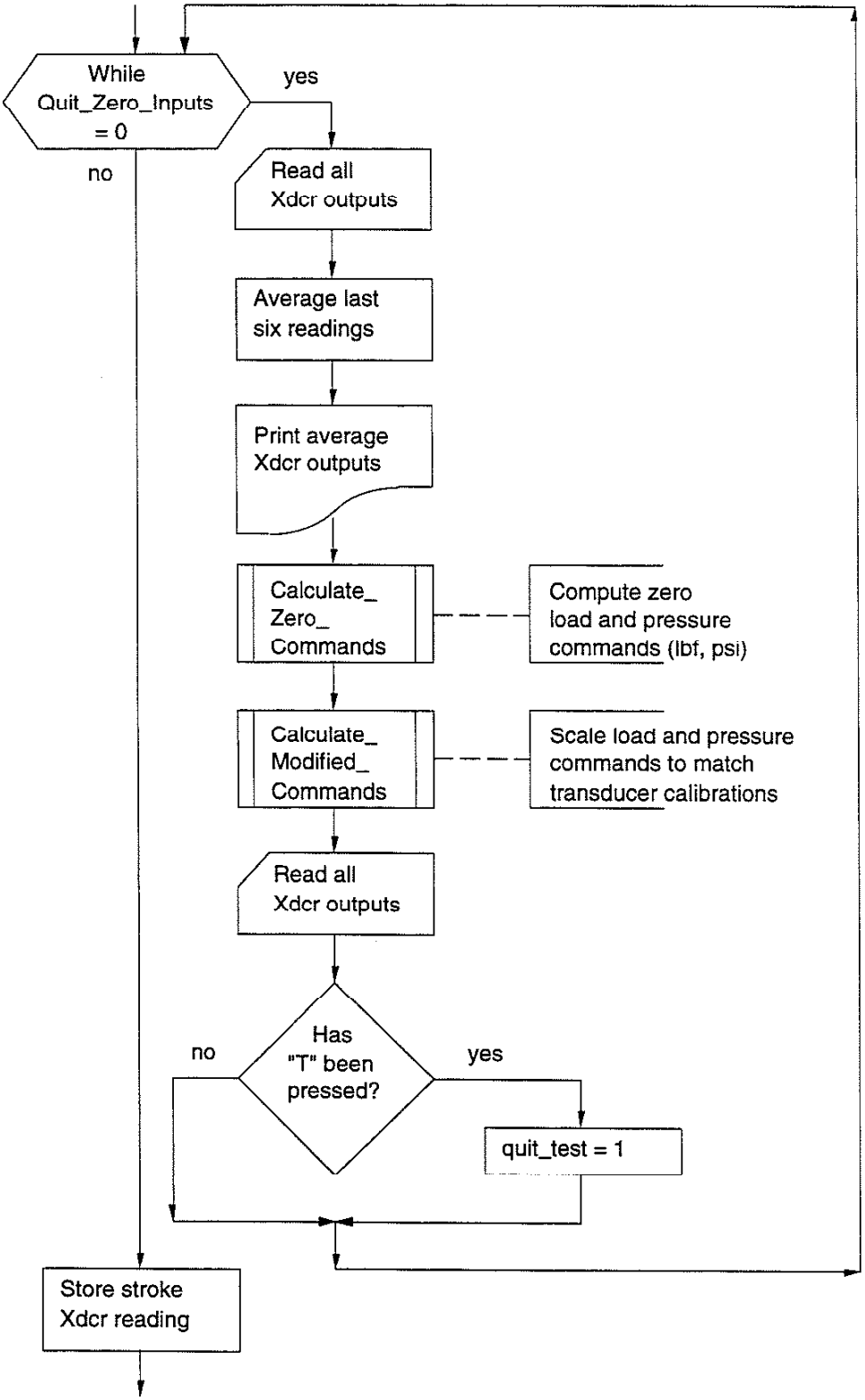
While
Quit_Zero_Inputs
= 0
yes
no
Read all
Xdcr outputs
Average last
six readings
Print average
Xdcr outputs
Calculate_
Zero_
Commands
Compute zero
load and pressure
commands (lbf, psi)
Calculate_
Modified_
Commands
Scale load and pressure
commands to match
transducer calibrations
Read all
Xdcr outputs
Has
"T" been
pressed?
no
yes
quit_test = 1
Store stroke
Xdcr reading

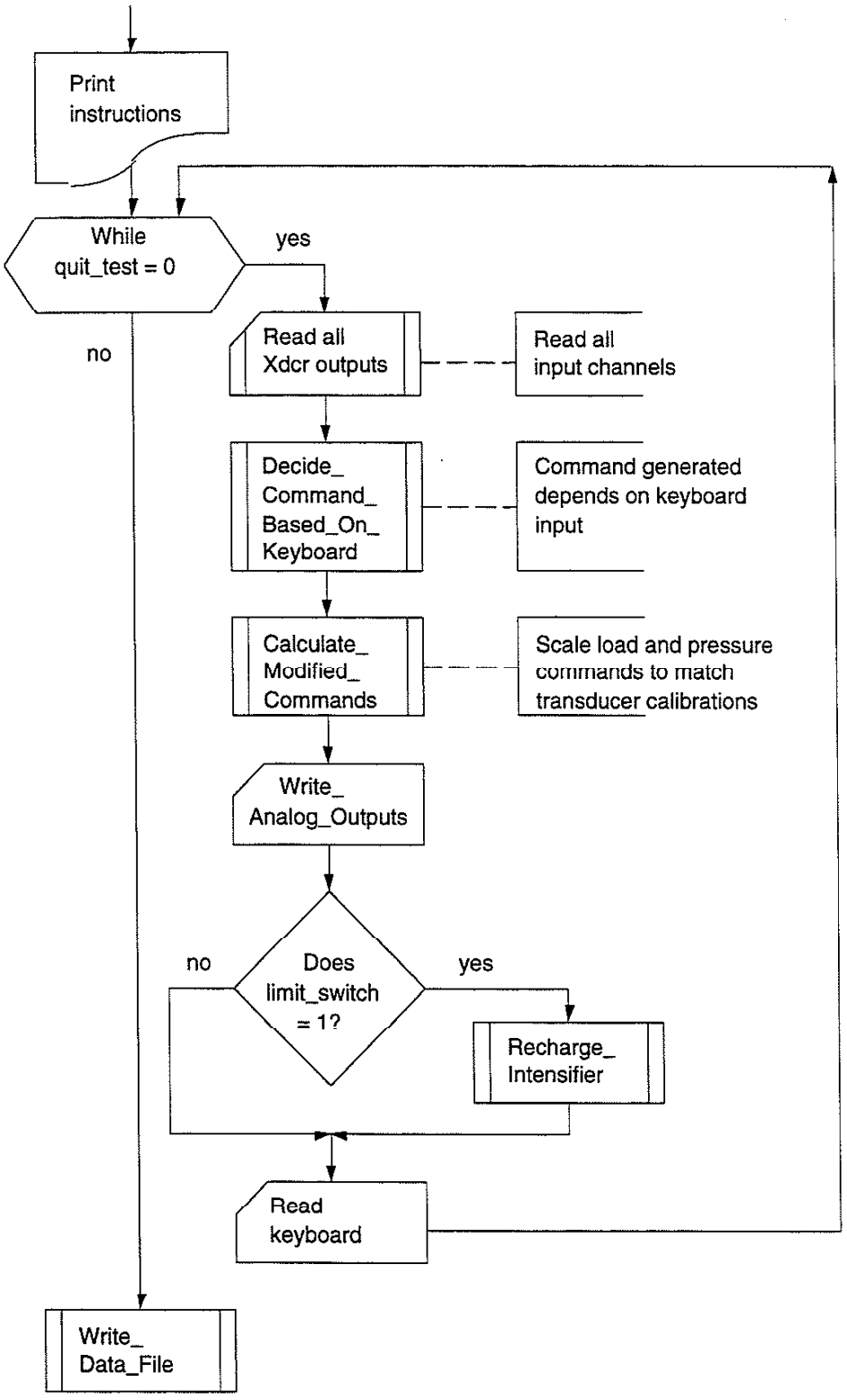

Figure 3.13: A flow chart for the test control program.

3.7.3 Dry Run Program

By suitable modifications to a copy of the control program just described, a "dry run" test simulation program was created to check for possible overload of the specimen shoulders. When running tests involving both high pressures and compressive gage section stress levels, it is possible to yield the specimen shoulders. To check for this condition, the "dry run" program calculates the axial stress in the sections of the specimen shoulders which lie both inside and outside the vessel, properly accounting for the pressure inside the vessel, and the stress due to seal frictional loads on the shoulders outside the vessel. Running the program produces a data file containing the shoulder stress history for the proposed test. Then it calculates the yield boundaries in axial-stress/pressure space for the shoulders, assuming a von Mises yield condition. Superimposing these yield boundaries on a plot of axial shoulder stress vs. pressure allows a simple, visual check for possible yielding of the shoulders. The yield boundaries are determined as follows:

σ_z = axial stress in the shoulders inside the vessel
σ_r = radial stress in the shoulders inside the vessel
σ_θ = circumferential stress in the shoulders inside the vessel
S_y = uniaxial yield stress of the shoulders

$$\sigma_{vm} = \sqrt{\frac{(\sigma_1 - \sigma_2)^2 + (\sigma_2 - \sigma_3)^2 + (\sigma_3 - \sigma_1)^2}{2}}$$

for σ_z greater than -P, i.e., ($\sigma_z > \sigma_r = \sigma_\theta = -P$),

$$\sigma_{vm} = \sqrt{\frac{(\sigma_z + P)^2 + (-P + P)^2 + (-P - \sigma_z)^2}{2}}$$

$$= P + \sigma_z$$

and tensile yielding begins when $\sigma_z = S_y - P$

for σ_z less than -P, i.e., ($\sigma_z < \sigma_r = \sigma_\theta = -P$),

$$\sigma_{vm} = \sqrt{\frac{(-P + P)^2 + (-P - \sigma_z)^2 + (\sigma_z + P)^2}{2}}$$

$$= P + \sigma_z$$

and compressive yielding begins when $\sigma_z = -S_y - P$.

Now two conditions must be checked: Inside the pressurized vessel, and outside the vessel.

Inside the vessel we have:

load on shoulder inside vessel = F = load in gage section - P(A - a)

$$\sigma_{z(shoulder)} = \frac{\text{load on shoulder inside vessel}}{A} = \frac{\sigma_{gage}\, a}{A} - \frac{P(A - a)}{A}$$

$$= \sigma_{gage}\left(\frac{a}{A}\right) + P\left(\frac{a}{A}\right) - P$$

$$\sigma_{z(shoulder)} = (\sigma_{gage} + P)\frac{a}{A} - P$$

thus, tensile yielding of the shoulders inside the vessel occurs when

$$\sigma_z = S_y - P$$

$$(\sigma_{gage} + P)\frac{a}{A} - P = S_y - P$$

$$\therefore \sigma_{gage} + P = \frac{a}{A}\sigma_y$$

and compressive yielding of the shoulders inside the vessel occurs when

$$\sigma_z = -S_y - P$$

$$(\sigma_{gage} + P)\frac{a}{A} - P = -S_y - P$$

$$\therefore \sigma_{gage} + P = -\frac{a}{A}\sigma_y$$

Outside the vessel we have:

load on shoulder outside vessel = F ± seal friction = load in gage section - P(A - a) ± seal friction

40,000 psi pressure on a seal supported with beveled brass back-up rings creates a seal friction which has been measured as equivalent to 7250psi of stress on a 0.25" diameter gage section. Converting this into a frictional force gives:

$$(7250 \text{ psi})(\frac{\pi}{4}(0.25)^2) = 356 \text{ lbf}$$

Pressure energizes the seal and forces it against the shoulder of the specimen. The higher the pressure, the greater this force. Therefore, as a first approximation it is reasonable to assume that

seal friction will be proportional to pressure. Converting the frictional force into a frictional force per psi of pressure gives:

$$356 \text{ lbf} / 40000 \text{ psi} = 0.0089 \frac{\text{lbf}}{\text{psi}}$$

Friction opposes the direction of motion at the seal/specimen interface.

$$\sigma_z = \frac{\text{load on shoulder outside vessel}}{A}$$

$$= \frac{\sigma_{gage}\, a}{A} + P\,\frac{a}{A} - P \pm \frac{(0.0089\ P)}{A}$$

when getting longer, $\sigma_z = (\sigma_{gage} + P)\,\frac{a}{A} - P + 0.0089\,\frac{P}{A}$

when getting shorter, $\sigma_z = (\sigma_{gage} + P)\,\frac{a}{A} - P - 0.0089\,\frac{P}{A}$

outside the vessel, $\sigma_r = \sigma_\theta = 0$; thus yielding will occur when $S_y = \sigma_z$.

Summarizing the two cases gives:

Shoulders inside the vessel remain elastic if

$$\left(\frac{A}{a} S_y\right) > (\sigma_{gage} + p) > \left(-\frac{A}{a} S_y\right)$$

Shoulders outside the vessel remain elastic if

$$S_y > \left[(\sigma_{gage} + p)\frac{a}{A} + p\left(\frac{0.0089}{A} - 1\right)\right] = \sigma_{z\,max}$$

and

$$-S_y < \left[(\sigma_{gage} + p)\frac{a}{A} + p\left(\frac{-0.0089}{A} - 1\right)\right] = \sigma_{z\,min}$$

To the user, setting up the "dry run" program is identical to setting up the control program, and it also provides an IGOR compatible output file. A quick glance at the yield boundaries superimposed on the shoulder stress vs. pressure plot is all it takes to see whether or not a proposed test can be safely conducted.

List of References

1. Arora, P. R., & Raghavan, M. R. Prediction of specimen strain from extensometer deflection measurements in a direct stress fatigue test specimen under static tensile loading. Journal of Testing and Evaluation, 1988, 16(4), 386-391.

2. Bridgman, P. W. The effect of pressure on the tensile properties of several metals and other materials. Journal of Applied Physics, 1953, 24(5), 560-570.

3. Bridgman, P. W. Studies in Large Flow and Fracture. Cambridge, MA: Harvard University Press, 1964.

4. Pugh, H. Ll. D. The mechanical properties and deformation characteristic of metals and alloys under pressure. ASTM STP 374 Irreversible Effects of High Pressure and Temperature on Materials, 1965, 68-139.

5. Crossland, B. The effect of fluid pressure on the shear properties of metals. Proceeding of the Institution of Mechanical Engineers, 1954, 168(40), 935-946.

6. Sakata, Masaru, Aoki, Sigeru, & Tsujimoto, Takashi. An experimental study on the deformation of materials under high hydrostatic pressures. Bulletin of the JSME, 1971, 14(74), 737-744.

7. Pugh. H. Ll. D., & Gunn, D. A. A strain gauge load cell for use under high hydrostatic pressure. Proceedings of the Institution of Mechanical Engineers 1967-68 (High Pressure Engineering), 1968, 182(3C), 260-265.

8. Gordon, Robert B., & Mike, Leslie F. Measurement of the mechanical properties of solids at high pressure. Review of Scientific Instruments, 1967, 38(4), 541-546.

9. Brandes, Marek, & Szlachcic, Henryk. Simple device for stretching test pieces under high hydrostatic pressures. The Review of Scientific Instruments, 1965, 36(7), 991-993.

10. Pugh, J. Ll. D., & Green, D. The effect of hydrostatic pressure on the plastic flow and fracture of metals. Proceedings of the Institution of Mechanical Engineers, 1964, 179(12), 415-437.

11. Pugh, H. Ll. D., Hodgson, G., & Gunn, D. A. Tensile strain measurement under high hydrostatic pressure using an optical method. Journal of Scientific Instrumentation, 1963, 40(5), 221-224.

12. Oguchi, Atsushi, & Yoshida, Susumu. A magnetostrictive load cell for use under high hydrostatic pressures. Japanese Journal of Applied Physics, 1968, 7(6), 672-678.

13. Birks, A. W., & Ludlow, C. A strain gauge load cell for the measurement of compressive loads under conditions of high hydrostatic pressure. Strain, 1969, 5, 218-220.

14. Fung, P. K. Instrumentation for measuring load and deformation under high pressure. Experimental Mechanics, February 1975, 61-66.

15. Gerdeen, J. C. Effects of pressure on small foil strain gages. Experimental Mechanics, Mar. 1963, 73-80.

16. Milligan, R. V. The effects of high pressure on foil strain gages. Experimental Mechanics, Feb. 1964, 25-36.

17. Milligan, R. V. The effects of high pressure on foil strain gages on convex and concave surfaces. Experimental Mechanics, Feb. 1965, 59-64.

18. MM Catalog 500, Part B - Strain Gage Technical Data, Measurements Group, Micro-Measurements Division, Raleigh, NC, p. 61

19. Experimental Stress Analysis, 3rd edition, by James W. Dally and William F. Riley, McGraw-Hill, Inc., 1991, pp. 166-167.

20. MicroMeasurements catalog A-110-5 MM Catalog A-110-5, Part B - M-Line Strain Gage Accessories, Measurements Group, Micro-Measurements Division, Raleigh, NC, p. 9.

21. Roark's Formulas for Stress and Strain, 6th edition, by Warren C. Young, McGraw-Hill, Inc., 1989.

4. EFFECT OF STRESS STATE ON THE STRESS-ASSISTED MARTENSITIC TRANSFORMATION OF CARBURIZED 4320 STEELS

4.1 Overview

The effect of stress state on the stress-assisted martensitic transformation of retained austenite was investigated in carburized 4320 steels having an initial retained austenite content of 15%. Utilizing conventional servohydraulic test machines as well as a specialized pressure test apparatus, monotonic experiments were conducted on specimens with different austenitization and tempering histories. When stress-strain behavior under various stress states were compared, experimental results indicated considerable asymmetry between tension and compression. The highest strength levels were observed for the untempered material tested under triaxial stress states. Transformation is responsible for the initial yield behavior and flow stress increases with decreasing triaxiality or hydrostatic stress. Carburized 4320 tempered at low temperatures contained fine carbide precipitates which increased the strength and ductility of the specimens and also changed the austenite to martensite transformation behavior.

4.2 Introduction

Basic machine elements such as bearings, gears, cams and sprockets require the combination of tough, ductile, fracture-resistant interiors and strong, hard, wear-resistant surfaces. In the majority of industrial applications, steel is the material of choice for these critical components. However in steels, the above-mentioned properties display a strong dependence on carbon content: low carbon steels can provide only the former properties and high carbon steels only the latter. To provide the required combination of properties in a single piece of steel, a heat treatment process called "carburizing" was developed which produces a predictable variation in carbon concentration through the thickness of a component.

In carburizing, low carbon steel components at or near net shape are heated in an atmosphere of carbonaceous gases until diffusional processes form a high carbon surface layer called a "case" around the low carbon "core." The temperatures used for carburizing are chosen high enough to transform the steel to its high temperature phase, austenite, since both the diffusion

coefficients and solubility of carbon in austenite are more than an order of magnitude greater than in its primary low temperature phase, ferrite. (In fact, to save costly furnace time the diffusion coefficient is often further raised by employing temperatures well above the austenitizing temperature.) Once the atmosphere and temperature are set, the length of time that a component spends in a carburizing furnace is determined by the desired thickness of the high carbon surface layer (the "depth of the case"). When this time is reached the temperature is often lowered to just above the austenitizing temperature (to minimize quench cracking and distortion). After soaking for a time at this temperature, the component is oil quenched. The high carbon case responds more vigorously to the quenching than does the low carbon core, resulting in the desired combination of a strong, hard, wear-resistant surface and a tough, ductile, fracture-resistant interior. Typically, carburized components are immediately tempered at a low temperature (150 - 200°C) to improve the toughness of the case, while maintaining their high strength. It has even been found that carburizing steel bearings, gears, cams and sprockets will improve their fatigue strength. The improvement is caused by the increased carbon content in the surface layer which converts the case to a higher strength material, and by the compressive residual stresses in the case which result from the volumetric expansion of the austenite as it transforms.

As is usual in any quenched high carbon steel, the room temperature microstructure of the case consists of both martensite and untransformed or "retained" austenite phases. Retained austenite exists because the thermodynamic driving force for the transformation to martensite is not strong enough to overcome the forces resisting the transformation. The austenite is severely strained by being forced to accomodate the volumetric expansion of the martensite transformation. These accomodation strains create internal stress fields which resist complete transformation. However, under a favorable applied stress or with further decreases in temperature, the metastable retained austenite will transform to martensite. Of course, any retained austenite that transforms to martensite will increase in volume by about 4% [1-2]. In the real world, the dimensional changes resulting from this volumetric expansion can exceed tight tolerances in roller bearings or loosen press fit bearing races [3]. These changes can influence fatigue and fracture behavior and lead to component failure: on heavily loaded railroad freight cars, such axle bearing problems can cause catastrophic derailments. Thus, to understand the dimensional changes of stressed components in service, it is important to understand how phase transformations are affected by applied stress conditions.

The effect of uniaxial stress on martensitic transformation was first extensively studied by Kulin *et al.* [4]. Since this work, numerous studies have considered the effects of stress state on martensitic transformation of ferrous alloys [2-9]. Within a specific temperature range above M_s (the martensite start temperature) a stress applied to an austenitic or a martensitic-austenitic composite sample causes "stress-assisted" transformation. In this regime, martensite nucleates on the same sites which are responsible when "spontaneous" transformation occurs without any

applied stress [6,10]. However, if martensite nucleates on sites formed by plastic deformation, the mechanism is called "strain-induced" transformation [10,11]. The initial yield behavior shows whether the mechanism is stress-assisted or strain-induced, according to the change in the yield strength with temperature. Recent studies show that stress-assisted transformation is the dominant mechanism for initial yield behavior of carburized 4320 steels [2,3]. The kinetics of stress-assisted transformation are complex, but generally related to the ambient temperature, M_s temperature, carbon content, amount of retained austenite, austenite and martensite strengths, and the hydrostatic and effective stresses [10,12,13]. The distinction between deformation due to different modes of transformation or even just due to slip becomes less obvious as deformation proceeds.

Although a large number of researchers have studied the effects of uniaxial stress *state* on the martensitic transformation of steels, there is a shortage of experimental work concentrating on the effect of multi-dimensional stress states on the mechanical behavior of carburized steels. Nishiyama reviewed the studies on the effect of pure hydrostatic pressure on the martensitic transformation of steels in terms of the pressure dependency of the M_s temperature, and the equilibrium concentration of vacancies and interstitial atoms [14]. Recent work on the strain-induced transformation describe the stress state dependence of the potency distribution of the martensitic nucleation sites [10,15]. The only studies to date which studied the effect of the triaxial stress states on the stress-assisted martensitic transformation are the works on two types of shape memory alloys, i.e. Ni-Ti and Cu-Zn-Al [16,17], which will be covered in a subsequent chapter.

Research efforts have also focused on the influence that uniaxial stress *sense* (tension vs. compression) has on stress-assisted martensitic transformation. The majority of these studies report asymmetry between tensile and compressive yield strength [2, 17-19]. It has been observed that in compression, very little or no transformation occurs due to the small number of variants available for transformation: consequently, the yield strength depends predominately on slip processes. However, in tension the first inelastic strain is produced by stress-assisted transformation which occurs before the stress is high enough to cause slip.

With the effects of pure hydrostatic pressure on many ferrous alloys already well-established [14], it is desirable to find out how hydrostatic pressure applied together with uniaxial compressive or tensile stresses will affect the asymmetry in stress-strain behavior. The Clausius-Clapeyron equation [5] predicts that equilibrium phase transition temperature should decrease with pure hydrostatic pressure for materials which exhibit a positive volume change upon transformation. Conversely, it predicts increases for materials which exhibit a negative volume change. Since transformation in carburized steels shows a positive volume change, the Clausius-Clapeyron equation suggests that high hydrostatic pressure should decrease the amount of stress-assisted transformation, regardless of the sense of the uniaxial stress. If the decrease is large enough, this may also change the deformation mechanism from stress-assisted transformation to slip. Hence, to understand the detailed stress-strain behavior of carburized steels, it is instructive

to study the roles of different stress states on the transformation. M_s

In carburized steels the stress (effective or uniaxial) at which retained austenite begins to transform is dependent on the amount and stability of the retained austenite. This in turn is dependent on the test temperature, the chemical composition, the austenitizing and quenching temperatures, and the tempering time and temperature. At higher austenitizing temperatures more carbon goes into solution. Since carbon and other alloying elements lower the M_S temperature [26], higher retained austenite levels result upon quenching to room temperature. Carbon steels are tempered at temperatures between 150°C and 200°C for up to 2 hours to improve toughness and undesirable residual stresses while maintaining hardness and strength at high levels [20-23]. In 1.4% C steel, Glover [24] found that these low tempering temperatures (LTT) produced a large reduction in M_S temperature, indicating that the retained austenite became more stable. This, of course, raises the barrier for stress-assisted transformation of austenite to martensite. Horn and Ritchie [25] found that increasing tempering temperature above the LTT range caused carbide precipitation. Since carbide precipitation reduces the carbon content of the austenite, it raises the M_S temperature and makes the retained austenite less stable.

All of the above results have motivated this experimental investigation into examining the effects of tempering, different austenitizing temperatures and different stress states on the stress-strain behavior of carburized 4320 steel. The following pages describe the determination of the transformation stress in tension, compression and under three-dimensional stress states at ambient temperature, coupled with an examination of the stress-strain behavior after transformation starts.

4.3 Experimental Techniques:

The material used in this study was 4320 special-quality ball and roller bearing steel per ASTM A535. The as-received 4320 steel composition was 0.21 C, 0.20 Si, 0.62 Mn, 1.73 Ni, 0.49 Cr, 0.20 Mo, 0.01 P, 0.018 S, and 0.16 Cu (wt. pct.). Two different specimen geometries were used: one for tension-compression tests and a second for triaxial pressure tests. Specimens were prepared with a nominal gage length of 12.7mm, and gage diameter of 5.08 mm. The gage section of each specimen was first rough machined to 5.60 mm diameter. Carburizing was performed on the gage section of these specimens in an endothermic atmosphere at a temperature of 955 °C for 18 hours. The carbon potential under these conditions was 1.10%. The long carburizing time was chosen to produce a specimen that was carburized all the way through its gage section, in order to simulate just the case of a carburized bearing race.

To investigate the effects of both austenitizing temperature and low temperature tempering, four different batches were prepared after carburizing, as described in Table 4.1. One batch was austenitized at 955 °C, above A_{cm} (upper critical temperature), and another one at 845 °C, below A_{cm}, each for 1 hour. Both batches were hardened by quenching in oil at 60 °C. A part of each batch was then tempered for 1.5 hours at 177 °C. The specimens were machined to final

Batch I.D.	Austenitizing parameters	Tempering parameters
I	1 hour @ 955 °C	untempered
II	1 hour @ 955 °C	1.5 hours @ 177 °C
III	1 hour @ 845 °C	untempered
IV	1 hour @ 845 °C	1.5 hours @ 177 °C

Table 4.1. Summary of specimen heat treatments. All specimens were carburized at 955 °C for 18 hours and quenched in oil at 60 °C.

dimensions utilizing a slow grinding process, and then polished. The magnitude of M_s was checked using a Differential Scanning Calorimeter (DSC) analysis. The martensite start temperature M_s was found to be ≈ 0 °C for the material austenitized at 955 °C, and ≈ 8 °C for the material austenitized at 845 °C. This shows that the retained austenite of the former is slightly more stable than that of the latter. The resulting volume fraction of the retained austenite on the surface of

Test Description	Applied Stress State	Hydrostatic Stress	Triaxiality
Pure Tension	$\sigma_{ij} = \begin{bmatrix} \sigma & 0 & 0 \\ 0 & 0 & 0 \\ 0 & 0 & 0 \end{bmatrix}$	$\sigma_H = \sigma / 3$	1/3
Pure Compression	$\sigma_{ij} = \begin{bmatrix} -\sigma & 0 & 0 \\ 0 & 0 & 0 \\ 0 & 0 & 0 \end{bmatrix}$	$\sigma_H = -\sigma / 3$	-1/3
Zero Hydrostatic	$\sigma_{ij} = \begin{bmatrix} 2\sigma & 0 & 0 \\ 0 & -\sigma & 0 \\ 0 & 0 & -\sigma \end{bmatrix}$	$\sigma_H = 0$	0
Axial Tension - Diametral Compression	$\sigma_{ij} = \begin{bmatrix} \sigma & 0 & 0 \\ 0 & -\sigma & 0 \\ 0 & 0 & -\sigma \end{bmatrix}$	$\sigma_H = -\sigma / 3$	-1/6
Triaxial Compression	$\sigma_{ij} = \begin{bmatrix} -5\sigma & 0 & 0 \\ 0 & -\sigma & 0 \\ 0 & 0 & -\sigma \end{bmatrix}$	$\sigma_H = -7\sigma / 3$	-7/12

Table 4.2. Experimental stress states applied to all batches in Table 1. Triaxiality represents the ratio of the hydrostatic stress component to deviatoric stress component of effective stress.

uniaxial test specimens was measured using X-ray diffraction techniques [26]. After testing, the austenite content was measured again by the same technique on the cross-sectional area perpendicular to the testing direction.

Both uniaxial and triaxial experiments were conducted at 20°C. Uniaxial tests were performed on an Instron 1331 servohydraulic test machine operating in axial strain control at a strain rate of 10^{-4} s^{-1}. MTS extensometers measured both axial and diametral strains. During all experiments, the axial load, axial strain, diametral strain (and pressure in triaxial tests) were stored via computer. The test apparatus described in chapter 3 was used for triaxial testing.

A summary of stress conditions studied is provided in Table 4.2. Tests were conducted at constant triaxiality values. A graphical representation in axial stress-pressure space is shown in Figure 4.1. For each of the triaxial stress state experiments, the axial and diametral stresses were ramped from zero initial conditions until either the specimen failed or the machine loading limit was reached. The stresses at the onset of the austenite to martensite transformation were determined using a 0.00025 strain offset method.

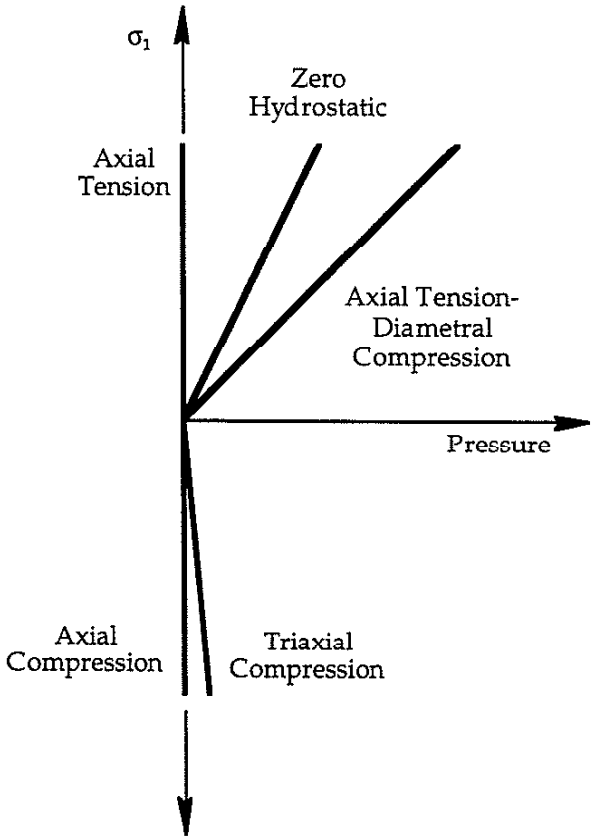

Figure 4.1. A graphical representation of the various tests in axial stress-pressure space.

4.4 Experimental Results:

For all tests, stress and strain data were collected in raw engineering quantities. Uniaxial test data was then converted to true stresses and strains using the following equations:

$$\sigma_{zz}^{true} = \frac{\sigma_{zz}}{(1 + \varepsilon_{rr})^2}$$

$$\varepsilon_{rr}^{true} = \varepsilon_{\theta\theta}^{true} = \ln(\varepsilon_{rr} + 1)$$

$$\varepsilon_{zz}^{true} = \ln(\varepsilon_{zz} + 1)$$

The conversion of pressure test data to true stresses and strains is detailed in chapter 3.

In order to compare uniaxial and triaxial test results, effective stress and strain quantities were calculated using the following equations:

$$\sigma_{eff} = \sqrt{\frac{(\sigma_{zz} - \sigma_{rr})^2 + (\sigma_{rr} - \sigma_{\theta\theta})^2 + (\sigma_{\theta\theta} - \sigma_{zz})^2}{2}}$$

$$\varepsilon_{eff} = \frac{\sqrt{2}}{3}\sqrt{(\varepsilon_{zz} - \varepsilon_{rr})^2 + (\varepsilon_{rr} - \varepsilon_{\theta\theta})^2 + (\varepsilon_{\theta\theta} - \varepsilon_{zz})^2}$$

Effective stress-effective strain curves for both tension and compression tests are shown in Figure 4.2 and 4.3 for untempered and tempered 4320 materials respectively. Note that the

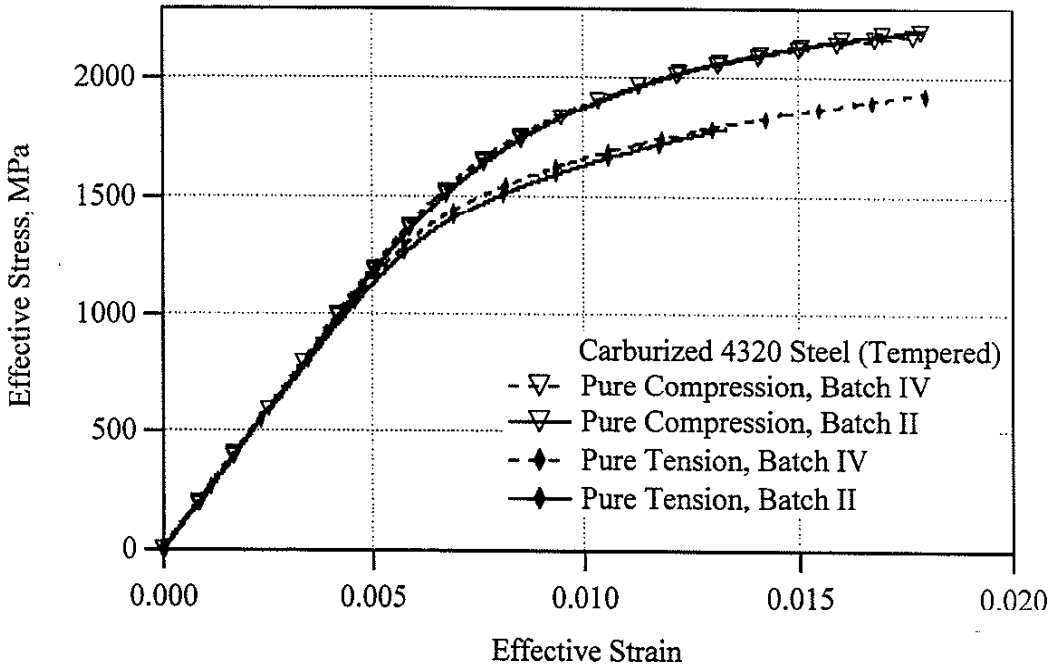

Figure 4.2. The effective stress-effective strain response of carburized 4320 steel under pure tension and pure compression. Specimens are only quenched.

tension-compression asymmetry is particularly remarkable. The effective flow stress (at 0.00025 offset) for untempered material austenitized at 955 °C was 26% lower in tension than in compression: for tempered material austenitized at 845 °C, it was 17% lower. The lower flow stress in tension was attributed to stress-assisted transformation of retained austenite to martensite. As determined by X-ray diffraction measurements, the initial retained austenite levels in the gage sections of the untempered specimens were 15%. As expected, tempered specimens had slightly lower austenite content (14%) than untempered ones. Retained austenite measurements conducted after testing indicated that under tension, the retained austenite transformed almost completely (retained austenite content ≈ 2%). The retained austenite content was slightly higher after the compression tests than after the tension tests, though the difference was within the accuracy of the measurements (± 2%).

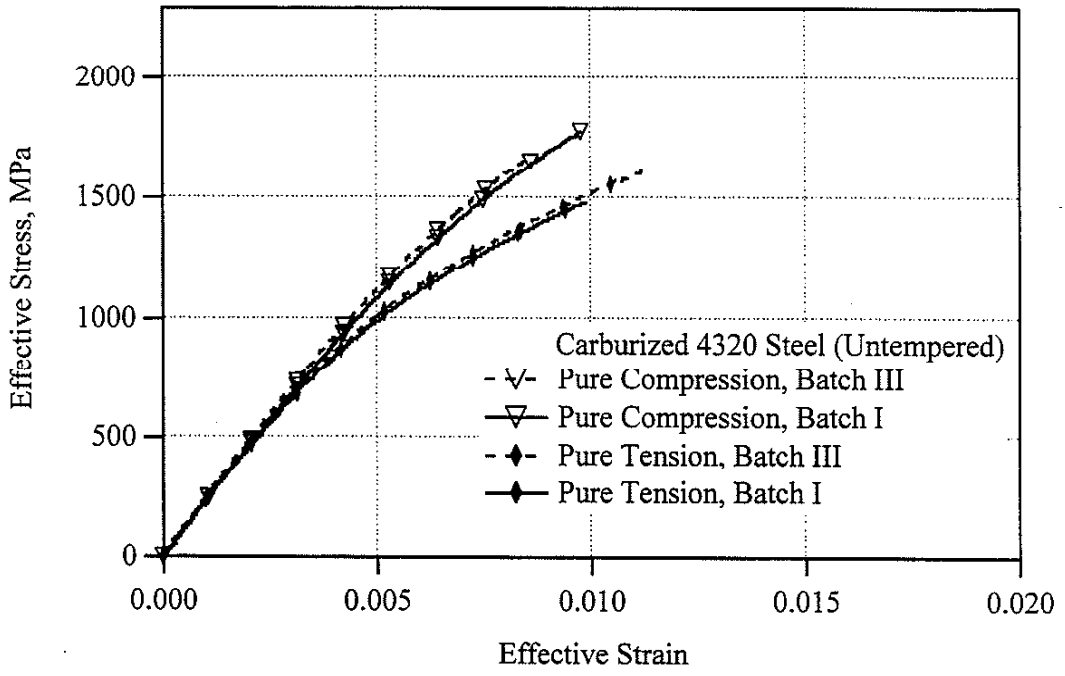

Figure 4.3. The effective stress-effective strain response of carburized 4320 steel under pure tension and pure compression. Specimens are tempered.

Both axial and circumferential strains, ε_{zz} and $\varepsilon_{\theta\theta}$, were measured during all tests. From these measurements, the volumetric strain $\frac{\Delta V}{V}$ can be determined as follows:

$$\Delta V = V_i - V_f$$

where in the cylindrical coordinate system used for the specimen (see Figure 4.4),

$V_i = \pi R^2 H$ = volume of specimen before straining,

$V_f = \pi (R + \Delta R)^2 (H + \Delta H)$ = volume of specimen after straining,

$$\Delta R = R\varepsilon_{rr}$$

$$\Delta H = H\varepsilon_{zz}$$

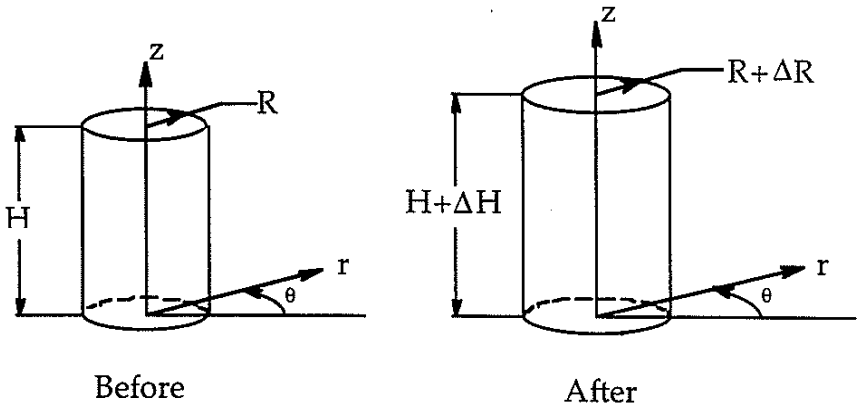

Figure 4.4. A slice taken from a test specimen's gage section, showing before and after dimensions used in volumetric strain derivation.

substituting gives:

$$\Delta V = \pi (R^2 + 2R^2\varepsilon_{rr} + R^2\varepsilon_{rr}^2) (H + H\varepsilon_{zz}) - \pi R^2 H$$

neglecting insignificant $R^2\varepsilon_{rr}^2$ term containing squares of strains we obtain:

$$\Delta V = \pi R^2 H [(1 + 2\varepsilon_{rr}) (1 + \varepsilon_{zz}) - 1]$$

Expanding, we obtain:

$$\Delta V = \pi R^2 H [1 + \varepsilon_{zz} + 2\varepsilon_{rr} + 2\varepsilon_{rr}\varepsilon_{zz} - 1]$$

neglecting insignificant $2\varepsilon_{rr}\varepsilon_{zz}$ term containing products of strains we obtain

$$\Delta V = \pi R^2 H [\varepsilon_{zz} + 2\varepsilon_{rr}]$$

but $\varepsilon_{rr} = \varepsilon_{\theta\theta}$, and $\varepsilon_{\theta\theta}$ is easily measured, so substituting we obtain

$$\Delta V = \pi R^2 H [\varepsilon_{zz} + 2\varepsilon_{\theta\theta}]$$

dividing by the original volume gives

$$\frac{\Delta V}{V} = \frac{\pi R^2 H[\varepsilon_{zz} + 2\varepsilon_{zz}]}{\pi R^2 H} = \varepsilon_{zz} + 2\varepsilon_{\theta\theta}$$

This total volumetric strain is calculated from the axial and circumferential strains. However, these axial and circumferential strain components are each comprised of elastic, plastic and transformation strain sub-components. Assuming that plastic strain occurs at constant volume, subtracting the elastic strain sub-components from the axial and circumferential strains before calculating total volumetric strain gives us volumetric *transformation* strain, $\left(\frac{\Delta V}{V}\right)^{tr}$. First the elastic strain is calculated:

$$\varepsilon_{zz} = (\varepsilon_{zz}^{tr} + \varepsilon_{zz}^{p} + \varepsilon_{zz}^{e}) = \varepsilon_{zz}^{tr} + \varepsilon_{zz}^{p} + \frac{1}{E}(\sigma_{zz} - \nu\,(\sigma_{\theta\theta} + \sigma_{rr}))$$

For the general triaxial case, we have:

$$\sigma_{\theta\theta} = \sigma_{rr} = -P$$

where P = Pressure, a compressive surface stress conventionally measured as a positive quantity. Substituting this gives:

$$\varepsilon_{zz} = (\varepsilon_{zz}^{tr} + \varepsilon_{zz}^{p} + \varepsilon_{zz}^{e}) = \varepsilon_{zz}^{tr} + \varepsilon_{zz}^{p} + \frac{1}{E}(\sigma_{zz} + 2\nu P)$$

Likewise, the same substitution into

$$\varepsilon_{\theta\theta} = (\varepsilon_{\theta\theta}^{tr} + \varepsilon_{\theta\theta}^{p} + \varepsilon_{\theta\theta}^{e}) = \varepsilon_{\theta\theta}^{tr} + \varepsilon_{\theta\theta}^{p} + \frac{1}{E}(\sigma_{\theta\theta} - \nu\,(\sigma_{zz} + \sigma_{rr}))$$

gives:

$$\varepsilon_{\theta\theta} = (\varepsilon_{\theta\theta}^{tr} + \varepsilon_{\theta\theta}^{p} + \varepsilon_{\theta\theta}^{e}) = \varepsilon_{\theta\theta}^{tr} + \varepsilon_{\theta\theta}^{p} + \frac{1}{E}(P(\nu - 1) - \nu\sigma_{zz})$$

Substituting these relations into our transformation strain equation gives

$$\left(\frac{\Delta V}{V}\right)^{tr} = (\varepsilon_{zz}^{tr} + \varepsilon_{\theta\theta}^{p} + 2(\varepsilon_{\theta\theta}^{tr} + \varepsilon_{\theta\theta}^{p})) = \varepsilon_{zz} + 2\,\varepsilon_{\theta\theta} - \frac{1}{E}(\sigma_{zz} + 2\nu P + 2P(\nu - 1) - 2\nu\sigma_{zz})$$

Using the constant volume plasticity assumption,

$$\varepsilon_{zz}^{p} + 2\varepsilon_{\theta\theta}^{p} = 0$$

gives, upon simplification:

$$\left(\frac{\Delta V}{V}\right)^{tr} = (\varepsilon_{zz}^{tr} + 2\,\varepsilon_{\theta\theta}^{tr}) = \varepsilon_{zz} + 2\,\varepsilon_{\theta\theta} - \left(\frac{1 - 2\nu}{E}\right)(\sigma_{zz} - 2P)$$

This is the general result. For the uniaxial case, P=0 and the volumetric transformation strain reduces to:

$$\left(\frac{\Delta V}{V}\right)^{tr} = \varepsilon_{zz} + 2\,\varepsilon_{\theta\theta}$$

The above calculations were made on the 4320 test data to gain insight on the overall volume change. The first significant effect observed was that transformation begins when the stress level reaches the elastic limit (see Figure 4.5). This result implies that the transformation is responsible for the initial yield behavior, as is expected in the case of stress-assisted transformations.

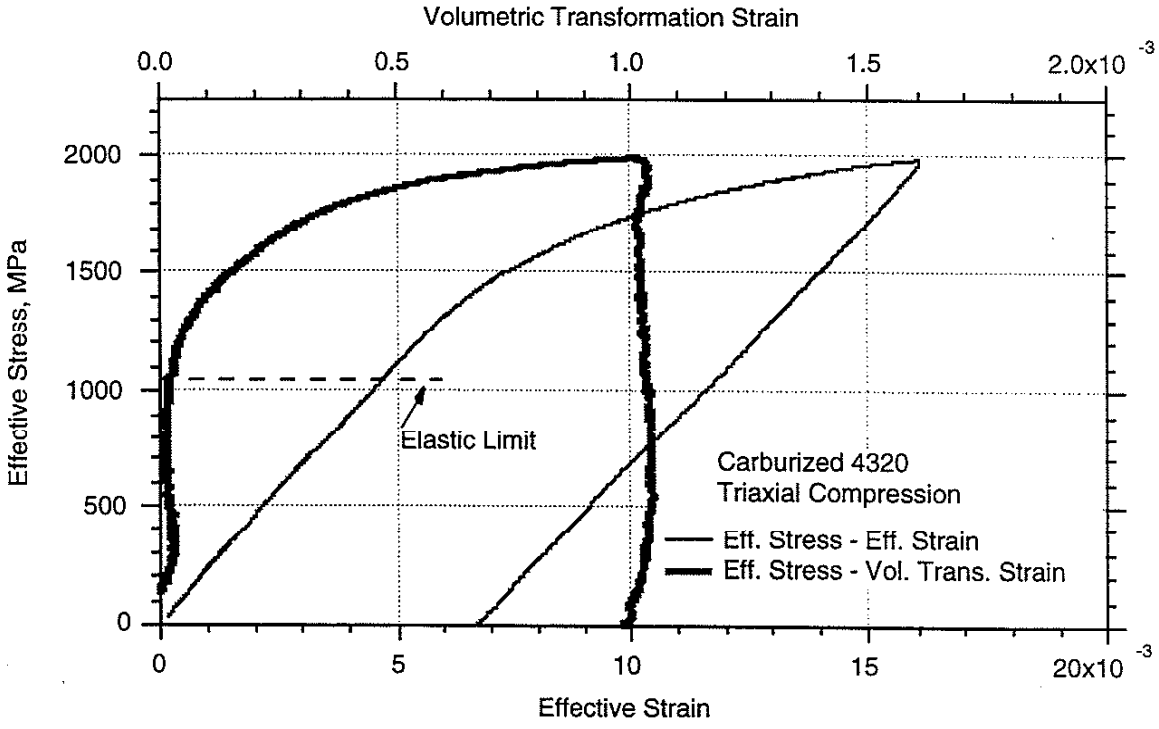

Figure 4.5. Development of volumetric transformation strain for triaxial compression test of carburized 4320. Note that transformation begins at the elastic limit.

The volumetric transformation strains vs. effective stress plots are shown in Figure 4.6 and 4.7. After initial transformation started, the volumetric transformation strain increased with effective stress until fracture. The volumetric transformation strain was much smaller in compression than in tension (Figure 4.3). In tension it was found to be 0.0015 at fracture for batch I and III while it was 0.002 for batch II and 0.0033 for batch IV. The smallest increase in the volumetric transformation strain (less than 0.0005) was observed under compressive load in

untempered batches strained to fracture, while in tempered batches it was between 0.001 and 0.002 up to an effective strain of 2%.

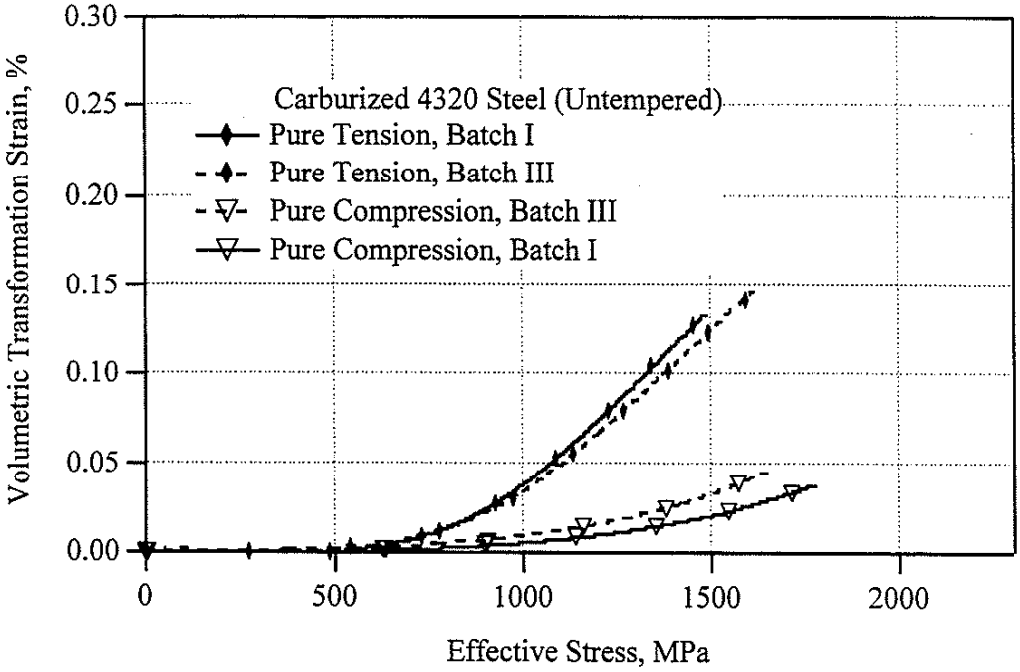

Figure 4.6. Development of volumetric transformation strain for pure tension and pure compression tests of carburized 4320. Specimens are only quenched.

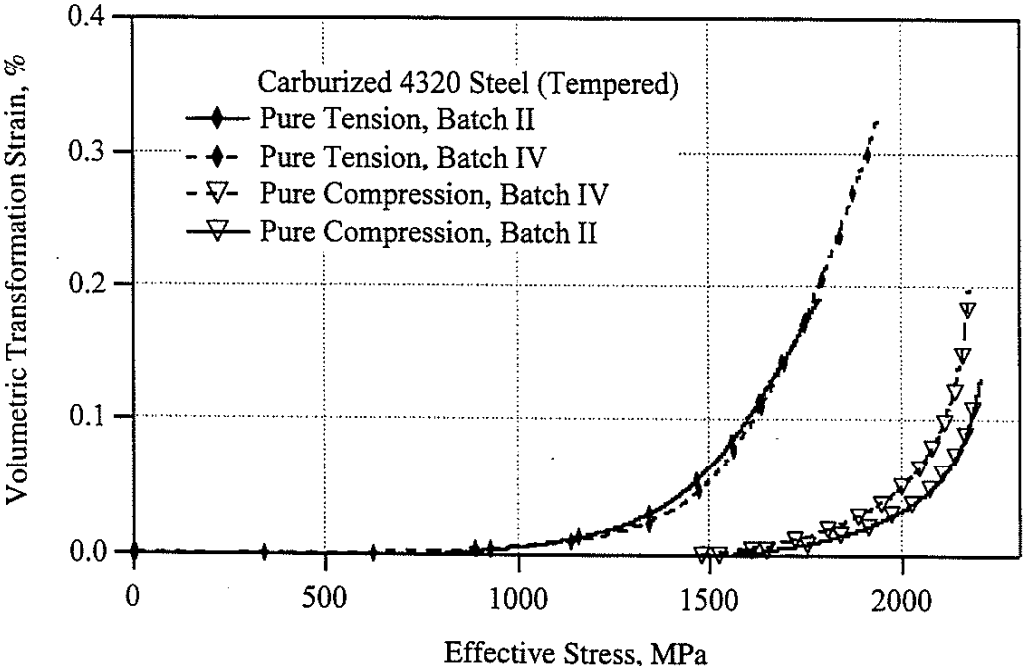

Figure 4.7. Development of volumetric transformation strain for pure tension and pure compression tests of carburized 4320. Specimens are tempered.

The effective stress-effective inelastic strain results for different triaxial stress states are shown in Figure 4.8 and 4.9. In untempered material the triaxial stress state results lie above the corresponding responses from the uniaxial stress states. However, in tempered material, the triaxial stress state results lie between the uniaxial tension and compression extremes.

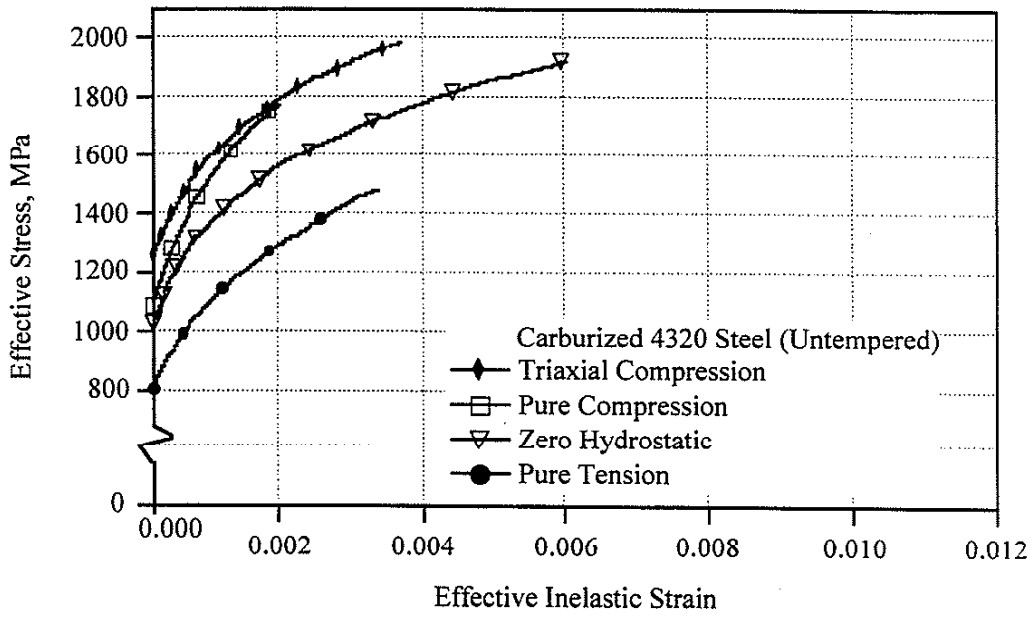

Figure 4.8. The effective stress-effective inelastic strain curves of carburized 4320 steel as a function of applied stress state. Specimens were austenitized at 955 ^{0}C and only quenched.

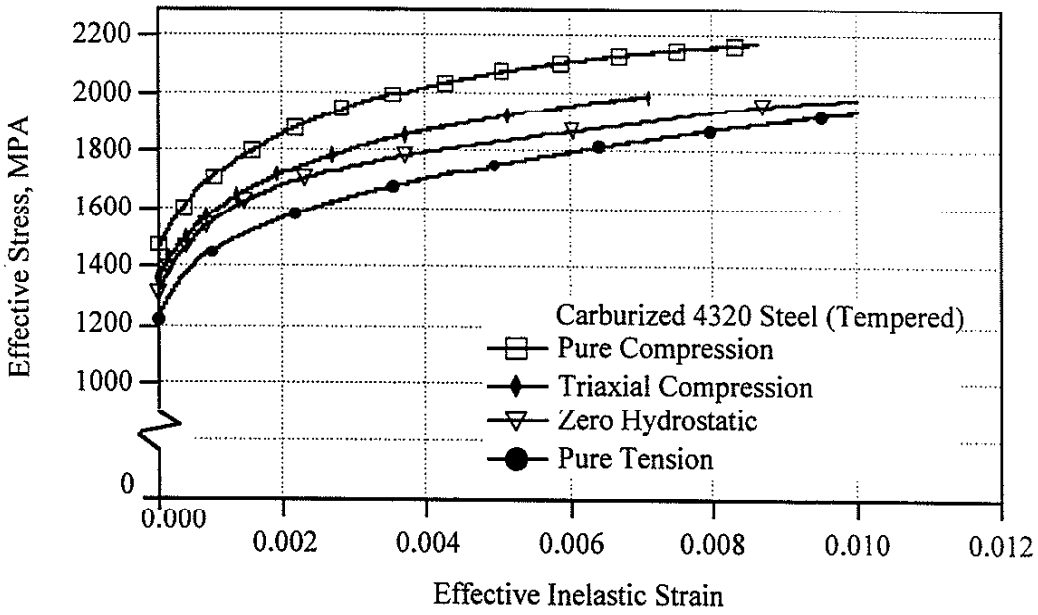

Figure 4.9. The effective stress-effective inelastic strain curves of carburized 4320 steel as a function of applied stress state. Specimens were austenitized at 845 ^{0}C for 1 hour and tempered at 177 ^{0}C for 1.5 hours.

The last two plots, figures 4.10 and 4.11, show the triaxiality and hydrostatic stress dependence of the effective flow stress for all the carburized 4320 cases investigated. In general the flow stress increases with decreasing triaxiality or hydrostatic stress. Note that all the data points represent tests conducted at constant triaxiality, and not the more common case of axial tests conducted under constant pressure.

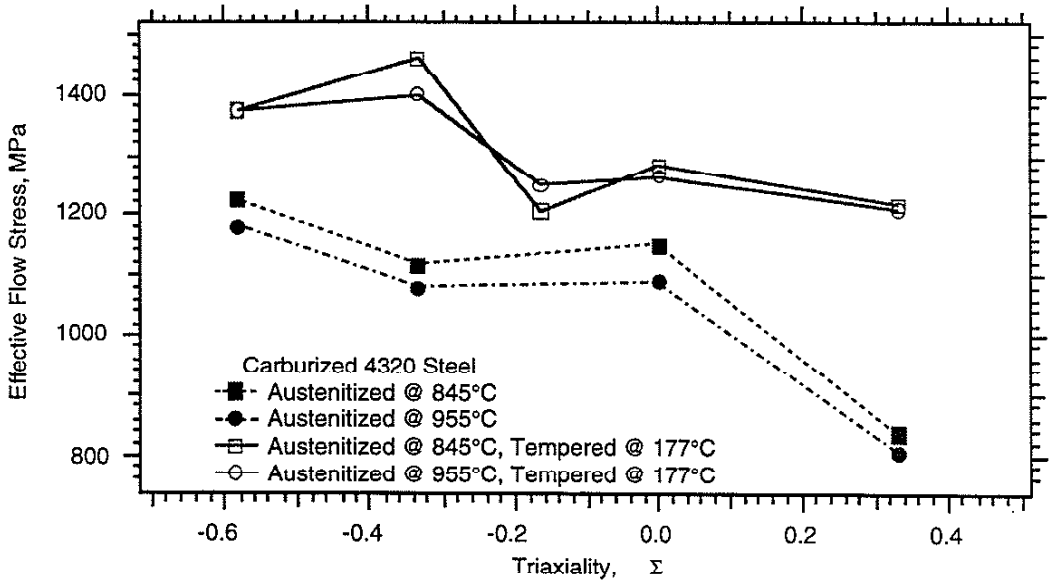

Figure 4.10. The effective flow stress for carburized 4320 steel as a function of triaxiality. Flow stress is calculated using a 0.025% offset method.

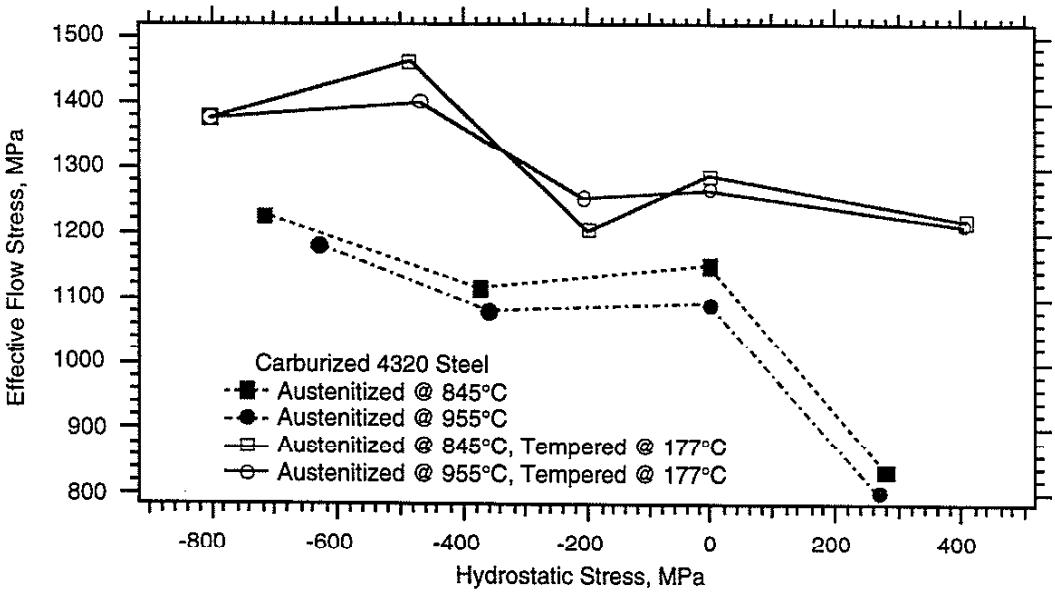

Figure 4.11. The effective flow stress for carburized 4320 steel as a function of hydrostatic stress. Flow stress is calculated using a 0.025% offset method.

4.5 Discussion of Results

The experiments conducted in this investigation have provided much insight into the understanding of the stress state effects on the stress-assisted martensitic transformation of carburized steels. The volumetric transformation strain and the plastic strain became non-zero at the same applied stress level, implying that the transformation is responsible for the initial yield behavior. The effective stress-effective inelastic strain results for different triaxial stress states revealed the differences in initial flow stresses between tempered and untempered specimens. Comparison of the initial yield strengths under tension and compression with previous results on similar material with 35% initial retained austenite [2] indicated that the greater the initial retained austenite content, the lower the flow stress and the earlier the transformation starts. It is evident from Figures 4.2, 4.3, 4.6 and 4.7 that the retained austenite is less stable under tensile loading conditions than under compressive loading.

The increase in strength and ductility in tempered specimens (see Figs. 4.2 and 4.3) was attributed to the effect of increasing the density of fine transition carbides in the martensitic structure. After quenching, low temperature tempering (150-200 °C) causes these fine transition carbides to precipitate in the martensite crystals, reducing the carbon content of the martensite. The martensite gains toughness [27], but the retained austenite content remains unchanged [28]. The overall strength improves as the fine carbides now act as obstacles to dislocation motion. Thus the only microstructural change during tempering occurs within the martensite plates on a very fine scale.

Austenitization treatments after carburizing reduce the as-quenched retained austenite content [27]. If the treatment is performed between A_1 (lower critical temperature) and A_{cm} (upper critical temperature) carbide particles might be retained, thereby reducing the carbon content of the austenite [22], which increases the M_S temperature. Retained carbide particles also restrain austenite grain growth and result in a fine austenite grain size. The 845 °C austenitization temperature used for some specimens was chosen to lie between A_1 and A_{cm}. Higher austenitization temperatures produce relatively higher retained austenite contents than those generated at lower austenitization temperatures [26]. The 955 °C austenitization temperature used for some specimens was chosen to lie above A_{cm}. Therefore we expected to observe more stress-assisted martensitic transformation in specimens austenitized at 955 °C. Unfortunately, the stress-strain plots show that the differences between the two treatments were not very notable. The small differences in the initial retained austenite contents were not enough to cause profound effects in the stress-strain behaviors.

The differences in the volumetric transformation strains in Figures 4.6 and 4.7 between tempered and untempered specimens were attributed to higher stress levels attained before fracture in the tempered case. The similar retained austenite contents between specimens having two distinct austenitization treatments led to the very small differences in volumetric transformation strains.

We have mentioned that the differences in stress-strain responses observed under various stress states, as in Figures 4.8 and 4.9, can be attributed to the amount and the stability of the retained austenite. But these differences can also be explained by a crystallographic approach. It is known that transformation only occurs along specified directions in a given crystallographic system [29] while slip may occur along conjugate directions in a slip system depending on the direction and amount of the applied stress. In some stress states there are a larger number of favorable martensite variants available for the transformation. Moreover, it is believed that retained austenite exists due to strong martensite plates interfering to create confining internal stresses which prevent the austenite from attaining the volume expansion required for transformation to martensite [27,30]. From these two approaches, two possible arguments can be inferred. Firstly, that different stress states activate a different number of variants for each grain during transformation, leading to a distinct stress-strain response for each stress state. Secondly, applied stress states either trigger or suppress the transformation by respectively assisting or opposing the previously existing internal stresses that the martensite plates have imposed on the austenite phase.

4.6 Conclusions

1. The monotonic stress-strain response of carburized 4320 steel with an average of 15% retained austenite is dependent on the applied stress state at room temperature. The most favorable stress state for stress-assisted transformation of austenite is tension. Much less transformation was observed under uniaxial compression and triaxial compression.

2. For a given stress state, the initial flow stress of the low temperature tempered specimens was higher than that of the untempered specimens. This difference was attributed to the amount and the stability of the retained austenite (the greater the initial retained austenite content, the lower the flow stress and the earlier the transformation starts), and to the effect that tempering has in increasing the density of the carbide precipitates in martensitic structures. Both tempered and untempered specimens showed the same trend with respect to hydrostatic stress.

3. The volumetric transformation strain and the plastic strain became non-zero at the same applied stress level, implying that the transformation is responsible for the initial yield behavior.

4. . The flow stress increases with decreasing triaxiality or hydrostatic stress.

5. Crystallographic effects combine with different stress states to activate a different number of variants for each grain during transformation, leading to a distinct stress-strain response for each stress state.

List of References

1. C.S. Roberts, *J. Metals Trans. A.I.M.E.* **203** (1953).
2. R. Neu and H. Sehitoglu, *Acta Metall. Mater.* **40**, 2257 (1992).
3. R. Neu and H. Sehitoglu, *Metall. Trans.* **22A**, 1491(1991).
4. S.A. Kulin, M. Cohen and B.L. Averbach, *J. Metals* **4**, 661 (1952).
5. J.R. Patel and M. Cohen, *Acta Metall.* **1**, 531 (1953).
6. G.B. Olson and M. Cohen, *J. Less-common Metals* **28**, 107 (1972).
7. R.H. Richman and R.W. Landgraf, *Metall. Trans.* **6A**, 955 (1975).
8. M. Cohen and C. M. Wayman, *Metallurgical Treatises* (edited by J.K. Tien and J.F. Elliot), 445, T.M.S.-A.I.M.E. (1981).
9. E. Gautier, J.S. Zhang and X.M. Zhang, *J. De Physique IV* **5**, C8-41 (1995).
10. R.G. Stringfellow, Ph.D. Thesis, Massachusetts Institute of Technology, Cambridge, MA (1990).
11. M.A. Zaccone, G. Krauss, *Metall. Trans.* **24A**, 2263 (1993).
12. G.N. Haidemenopoulos, M. Grujicic, G.B. Olson and M. Cohen, *Acta Metall.* **37**, 1677 (1989).
13. P.G. McDougall, C.M. Wayman, Martensite (edited by G.B. Olson and W.S. Owen)), 59, ASM International (1992).
14. Z. Nishiyama, *Martensitic Transformation.* Academic Press, London (1978).
15. C.C. Young, Ph.D. Thesis, Massachusetts Institute of Technology, Cambridge, MA (1988).
16. K. Jacobus, H. Sehitoglu and M. Balzer, *Metall. Trans.* **27A**, 3066 (1996).
17. K. Gall, H. Sehitoglu, H.J. Maier and K. Jacobus, *Met. and Mater. Trans.*, in press.
18. M.W. Burkart, T.A. Read, *Trans. Met. Soc. AIME* **197**, 1516 (1953).
19. E. Patoor, M. El Amrani, A. Eberhardt, M. Berveiller, *J. De Physique IV* **5**, C2-495 (1995).
20. R.S. Hyde, G. Krauss, D.K. Matlock, *Metall. Trans.* **25A**, 1229 (1994).
21. G. Krauss, D.K.Matlock, *J. De Physique IV* **5**, C8-51 (1995).
22. G. Krauss, *ISIJ International* **35**, 349 (1995a).
23. G.R. Speich, K.A. Taylor, Martensite (edited by G.B. Olson and W.S.Owen), ASM International (1992).
24. S.G. Glover, *J. Iron Steel Inst.* **200**, 102 (1962).
25. R.M. Horn and R.O. Ritchie, *Metall. Trans.* **9A**, 1039 (1978).
26. C.F. Jatzcak, J.A. Larson, S.W. Shin, *Retained Austenite and Its Measurement by X-ray Diffraction*, SP-453. SAE, Warrendale, PA (1980).
27. G. Krauss, *Advanced Materials &Processes* **148**, 7, 48U (1995c).
28. G. Krauss, *Advanced Materials& Processes* **147**, 5, 40Y (1995b).
29. M. Kumosa, *J. Physics* **24**, 1816 (1991).
30. E.J. Klimek, *Metals Eng. Quarterly*, 55 (1975).

5. EFFECT OF STRESS STATE ON THE STRESS-STRAIN BEHAVIOR OF Ni-Ti SHAPE MEMORY ALLOY

5.1 Overview

Using uniaxial and triaxial stress tests, the effect of stress state on the character and extent of the stress-induced martensitic transformation in polycrystalline Ni-Ti shape memory alloy was investigated. Tests conducted under different stress states were compared using effective stress and effective strain quantities. A strain offset method was utilized to determine the effective stress required for transformation under a given stress state. Tests conducted under different stress states show that:

(i) despite the negative volumetric strain associated with the austenite-to-martensite transformation in Ni-Ti, the effective stress for the onset of transformation *decreases* with increasing hydrostatic stress,

(ii) effective stress vs. effective strain behavior varies greatly with stress state, and

(iii) austenite in Ni-Ti is fully stable under large values of compressive hydrostatic stress.

5.2 Introduction

Due to its high strength, high stiffness, chemical inertness and strain recoverability, polycrystalline Ni-Ti is currently the most widely utilized shape memory alloy system. Though recently discovered (in 1963) [1], it is seeing increasing widespread use, in applications ranging from orthodontics to aircraft hydraulic fittings. However in this case, materials science has not yet caught up with technology: there is still very little known about the effect of stress states other than tension on its stress-strain behavior.

When loaded at temperatures above their Ms temperature, certain shape memory alloys possess the ability to deform as much as 8%, and then, upon removal of the load, return to their original shape. This unique property is called *pseudoelasticity* and it is caused by a reversible, stress-induced transformation from parent phase to martensite.

Normally, the large strains associated with stress-induced martensitic transformations can only be accommodated through plastic deformation of the martensite phase. This plastic

deformation damages the martensite, rendering it unable to easily transform back to its parent phase. Therefore, general stress-induced martensitic phase transformations are found to be irreversible. However, there exists a special class of materials called shape memory alloys that exhibit reversible stress-induced martensitic transformations. Instead of accommodating transformation shape changes by dislocation motion, their *thermoelastic* martensitic transformations employ a twinning-type mechanism to accommodate the transformation strains. Upon removal of the applied loading, detwinning of the stress-induced martensite occurs in reverse order of its formation. Through this mechanism, the material returns to its undeformed state.

Figure 5.1 shows a somewhat idealized pseudoelastic stress-strain curve for a uniaxially loaded polycrystalline shape memory alloy.

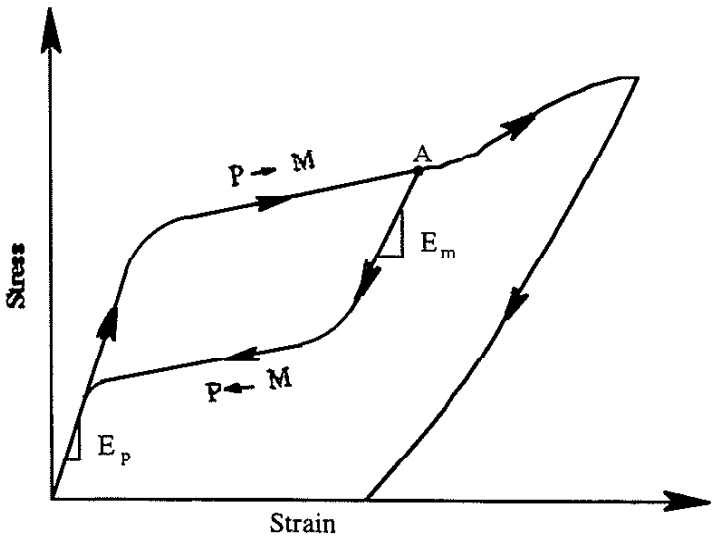

Figure 5.1 Representative stress-strain curve for a polycrystalline shape memory alloy displaying pseudoelasticity. Parent and martensite moduli are indicated.

As the load is initially placed upon the specimen, the material displays the elastic modulus of the parent phase. Flow begins due to the onset of transformation, and continued transformation from parent to martensite is characterized by a reduced modulus. In a polycrystalline specimen with random grain orientation, favorably oriented grains transform at low applied stress levels, less favorably oriented grains transform at higher levels. These combine to produce a monotonically increasing curve. If the specimen is loaded past the point at which transformation is complete, deformation continues by slip mechanisms. If the specimen is unloaded at point A before slip commences, a linear region is first seen with a slope equal to the martensite modulus. Upon further unloading, the slope changes dramatically, indicating the reversion of the stress induced martensite to its parent phase. The final recovery traces the same curve as the initial loading and is once again the linear-elastic response of the parent phase. In reality, polycrystalline specimens are

rarely able to fully recover pseudoelastic strains because of irreversible deformation processes in the martensite structures (grain boundary slip, intergranular cracking).

Much effort has been devoted to the effect of uniaxial stress *sense* (tension vs. compression) on the pseudoelastic stress-assisted martensitic transformation. The majority of investigators [2-6] find at least some degree of asymmetry between tensile and compressive behavior, with higher stresses being required for the onset of transformation in compression than in tension.

A number of previous investigations [7-9] have considered the effect of stress state on pseudoelastic stress-assisted martensitic transformations, focusing primarily on the effect of hydrostatic compression. The results of these studies indicate that the effect of pressure on martensitic transformation is linked to the volumetric change ($\Delta V = V_m - V_p$) associated with the parent to martensite transformation: hydrostatic pressure normally favors transformations that result in a negative volumetric change and hinders those that result in a positive volumetric change.

The transformation strains give rise to the unique mechanical behavior of Ni-Ti. To optimally utilize this behavior, the governing stress-assisted martensitic transformation in Ni-Ti must be thoroughly understood. This level of understanding requires studies in which both the effective and hydrostatic stresses are systematically changed and the pseudoelastic transformation strains are measured. As no such studies are currently available, the series of uniaxial and triaxial stress-controlled tests on polycrystalline Ni-Ti presented here provides valuable new information.

With this background, the purpose of the present investigation of Ni-Ti is :

(i) to determine the transformation stress in tension, compression and under varying hydrostatic stress levels,

(ii) to establish the stress-strain behavior beyond the initial transformation stress.

5.3 Experimental Techniques

In the Ni-Ti alloy system, only a very limited range of compositions -- 49-51 wt% Ti, balance Ni -- is capable of producing the ordered b.c.c. austenite structure necessary for stress-assisted martensitic transformations. Additionally, in this compositional range, transformation temperatures from -200 to 110 °C can be achieved depending upon the specific heat treatment chosen [10]. With this in mind, a single heat of 50% Ni and 50% (by weight) alloy was purchased from Special Metals Inc. of New Hartford, NY. The heat treatment for all specimens consisted of soaking at 550 °C for 15 minutes followed by quenching in ambient temperature water. This heat treatment was chosen to produce pseudoelastic behavior at room temperature and to avoid the R-phase transformation. It was was conducted by Memry Corporation of Brookfield, CT. The resulting microstructure was polycrystalline with an average grain diameter of 19 microns.

Differential scanning calorimetry was performed on the heat treated Ni-Ti specimen blanks. Ni-Ti samples were tested between temperature limits of -70 and +70 °C; samples were

heated/cooled at a rate of 10°C/min. Average transformation temperatures were as follows: Austenite finish temperature, A_f = 8.6 °C; Austenite start temperature, A_s = -0.3 °C; Martensite start temperature, M_s = -18.1 °C; Martensite finish temperature, M_f = -34.2 °C. [11] (Although "parent phase" is the correct term, many people use the term "austenite" for any pre-martensitic phase, even though austenite is an technically an iron-carbon phase).

After heat treating, a variety of test specimens were machined from the heat treated blanks. For triaxial tests under pressure, specimens had a nominal gage length of 12.7 mm and gage diameter of 5.59 mm (see drawings in Appendix D). For uniaxial tensile testing, cylindrical "dogbone" specimens had a nominal gage length of 25.4 mm and a gage diameter of 7.37 mm. For uniaxial compression testing, constant diameter cylindrical specimens had an overall length of 19.1 mm and a diameter of 11.13 mm.

A summary of experimental conditions is provided in Table 1. Note that five distinctly differing applied stress states were investigated: uniaxial tension (UT), uniaxial compression (UC), hydrostatic compression (HC), zero hydrostatic stress (ZH) and triaxial compression (TC). For

Experiment	Applied Stress State	Hydrostatic Stress	Triaxiality
UT (uniaxial tension)	$\sigma_{ij} = \begin{bmatrix} \sigma & 0 & 0 \\ & 0 & 0 \\ & & 0 \end{bmatrix}$	$\sigma_H = \frac{\sigma}{3}$	$\frac{1}{3}$
UC (uniaxial compression)	$\sigma_{ij} = \begin{bmatrix} -\sigma & 0 & 0 \\ & 0 & 0 \\ & & 0 \end{bmatrix}$	$\sigma_H = -\frac{\sigma}{3}$	$-\frac{1}{3}$
HC (hydrostatic compression)	$\sigma_{ij} = \begin{bmatrix} -\sigma & 0 & 0 \\ & -\sigma & 0 \\ & & -\sigma \end{bmatrix}$	$\sigma_H = -\sigma$	∞
ZH (zero hydrostatic stress)	$\sigma_{ij} = \begin{bmatrix} 2\sigma & 0 & 0 \\ & -\sigma & 0 \\ & & -\sigma \end{bmatrix}$	$\sigma_H = 0$	0
TC (triaxial compression)	$\sigma_{ij} = \begin{bmatrix} -3\sigma & 0 & 0 \\ & -\sigma & 0 \\ & & -\sigma \end{bmatrix}$	$\sigma_H = -\frac{5\sigma}{3}$	$-\frac{5}{6}$

Table 5.1 Experimental stress states.

each of these applied stress states, every test was run from the initial condition of all stress components being (essentially) zero in magnitude. In all stress controlled tests, the stresses were simultaneously, linearly ramped until either the specimen failed, or predetermined strain or machine limits were reached. Thus for the zero hydrostatic stress (ZH) condition the specimen was subjected to simultaneous axial stress and lateral pressure such that the axial stress was tensile in sign with a magnitude equal to twice the instantaneous magnitude of the lateral pressure.

Uniaxial tension tests of Ni-Ti were performed on an Instron Model 1331 servohydraulic test machine operating in axial strain control at room temperature. An MTS 25.4 mm gage length extensometer was used to monitor axial strains and an MTS diametral extensometer was used to monitor specimen diametral strains. Test definition, control and data collection were accomplished by Instron FLAPS software.

Uniaxial compression tests were performed on a MTS 100kip servohydraulic test machine operating in axial load control at room temperature. Axial and diametral strains were monitored by foil strain gages bonded to the specimen gage section. Test definition, control and data collection were accomplished using software written in Labview.

The test apparatus described in chapter 3 was used for triaxial testing.

For all tests, stress and strain data were collected in raw engineering quantities. Uniaxial test data was then converted to true stresses and strains using the following equations:

$$\sigma_{zz}^{true} = \frac{\sigma_{zz}}{(1 + \varepsilon_{rr})^2}$$

$$\varepsilon_{rr}^{true} = \varepsilon_{\theta\theta}^{true} = \ln(\varepsilon_{rr} + 1)$$

$$\varepsilon_{zz}^{true} = \ln(\varepsilon_{zz} + 1)$$

The conversion of pressure test data to true stresses and strains is detailed in chapter 3.

In order to compare uniaxial and triaxial test results, effective stress and strain quantities were calculated using the following equations:

$$\sigma_{eff} = \sqrt{\frac{(\sigma_{zz} - \sigma_{rr})^2 + (\sigma_{rr} - \sigma_{\theta\theta})^2 + (\sigma_{\theta\theta} - \sigma_{zz})^2}{2}}$$

$$\varepsilon_{eff} = \frac{\sqrt{2}}{3}\sqrt{(\varepsilon_{zz} - \varepsilon_{rr})^2 + (\varepsilon_{rr} - \varepsilon_{\theta\theta})^2 + (\varepsilon_{\theta\theta} - \varepsilon_{zz})^2}$$

Volumetric transformation strains were calculated as described in chapter 4. Transformation stresses, $\sigma_{P->M}$, required to bring about the austenite to martensite transformation under test conditions were determined from the axial stress vs. axial strain (effective stress vs. effective strain for triaxial tests) using a 0.001 strain offset.

5.4 Experimental Results

Representative stress-strain curves from the uniaxial tension (UT) and uniaxial compression (UC) experiments are shown in Figure 5.1. In the figure, deformation to strains beyond 0.10 (10%) are shown including unloading behavior to zero stress. When the deformation is driven past the maximum transformation strain (~0.06), plasticity becomes the dominant mechanism and the strains become essentially non-recoverable. Note the enormous tension-compression asymmetry.

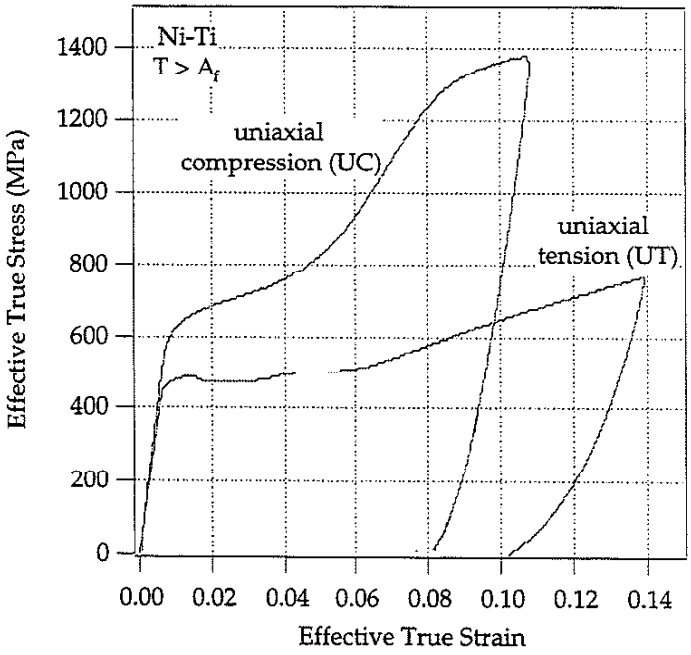

Figure 5.1 Comparison of Ni-Ti behavior in uniaxial tension (UT) and compression (UC).

In order to understand the effect of strain rate on mechanical behavior and to assess its influence in the stress-controlled triaxial tests (in which strain rate was not constant), uniaxial tensile tests with strain rates differing by two orders of magnitude were performed (10^{-4} s^{-1} and 10^{-2} s^{-1}). The results of these tests are provided in Figure 5.2. As the figure indicates, the stresses for the onset of transformation are nearly the same for the different strain rates. The major difference arises in the transformation region (after yield to $\varepsilon = 0.06$), where the high strain rate test shows linear hardening and the low strain rate test shows transformation at a nearly uniform value of stress. (The linear hardening in the high strain rate specimen results from the temperature rise during the transformation - measured to be roughly 8°C - and the resulting increase in stress required to begin the transformation at higher temperatures. Corroborating results have been

reported by previous researchers [12,13]. A nearly constant stress over this region is observed in the low strain rate test - for which the temperature change was negligible).

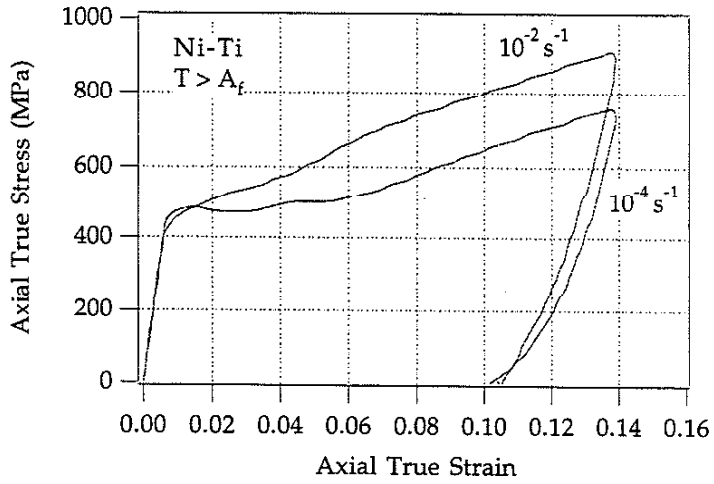

Figure 5.2 Effect of strain rate on uniaxial tensile behavior.

Aside from this difference in hardening behavior in the transformation region, we see that the elastic behavior, the stress for the onset of transformation and the hardening rate in the plasticity dominated region are in agreement for the two strain rates. Thus comparisons on these three points are made with confidence for the stress controlled triaxial tests discussed below.

The first experiment discussed here is the hydrostatic compression (HC) experiment in which the specimen is loaded under identical compressive stress in both the axial and lateral

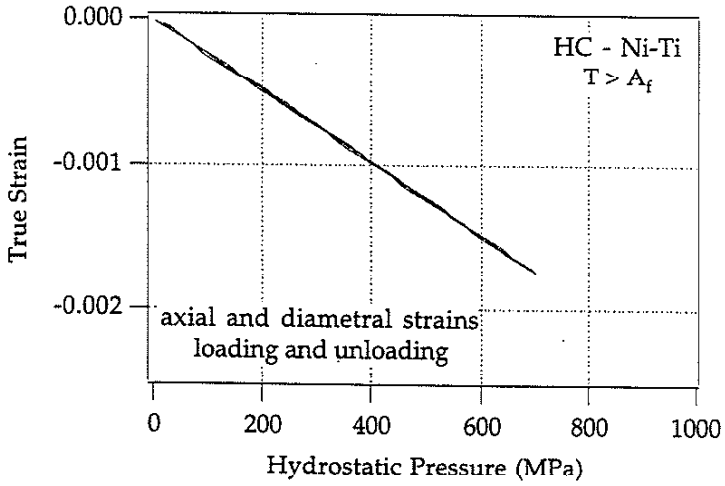

Figure 5.3 HC stress state, true axial and diametral strain vs. hydrostatic pressure.

directions. Under this hydrostatic stress state, linear elasticity predicts the following strain in all directions:

$$\varepsilon = \frac{-P(1 - 2\nu)}{E}$$

Note that the above equation predicts a linear change of strains in all directions and identical paths in loading and unloading. As observed in Figure 5.3, the specimen behavior displays all of these characteristics as well as a slope nearly identical to that computed using average values for elastic modulus and Poisson's ratio (E = 72 GPa, ν = 0.420) gathered from earlier uniaxial tests. As such it can be concluded that the behavior of the specimen up to a hydrostatic pressure of 700 MPa is fully elastic and thus no transformation behavior is observed. Thus hydrostatic pressure of 700 MPa is unable to induce the martensitic transformation in polycrystalline Ni-Ti.

A comparison of representative data from the four remaining stress states (UT, UC, ZH, TC) is provided in Figures 5.4 and 5.5. In Figure 5.4 it is clear that the shapes of the curves differ beyond yield. This difference is predominately the result of the varying strain rates imposed beyond yield (due to the stress-controlled nature of the testing apparatus) and their effect on the stress strain behavior.

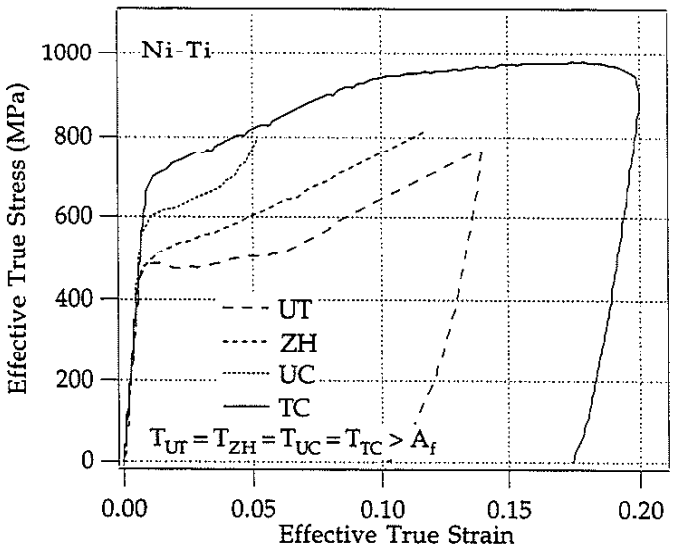

Figure 5.4 Summary of experimental results indicating the role of hydrostatic stress in the stress-strain behavior.

For this reason we focus our attention on the small strain regime where strain rates are nearly identical and use Figure 5.5 to examine the effect of the imposed stress state on the stress required for transformation. Using a 0.001 strain offset method we find that the UT stress state yields first at 422 MPa followed by the ZH stress state at 458 MPa, the UC stress state at 548 MPa and finally

the TC at 658 MPa. Thus the general trend of increasing effective stress for transformation with decreasing hydrostatic component is observed.

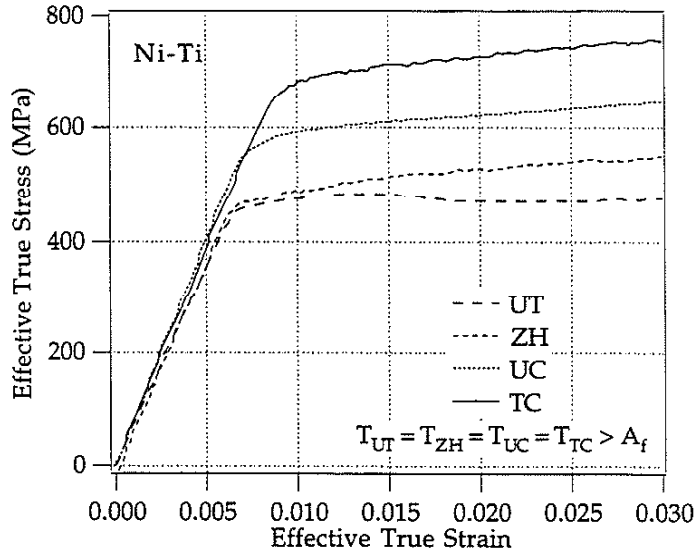

Figure 5.5 Replot of Figure 5.4 focusing on small strain regime.

The dependence on hydrostatic stress is made more clear when replotted as in Figure 5.6. Note that the tension-compression yield asymmetry is particularly striking.

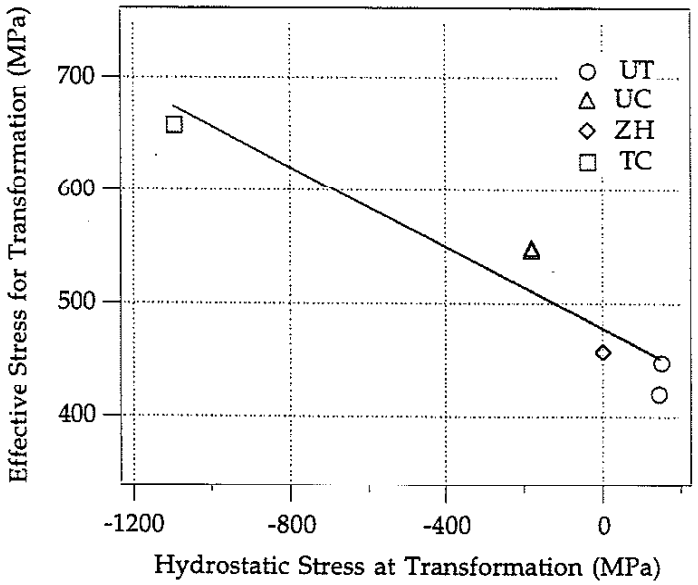

Figure 5.6 Effective stress for transformation as a function of hydrostatic stress component at transformation for differing stress states at 20°C.

Next a cyclic experiment was conducted in which the axial stress and pressure were varied in so that the hydrostatic stress was maintained equal to zero. The principal stress state can be described as $(2\sigma, -\sigma, -\sigma)$.

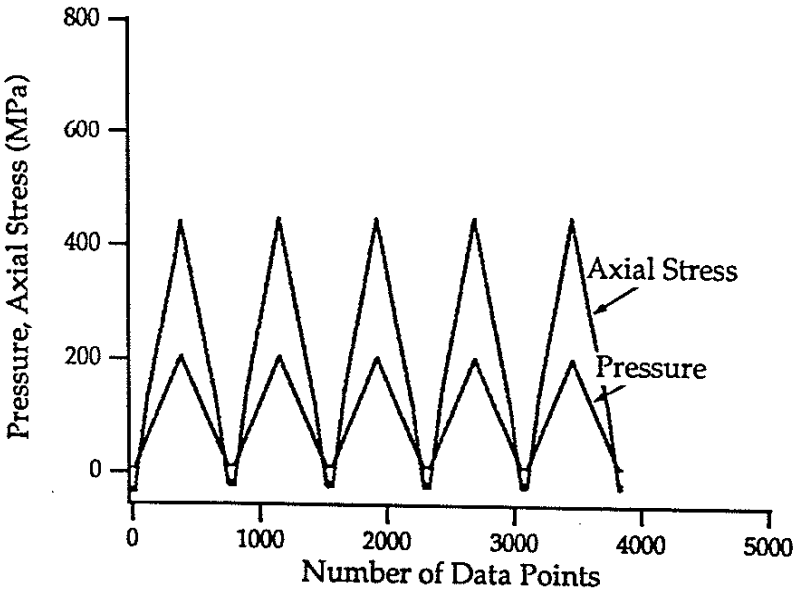

Figure 5.7 Effective stress/axial stress/pressure history during the cyclic experiment.

In Figure 5.7 we note that the axial stress is controlled from a peak value to a slightly negative value, while the pressure also reaches a peak at the same time as the axial stress. The data acquisition rate is 125 Hertz, so the cycle time is approximately 6 seconds.

The cyclic loading is conducted under stress control and therefore ratchetting of the material is expected. We note that the ratchetting strain (both in axial and circumferential directions) rate gradually decreases. This polycrystalline material undergoes stress induced phase transformation which is mostly recoverable at small strains (see Figure 5.8),

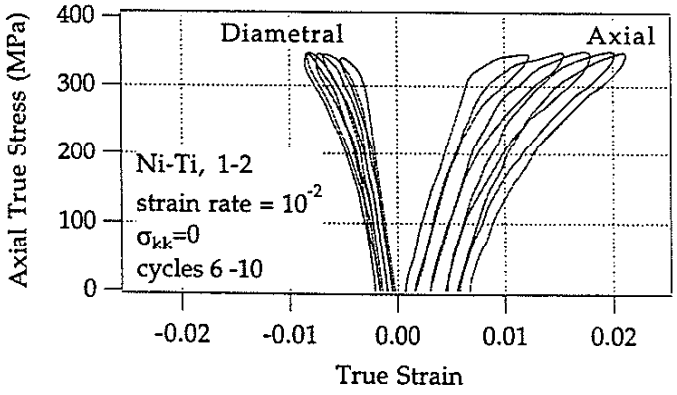

Figure 5.8 Zero hydrostatic stress cyclic experiment.

but non-recoverable at higher strains (see Figure 5.9). The deformation levels presented in Figure 5.9 include a considerable non-recoverable (plastic) strain component.

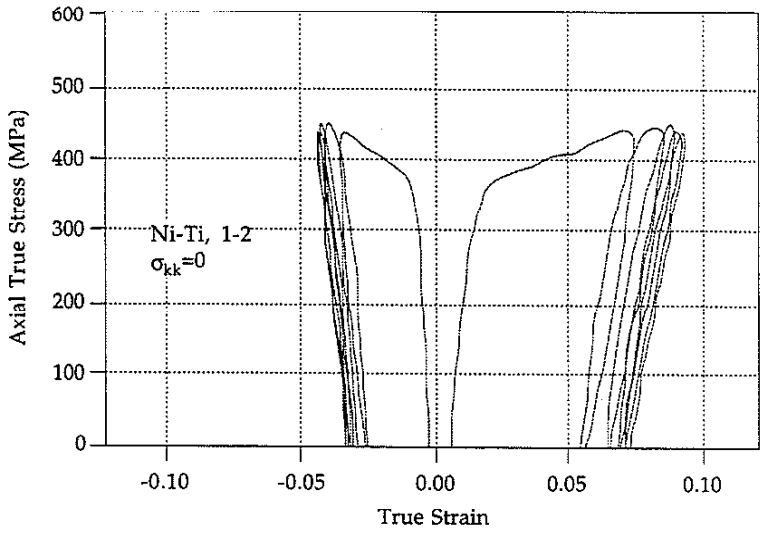

Figure 5.9 Zero hydrostatic stress cyclic experiment.

In Figure 5.10 the output of a thermocouple attached to the specimen shows the temperature rise which occurs as the specimen is strained under pressure. Note that the peak temperature decreases with the amount of plastic strain in the cycle.

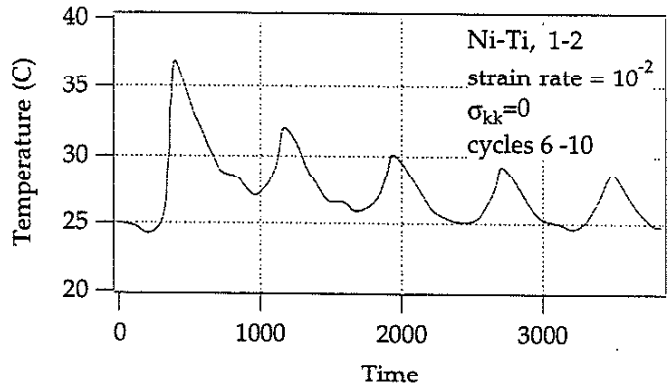

Figure 5.10 Temperature rise in cyclic experiment.

5.5 Discussion of Results

The effect of applied stress *sense* on martensitic transformation was proposed by Patel and Cohen [14] for steels, and numerous models have been proposed in the literature to describe all aspects of the martensitic transformation. It is well recognized that in shape memory alloys that the transformation strains are considerably larger than the hydrostatic strain components. Therefore,

the effect of the hydrostatic stress, or asymmetry between tension and compression should be rather small, and even negligible. The present experimental results, however, show that the effect is considerable and cannot be ignored.

Previous attempts to predict the bending behavior of Ni-Ti have not been successful and the interpretation of bending experiments has been difficult due to the tension-compression asymmetry of these materials. It is clear that the experimental findings in the present work must be addressed fully in any future model expected to predict true material behavior.

The reasons behind the tension-compression assymetry have recently been investigated by Gall [15]. They are believed to stem from the fact that twin formation associated with martensitic transformation is fundamentally different from the dislocation slip processes responsible for plastic deformation in non-shape-memory materials. While both slip and twinning occur in certain specific planes and directions, twinning is essentially unidirectional and cannot occur in conjugate (forward and reverse) directions the way that slip can. Thus, a system (martensite variant) that is favorably oriented to twin under tension, will not be favorably oriented to twin under compression... some other variant must be activated and since it is likely to be less favorably oriented, the stress required to activate it will be necessarily higher. This higher stress in conjugate directions gives rise to the tension-compression assymetry.

In the case of near 50-50 weight % NiTi alloy, the austenite phase takes the form of an ordered b.c.c. superlattice (designated B2) β phase with $a \approx 3$Å [16,17]. With sufficient cooling and/or stress, the β phase in Ni-Ti will, in a diffusionless and shear dominated reaction, transform to martensite. It is accepted that the Ni-Ti martensite is a monoclinic distortion of a B19 lattice ($a \approx 2.883$Å, $b \approx 4.623$Å, $c \approx 4.117$Å, $\gamma \approx 96.8°$) [18,19]. Calculations based on the lattice parameters of the austenite and martensite crystal structures in Ni-Ti indicate that the austenite to martensite transformation in Ni-Ti results in a shear strain, g, of 0.13 and a volume change, $\Delta V^{tr}/V$, of -0.0034 [20].

During the low and high strain-rate UT experiments both the axial and diametral strain were monitored, and the volumetric transformation strains were determined. Upon completion of the stress-induced transformation, the values of volumetric transformation strain were found to be -0.0037 and -0.0031, respectively. These values are in exceptionally strong agreement with the expected value of -0.0034 calculated from lattice constants.

The Clausius-Clapeyron equation predicts that decreasing hydrostatic stress should decrease the effective stress necessary for transformation in materials which have negative volume changes during dransformation. However, the experiments described here show the opposite effect. This can be explained due to stress-state-dependent crystallographic effects which overshadow the dependence of the transformation behavior on the volume change during the transformation [21].

5.6 Conclusions

The experimental results from polycrystalline specimens of Ni-Ti support the following conclusions:

1.) The stress required to begin the stress-assisted martensitic transformation in polycrystalline Ni-Ti is significantly greater in uniaxial compression than in uniaxial tension. The remarkable difference in the hardening behavior after the conclusion of transformation for tension and compression cases points out that the martensite flow behavior is distinctly different in tension versus compression, at least in the high strain regime.

2.) Raising the strain rate caused the specimen temperature to rise. The elevated temperature increased the stress required to sustain the austenite to martensite transformation in polycrystalline Ni-Ti, and these increases are consistent with predictions from the Clausius-Clapeyron equation.

3.) Austenite in Ni-Ti does not transform under compressive hydrostatic stress of up to -700MPa.

4.) Over the range of stress states examined, there appears to be a linear relationship between the hydrostatic stress and the effective stress to begin transformation: the effective stress required to induce pseudoelastic martensite in polycrystalline Ni-Ti increases with decreasing values of hydrostatic stress. This occurs despite the contrary predictions of the Clausius-Clapeyron equation, and is attributed to stress-state-dependent crystallographic effects.

5.) The capabilities of the pressure test apparatus were proven via several short cyclic tests in which both pressure and axial stress were varied in phase. 5 cycles were run at several different stress/pressure levels, each corresponding to zero hydrostatic stress. A thermocouple was used to measure specimen temperature during loading under pressure. Small pseudoelastic strains were seen to recover while large plastic strains were permanent.

List of References

1. Buehler, W.J., J.V. Gilfrich, and R. C. Wiley, "Effect of Low Temperature Phase Changes on the Mechanical Properties of Alloys Near Composition TiNi," *J. Appl. Phys.*, 1963, vol. 34, pp. 1475-1477.
2. M. W. Burkart and T. A. Read: *Trans. Met. Soc. AIME*, 1953, vol. 197, pp. 1516-1524.
3. H. Sakamoto, M. Tanigawa, K. Otsuka and K. Shimizu: *Proceedings. International Conference on Martensitic Transformations*, ICOMAT 79, Cambridge, MA, 1979, pp. 633-638.
4. P. Vacher and C. Lexcellent: *Proceedings, Mechanical Behavior of Materials IV*, M. Jono ed., Plenum Press, New York, NY, 1991, pp. 231-236.
5. P. Roumagnac, Thesis, Université Technologique de Compiegne, France, 1993.
6. E. Patoor, M. El Armani, A. Eberhardt, and M. Berveiller: *J. de Physique IV*, vol. 5, pp. C2-495 -500, 1995.
7. Y. Gefen, A. Halwany and M. Rosen: *Phil. Mag.*, 1973, vol. 28, pp. 1-9.
8. T. Kakeshita, Y. Yoshimura, K. Shimizu, S. Endo, Y. Akahama, and F. E. Fujita: *Trans. JIM*, 1988, vol. 29, pp. 781-789.
9. T. Kakeshita, K. Shimizu, S. Nakamichi, R. Tanaka, S. Endo, and F. Ono: *Mat. Trans. JIM*, 1992, vol. 33, pp. 1-6.
10. T. W. Duerig, A. R. Pelton: Materials Properties Handbook, Titanium Alloys, ASM International, Metals Park, OH, 1994, pp. 1035-1048.
11. M. Wu : private communication, 1995.
12. K. Mukherjee, S. Sircar and N. B. Dahotre: *Mater. Sci. and Eng.*, 1985, vol. 74, pp. 75-84.
13. P. H. Leo, T. W. Shield and O. P. Bruno: *Acta Metall. Mater.*, 1993, vol. 41, pp.2477-2485.
14. Patel, J. R and Cohen, M., 1953, Criterion for the Action of Applied Stress in the Martensitic Transformation, Acta Metallurgica, 1, 531
15. Gall, K. A., The Effect of Stress State and Precipitation on Stress-Induced Martensitic Transformations in Polycrystalline and Single Crystal Shape Memory Alloys: Experiments and Micro-Mechanical Modeling. PhD Thesis, UIUC, Urbana, IL 1998
16. A. Nagasawa: *J. Phys. Soc. Jpn.*, 1970, vol. 29, p. 1386-1391.
17. J. Perkins: *Metals Forum*, 1991, vol. 4, pp. 153-163.
18. K. Otsuka, T. Sawamura and K. Shimizu :*Phys. Status Solidi (a)* , 1971, vol 5, pp. 457-462.
19. R.F. Hehemann and G.D. Sandrock: *Scripta Met.*, 1971, vol. 5, pp. 801-805.
20. K. Okamoto, S. Ichinose, K. Morii, K. Otsuka, and K. Shimizu: *Acta Met.*, 1986, vol. 34, pp. 2065-2073.
21. Patoor, E., M. El Amrani, A. Eberhardt and M. Berveiller: *J. Phys. IV*, 1991, vol 5, no. C2, pp. 495-500.

6. EFFECT OF STRESS STATE ON THE STRESS-STRAIN BEHAVIOR OF 4340 STEEL

6.1 Overview

The effect of different stress states on the stress-assisted martensitic transformation of retained austenite was investigated in 4340 steel in two different heat treat conditions. Utilizing conventional servohydraulic test machines as well as a specialized pressure test apparatus, monotonic experiments were conducted on specimens with different austenitization and tempering histories to compare the stress-strain behavior under various stress states. Experimental results indicated asymmetry between tension and compression, and pressure dependent yield behavior and stress-strain behavior. As triaxiality values decreased, larger effective stress magnitudes were required to begin transformation. The highest yield strength level was observed for the Batch 1 material tested under triaxial compression.

6.2 Introduction

Spitzig *et al.* was the first to make an extensive study into the stress-strain behavior of 43 series steel specimens under a variety of stress states [1]. Their material was a forged and normalized 4330, which they austenitized at 900°C and quenched into agitated, iced brine and then liquid nitrogen in an effort to completely transform the steel to martensite. After tempering at 260°C for 1 hour, the retained austenite content was measured to be less than 0.01%. Conventional monotonic tension and compression tests were conducted at atmospheric pressure, but they also used a modernized copy of Pugh and Green's 1954 Type I pressure test apparatus to conduct monotonic tension and compression tests at constant pressures of 20,000, 40,000, 80,000, 120,000, and 160,000 psi. Since they were interested in the initial flow behavior, all tests were stopped when a maximum of 4% strain was reached.

In 4330, Spitzig *et al.* found that the strength in compression was 5.5% higher than in tension (see figure 6.1), and that neither this result nor the strain hardening characteristics were affected by constant pressure (see fig 6.2). However, pressure did affect other quantities: they

found that testing under constant pressure raised the stress-strain curve and they measured a larger pressure dependence of the yield strength than Pugh and Bridgman observed in mild steels. Nevertheless, their goal was to test a material that could *not* transform.

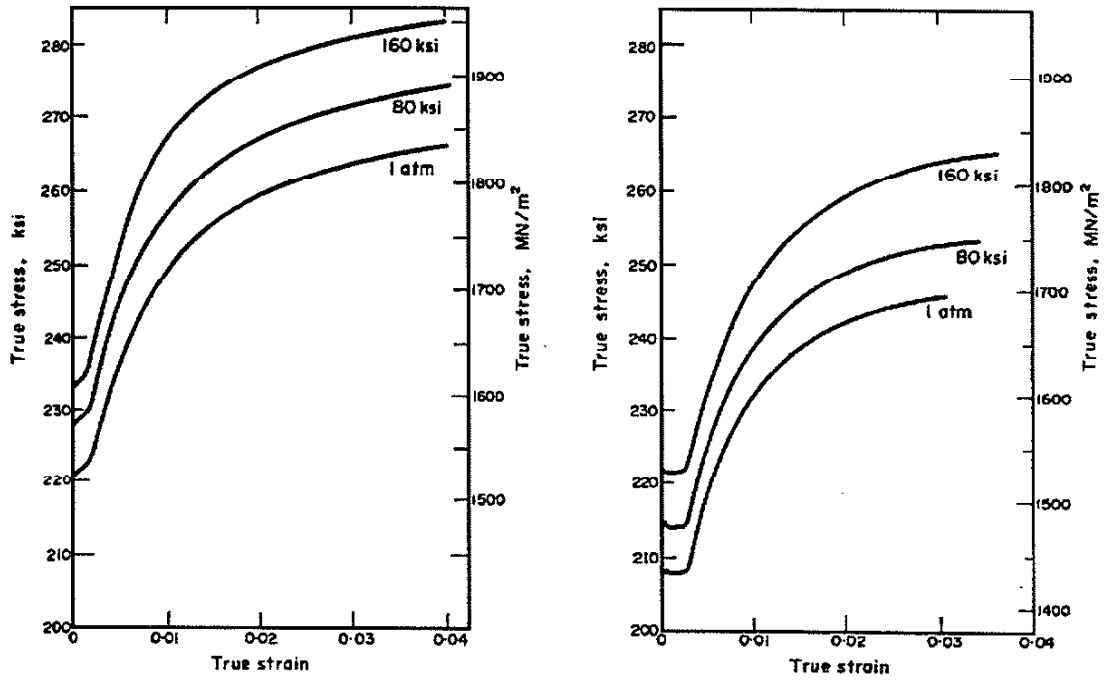

Figure 6.1: Effect of hydrostatic pressure on the tensile (left) and compressive (right) stress-strain curves for Q&T 4330 steel [1] Note the tension-compression asymmetry.

In 1988, Haidemenopoulis *et al.* set about to find the M_S^σ temperature of a 4340VAR steel by determining the temperature dependence of the elastic limit [2]. Their 4340VAR steel (0.4C, 0.46Mn, 0.28Si, 1.74Ni, 0.89Cr, 0.21Mo, wgt %) was austenitized at the relatively high temperature of 1200°C for 1 hour, then oil quenched and tempered at 200°C for 1 hour. The high austenitizing temperature was chosen to ensure solution of all the carbon and other alloying elements, so as to produce a material with a low M_S temperature and higher-than-normal retained austenite levels. They measured 9% retained austenite in their samples.

Their method for determining the M_S^σ temperature relied on the hypothesis that stress-assisted transformation of retained austenite to martensite, not dislocation slip, was responsible for and would indicate the elastic limit. If the stress-assisted transformation occured at lower stresses than was necessary to initiate slip, the transformation strains could be measured and would display their characteristic Clausius-Clayeyron temperature dependence. They tested their samples in uniaxial tension at temperatures between 20 and 50°C and successfully found the cusp in the uniaxial stress vs temperature plot (at 40°C) corresponding to the boundary between stress-assisted

and strain-induced modes of transformation - the M_S^{σ} temperature (see figure 2.23). Based on their uniaxial tension test results, Haidemenopoulis *et al.* developed a model which predicted the initial yielding due transformation of the retained austenite.

In an attempt to bridge the gaps in the existing works, a series of experiments were conducted on 4340VAR specimens which were given the same heat treatment used by Haidemenopoulis *et al.* These include uniaxial compression and a number of triaxial stress-states spanning a wide range of hydrostatic stress levels. These experiments, described in the next section, provide a wealth of data which can be used to test the range of applicability of the Haidemenopoulis and Stringfellow[3] models and/or permit the observed hydrostatic stress dependence of the transformation (or elastic limit) to be included. Additionally, to further expand the 4340VAR database, 4340VAR in a more conventional heat treatment condition was also tested.

6.3 Experimental Techniques

12.5mm thick, cross (hot) rolled plates from a single heat of 4340VAR steel were obtained from the US Army Research Laboratory in Watertown, MA. The plates were cut into specimen blanks along the rolling direction. Two different batches were prepared, as described in Table 6.1. The blanks were separated into 2 batches. Batch 1 was austenitized at 1200°C, above A_{cm} (upper critical temperature), in a protective atmosphere for 1 hour, oil quenched and then tempered at 200°C for 1 hour (hardness was approximately Rc 50). The quench from 1200°C is a severe one and several of the specimen blanks cracked during quenching. Batch 2 was austenitized at 840°C, below A_{cm}, in a protective atmosphere for 1 hour, oil quenched and then tempered at 535°C for 1 hour (hardness was approximately Rc 40). The specimens were machined to final dimensions utilizing a slow grinding process, and then polished.

Batch I.D.	Austenitizing parameters	Tempering parameters
I	1 hour @ 1200 °C	1.0 hour @ 200 °C
II	1 hour @ 840 °C	1.0 hour @ 535 °C

Table 6.1. Summary of specimen heat treatments. All specimens were quenched in oil.

Both uniaxial and triaxial experiments were conducted at 20 °C. Uniaxial tests were performed on an Instron 1331 servohydraulic test machine operating in axial strain control at a strain rate of 10^{-4} s^{-1}. MTS extensometers measured both axial and diametral strains. During all experiments, the axial load, axial strain, diametral strain (and pressure in triaxial tests) were stored via computer. The test apparatus described in chapter 3 was used for triaxial testing.

It has been proposed that the thermodynamic driving force and nucleation rate depend on the "triaxiality" of the stress state where (see chapter 2):

$$\Sigma = \frac{\sigma_H}{\sigma_{eff}}$$

In the following set of experiments, the specimens were deformed while maintaining Σ constant (pressure proportional to σ_z) to establish the evolution of transformation strains as a function of the tensile principal stress, σ_z.

Pressure P	Axial Stress σ_z	Hydrostatic Stress σ_H	Triaxiality Σ
0	$\sigma_z > 0$	$\sigma_z / 3$	1/3
0.5 σ_z	+2 p	0	0
σ_z	+	-1/3 p	-1/6
σ_z	+ p	-1/3 p	-1/6
0	$\sigma_z < 0$	$\sigma_z / 3$	-1/3
0	$\sigma_z < 0$	$\sigma_z / 3$	-1/3
-0.2 σ_z	-5 p	-7/3 p	-7/12

Table 6.2: Monotonic Pressure Experiments, Batch I

Pressure P	Axial Stress σ_z	Hydrostatic Stress σ_H	Triaxiality Σ
0	$\sigma_z > 0$	$\sigma_z / 3$	1/3
0.5 σ_z	+2 p	0	0
0.5 σ_z	+2 p	0	0
σ_z	+ p	-1/3 p	-1/6
0	$\sigma_z < 0$	$\sigma_z / 3$	-1/3
0	$\sigma_z < 0$	$\sigma_z / 3$	-1/3
-0.3 σ_z	-3.3 p	-5.3/3 p	-.768

Table 6.3: Monotonic Pressure Experiments, Batch II

A summary of stress conditions studied is provided in Tables 6.2 and 6.3. For each of the triaxial stress state experiments, the axial and diametral stresses were ramped from zero initial conditions until either the specimen failed or the machine loading limit was reached. The stresses at

the onset of the austenite to martensite transformation were determined using a 0.00025 strain offset method.

6.4 Experimental Results:

For all tests, stress and strain data were collected in raw engineering quantities. Uniaxial test data was then converted to true stresses and strains using the following equations:

$$\sigma_{zz}^{true} = \frac{\sigma_{zz}}{(1 + \varepsilon_{rr})^2}$$

$$\varepsilon_{rr}^{true} = \varepsilon_{\theta\theta}^{true} = \ln(\varepsilon_{rr} + 1)$$

$$\varepsilon_{zz}^{true} = \ln(\varepsilon_{zz} + 1)$$

The conversion of pressure test data to true stresses and strains is detailed in chapter 3. Volumetric transformation strains were calculated as described in chapter 4.

In order to compare uniaxial and triaxial test results, effective stress and strain quantities were calculated using the following equations:

$$\sigma_{eff} = \sqrt{\frac{(\sigma_{zz} - \sigma_{rr})^2 + (\sigma_{rr} - \sigma_{\theta\theta})^2 + (\sigma_{\theta\theta} - \sigma_{zz})^2}{2}}$$

$$\varepsilon_{eff} = \frac{\sqrt{2}}{3}\sqrt{(\varepsilon_{zz} - \varepsilon_{rr})^2 + (\varepsilon_{rr} - \varepsilon_{\theta\theta})^2 + (\varepsilon_{\theta\theta} - \varepsilon_{zz})^2}$$

Effective stress-effective strain curves for uniaxial compression and tension tests, plus a zero hydrostatic stress triaxial test are shown in Figure 6.2 for the Batch I 4340VAR and in Figure 6.3 for the Batch II 4340VAR. In Figure 6.2 the compressive curve is approximately 7.5% greater than the tensile curve, and pressure is seen to raise the tensile stress-strain curve. The lower flow stress in tension was attributed to stress-assisted transformation of retained austenite to martensite. In Figure 6.2 the compressive curve is approximately 3.3% greater than the tensile curve, and no pressure dependence is seen. The difference in the shape of the curves is due to the different heat treatments.

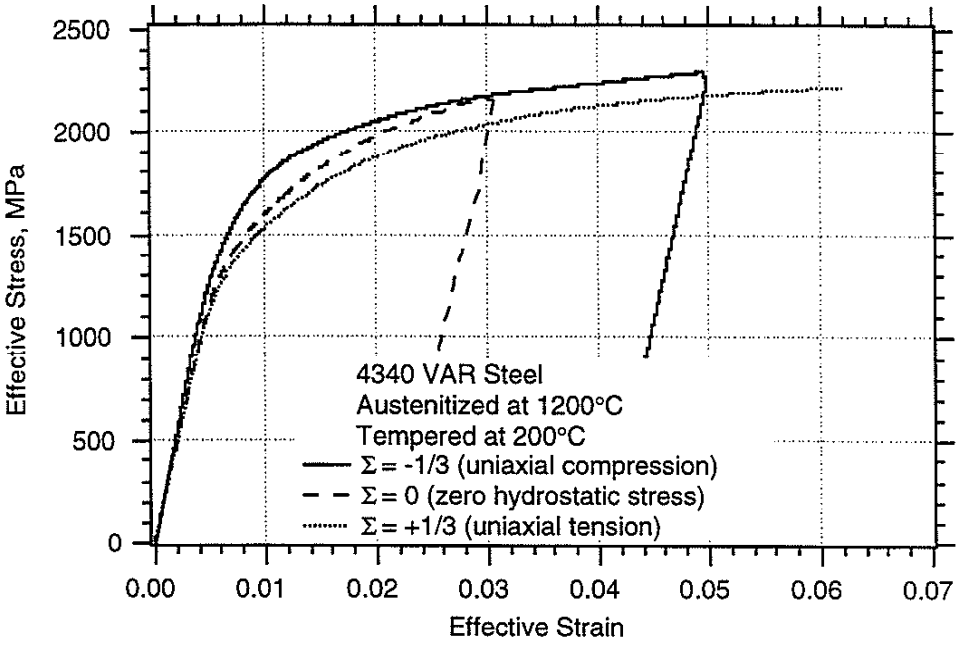

Figure 6.2: Effect of stress state on the stress-strain curves for Batch I Q&T 4340VAR steel.

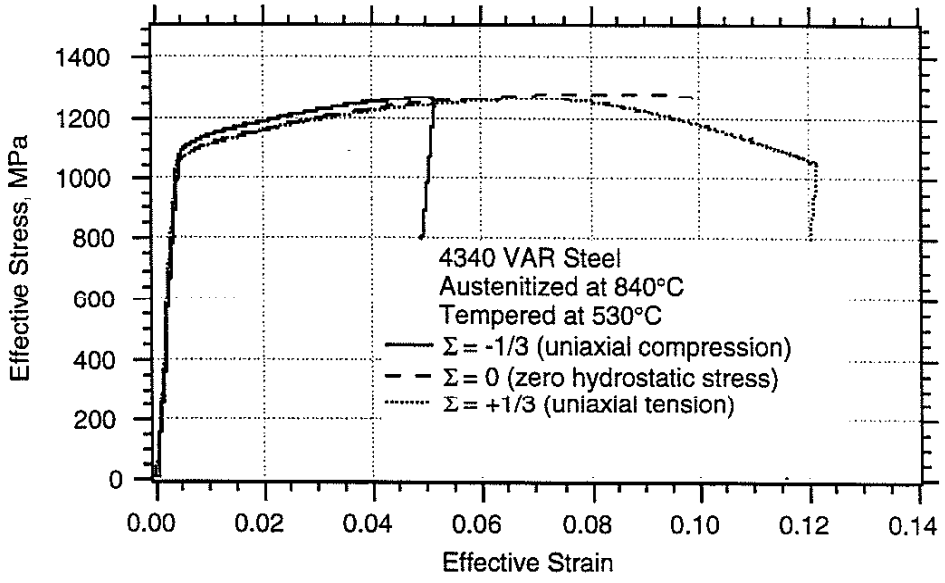

Figure 6.3: Effect of stress state on the stress-strain curves for Batch II Q&T 4340VAR steel.

The volumetric transformation strains were calculated using the methods described in chapter 4. A plot of the volumetric transformation strains vs. effective stress is presented in Figure 6.4. This shows that the effective stress required for the onset of transformation increases as the triaxiality decreases. The initial rate of transformation is seen to be highest for the specimen with the positive triaxiality value.

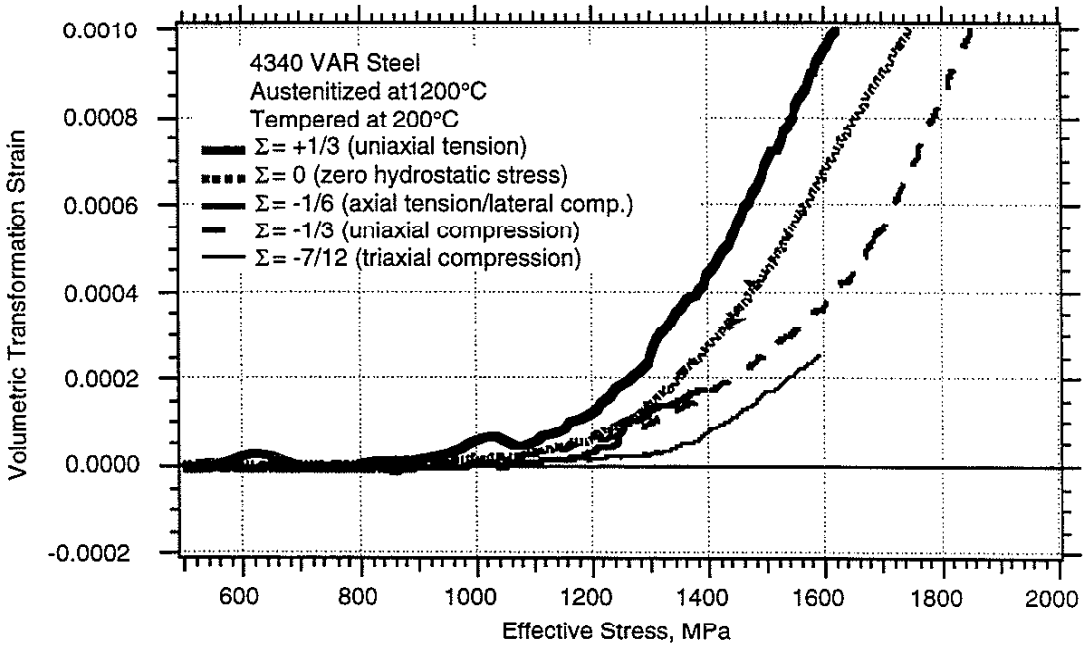

Figure 6.4: Development of volumetric transformation strain for Batch I Q&T 4340VAR steel under a variety of uniaxial and triaxial stress states.

A significant effect observed was that transformation begins when the stress level reaches the elastic limit (see Figure 6.5). This result implies that the transformation is responsible for the initial yield behavior, as is expected in the case of stress-assisted transformations.

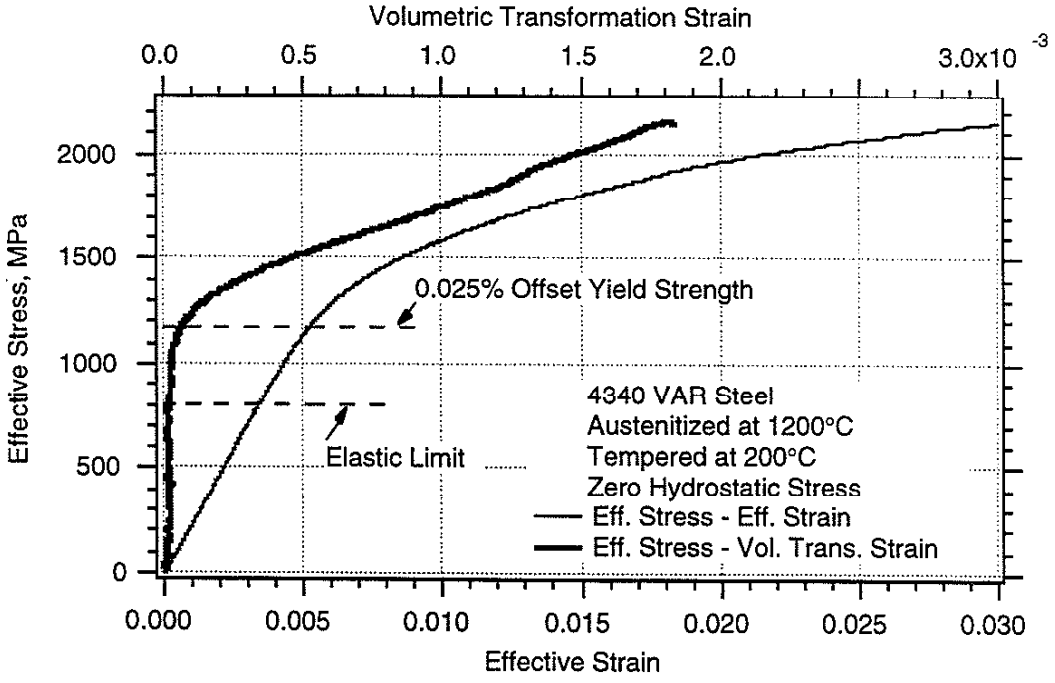

Figure 6.5. Development of volumetric transformation strain for zero hydrostatic stress test of carburized 4320. Note that transformation begins at the elastic limit.

Carrying this idea one step further, the effective flow stress in the microyield regime is plotted vs triaxiality for all the tests run on both batches of 4340VAR steel. This graph, shown in figure 6.6, reveals at once the hydrostatic stress dependence of the microyield strength and the underlying stress dependence of the transformation responsible for the microyielding.

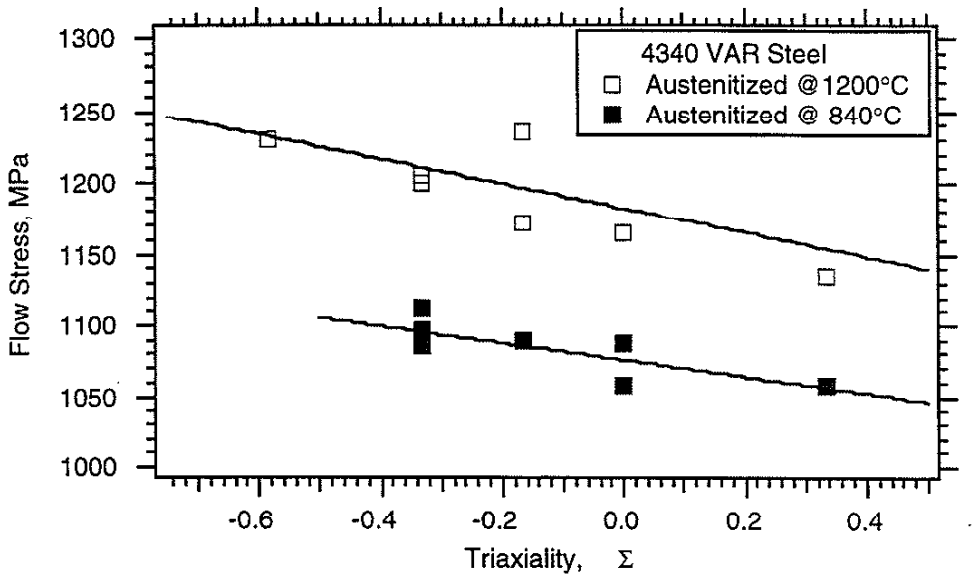

Figure 6.6: Flow Stress vs. Triaxiality for 4340VAR steel.

6.5 Discussion Of Results

Spitzig's *et al.* 4330 tests were as thorough as always, and his results in Figure 6.7 show a linear dependence of yield strength on hydrostatic stress. Additionally, he found the tension-compression asymmetry to be independent of hydrostatic pressure (see Figure 6.1).

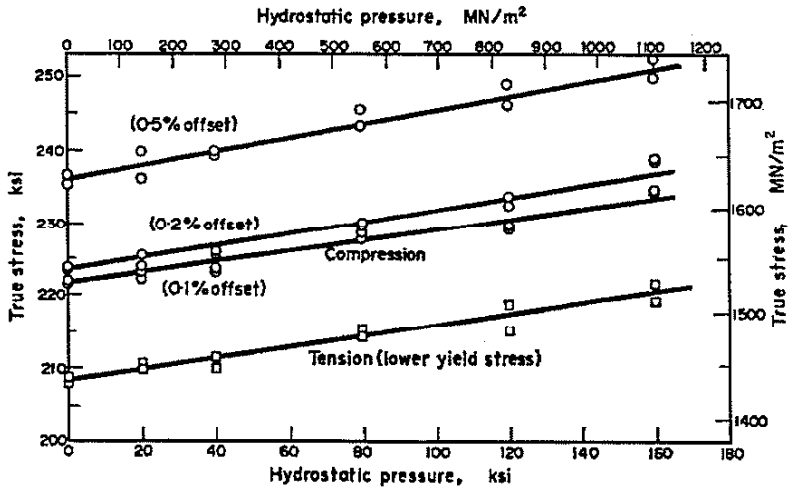

Figure 6.7: Effect of hydrostatic pressure on the yield strength of Q&T 4330 steel [1].

Nevertheless, his tests were conducted at constant pressure, and on a material that was specially processed to *not* transform.

In our 4340VAR tests conducted at constant triaxiality, we also found similar magnitudes of tension-compression asymmetry, though the exact values differed between the two batches we tested. In Batch 1 the compressive curve shows the same 7.5% increase over the tensile curve that Spitzig found, and pressure is also seen to raise the tensile stress-strain curve though the different test methods prevent simple comparison. Spitzig attempted to explain his tension-compression assymetry in terms of a "volume-expansion hypothesis based upon the normality flow rule of continuum plasticity theory which requires that materials exhibiting plastic volume expansion also show a pressure dependence of the yield and flow stresses." [1]. Unfortunately, his calculations did not pan out. In our case, we attribute the lower flow stress observed in tension in batch 1 to the stress dependence of the stress-assisted transformation of retained austenite to martensite.

The effective flow stress in the microyield regime in figure 6.6 reveals the hydrostatic stress dependence of the yield strength and the underlying stress dependence of the transformation responsible for the microyielding.

6.7 Conclusions

This work supports the following conclusions:

1. Stress-controlled, triaxial monotonic stress/strain tests have been conducted on two batches of quenched and tempered 4340VAR steel specimens.

Asymmetry was found between tension and compression, though its magnitude differed between the two batches we tested. For Batch 1, the compressive curve is approximately 7.5% higher than the tensile curve.

2. Pressure is seen to raise the tensile stress-strain curve. The highest yield strength level was observed for the Batch 1 material tested under triaxial compression.

3. The volumetric transformation strains show that as triaxiality values decreased, larger effective stress magnitudes were required to begin transformation. The initial rate of transformation is seen to be highest for the specimen with the positive triaxiality value.

4. The effective flow stress in the microyield regime is plotted vs triaxiality for all the tests run on both batches of 4340VAR steel. This graph, shown in figure 6.6, reveals at once the hydrostatic stress dependence of the yield strength and the underlying stress dependence of the transformation responsible for the microyielding. The lower flow stress in tension was attributed to stress-assisted transformation of retained austenite to martensite. Our results agree with Haidemenopoulis *et al.* that stress-assisted transformation of retained austenite to martensite, not dislocation slip, appears to be responsible for initial yield behavior and indicates the elastic limit, as is expected in the case of stress-assisted transformations.

List of References

1. Spitzig, W. A., Sober, R. J., & Richmond, O. Pressure dependece of yielding and associated volume expansion in tempered martensite. Acta Metallurgica, 1975, 23, 885-893.

2. Haidemenopoulis, G.N., Grujicic, M., Olson, G.B., Cohen, M., Transformation Microyielding of Retained Austenite, Acta metall., vol 37, no. 6, pp. 1677-1682, 1989.

3. Stringfellow, R. G., Mechanics of Strain-Induced Transformation Toughening in Metastable Austenitic Steels, PhD Thesis, MIT, Cambridge, MA, 1990.

7. EFFECT OF STRESS STATE ON THE FATIGUE BEHAVIOR OF 1070 STEEL

7.1 Overview

The effect of stress state on stress-strain response and fatigue life was investigated in normalized 1070 steel. Utilizing conventional servohydraulic test machines as well as a specialized pressure test apparatus, monotonic and cyclic experiments were conducted. When stress-strain behavior under various stress states were compared, experimental results indicated no pressure dependence of flow stress. Fatigue tests allowed the first successful use of the model described in chapter 3 which converts raw data from the externally mounted extensometer to gage section axial stress and strain. These fatigue tests under pressure show that the fatigue life of 1070 steel increases with pressure in the low cycle regime. Pressure had no effect on the appearance of the fracture surfaces.

7.2 Introduction

Rolling contact fatigue is the major cause of railroad wheel shelling and spalling, two phenomena which effectively determine the service life of heavily loaded, tread-braked wheels and the subject of much on-going research [1]. This type of fatigue occurs at the wheel tread and is characterized by a state of high compressive mean stress coupled with reversed shear. The compressive normal stress magnitudes are greater than the uniaxial yield strength, yet gross yielding is prevented due to the triaxial nature of the Hertzian stress field and the constraint provided by the material surrounding the contact patch.

Attempts have been made to model rolling contact as multiaxial fatigue, based on existing data from tensile mean stress regimes [2]. However, with primarily compressive mean stresses acting on the critical planes, one would expect the damage accumulated per cycle to be lower than if the mean normal stresses were zero or tensile. Attempts to impose the large rolling contact stress-strain magnitudes on uniaxial test specimens are not successful due to ratchetting or fracture in stress-controlled testing, or rapid mean stress relaxation in strain controlled testing [3]. As triaxial test data at high compressive mean stress levels is not available, the available models must therefore rely on assumptions of material behavior, limiting their value as predictive tools [2].

To demonstrate how the pressure test apparatus may be used to produce this needed triaxial data, we chose to run a series of experiments on 1070 steel specimens. Monotonic data will be obtained to identify possible pressure dependence of the flow strength. Fatigue data will be generated at triaxial compressive stress levels and then used to evaluate the Findley type of multiaxial fatigue life prediction model. Hysteresis loops will also be recorded under pressure for investigation of cyclic stress-strain behavior.

7.3 Experimental Techniques

According to Association of American Railroad specifications, railroad wheels begin life as 1070 steel castings. Cast wheels are used in either the as-cast condition (termed "Class U") or in an austenitized and rim-quenched condition (termed "Class C"). Class U wheels display a coarse pearlite morphology, whereas the increased cooling rate provided by the quench given to Class C wheels results in a finer pearlite structure in the tread and the production of beneficial residual stresses in the wheel. Unlike the other materials examined in this thesis, this 1070 contains no martensite nor does it transform to martensite under load.

A single heat of EF grade, bearing quality 1070 steel was purchased from Republic Engineered Steels in 2.4 inch diameter hot rolled bars. Its chemical composition was 0.68% C, 0.95% Mn, 0.25% Si, 0.16% Cu, 0.06% Ni, 0.15%Cr, 0.02% Mo, 0.015% P and 0.031% S. At UIUC, the bars were normalized for 4 hours at 870°C and cooled in still air. This heat treatment was chosen to produce a coarse pearlite microstructure characteristic of a Class U wheel. The average hardness after heat-treatment was 18.7 HRC. After heat treating, specimens were cut from the bars with their longitudinal axes parallel to the rolling direction. For uniformity, specimens were made only from material distributed about the half-radius point of the bars: a cylindrical volume of 0.7 inch inner diameter and 1.7 inch outer diameter. For triaxial tests under pressure, specimens had a nominal gage length of 12.7 mm and gage diameters of 5.1 to 7.4 mm (see drawings in Appendix D). The test apparatus described in chapter 3 was used for triaxial testing.

To provide data for evaluating the Findley type of "critical plane" model for multiaxial fatigue life under proportional loading (where maximum shear and normal stress in the cycle coincide), two groups of experiments were conducted. The Findley model says that fatigue life depends on the shear stress range acting on the critical plane where cracks are found to initiate, with the normal stress having a modifying influence. Expressed mathematically for a given life, it appears as $\Delta\tau + k\Delta\sigma_n = \text{constant}$. A summary of experimental conditions is provided in Table 1. Two specimens were tested in each group in which the shear stress was kept constant while the normal stress was systematically varied. No axial ratchetting was expected in these tests, since the effective stress $\sigma_z + P$, is the same in the forward and backward directions.

Group	constant pressure P	max axial stress $\sigma_{z\,max}$	min axial stress $\sigma_{z\,min}$	axial mean stress $\sigma_{z\,mean}$	max shear stress τ_1	min shear stress τ_1	shear stress range $\Delta\tau$	Life N_f
Group 1	20 ksi	60 ksi	-100 ksi	-20 ksi	40 ksi	-40 ksi	80 ksi	2,275 cycles
	50	30	-130	-50	40	-40	80	4,086
Group 2	20 ksi	40 ksi	-80 ksi	-20 ksi	30 ksi	-30 ksi	60 ksi	16,178 cycles
	50	10	-110	-50	30	-30	60	23,467

Table 7.1 Experimental stress states.

For each of these applied stress states, every test was run from the initial condition of all stress components being (essentially) zero in magnitude. The normal stresses were simultaneously, linearly ramped to a state of hydrostatic stress and then the pressure was held constant while the axial stress was cycled between its maximum and minimum limits.

7.4 Experimental Results

For all tests, stress and strain data were collected in raw engineering quantities. Uniaxial test data was then converted to true stresses and strains using the following equations:

$$\sigma_{zz}^{true} = \frac{\sigma_{zz}}{(1+\varepsilon_{rr})^2}$$

$$\varepsilon_{rr}^{true} = \varepsilon_{\theta\theta}^{true} = \ln(\varepsilon_{rr}+1)$$

$$\varepsilon_{zz}^{true} = \ln(\varepsilon_{zz}+1)$$

The conversion of pressure test data to true stresses and strains is detailed in chapter 3.

Concentrating on the small strain regime, true axial stress-strain curves from the tension experiments under 0 to 414 MPa pressure are shown in Figure 7.1 to examine the effect of the imposed stress state on the stress-strain response. In the figure, the ramps leading from (0,0) to the start of the stress-strain curves are the hydrostatic stress trajectories followed to set the initial conditions for the test. Once at this state of hydrostatic stress, the pressure was held constant while the axial stress was increased. In the normalized condition, this 1070 steel has a uniaxial yield strength of 449 MPa, an ultimate strength of 825 MPa, an elongation of 21% and a reduction in area of 30% [3].

When the results shown in Figure 7.1 are converted to effective stress-effective strain quantities, the four curves plot directly on top of each other, and no information can be obtained.

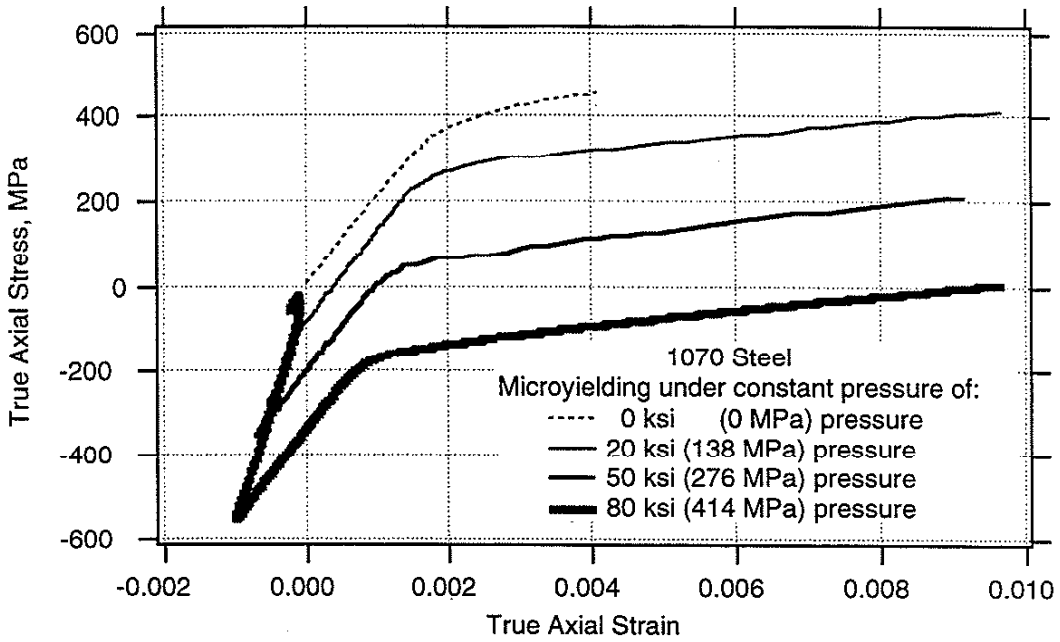

Figure 7.1 True axial stress-true axial strain curves at constant 0 - 414 MPa pressures.

However, it is instructive to obtain the flow strength values at 0.2% and 0.025% from the individual plots and graph them vs. pressure. When this is done, it is clear that there is essentially no pressure dependence to the flow strength for normalized 1070 steel.

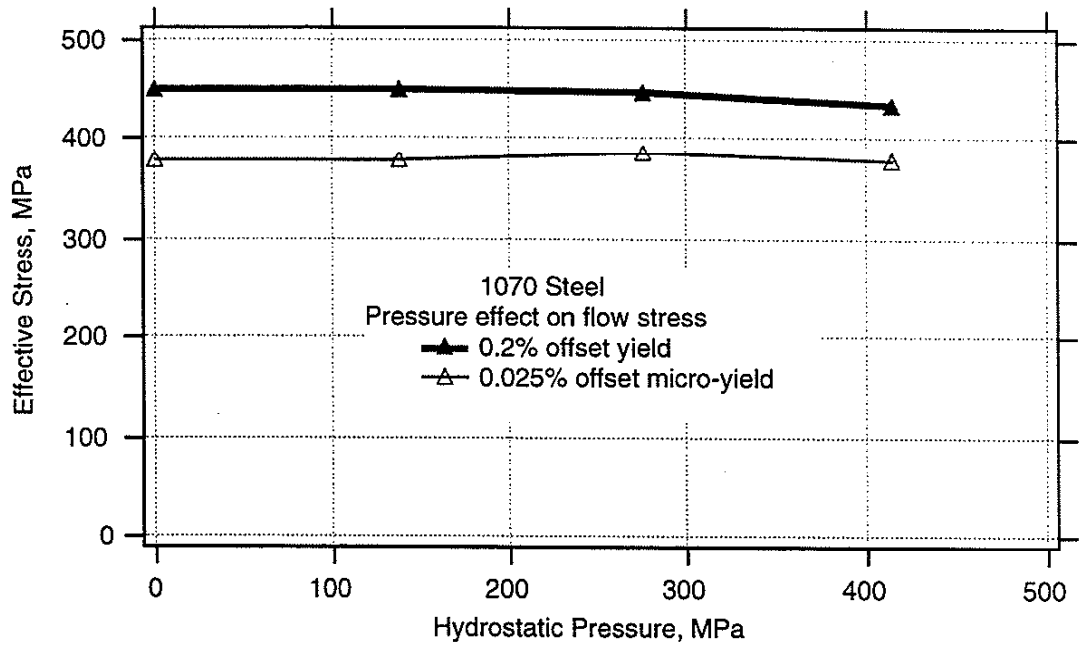

Figure 7.2 Pressure dependence of 0.2% and 0.025% flow strength of 1070 steel tested at constant 0 - 414 MPa pressures.

Representative stress-strain curves from two of the fatigue experiments are shown in Figures 7.3 and 7.4. In the figures, hysteresis loops show the cyclic stress response of the material under pressure. The solid loops show data obtained from the strain gages mounted on the specimen. The dotted loops show data obtained after the strain gages have failed in fatigue. They

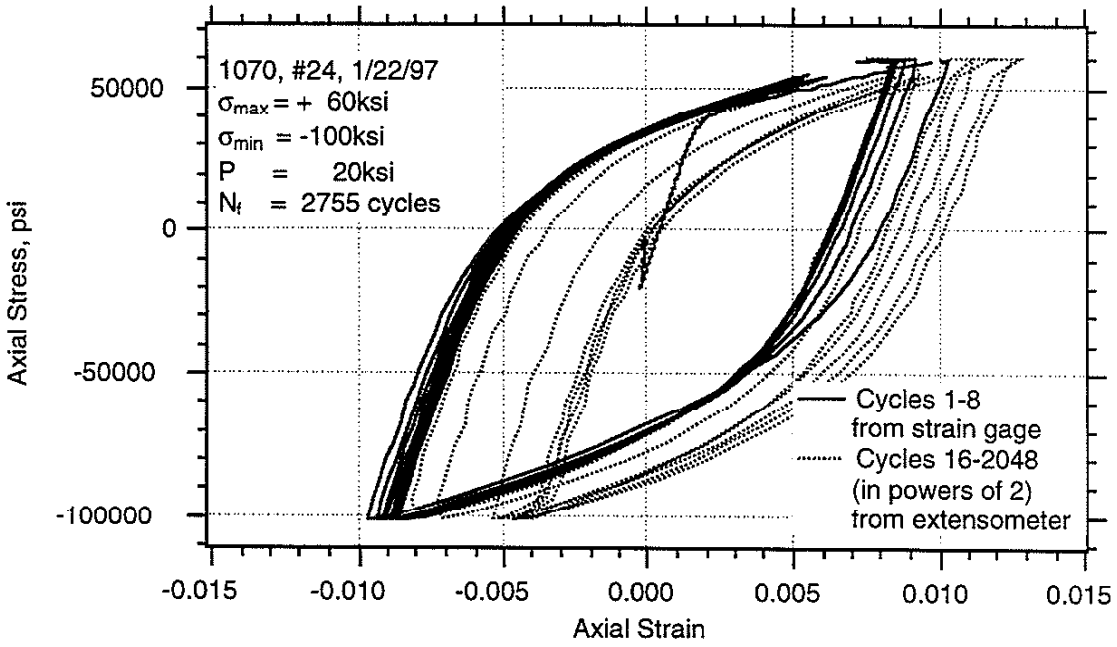

Figure 7.3 Cyclic axial stress vs. strain for Group 1, Test 1

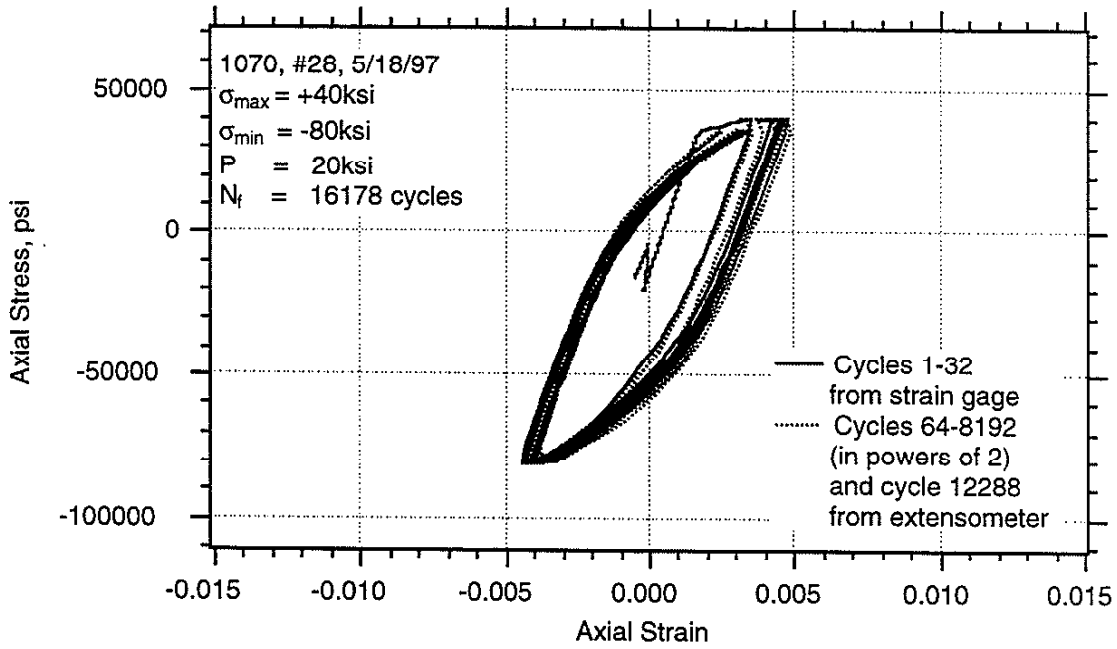

Figure 7.4 Cyclic axial stress vs. strain for Group 2, Test 1

have been calculated using the raw data from the externally mounted extensometer and the model described in chapter 3 which converts extensometer output to gage section axial stress and strain. As with the monotonic tests under pressure, the ramps leading from (0,0) to the start of the stress-strain curves are the hydrostatic stress trajectories followed to set the initial conditions for the test. Once at this state of hydrostatic stress, the pressure was held constant while the axial stress was cycled. Since the stress cycle was symmetric about the initial hydrostatic stress point, no ratchetting was expected and essentially none was seen.

A comparison of data from the cyclic tests under pressure is provided in Figure 7.5. Increasing pressure raises the fatigue life curve.

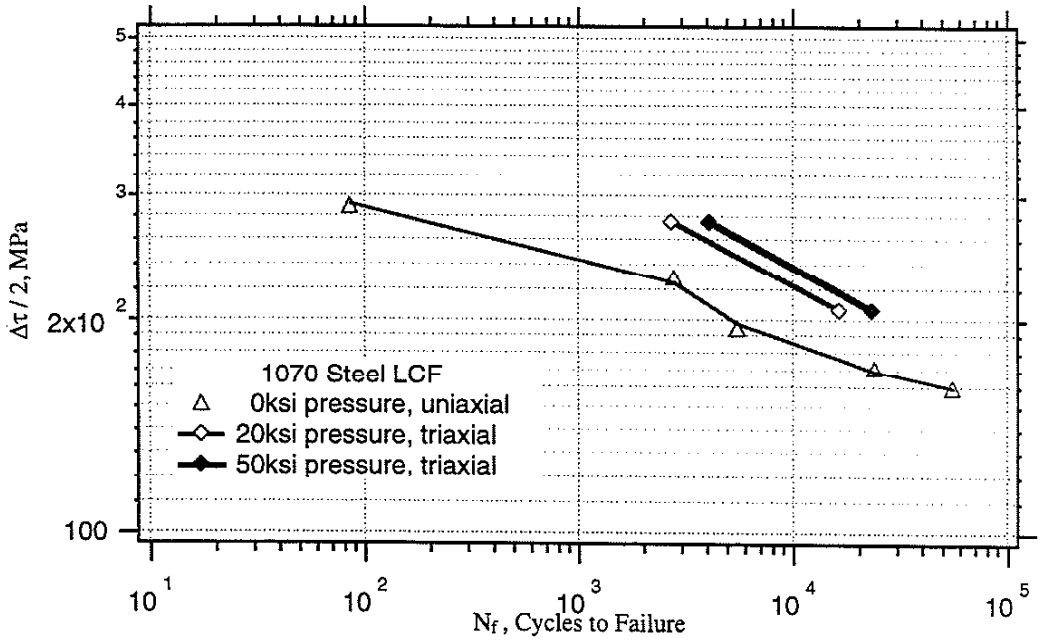

Figure 7.5 Shear stress range vs. life as a function of pressure for normalized 1070 steel.

7.5 Discussion of Results

Unlike the other materials appearing in this thesis, the flow stress of normalized 1070 steel shows essentially no dependence on pressure, even up to pressure magnitudes 25% greater than the uniaxial yield strength of the 1070. This result applies to both the microyield point and the 0.2% offset yield strength, and validates the assumption of pressure-independent yield surface models in rolling contact simulations incorporating plasticity of 1070.

As discussed in chapter 2, the majority of the existing published data regarding fatigue under pressure is unreliable. The few credible papers show that fatigue life generally increases with pressure. The experimental findings in the present work corroborate this trend and present new data for 1070 steel. Fractures were centered in the gage section and fracture surfaces were

essentially perpendicular to the axial stress. As examined under an optical microscope, it is clear that pressure had no effect on the appearance of the fracture surfaces.

7.6 Conclusions

The experimental results from specimens of normalized 1070 steel support the following conclusions:

1.) As evidenced by Figure 7.2, there is essentially no pressure dependence to the 0.025% and 0.2% offset flow strengths for normalized 1070 steel up to pressure magnitudes 25% greater than its uniaxial yield strength. This validates the assumption of pressure-independent yield surface models in rolling contact simulations incorporating plasticity of 1070.

2.) Additional capabilities of the pressure test apparatus were proven via extended cyclic tests at different stress/pressure levels. Each test involved ramping to an initial hydrostatic stress state, from which pressure was held constant and axial stress was cyclically varied. The raw data from the externally mounted extensometer was successfully converted to gage section axial stress and strain using the model described in chapter 3.

3.) Fatigue tests under pressure show that the fatigue life of 1070 steel increases with pressure in the low cycle regime. Pressure had no effect on the appearance of the fracture surfaces.

List of References

1. M. Balzer, H. Sehitoglu, G.J. Moyar, "An Inelastic Finite Element Analysis of the Contribution of Rail Chill to Braked Tread Surface Fatigue." RTD-Vol 5, Rail Transportation, ASME WAM 1992, pp. 117-122.

2. Y. Jiang and H. Sehitoglu, "Contact Fatigue Life Prediction Methods, Report No. 1" in "Fatigue Stress and Analyses of Rolling Contact," UIUC College of Engineering Report No. 161/UILU-ENG 92-3602, 1992.

3. Y. Jiang and H. Sehitoglu, "Multiaxial Fatigue of 1070 Steel under Proportional and Non-Proportional Loading, Report No. 3" in "Fatigue Stress and Analyses of Rolling Contact," UIUC College of Engineering Report No. 161/UILU-ENG 92-3602, 1992.

APPENDIX A - TEST MACHINE OPERATION MANUAL

Table of Contents

Pressure Tests - Monotonic Or Cyclic

Setup

Specimen And/Or Dummy Gage Preparation
Specimen Installation
Bleed The Vessel
Zero The Pressure Transducer
Zero The External Load Cell
Complete Test Set-Up Procedure
Run Test Simulation
Adjust Internal Load Cell Gain
Raise The Lower Grip
"Zero" The Transducers
Pre-Pressurizing
Find Strain Calibration Factors
Find Pressure Calibration Factors

Run Test

Teardown

Lower The Lower Grip
Specimen Removal

Reduce The Test Data

Plotting the Data

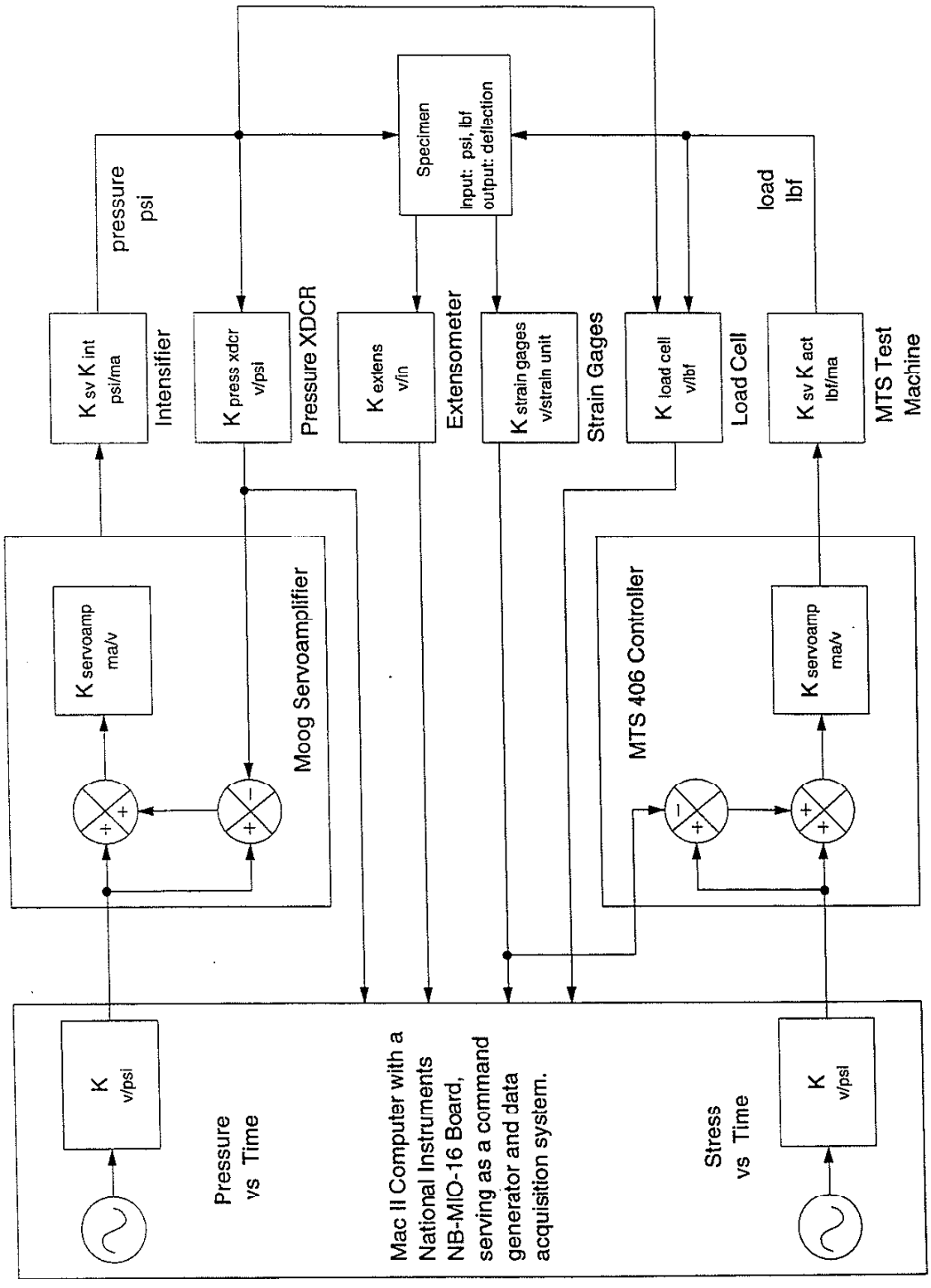
Specimen
input: psi, lbf
output: deflection
pressure
psi
load
lbf
K sv K int
psi/ma
Intensifier
K press xdcr
v/psi
Pressure XDCR
K extens
v/in
Extensometer
K strain gages
v/strain unit
Strain Gages
K load cell
v/lbf
Load Cell
K sv K act
lbf/ma
MTS Test
Machine
K servoamp
ma/v
Moog Servoamplifier
MTS 406 Controller
K servoamp
ma/v
K
v/psi
Pressure
vs Time
Mac II Computer with a
National Instruments
NB-MIO-16 Board,
serving as a command
generator and data
acquisition system.
Stress
vs Time
K
v/psi

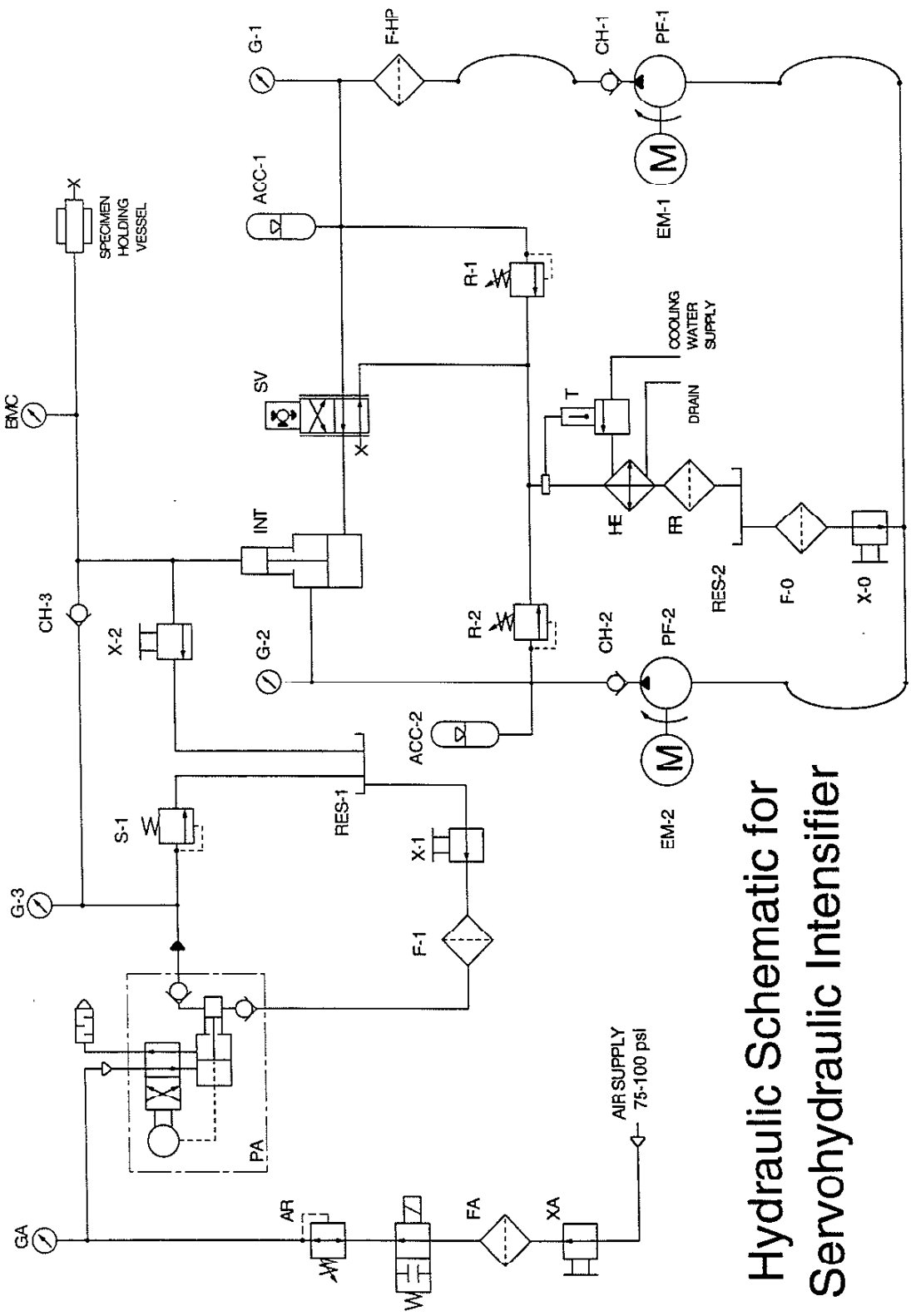

Hydraulic Schematic for Servohydraulic Intensifier

Introduction

This operating manual contains information required to calibrate, set-up and operate the HTML high pressure test machine.

The HTML high pressure test machine is designed to conduct various material tests, acquire data during the tests and store it for subsequent analysis. Software programs, written in C and used with the HTML high pressure test machine, allow the machine to be set-up and calibrated. Two separate test control programs, **Mono Load Control** and **Cyclic Load Control**, are used to conduct the actual tests.

Mono Load Control allows stress-controlled monotonic tests to be conducted. This program displays the transducer outputs on the screen for zeroing, provides ramp up, & ramp down command signals for load & pressure during the test, and stores the test data. Test variables are specified in the file named "initialize.c" Below is a plot which graphically illustrates the variables which control command generation.

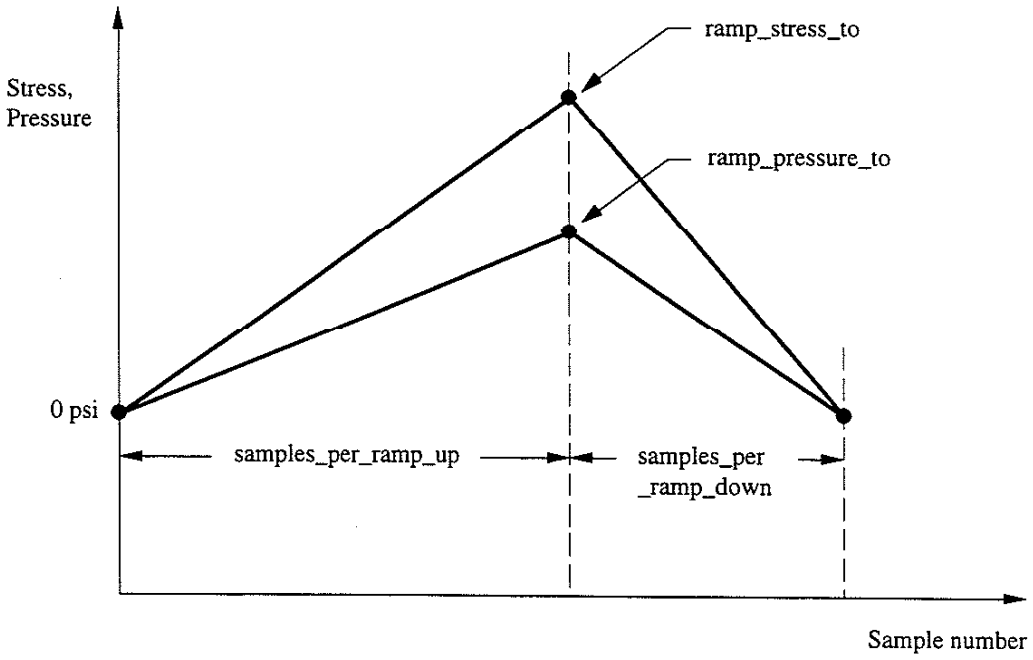

The two-step ramp before the start of cyclic command generation provides a variety of loading options, including the ability to begin cycling from a hydrostatic stress state. **Mono Load Control** runs at approximately 125 samples per second.

Cyclic Load Control allows cyclic tests to be conducted. This program displays the transducer outputs on the screen for zeroing, displays the current cycle number on a counter, provides ramp up, cyclic, & ramp down command signals for load & pressure during the test, and stores the test data. Test variables are specified in the file named "initialize.c" Below is a plot which graphically illustrates the variables which control command generation.

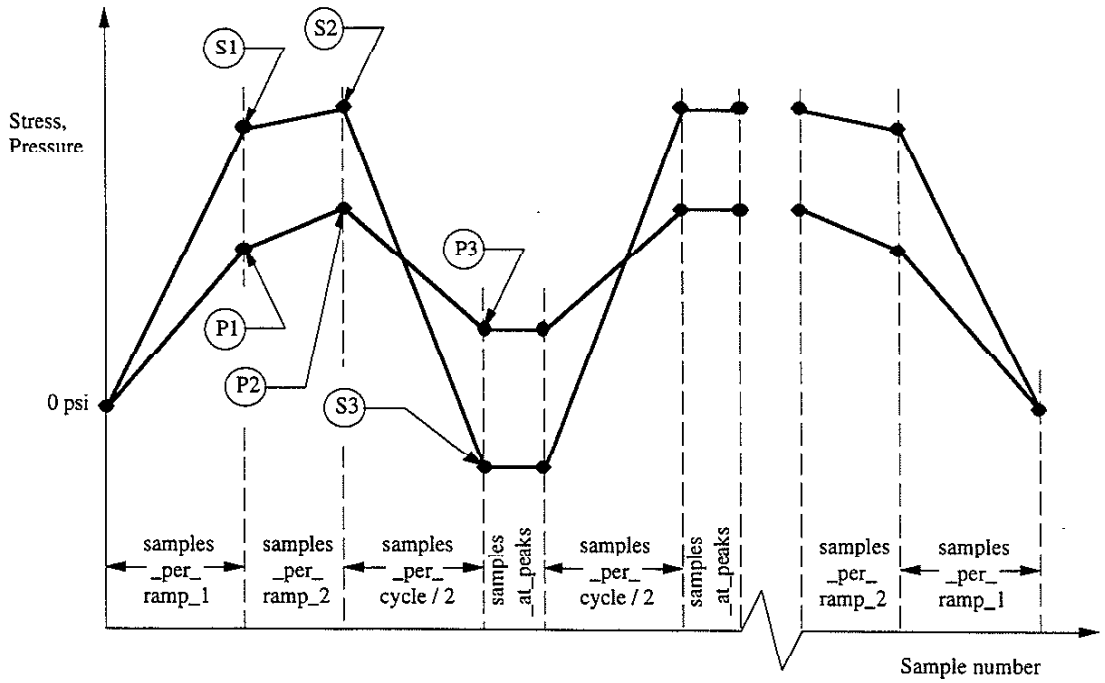

Key: S1 = ramp_stress_to P1 = ramp_pressure_to
S2 = cycle_stress_from P2 = cycle_pressure_from
S3 = cycle_stress_to P3 = cycle_pressure_to

The two-step ramp before the start of cyclic command generation provides a variety of loading options, including the ability to begin cycling from a hydrostatic stress state. The "samples_per_cycle" and "samples_at_peaks" variables allow the cyclic command to be tailored from a triangular waveform, to a triangular wave with a dwell (to ensure that the peak values are achieved), to a square waveform. **Cyclic Load Control** runs at approximately 125 samples per second.

Transducer Calibrations

Pressure Transducer Calibration

These are sequential instructions which must be followed in order.

CHECK HERE

☐ Open the cooling water valves for the Harwood Engineering pressure intensifier and the MTS HPU.

☐ On the Harwood Engineering pressure intensifier front panel, unscrew the knob marked "AR" until it stops.

☐ Behind the Harwood Engineering pressure intensifier front panel, open the needle valve marked "X-2". The gage marked "G-3" will then read zero.

☐ Using the Macintosh Mac II, open the folder labeled "Development". Then open the folder labeled "Current 16 bit Programs". Then open the folder labeled "Zero Inputs". From THINK C, run the program "Zero Inputs". This program provides a zero load command signal and a full scale pressure command signal while it displays the transducer and load cell outputs on the screen.

☐ Use the GP:50 New York Limited Model 312-SF-CA/GJ pressure transducer/transmitter as a 30,000 psi standard. Install the pressure transducer/transmitter in place of the tube connecting the intensifier to the specimen holding vessel. Connect a 24.00 vdc power supply and a 500 ohm precision resistor in series with the pressure transducer/transmitter. Use a DVM to make sure that there is a 2.00 vdc reading across the resistor (4.00 ma flowing thru the circuit).

☐ Zero the pressure transducer output using the trim-pots marked "ZERO" on the Ectron Model 687 marked "Pressure XDCR". Turn the knob marked "GAIN" to "1K". Adjust the "RTI ZERO" trim-pots until you get the following output on the Mac II screen:

p_xdcr = 0 (bits)

Turn the knob marked "GAIN" to "10". Adjust the "RTO ZERO" trim-pot until you get the following output on the Mac II screen:

p_xdcr = 0 (bits)

Set the pressure transducer gain to "1K" using the knob marked "GAIN". The "GAIN VERN" switch should be in the "IN" position.

☐ Behind the Harwood Engineering pressure intensifier front panel, close the needle valve marked "X-2".

☐ On the Harwood Engineering pressure intensifier front panel, open the valve marked "XA". Then adjust the knob marked "AR" until the gage marked "G-3" reads 1000 psi.

☐ On the Harwood Engineering pressure intensifier front panel, push the green button marked "CONTROL POWER ON". The red indicator light labeled "CONTROL POWER ON" and the yellow indicator light labeled "BOTTOM LIMIT SWITCH ACTIVATED" will light up. Then push the green button marked "SYSTEM START" to start the hydraulic pumps. The green indicator lights labeled "DRIVE PUMP RUN" and "RETRACTING PUMP RUN" will light up. The gage marked "G-2" should read 500 psi.

Protect your hearing; put on the sound suppressors!

☐ On the Harwood Engineering pressure intensifier front panel, slowly adjust the regulator marked "R-1" until the voltage across the 500 Ohm resistor is 10.00 vdc, signifying 30,000 psi (20.00 ma flowing thru the circuit). On the Harwood Engineering pressure intensifier front panel, the yellow indicator light labeled "BOTTOM LIMIT SWITCH ACTIVATED" will go out.

☐ Adjust the gain using the trim-pot marked "VERN" on the Ectron Model 687 until you get the following output on the Mac II screen:

p_xdcr = 7864 (bits)

This pressure transducer setting is derived as follows:

•"ten_volt_pressure" is the value of this calibration in subroutine "Calibrations()" in file "Initialize.c".
•There are 32,767 bits per 10 volts

$$\frac{\text{pressure}}{\text{ten\_volt\_pressure}} * 32{,}767 = \frac{30000}{125000} * 32{,}767 = 7864 \text{ bits}$$

☐ On the Harwood Engineering pressure intensifier front panel, adjust the regulator marked "R-1" until the gage marked "G-1" reads zero psi. On the Harwood Engineering pressure intensifier front panel, the yellow indicator light labeled "BOTTOM LIMIT SWITCH ACTIVATED" will light up.

☐ On the Harwood Engineering pressure intensifier front panel, adjust the knob marked "AR" until the gage marked "GA" reads zero psi. Then close the valve marked "XA".

☐ Behind the Harwood Engineering pressure intensifier front panel, open the needle valve marked "X-2".

☐ Once again, there will be a 2.00 vdc reading across the resistor (4.00 ma flowing thru the circuit). Zero the pressure transducer output using the trim-pots marked "ZERO" on the Ectron Model 687. Turn the knob marked "GAIN" to "1K." Adjust the "RTI ZERO" trim-pots until you get the following output on the Mac II screen:

p_xdcr = 0 (bits)

Turn the knob marked "GAIN" to "10". Adjust the "RTO ZERO" trim-pot until you get the following output on the Mac II screen:

p_xdcr = 0 (bits)

Set the pressure transducer gain to "1K" using the knob marked "GAIN". The "GAIN VERN" switch should be in the "IN" position.

☐ 2 Behind the Harwood Engineering pressure intensifier front panel, close the needle valve marked "X-2".

☐ 3 On the Harwood Engineering pressure intensifier front panel, open the valve marked "XA". Then adjust the knob marked "AR" until the gage marked "G-3" reads 1000 psi.

☐ 4 On the Harwood Engineering pressure intensifier front panel, slowly adjust the regulator marked "R-1" until the voltage across the 500 Ohm resistor is 10.00 vdc, signifying 30,000 psi (20.00 ma flowing thru the circuit). On the Harwood Engineering pressure intensifier front panel, the yellow indicator light labeled "BOTTOM LIMIT SWITCH ACTIVATED" will go out.

☐ 5 Adjust the gain using the trim-pot marked "VERN" on the Ectron Model 687 until you get the following output on the Mac II screen:

p_xdcr = 7864 (bits)

This pressure transducer setting is derived as follows:

•"ten_volt_pressure" is the value of this calibration in subroutine "Calibrations()" in file "Initialize.c".
•There are 32,767 bits per 10 volts

$$\frac{\text{pressure}}{\text{ten\_volt\_pressure}} * 32{,}767 = \frac{30000}{125000} * 32{,}767 = 7864 \text{ bits}$$

☐ 6 On the Harwood Engineering pressure intensifier front panel, adjust the regulator marked "R-1" until the gage marked "G-1" reads zero psi. On the Harwood Engineering pressure intensifier front panel, the yellow indicator light labeled "BOTTOM LIMIT SWITCH ACTIVATED" will light up.

☐ 7 On the Harwood Engineering pressure intensifier front panel, adjust the knob marked "AR" until the gage marked "GA" reads zero psi. Then close the valve marked "XA".

☐ 8 Behind the Harwood Engineering pressure intensifier front panel, open the valve marked "X-2

☐ Repeat the last 8 steps until the bit readouts are stable. Once they are stable, proceed.

☐ On the Harwood Engineering pressure intensifier front panel, push the red button marked "STOP". The green indicator lights labeled "DRIVE PUMP RUN" and "RETRACTING PUMP RUN" will go out, but the red indicator light labeled "CONTROL POWER ON" and the yellow indicator light labeled "BOTTOM LIMIT SWITCH ACTIVATED" will remain lit. Then push the red button labeled"OFF" to extinguish these remaining indicator lights.

☐ Disconnect the 24 vdc power supply and the 500 ohm resistor that are in series with the pressure transducer/transmitter. Remove the pressure transducer/transmitter and replace the tube connecting the intensifier to the specimen holding vessel.

☐ Using the Macintosh Mac II, push "Q" to end execution of the program "Zero Inputs".

☐ Close the cooling water valve for the Harwood Engineering pressure intensifier.

Extensometer Calibration

This calibration method ensures that the mechanical zero of the extensometer and the electrical zero of its amplifier are synchronized. Electrical offsets may be entered into the test program.

CHECK HERE

☐ Set the calibration stand for a 0.550" gage length. Install the 3/8" diameter extensometer extension on the calibration stand. Mount the extensometer on the calibration stand.

☐ Using the Macintosh Mac II, open the folder labeled "Development". Then open the folder labeled "Current 16 bit Programs". Then open the folder labeled "Zero Inputs". From THINK C, run the program "Zero Inputs". This program provides a zero load command signal and a full scale pressure command signal while it displays the transducer outputs on the screen.

☐ Zero the extensometer using the trim-pots marked "ZERO" on the Ectron Model 687. Turn the knob marked "GAIN" to "1K". Adjust the "RTI ZERO" trim-pots until you get the following output on the Mac II screen:

exten = 0 (bits)

Turn the knob marked "GAIN" to "10". Adjust the "RTO ZERO" trim-pot until you get the following output on the Mac II screen:

exten = 0 (bits)

☐ Choose a maximum deflection that you would like to record during your test. Try to keep this number as small as possible without risking the loss of any important data. The value of this deflection will be entered as "ten_volt_deflection" in subroutine "Calibrations()" in file "Initialize.c" of programs "Mono Load Control" and "Cyclic Load Control".

☐ Use the highest gain setting that will allow the maximum deflection to be reached, thus providing maximum resolution. (If the amplifier output exceeds ±10.0 volts, your data will be lost.) Set the extensometer gain using the knob marked "GAIN". The "GAIN VERN" switch should be in the "IN" position.

For the best resolution possible when measuring strains that are essentially unidirectional, choose an Amp Gain that provides a $|\Delta E|$ between 10 and 20 volts. Then when mounting the extensometer, open or close it to mechanically (and thus electrically) bias the amplifier output in the direction opposite to the direction of the expected voltage change during the test.

Example: for a tension test the axial strain will be positive. Choose a gain that will give +15V for the maximum deflection, and then mount the extensometer so that the amplifier is putting out -7.5V before the test starts. ie, mount the extensometer so that you get the following output on the Mac II screen:

exten = -24575 (bits)

and enter -24575 as the "extensometer_offset" in the Calibrations() subroutine of Initialize.c in either "Mono Load Control" or "Cyclic Load Control."

This extensometer setting is derived as follows:

•There are 32,767 bits per 10 volts

$$-7.5V * \frac{32767 \text{ bits}}{10V} = -24575 \text{ bits}$$

[1] Set the calibration stand set for a positive deflection equal to the full scale deflection chosen. Adjust the gain using the trim-pot marked "VERN" on the Ectron Model 687 until you get the following output on the Mac II screen:

exten = 32767 (bits)

This extensometer setting is derived as follows:

•"ten_volt_deflection" is the value of this calibration in subroutine "Calibrations()" in file "Initialize.c".
•There are 32,767 bits per 10 volts

$$\frac{\text{deflection}}{\text{ten\_volt\_deflection}} * 32{,}767 = +1 * 32{,}767 = +32767 \text{ bits}$$

[2] Zero the extensometer using the trim-pots marked "ZERO" on the Ectron Model 687. Adjust the "RTI ZERO" trim-pots until you get the following output on the Mac II screen:

exten = 0 (bits)

[3] Set the calibration stand set for a negative deflection equal to the full scale deflection chosen. Adjust the gain using the trim-pot marked "VERN" on the Ectron Model 687 until you get the following output on the Mac II screen:

exten = -32767 (bits)

This extensometer setting is derived as follows:

•"ten_volt_deflection" is the value of this calibration in subroutine "Calibrations()" in file "Initialize.c".
•There are 32,767 bits per 10 volts

$$\frac{\text{deflection}}{\text{ten\_volt\_deflection}} * 32{,}767 = -1 * 32{,}767 = -32767 \text{ bits}$$

[4] Zero the extensometer using the trim-pots marked "ZERO" on the Ectron Model 687. Adjust the "RTI ZERO" trim-pot until you get the following output on the Mac II screen:

exten = 0 (bits)

[ ] Repeat the last 4 steps until the bit readouts are stable. Once they are stable, proceed.

[ ] Using the Macintosh Mac II, push "Q" to end execution of the program "Zero Inputs".

Internal Load Cell Calibration

The output of the internal load cell is affected by both axial compressive load and by external pressure. Two calibrations are therefore necessary to map its output voltage over its operating load & pressure range.

- Only load (not pressure) is applied in the first calibration, using a "solid bar" specimen capable of withstanding high compressive loads without yielding. **The external load cell on the MTS test machine provides load feedback here.**
- Pressure and load are applied in the second calibration, using a special "plug" specimen that allows simultaneous application of an axial load proportional to the applied pressure. **The MTS test machine is not used here.**
- As a check, pressure and load may be applied in a third calibration, using a solid specimen and applying dither, then waiting for the seal friction to drop to zero. **The external load cell on the MTS test machine provides load feedback here.**

1. Solid Bar Specimen W/O Pressure

Solid Bar Specimen Installation

These are sequential instructions which must be followed in order.

CHECK HERE

- ☐ Obtain a "Solid Bar Specimen." This is a 0.4375 diameter specimen made from hardened steel which does not have a reduced gage section machined into it, nor strain gages bonded to it.
- ☐ Clean vessel with an aerosol cleaning solvent available at the EE Storeroom. Wash from top to bottom, allowing the liquid to flush away any dirt and grease. Clean the vessel support arm and place the vessel on it.
- ☐ Lubricate the vessel bores with the high pressure fluid. Remove any fluid puddles from the thread undercut for the electrical feedthru bore.
- ☐ Handling them with extreme care, select and clean a new set of O-ring seals with electronics parts cleaner. Alternately, you may clean and reuse O-ring seals which are known to have not leaked, if they pass a careful visual inspection for damage. Discard any O-ring seals which are damaged.
- ☐ After checking and/or replacing the backup rings, install the cleaned O-ring seals on the Load Cell Housing. Lubricate the specimen shoulder near the conical end with the high presure fluid. With a gentle twisting motion, insert the specimen into the Load Cell Housing until the conical surfaces mate. Be careful not to crush the internal backup ring, which is easily done if it falls out of position.
- ☐ Lubricate the outer diameter of the Load Cell Housing O-ring seal with the high pressure fluid.
- ☐ Insert the assembly into the bore of the vessel, sliding the specimen down the main bore. Insert the assembly until the top of the Load Cell Housing is slightly above the top surface of the vessel. Do NOT push it in too far!

☐ Install the four 3/8-16 x 1.75 SHCS into their counterbores in the Upper Adapter. Using a torque wrench and the reaction-torque tool to prevent the vessel from rotating, torque these fasteners to 30 ft-lbs in a star pattern (this will seat the Load Cell Housing in the vessel bore). Position the torque wrench so that it is parallel to the handle of the reaction-torque tool during the final stages of tightening. Be careful not to knock the vessel off the support arm!

☐ Lubricate the threads and underneath the heads of the six 3/8-16 x 6.5 SHCS with all purpose grease. Insert them into the lower endcap for the vessel. Hold your hand underneath the lower endcap to support it and keep the SHCS's from dropping out of their holes.

☐ Position the lower endcap so that the word "FRONT" is facing you, and from below insert the SHCS's into their respective holes in the vessel. Raise the lower endcap, so that the specimen passes thru the hole in the lower end cap. Continue raising the lower endcap as the SHCS's pass thru upper collet adapter.

☐ Rotate the support arm underneath the upper grip, ensuring that the high pressure tubing enters the port on the left side of the vessel. Raising the lower endcap against the vessel. Ensure that the pins in the lower end cap enter the holes in the bottom of the vessel. Thread the SHCS's into the upper grip.

☐ Snug, and then torque the SHCS's to 30 ft-lbf in a star pattern.

☐ Tighten the nut for the high pressure tubing connection to the vessel.

☐ **The lower seal, lower backup rings, dummy gages, feedthru and the extensometer are not used in this calibration.**

Zero the External Load Cell

CHECK HERE

☐ Using the Macintosh Mac II, open the folder labeled "Development". Then open the folder labeled "16 bit Programs". Open the folder labeled "Calibrate Int LC". Open the folder labeled "Calibrate Int LC W/O Pressure". Save the old file "Output.dat" under a new name, if you have not already done this. Open the file "Initialize.c". Enter all necessary info into the subroutine "Calibrations()". **Be sure to set:**

int_l_c_gain_factor = 1.0
zero_offset_load = -30.0

Save the file "Initialize.c". From THINK C, run the program "Calibrate Int LC W/O Pressure". This program displays the transducer outputs on the screen for zeroing, displays the current cycle number on a counter, provides ramp up, cyclic, & ramp down command signals for load & pressure during the test, and stores the test data.

☐ With the lower grip lowered, zero the external load cell using the ten-turn-pot marked "XDCR 2" "ZERO" on the MTS 406 Controller. Adjust the "ZERO" pot until you get the following output on the Mac II screen:

Ext_LC = 0 (bits)

The pressure and the strain gage signals need not be zeroed for this calibration.

Raise the lower grip

CHECK HERE

- [ ] Open the cooling water valve for the MTS HPU.

- [ ] Open the release valve on the Enerpac P18 hand pump.

- [ ] Check that at least 5 threads are visible on each of the collet releasing screws on the lower collet adapter. If not, unscrew them.

- [ ] **On the MTS 406 Controller, turn the switch marked "FDBK SELECT" to the position marked "XDCR 2." Then adjust the knob marked "GAIN" to 6.5 and the knob marked "RATE" to 8.5.**

- [ ] On the MTS 406 Controller, turn the switch under the panel meter to the position marked "ERROR".

- [ ] On the panel located above the MTS 406 Controller, turn the switch to the position marked "XDCR 2" "DC" to display the external load cell output on the Digital Read Out (DRO).

- [ ] **On the MTS 406 Controller, turn the knob marked "SET POINT" so that the panel meter on the MTS 406 reads a negative value.**

- [ ] On the MTS 413 Master Control Panel, push the blue button marked "RESET." Then push the white button marked "HYDRAULIC PRESSURE""HIGH LOW"" once to turn the HPU on. Then push the white button marked "HYDRAULIC PRESSURE""HIGH LOW" a second time. If the lower grip is not in its lowest position, it will move downward.

- [ ] Check the MTS HPU pressure and if necessary, adjust the regulator (the knob marked "PRESSURE CONTROL") so that the gage reads 3000psi. Tighten the locknut.

- [ ] On the MTS 406 Controller, turn the knob marked "SET POINT" clockwise until the lower grip begins to rise. The panel meter on the MTS 406 Controller will read a positive value. Let the grip slowly rise until the specimen bottoms against the collet stop.

- [ ] When the specimen bottoms against the collet stop, close the release valve on the Enerpac P18 hand pump.

- [ ] Slowly pump the Enerpac P18 hand pump to 3000psi. The lower grip should move downward slightly as the lower collet protrudes out of its opening, signifying that the specimen is indeed bottomed against the collet stop.

- [ ] **Do not turn off the MTS HPU while the specimen is gripped in the lower grip.**

Run Calibration

Complete several calibration runs to "bed-in" the set-up before taking your data.

CHECK HERE

☐ Ensure that all safety guards are in place.

☐ The external load cell must now be synchronized to the command signal from the MAC II. Adjust the knob marked "SET POINT" on the MTS 406 Controller until you get the following output on the Mac II screen.

Ext_LC = -49.2 (bits)

This external load cell setting is derived as follows:

- "zero_offset_load" is the value of the user-specified compressive load in subroutine "Calibrations()" in file "Initialize.c".
- The external load cell calibration is 20,000 lbf per 10VDC.
- "ten_volt_load" is the value of this calibration (modified by the NIDAQ board gain) in subroutine "Calibrations()" in file "Initialize.c".
- There are 32,767 bits per 10 volts

$$\frac{\text{zero\_offset\_load}}{\text{ten\_volt\_load}} * 32{,}767 = \frac{-30}{20000} * 32{,}767 = -49.2 \text{ bits}$$

☐ The internal load cell output should now be set to zero. This offset will be taken into account later when the calibration data is examined. Zero the internal load cell output using the trim-pots marked "ZERO" on the Ectron Model 687. Adjust the "RTI ZERO" trim-pots until you get the following output on the Mac II screen:

Int_LC = 0 (bits)

☐ Using the Macintosh Mac II, push "T" to bring up the Test command menu. Then push "B" to begin the command generation.

☐ The reading on the DRO will change. When the test is complete, the load command will be "zero_offset_load". This event will be evidenced by a steady reading on the DRO.

☐ Using the Macintosh Mac II, push "Q" and then "Y" to save the data and end execution of the program.

☐ Using the Macintosh Mac II, rename the file "Output.dat" for future examination using IGOR.

Lower The Lower Grip

CHECK HERE

- [ ] Open the release valve on the Enerpac P18 hand pump.

- [ ] Simultaneously screw in each of the two collet releasing screws on the lower collet adapter. This will free the specimen from the self-holding action of the collet.

- [ ] On the MTS 406 Controller, turn the switch under the panel meter to the position marked "ERROR".

- [ ] On the MTS 406 Controller, turn the knob marked "SET POINT" counterclockwise so that the panel meter on the MTS 406 reads a negative value. The lower grip will move downward.

- [ ] On the MTS 413 Master Control Panel, push the red button marked "HYDRAULIC OFF" to stop the hydraulic pump. The blue button marked "RESET" will light up.

- [ ] Close the cooling water valve for the MTS HPU.

Specimen Removal

CHECK HERE

- [ ] Loosen and unscrew the nut for the high pressure tubing connection to the intensifier.

- [ ] Loosen the SHCS's which mount the vessel. Unscrew them, lowering the vessel onto the support arm, and freeing the lower endcap.

- [ ] Rotate the support arm out from underneath the upper grip, ensuring that the high pressure tubing exits the port on the left side of the vessel. Remove the SHCS's and the lower endcap by sliding it down and off of the specimen.

- [ ] Using the torque bar to prevent the vessel from rotating, loosen the 4 SHCS in the upper adapter. Remove the SHCS and then carefully lift the upper adapter straight up by 1 inch. Carefully reach underneath and hold the load cell wire to prevent it from being tugged while you place the upper adapter on the support arm, to the left of the vessel.

- [ ] Carefully push the specimen and Load Cell Housing upward, until they come out of the vessel bore.

Reduce The Calibration Data

CHECK HERE

☐ Using the Macintosh Mac II, read the data file using IGOR and plot WOP_Int_LC_Volts vs WOP_Sho_Stress.
Append WOP_Int_LC_Volts_1 vs WOP_Sho_Stress_1,
WOP_Int_LC_Volts_2 vs WOP_Sho_Stress_2,
WOP_Int_LC_Volts_3 vs WOP_Sho_Stress_3, and
WOP_Int_LC_Volts_4 vs WOP_Sho_Stress_4.

• Fit a line to this data. Extrapolate the line to zero Shoulder Stress to find the (positive) Y-intercept.

• Make a note of this Y-intercept value because it will be used in section 3 of this calibration, "3. SOLID BAR W/PRESSURE CALIBRATION CHECK"

• Subtract this value from the y values of the curve-fit line so that the new line passes through the origin.

• The equation of this new line (y = m1*x + 0) will be inserted into the subroutine "Modify Commands.c" of projects "Mono Load Control" and "Cyclic Load Control" in the following form:

```
int_l_c_no_pressure = m1 * stress_in_shoulder
```

2. Plug Specimen W/Pressure

Plug Specimen Installation

These are sequential instructions which must be followed in order.

CHECK HERE

- ☐ Obtain a "Plug Specimen." This is a 0.4375 diameter upper shoulder cut from an old specimen. Also obtain a vessel plug for the bottom of the vessel where the specimen usually protrudes.

- ☐ Clean vessel with an aerosol cleaning solvent available at the EE Storeroom. Wash from top to bottom, allowing the liquid to flush away any dirt and grease. Clean the vessel support arm and place the vessel on it.

- ☐ Lubricate the vessel bores with the high pressure fluid. Remove any fluid puddles from the thread undercut for the electrical feedthru bore.

- ☐ Handling them with extreme care, select and clean a new set of 0-ring seals with electronics parts cleaner. Alternately, you may clean and reuse O-ring seals which are known to have not leaked, if they pass a careful visual inspection for damage. Discard any O-ring seals which are damaged.

- ☐ After checking and/or replacing the backup rings, install the cleaned O-ring seals on the Load Cell Housing. Lubricate the plug specimen shoulder near the conical end with the high presure fluid. With a gentle twisting motion, insert the plug specimen into the Load Cell Housing until the conical surfaces mate. Be careful not to crush the internal backup ring, which is easily done if it falls out of position.

- ☐ Lubricate the outer diameter of the Load Cell Housing O-ring seal with the high pressure fluid.

- ☐ Insert the assembly into the bore of the vessel, sliding the specimen down the main bore. Insert the assembly until the top of the Load Cell Housing is slightly above the top surface of the vessel. Do NOT push it in too far!

- ☐ Install the four 3/8-16 x 1.75 SHCS into their counterbores in the Upper Adapter. Using a torque wrench and the reaction-torque tool to prevent the vessel from rotating, torque these fasteners to 30 ft-lbs in a star pattern (this will seat the Load Cell Housing in the vessel bore). Position the torque wrench so that it is parallel to the handle of the reaction-torque tool during the final stages of tightening. Be careful not to knock the vessel off the support arm!

- ☐ Clean and grease the mating surfaces of an anti-extrusion ring and install it on the vessel plug. Then dip a cleaned O-ring seal into the high presure fluid and install it on the vessel plug.

- ☐ Lubricate the threads and underneath the heads of the six 3/8-16 x 6.5 SHC screws with all purpose grease. Insert them into the lower endcap for the vessel. Hold your hand underneath the lower endcap to support it and keep the SHCS's from dropping out of their holes.

- [ ] Position the lower endcap so that the word "FRONT" is facing you, and from below, insert the SHCS's into their respective holes in the vessel. Place the vessel plug on the lower endcap, in the center. Raise the lower endcap, so that the SHCS's pass thru upper collet adapter.

- [ ] Rotate the support arm underneath the upper grip, ensuring that the high pressure tubing enters the port on the left side of the vessel. Raising the lower endcap against the vessel inserts the seal, anti-extrusion rings and the vessel plug into the bore of the vessel. Ensure that the pins in the lower end cap enter the holes in the bottom of the vessel. Thread the SHCS's into the upper grip.

- [ ] Snug, and then torque the SHCS's to 30 ft-lbf in a star pattern.

- [ ] Tighten the nut for the high pressure tubing connection to the vessel.

- [ ] Tighten the nut for the bleed port behind the vessel.

- [ ] Check the condition of the o-ring on the feedthru plug. Replace if necessary. Lubricate the o-ring on the feedthru plug with the high pressure fluid.

- [ ] The dummy gages are not used in this calibration.

- [ ] Insert the electrical feedthru into the feedthru bore in the vessel.

- [ ] Thread in and tighten the nut which retains the electrical feedthru plug.

- [ ] The Extensometer is not used in this calibration.

Bleed The Vessel

CHECK HERE

☐ On the Harwood Engineering pressure intensifier front panel, unscrew the knob marked "AR" until it stops.

☐ Behind the Harwood Engineering pressure intensifier front panel, open the needle valve marked "X-2". The gage marked "G-3" will then read zero.

☐ Using the Macintosh Mac II, open the folder labeled "Development". Then open the folder labeled "16 bit Programs". Open the folder labeled "Calibrate Int LC". Open the folder labeled "Calibrate Int LC W/Press (Plug)". Save the old file "Output.dat" under a new name, if you have not already done this. Open the file "Initialize.c". Enter all necessary info into the subroutine "Calibrations()". Save the file "Initialize.c". From THINK C, run the program "Calibrate Int LC W/Plug". This program displays the transducer outputs on the screen for zeroing, displays the current cycle number on a counter, provides ramp up, cyclic, & ramp down command signals for load & pressure during the test, and stores the test data.

☐ Put on the white hard hat and lower the face shield.

☐ On the Harwood Engineering pressure intensifier front panel, open the valve marked "XA". Then adjust the knob marked "AR" until you can hear the charge pump slowly cycling.

☐ Loosen the plug closing the bleed port behind the pressure vessel until fluid begins to come out. When a stream of fluid comes out with no entrained air bubbles, tighten the plug.

☐ On the Harwood Engineering pressure intensifier front panel, adjust the knob marked "AR" until the gage marked "GA" reads zero psi. Then close the valve marked "XA".

Zero The Pressure Transducer

CHECK HERE

☐ Zero the pressure transducer using the trim-pot marked "RTI ZERO F" on the Ectron R687 marked "Pressure XDCR." Adjust the "RTI ZERO F" trim-pot until you get the following output on the Mac II screen:

p_xdcr = 0 (bits)

The external load cell and the strain gage signals are not used in this calibration.

Zero The Internal Load Cell

CHECK HERE

☐ The internal load cell output should now be set to zero. This offset will be taken into account later when the calibration data is examined. Zero the internal load cell output using the trim-pots marked "ZERO" on the Ectron Model 687. Adjust the "RTI ZERO" trim-pots until you get the following output on the Mac II screen:

Int_LC = 0 (bits)

Run Calibration

Complete several calibration runs to "bed-in" the set-up before taking your data.

CHECK HERE

☐ Open the cooling water valves for the Harwood Engineering pressure intensifier.

☐ On the Harwood Engineering pressure intensifier front panel, unscrew the knob marked "AR" until it stops.

☐ Ensure that all safety guards are in place.

☐ On the Harwood Engineering pressure intensifier front panel, push the green button marked "CONTROL POWER ON". The red indicator light labeled "CONTROL POWER ON" and the yellow indicator light labeled "BOTTOM LIMIT SWITCH ACTIVATED" will light up. Then push the green button marked "SYSTEM START" to start the hydraulic pumps. The green indicator lights labeled "DRIVE PUMP RUN" and "RETRACTING PUMP RUN" will light up. The gage marked "G-2" should read 500 psi.

Protect your hearing; put on the sound suppressors!

☐ Behind the Harwood Engineering pressure intensifier front panel, close the needle valve marked "X-2".

☐ On the Harwood Engineering pressure intensifier front panel, open the valve marked "XA". Then adjust the knob marked "AR" until the gage marked "G-3" reads 1000 psi.

☐ On the Harwood Engineering pressure intensifier front panel, adjust the regulator marked "R-1" until the gage marked "G-1" reads 4500 psi.

☐ Using the Macintosh Mac II, push "T" to bring up the Test command menu. Then push "B" to begin the command generation.

☐ On the Harwood Engineering pressure intensifier front panel, the yellow indicator light labeled "BOTTOM LIMIT SWITCH ACTIVATED" will go out. When the test is complete, the pressure command will be zero. This event will be evidenced by the lighting of the yellow indicator light labeled "BOTTOM LIMIT SWITCH ACTIVATED" on the Harwood Engineering pressure intensifier front panel.

Emergency shut down procedure if there is a fluid leak

If there is a fluid leak, stop the test by pushing "S" and then continue with the instructions.

☐ On the Harwood Engineering pressure intensifier front panel, adjust the regulator marked "R-1" until the gage marked "G-1" reads zero psi.

☐ On the Harwood Engineering pressure intensifier front panel, adjust the knob marked "AR" until the gage marked "GA" reads zero psi. Then close the valve marked "XA".

☐ Behind the Harwood Engineering pressure intensifier front panel, open the needle valve marked "X-2".

- [ ] On the Harwood Engineering pressure intensifier front panel, push the red button marked "STOP". The green indicator lights labeled "DRIVE PUMP RUN" and "RETRACTING PUMP RUN" will go out, but the red indicator light labeled "CONTROL POWER ON" and the yellow indicator light labeled "BOTTOM LIMIT SWITCH ACTIVATED" will remain lit. Then push the red button labeled"OFF" to extinguish these remaining indicator lights.

- [ ] Using the Macintosh Mac II, push "Q" and then "Y" to save the data and end execution of the program.

- [ ] Using the Macintosh Mac II, rename the file "Output.dat" for future examination using IGOR.

- [ ] Close the cooling water valve for the Harwood Engineering pressure intensifier.

Plug Specimen Removal

CHECK HERE

- [ ] Loosen and unscrew the nut which retains the electrical feedthru plug. Be careful not to let the weight of the nut hang on the wire.

- [ ] Loosen and unscrew the nut for the high pressure tubing connection to the intensifier.

- [ ] Loosen the SHCS's which mount the vessel. Unscrew them, lowering the vessel onto the support arm, and freeing the lower endcap.

- [ ] Rotate the support arm out from underneath the upper grip, ensuring that the high pressure tubing exits the port on the left side of the vessel. Remove the SHCS's and the lower endcap. The vessel plug will now be unsupported and may drop out of the vessel bore.

- [ ] Using a torque wrench and the reaction-torque tool to prevent the vessel from rotating, loosen the 4 SHCS in the upper adapter. Be careful not to knock the vessel off the support arm! Remove the SHCS and then carefully lift the upper adapter straight up by 1 inch. Carefully reach underneath and hold the load cell wire to prevent it from being tugged while you place the upper adapter on the support arm, to the left of the vessel.

- [ ] Thread the puller provided into the tapped holes in the plug in the feedthru bore

- [ ] Remove the feedthru from its bore.

- [ ] With a plastic drift punch inserted from below, carefully push the plug specimen and Load Cell Housing upward, until they come out of the vessel bore. The lower seal will remain in the vessel.

- [ ] Remove the lower anti-extrusion rings and seal from the vessel bore by tapping them out with a plastic drift punch inserted down the vessel bore.

Reduce The Calibration Data

CHECK HERE

☐ Using the Macintosh Mac II, read the data file using IGOR and plot WPlug_Int_LC_Volts vs WPlug_Sho_Stress.
Append WPlug_Int_LC_Volts_1 vs WPlug_Sho_Stress_1,
WPlug_Int_LC_Volts_2 vs WPlug_Sho_Stress_2,and
WPlug_Int_LC_Volts_3 vs WPlug_Sho_Stress_3.

• Fit a line to this data. Extrapolate the line to zero Shoulder Stress to make sure that it passes through the origin. If it doesn't, drop the Y-intercept to create a new curve-fit line that does.

• The equation of the curve fit line found in calibration 1 (y = m1*x + 0) will be subtracted from the equation of this new line (y = m2*x + 0) and the difference will be inserted into the subroutine "Modify Commands.c" of projects "Mono Load Control" and "Cyclic Load Control" in the following form:

int_l_c_pressure_effect = (m2 - m1) * stress_in_shoulder

3. Solid Bar W/Pressure Calibration Check

Solid Bar Specimen Installation

These are sequential instructions which must be followed in order.

CHECK HERE

- ☐ Obtain a "Solid Bar Specimen." This is a 0.4375 diameter specimen made from hardened steel which has no reduced gage section machined into it, and no strain gages attached.

- ☐ Clean vessel with an aerosol cleaning solvent available at the EE Storeroom. Wash from top to bottom, allowing the liquid to flush away any dirt and grease. Clean the vessel support arm and place the vessel on it.

- ☐ Lubricate the vessel bores with the high pressure fluid. Remove any fluid puddles from the thread undercut for the electrical feedthru bore.

- ☐ Handling them with extreme care, select and clean a new set of 0-ring seals with electronics parts cleaner. Alternately, you may clean and reuse O-ring seals which are known to have not leaked, if they pass a careful visual inspection for damage. Discard any O-ring seals which are damaged.

- ☐ After checking and/or replacing the backup rings, install the cleaned O-ring seals on the Load Cell Housing. Lubricate the specimen shoulder near the conical end with the high presure fluid. With a gentle twisting motion, insert the specimen into the Load Cell Housing until the conical surfaces mate. Be careful not to crush the internal backup ring, which is easily done if it falls out of position.

- ☐ Lubricate the outer diameter of the Load Cell Housing seal with the high pressure fluid.

- ☐ Insert the assembly into the bore of the vessel, sliding the specimen down the main bore. Insert the assembly until the top of the Load Cell Housing is slightly above the top surface of the vessel. Do NOT push it in too far!

- ☐ Install the four 3/8-16 x 1.75 SHCS into their counterbores in the Upper Adapter. Using a torque wrench and the reaction-torque tool to prevent the vessel from rotating, torque these fasteners to 30 ft-lbs in a star pattern (this will seat the Load Cell Housing in the vessel bore). Position the torque wrench so that it is parallel to the handle of the reaction-torque tool during the final stages of tightening. Be careful not to knock the vessel off the support arm!

- ☐ Lubricate the specimen shoulder with the high presure fluid. Then dip a cleaned O-ring seal into the high presure fluid and install it on the shoulder. Taking extreme care not to move the specimen axially, push the seal 2.00 inches onto the shoulder.

- ☐ Clean and grease the mating surfaces of an anti-extrusion ring and install it on the long shoulder.

- [ ] Lubricate the threads and underneath the heads of the six 3/8-16 x 6.5 SHC screws with all purpose grease. Insert them into the lower endcap for the vessel. Hold your hand underneath the lower endcap to support it and keep the SHCS's from dropping out of their holes. Place the steel spacer over the specimen hole in the lower endcap.

- [ ] Position the lower endcap so that the word "FRONT" is facing you, and from below, insert the SHCS's into their respective holes in the vessel. Raise the lower endcap, so that the specimen passes thru the spacer. Continue raising the lower endcap as the SHCS's pass thru upper collet adapter.

- [ ] Rotate the support arm underneath the upper grip, ensuring that the high pressure tubing enters the port on the left side of the vessel. Raising the lower endcap against the vessel inserts the seal, anti-extrusion rings and spacer into the bore of the vessel. Ensure that the pins in the lower end cap enter the holes in the bottom of the vessel. Thread the SHCS's into the upper grip.

- [ ] Snug, and then torque the SHCS's to 30 ft-lbf in a star pattern.

- [ ] Tighten the nut for the high pressure tubing connection to the vessel.

- [ ] Tighten the nut for the bleed port behind the vessel.

- [ ] Check the condition of the o-ring on the feedthru plug. Replace if necessary. Lubricate the o-ring on the feedthru plug with the high pressure fluid.

- [ ] The dummy gages are not used in this calibration.

- [ ] Insert the electrical feedthru into the feedthru bore in the vessel.

- [ ] Thread in and tighten the nut which retains the electrical feedthru plug.

- [ ] The Extensometer is not used in this calibration.

Bleed The Vessel

CHECK HERE

☐ On the Harwood Engineering pressure intensifier front panel, unscrew the knob marked "AR" until it stops.

☐ Behind the Harwood Engineering pressure intensifier front panel, open the needle valve marked "X-2". The gage marked "G-3" will then read zero.

☐ Using the Macintosh Mac II, open the folder labeled "Development". Then open the folder labeled "16 bit Programs". Open the folder labeled "Calibrate Int LC". Open the folder labeled "Calibrate Int LC W/Press". Save the old file "Output.dat" under a new name, if you have not already done this. Open the file "Initialize.c". Enter all necessary info into the subroutine "Calibrations()". **Set:**

ramp_pressure_to = 20000.
cycle_pressure_from = 20000.
cycle_pressure_to = 20000.
ramp_stress_to = 20000.
cycle_stress_from = 20000.
cycle_stress_to = 20000.
int_l_c_gain_factor = 1.0
zero_offset_load = -30.0

in the "Calibrations()" subroutine in Initialize.c Save the file "Initialize.c". From THINK C, run the program "Calibrate Int LC W/O Pressure". This program displays the transducer outputs on the screen for zeroing, displays the current cycle number on a counter, provides ramp up, cyclic, & ramp down command signals for load & pressure during the test, and stores the test data.

☐ Put on the white hard hat and lower the face shield.

☐ On the Harwood Engineering pressure intensifier front panel, open the valve marked "XA". Then adjust the knob marked "AR" until you can hear the charge pump slowly cycling.

☐ Loosen the plug closing the bleed port behind the pressure vessel until fluid begins to come out. When a stream of fluid comes out with no entrained air bubbles, tighten the plug.

☐ On the Harwood Engineering pressure intensifier front panel, adjust the knob marked "AR" until the gage marked "GA" reads zero psi. Then close the valve marked "XA".

Zero The Pressure Transducer

CHECK HERE

☐ Zero the pressure transducer using the trim-pot marked "RTI ZERO F" on the Ectron R687 marked "Pressure XDCR." Adjust the "RTI ZERO F" trim-pot until you get the following output on the Mac II screen:

p_xdcr = 0 (bits)

Zero The External Load Cell

CHECK HERE

☐ With the lower grip lowered, zero the external load cell using the ten-turn-pot marked "XDCR 2" "ZERO" on the MTS 406 Controller. Adjust the "ZERO" pot until you get the following output on the Mac II screen:

Ext_LC = 0 (bits)

The strain gage signals need not be zeroed for this calibration.

Raise The Lower Grip

CHECK HERE

- [ ] Open the cooling water valves for the Harwood Engineering pressure intensifier and the MTS HPU.

- [ ] On the Harwood Engineering pressure intensifier front panel, adjust the knob marked "AR" until the gage marked "GA" reads zero.

- [ ] Behind the Harwood Engineering pressure intensifier front panel, open the needle valve marked "X-2". The gage marked "G-3" will then read zero.

- [ ] Open the release valve on the Enerpac P18 hand pump.

- [ ] Check that at least 5 threads are visible on each of the collet releasing screws on the lower collet adapter. If not, unscrew them.

- [ ] **On the MTS 406 Controller, turn the switch marked "FDBK SELECT" to the position marked "XDCR 2." Then adjust the knob marked "GAIN" to 6.5 and the knob marked "RATE" to 8.5.**

- [ ] On the MTS 406 Controller, turn the switch under the panel meter to the position marked "ERROR".

- [ ] On the panel located above the MTS 406 Controller, turn the switch to the position marked "XDCR 2" "DC" to display the external load cell output on the Digital Read Out (DRO).

- [ ] **On the MTS 406 Controller, turn the knob marked "SET POINT" so that the panel meter on the MTS 406 reads a negative value.**

- [ ] On the MTS 413 Master Control Panel, push the blue button marked "RESET." Then push the white button marked "HYDRAULIC PRESSURE""HIGH LOW"" once to turn the HPU on. Then push the white button marked "HYDRAULIC PRESSURE""HIGH LOW" a second time. Increase the hydraulic pump pressure to 3000 psi by turning the knob marked "PRESSURE CONTROL" on the MTS HPU cw. If the lower grip is not in its lowest position, it will move downward.

- [ ] Check the MTS HPU pressure and if necessary, adjust the regulator (the knob marked "PRESSURE CONTROL") so that the gage reads 3000psi. Tighten the locknut.

- [ ] On the MTS 406 Controller, turn the knob marked "SET POINT" clockwise until the lower grip begins to rise. The panel meter on the MTS 406 Controller will read a positive value. Let the grip slowly rise until the specimen bottoms against the collet stop.

- [ ] When the specimen bottoms against the collet stop, close the release valve on the Enerpac P18 hand pump.

☐ Slowly pump the Enerpac P18 hand pump to 3000psi. The lower grip should move downward slightly as the lower collet protrudes out of its opening, signifying that the specimen is indeed bottomed against the collet stop.

☐ **Do not turn off the MTS HPU while the specimen is gripped in the lower grip.**

Synchronize The Load Cells

CHECK HERE

☐ The internal and external load cells must now be synchronized to each other and to the command signal from the MAC II. Adjust the knob marked "SET POINT" on the MTS 406 Controller until you get the following output on the Mac II screen.

Ext_LC = -49.2 (bits)

This external load cell setting is derived as follows:

- "zero_offset_load" is the value of the user-specified compressive load in subroutine "Calibrations()" in file "Initialize.c".
- The external load cell calibration is 20,000 lbf per 10VDC.
- "ten_volt_load" is the value of this calibration (modified by the NIDAQ board gain) in subroutine "Calibrations()" in file "Initialize.c".
- There are 32,767 bits per 10 volts

$$\frac{\text{zero\_offset\_load}}{\text{ten\_volt\_load}} * 32{,}767 = \frac{-30}{20000} * 32{,}767 = -49.2 \text{ bits}$$

☐ The internal load cell output should now be set as follows: Zero the internal load cell output using the trim-pots marked "ZERO" on the Ectron Model 687. Adjust the "RTI ZERO" trim-pots until you get the following output on the Mac II screen:

$$\text{Int\_LC} = \frac{-1.0 * (\text{Y-intercept from calibration 1 in Volts}) * 32767}{10.0}$$

☐ Check the transducer readings on all channels, and readjust if necessary.
The strain gage amplifiers are not used in this calibration.

Run Calibration Check

Complete several calibration runs to "bed-in" the set-up before taking your data.

CHECK HERE

☐ Ensure that all safety guards are in place.

☐ On the Harwood Engineering pressure intensifier front panel, push the green button marked "CONTROL POWER ON". The red indicator light labeled "CONTROL POWER ON" and the yellow indicator light labeled "BOTTOM LIMIT SWITCH ACTIVATED" will light up. Then push the green button marked "SYSTEM START" to start the hydraulic pumps. The green indicator lights labeled "DRIVE PUMP RUN" and "RETRACTING PUMP RUN" will light up. The gage marked "G-2" should read 500 psi.

Protect your hearing; put on the sound suppressors!

☐ Behind the Harwood Engineering pressure intensifier front panel, close the needle valve marked "X-2".

☐ On the Harwood Engineering pressure intensifier front panel, open the valve marked "XA". Then adjust the knob marked "AR" until the gage marked "G-3" reads 1000 psi.

☐ On the Harwood Engineering pressure intensifier front panel, adjust the regulator marked "R-1" until the gage marked "G-1" reads 4500 psi.

☐ Using the Macintosh Mac II, push "T" to bring up the Test command menu. Then push "B" to begin the command generation.

☐ On the Harwood Engineering pressure intensifier front panel, the yellow indicator light labeled "BOTTOM LIMIT SWITCH ACTIVATED" will go out, and the reading on the DRO will change. When the test is complete, the pressure command will be zero and the load command will be "zero_offset_load". This event will be evidenced by the lighting of the yellow indicator light labeled "BOTTOM LIMIT SWITCH ACTIVATED" on the Harwood Engineering pressure intensifier front panel, and a steady reading on the DRO.

Emergency shut down procedure if there is a fluid leak

If there is a fluid leak, stop the test by pushing "S" and then continue with the instructions.

☐ On the Harwood Engineering pressure intensifier front panel, adjust the regulator marked "R-1" until the gage marked "G-1" reads zero psi.

☐ On the Harwood Engineering pressure intensifier front panel, adjust the knob marked "AR" until the gage marked "GA" reads zero psi. Then close the valve marked "XA".

☐ Behind the Harwood Engineering pressure intensifier front panel, open the needle valve marked "X-2".

☐ On the Harwood Engineering pressure intensifier front panel, push the red button marked "STOP". The green indicator lights labeled "DRIVE PUMP RUN" and "RETRACTING PUMP RUN" will go out, but the red indicator light labeled "CONTROL POWER ON" and

the yellow indicator light labeled "BOTTOM LIMIT SWITCH ACTIVATED" will remain lit. Then push the red button labeled"OFF" to extinguish these remaining indicator lights.

☐ Using the Macintosh Mac II, push "Q" and then "Y" to save the data and end execution of the program "Load Control".

☐ Using the Macintosh Mac II, rename the file "Output.dat" to "20000psi" for future examination using IGOR.

• Each run of this "check" gives a file from which you will extract one data point. To get the second file, **set:**

ramp_pressure_to = 40000.
cycle_pressure_from = 40000.
cycle_pressure_to = 40000.
ramp_stress_to = 40000.
cycle_stress_from = 40000.
cycle_stress_to = 40000.

in the "Calibrations()" subroutine in Initialize.c Save the file "Initialize.c". From THINK C, run the program "Calibrate Int LC W/Press".

• Now repeat the instructions from "ZERO" THE TRANSDUCERS. When that check run is complete, rename the file "Output.dat" to "40000psi" for future examination using IGOR.

• Continue to increment in steps of 20,000 psi until you reach 100,000 psi.

• A zero data point will be:

WP_Sho_Stress	WP_Pressure	WP_Int_LC_Volts
approx 0 psi	0 psi	0.0 volts

Lower The Lower Grip

CHECK HERE

- [ ] Open the release valve on the Enerpac P18 hand pump.

- [ ] Simultaneously screw in each of the two collet releasing screws on the lower collet adapter. This will free the specimen from the self-holding action of the collet.

- [ ] On the MTS 406 Controller, turn the switch under the panel meter to the position marked "ERROR".

- [ ] On the MTS 406 Controller, turn the knob marked "SET POINT" counterclockwise so that the panel meter on the MTS 406 reads a negative value. The lower grip will move downward.

- [ ] On the MTS 413 Master Control Panel, push the red button marked "HYDRAULIC OFF" to stop the hydraulic pump. The blue button marked "RESET" will light up.

- [ ] Close the cooling water valves for the Harwood Engineering pressure intensifier and the MTS HPU.

Specimen Removal

CHECK HERE

- [ ] Loosen and unscrew the nut which retains the electrical feedthru plug. Be careful not to let the weight of the nut hang on the wire.

- [ ] Loosen and unscrew the nut for the high pressure tubing connection to the intensifier.

- [ ] Loosen the SHCS's which mount the vessel. Unscrew them, lowering the vessel onto the support arm, and freeing the lower endcap.

- [ ] Rotate the support arm out from underneath the upper grip, ensuring that the high pressure tubing exits the port on the left side of the vessel. Remove the SHCS's and the lower endcap by sliding it down and off of the specimen. The anti-extrusion rings and the spacer will now be unsupported and may drop out of the vessel bore.

- [ ] Using a torque wrench and the reaction-torque tool to prevent the vessel from rotating, loosen the 4 SHCS in the upper adapter. Be careful not to knock the vessel off the support arm! Remove the SHCS and then carefully lift the upper adapter straight up by 1 inch. Carefully reach underneath and hold the load cell wire to prevent it from being tugged while you place the upper adapter on the support arm, to the left of the vessel.

- [ ] Thread the puller provided into the tapped holes in the plug in the feedthru bore

- [ ] Taking extreme care not to move the specimen axially, remove the feedthru from its bore.

- [ ] Carefully push the specimen and Load Cell Housing upward, until they come out of the vessel bore. The lower seal will remain in the vessel.

- [ ] Remove the lower anti-extrusion rings and seal from the vessel bore by tapping them out with a plastic drift punch inserted down the vessel bore.

Reduce The Calibration Data

- [ ] Using the Macintosh Mac II, read the data file "20000psi" using IGOR and plot WP_Sho_Stress_64, WP_Pressure_64, and WP_Int_LC_Volts_64 vs the number of data points. Find the average values of each.

  • Plot (WP_Int_LC_Volts_64, WP_Sho_Stress_64) on the graph you made in calibration 2. The point should fall on the line.

  • Repeat for data file "40000psi" and all other data files.

Specimen and/or Dummy Gage Preparation

These are sequential instructions which must be followed in order.

CHECK HERE

☐ Using 400 grit sandpaper, wetted with water and detergent, sand and polish the specimen shoulders axially until no grinding marks are visible. Sand and polish the chamfered ends of the specimen so that the seals will not be damaged during installation. Polish the specimen with the motor setup and wet 600 grit paper.

☐ With soap and hot water, clean the specimen to remove all polishing residue. Blow dry with compressed air.

☐ Using a micrometer, measure and record the gage section diameter and the diameter of the shoulder. These will be entered into the "Calibrations()" subroutine in Initialize.c of programs "Mono Load Control" and "Cyclic Load Control".

☐ Mix a batch of Adhesive. **READ ALL APPLICABLE MSDS SHEETS BEFORE CONTINUING! THE CHEMICALS YOU WILL BE USING NEXT CAN BE FATAL IF INHALED, AND CAN CAUSE SERIOUS BURNS IF SPILLED ON THE SKIN OR EYES!**

• Measurements Group M-Bond 610: These are two component, high performance epoxy-resin adhesive systems, supplied in "Adhesive" and "Curing Agent" bottles. They must be at room temperature before opening. Using a disposible pipette, pipette 1 unit of the clear "Adhesive" into a small, clean specimen bottle. Discard this pipette. Using a disposible pipette, pipette .84 units of the yellow "Adhesive" into the specimen bottle. Discard this pipette. Thoroughly mix for 10 seconds, and then let the freshly mixed adhesive stand for one hour before using. Write the date on the specimen bottle. Pot life is two weeks.

• Measurements Group M-Bond AE-15: These are two component, 100% solids epoxy-resin adhesive systems, supplied in "Adhesive Resin AE" and "Curing Agent 15" bottles. They must be at room temperature before opening. Fill one of the calibrated droppers with Curing Agent 15 exactly to the number 15 and dispense it into the center of the jar of Resin AE. Discard this dropper and immediately cap the Curing Agent 15. Using a plastic stirring rod, thoroughly mix for 5 minutes. Pot life is 1.5 hours.

☐ The specimens will now be cleaned and prepared for strain gage installation. Do not touch the cleaned surfaces with your fingers! Do not allow a cleaned surface to sit for more than a few minutes before gage installation! Do not allow a partially cleaned surface to sit for more than a few minutes between steps in the cleaning procedure!

☐ Solvent degrease the specimens using aerosol spray cans of Measurements Group CSM-1 Degreaser or an equivalent such as an aerosol cleaning solvent available at the EE Storeroom. Under an operating exhaust hood, wash specimens from top to bottom, allowing the liquid to flush away dissolved dirt and grease. Do not be excessive here, because the evaporating solvent cools the specimen and humidity in the air will condense upon it. Do not dust with compressed air, as the oil and water vapors present can recontaminate the specimen.

☐ **DO NOT USE "Measurements Group M-Prep Conditioner A" NOR "M-Prep Neutralizer 5" ON SPECIMENS WHICH ARE SUSCEPTIBLE TO HYDROGEN EMBRITTLEMENT (eg. irons, steels, titaniums, etc). SUBSTITUTE "Measurements Group CSM-1 Degreaser" OR AN EQUIVALENT SUCH AS "Chemtronics TF Solvent", OR "TF Plus Electronic Solvent/Degreaser" AVAILABLE AT THE EE STOREROOM.**

☐ Using Measurements Group M-Prep Conditioner A, wet the specimen's gage section and the short shoulder just above where it intersects the fillet radius. Abrade these surfaces with 400 grit silicon carbide production paper, while keeping the surfaces wet - do not allow the M-Prep Conditioner A to dry on the surfaces, as this will leave a contaminating film!

☐ Using a fine point marker, draw any necessary gage alignment marks on the specimen.

☐ Repeatedly apply Measurements Group M-Prep Conditioner A to the specimen's gage section and the short shoulder just above where it intersects the fillet radius. Scrub these surfaces with cotton tipped applicators until a clean tip is no longer discolored by the scrubbing, while keeping the surfaces wet - do not allow the M-Prep Conditioner A to dry on the surfaces, as this will leave a contaminating film!

☐ **DO NOT USE "Measurements Group M-Prep Conditioner A" NOR "M-Prep Neutralizer 5" ON SPECIMENS WHICH ARE SUSCEPTIBLE TO HYDROGEN EMBRITTLEMENT (eg. irons, steels, titaniums, etc). SUBSTITUTE "Measurements Group CSM-1 Degreaser" OR AN EQUIVALENT SUCH AS "Chemtronics TF Solvent", OR "TF Plus Electronic Solvent/Degreaser" AVAILABLE AT THE MRL STOREROOM.**

☐ When clean, the surface should be dried by wiping through the cleaned area with a single slow stroke of a gauze sponge. The stroke should begin inside the cleaned area to avoid dragging contaminants in from the boundary of the cleaned area. Then using a fresh sponge, wipe with a single slow stroke in the opposite direction, again beginning inside the cleaned area. The sponge should never be wiped back and forth, since this may redeposit contaminants on the cleaned surface.

☐ Liberally apply Measurements Group M-Prep Neutralizer 5 to the specimen's gage section and the short shoulder just above where it intersects the fillet radius. Scrub these surfaces with a clean cotton tipped applicator, while keeping the surfaces wet - do not allow the M-Prep Neutralizer 5 to dry on the surfaces, as this will leave a contaminating film!

☐ When neutralized, the surface should be dried by wiping through the cleaned area with a single slow stroke of a gauze sponge. The stroke should begin inside the cleaned area to avoid dragging contaminants in from the boundary of the cleaned area. Then using a fresh sponge, wipe with a single slow stroke in the opposite direction, again beginning inside the cleaned area. The sponge should never be wiped back and forth, since this may redeposit contaminants on the cleaned surface.

☐ Remove each gage from its mylar envelope with tweezers, making certain not to touch any exposed foil. Using tweezers and/or a clean dental probe, place the gage in position on a piece of MM MJG-2 Mylar Tape. (The MJG-2 tape has a silicone mastic which can withstand the elevated temperature curing cycle.) With biaxial rosette gages, align the gage/tape assemblies so that with the long specimen shoulder towards you, the solder tab side of the gage is to your right. This makes gage 1 the axial gage. This is desireable since gage 1 displays superior fatigue properties compared to gage 2 (due to directional property variations induced when the metal foil is cold rolled). Align the gage/tape assembly on the specimen and press the tape down. Peel it part way back so that the gage backing and the specimen are exposed.

☐ If using M-Bond AE-15, coat the gage backing and prepared specimen surfaces with a thin layer of adhesive.
[If using M-Bond 610, coat the gage backing and prepared specimen surfaces with a thin layer of adhesive, and permit the adhesive to air dry for 30 minutes by solvent evaporation.]
Then press the tape down with a mylar gage envelope between the gage and your fingers. Wipe off any adhesive that is squeezed out. Wrap another small piece of tape over the first one to prevent it from moving.

☐ Overlay the gage areas with thin teflon sheets (.003 thick, available from the chemistry storeroom) and then with 1/16" thick silicone rubber pads (available from McMaster-Carr). Clamp these down against the specimen with a pressure of 40-50 psi using the clamp blocks provided.

☐ Make sure that the oven is cool. Place the clamped gage/specimen assemblies into the oven. Turn on the oven.

- The temperature must be raised to the curing temperature at a rate of 5 to 20 °F (3 to 11°C) per minute. Air bubbles trapped in the adhesive, uneven gluelines, and high adhesive film stresses WILL result from starting with a hot oven.
- The adhesive must remain at the curing temperature for 1 hour.
  [This will also provide reduced chemical sensitivity of the adhesive to the vinyl placticizer high pressure fluid.]
- Allow the oven temperature to slowly drop at least 100°F (55°C) before removing the specimen.

  Curing Temperature for M-Bond 610 = 350°F (180°C)
  Curing Temperature for M-Bond AE-15 = 175°F (80°C)

- If this temperature will age or temper the specimen, choose another curing time/temperature combination from the graph on the instruction sheet supplied with the adhesive.

☐ Using the Macintosh Mac II, open the folder labeled "Development". Then open the folder labeled "Oven Control". Double-click on the application "Oven Control." Open the file "Initialize.c". Enter all necessary info into the subroutine "Calibrations()". Save the file "Initialize.c". From THINK C, run the program "Oven Control". This program provides ramp up, hold, and ramp down temperature command signals to the oven.

☐ When the program "Oven Control" indicates that the curing cycle is complete, push "Q" to exit the program, and then return. **Turn off the oven.** When they have cooled, remove the specimens from the oven, and carefully remove the clamps, the silicone pads and the teflon pads. Carefully begin to unwrap the tape from the gage, stopping when the solder tabs are exposed, but the foil grid is still protected by a layer of tape.

☐ Form the strain gage leads from 8 inch long pieces of Alpha Wire Corporation P/N 2841/1, 30 AWG silver plated solid copper wire with PTFE insulation, available at the EE Storeroom. Use:

red wire for the axial gage lead,
black wire for the common gage lead,
green wire for the circumferential gage lead.

[Optionally, form the strain gage leads from MM 134-AWQ polyimide enamel coated, 34 AWG solid copper wire. Using a razor blade, remove 1/16 inch of the polyimide enamel coating from the ends of the wires without damaging the wire itself. If this optional wire was used for the strain gage leads, differentiate each lead by soldering:

a short piece of red wire to the axial gage lead,
a short piece of black wire to the common gage lead,
a short piece of green wire to the circumferential gage lead.]

☐ Orient and solder the leads to the strain gage solder tabs so that when viewing the specimen from the short shoulder end, the biaxial gage leads come off that gage in a counter-clockwise direction. Under an operating exhaust hood, remove any flux residue using aerosol spray cans of Measurements Group CSM-1 Degreaser or an equivalent such as an aerosol cleaning solvent available at the EE Storeroom. Wash specimens from top to bottom, allowing the liquid to flush away dissolved dirt and grease. Check the electrical resistance of the gage by measuring across the leads using an ohmmeter.

Specimen Installation

These are sequential instructions which must be followed in order.

CHECK HERE

☐ Clean vessel with an aerosol cleaning solvent available at the EE Storeroom. Wash from top to bottom, allowing the liquid to flush away any dirt and grease. Clean the vessel support arm and place the vessel on it.

☐ Lubricate the vessel bores with the high pressure fluid. Remove any fluid puddles from the thread undercut for the electrical feedthru bore.

☐ Wrap the wires 1 to 2 turns counter clockwise around the specimen gage section as viewed from the short shoulder end. With a very small piece of MM MJG-2 Mylar Tape, tape the ends of the wires together near their free ends.

☐ Handling them with extreme care, select and clean a new set of O-ring seals with electronics parts cleaner. Alternately, you may clean and reuse O-ring seals which are known to have not leaked, if they pass a careful visual inspection for damage. Discard any O-ring seals which are damaged.

☐ After checking and/or replacing the backup rings, install the cleaned O-ring seals on the Load Cell Housing. Lubricate the short specimen shoulder with the high presure fluid and with a gentle twisting motion, insert the specimen into the Load Cell Housing until the conical surfaces mate. Be careful not to crush the internal backup ring, which is easily done if it falls out of position.

☐ Lubricate the outer diameter of the Load Cell Housing seal with the high pressure fluid.

☐ For specimens with gage section diameters less than 0.250", put the 2 gage section bushings into position around the gage section. Let the wires feed out through the vertical slot. These bushings reduce the volume of (compressible) fluid in the vessel.

☐ Insert the assembly into the bore of the vessel. The wires should make their way out of the feedthru bore, as the specimen slides down the main bore. Insert the assembly until the top of the Load Cell Housing is slightly above the top surface of the vessel. Do NOT push it in too far!

☐ Using great care not to pull on the wire attached to the Load Cell Housing, install the Upper Adapter so that the 2 alignment pins fit into their mating holes. Do not let the wire get pinched between the Upper Adapter and the vessel.

☐ Install the four 3/8-16 x 1.75 SHCS into their counterbores in the Upper Adapter. Using a torque wrench and the reaction-torque tool to prevent the vessel from rotating, torque these fasteners to 30 ft-lbs in a star pattern (this will seat the Load Cell Housing in the vessel bore). Position the torque wrench so that it is parallel to the handle of the reaction-torque tool during the final stages of tightening. Be careful not to knock the vessel off the support arm!

- [ ] Lubricate the long specimen shoulder with the high presure fluid. Then dip a cleaned O-ring seal into the high presure fluid and install it on the long shoulder. Taking extreme care not to move the specimen axially, push the O-ring seal 2.00 inches onto the shoulder with one of the steel spacers.

- [ ] Clean and grease the mating surfaces of an anti-extrusion ring and install it on the long shoulder.

- [ ] Lubricate the threads and underneath the heads of the six 3/8-16 x 6.5 SHC screws with all purpose grease. Insert them into the lower endcap for the vessel. Hold your hand underneath the lower endcap to support it and keep the SHCS's from dropping out of their holes. Place the steel spacer over the specimen hole in the lower endcap.

- [ ] Position the lower endcap so that the word "FRONT" is facing you, and from below, insert the SHCS's into their respective holes in the vessel. Raise the lower endcap, so that the specimen passes thru the spacer. Continue raising the lower endcap as the SHCS's pass thru upper collet adapter.

- [ ] Rotate the support arm underneath the upper grip, ensuring that the high pressure tubing enters the port on the left side of the vessel. Raising the lower endcap against the vessel inserts the seal, anti-extrusion rings and spacer into the bore of the vessel. Ensure that the pins in the lower end cap enter the holes in the bottom of the vessel. Thread the SHCS's into the upper grip.

- [ ] Snug, and then torque the SHCS's to 30 ft-lbf in a star pattern.

- [ ] Tighten the nut for the high pressure tubing connection to the vessel.

- [ ] Tighten the nut for the bleed port behind the vessel.

- [ ] Check the condition of the o-ring on the feedthru plug. Replace if necessary.

- [ ] Check the condition of the dummy gages and replace them if necessary. Prolonged exposure to the vinyl plasticizer degrades the epoxy and the gage backing.

- [ ] The strain gage leads will be visible when looking down the electrical feedthru bore. Slide the white plastic bushing over the leads.

- [ ] Place the electrical feedthru in the vice and position it in front of the feedthru bore in the vessel.

- [ ] Cut the strain gage leads to length. Strip and tin the ends.

☐ Solder the leads to their respective connections and dummy (pressure compensating) gages using standard rosin core solder. Remember to TURN THE AMPS OFF BEFORE SOLDERING!

Atmospheric side of the feedthru	High pressure side of the feedthru
black	black wire from the specimen axial gage
blue	black wire from the specimen circumferential gage
green	green wires for the circumferential specimen and dummy gages
red	black wires from the dummy axial gage
brown	black wire from the dummy circumferential gage
white	red wire from the specimen and dummy axial gages

☐ Slide the white plastic bushing over the dummy gage holder so that it covers the solder terminals.

☐ Using the Macintosh Mac II, open the folder labeled "Development". Then open the folder labeled "16 bit Programs". Then open the folder labeled "Zero Inputs". From THINK C, run the program "Zero Inputs". This program provides a zero load command signal and a full scale pressure command signal while it displays the transducer outputs on the screen. If you can zero the strain gage signals, this ensures that all solder connections are good.

☐ Lubricate the o-ring on the feedthru plug with the high pressure fluid.

☐ Remove the electrical feedthru from the vice and manually insert it into the feedthru bore in the vessel.

☐ Install the Extensometer Extension on the specimen shoulder to assist in rotating the specimen. Taking extreme care not to pull the specimen axially (you may push upward however), rotate the specimen clockwise to wind the strain gage leads around the gage section of the specimen as you simultaneously insert the plug into the feedthru bore. Then remove the Extensometer Extension.

☐ Thread in and tighten the nut which retains the electrical feedthru plug.

☐ Mount the 1/2" extensometer. Position the upper rod in the dimple provided on the pressure vessel cap. Position the lower rod on the shoulder such that the extensometer output is as close to zero as possible, while ensuring that it is properly oriented - an imaginary line drawn thru the upper and lower rod centers should be parallel to the specimen axis.

For the best resolution possible when measuring strains that are essentially unidirectional, choose an Amp Gain that provides a $|\Delta E|$ between 10 and 20 volts. Then when mounting the extensometer, open or close it to mechanically (and thus electrically) bias the amplifier output in the direction opposite to the direction of the expected voltage change during the test.

Example: for a tension test the axial strain will be positive. Choose a gain that will give +15V for the maximum deflection, and then mount the extensometer so that the amplifier is putting out -7.5V before the test starts. ie, mount the extensometer so that you get the following output on the Mac II screen:

exten = -24575 (bits)

and enter -24575 as the "extensometer_offset" in the Calibrations() subroutine of Initialize.c in either "Mono Load Control" or "Cyclic Load Control."

This extensometer setting is derived as follows:

•There are 32,767 bits per 10 volts

$$-7.5V * \frac{32767 \text{ bits}}{10V} = -24575 \text{ bits}$$

Bleed The Vessel

CHECK HERE

☐ On the Harwood Engineering pressure intensifier front panel, unscrew the knob marked "AR" until it stops.

☐ Behind the Harwood Engineering pressure intensifier front panel, open the needle valve marked "X-2". The gage marked "G-3" will then read zero.

☐ Using the Macintosh Mac II, open the folder labeled "Development". Then open the folder labeled "Current 16 bit Programs". Then open the folder labeled "Zero Inputs". From THINK C, run the program "Zero Inputs". This program provides a zero load command signal and a full scale pressure command signal while it displays the transducer outputs on the screen.

☐ Put on the white hard hat and lower the face shield.

☐ On the Harwood Engineering pressure intensifier front panel, open the valve marked "XA". Then adjust the knob marked "AR" until you can hear the charge pump slowly cycling.

☐ Loosen the plug closing the bleed port behind the pressure vessel until fluid begins to come out. When a stream of fluid comes out with no entrained air bubbles, tighten the plug.

☐ On the Harwood Engineering pressure intensifier front panel, adjust the knob marked "AR" until the gage marked "GA" reads zero psi. Then close the valve marked "XA".

Zero The Pressure Transducer

CHECK HERE

☐ Zero the pressure transducer using the trim-pot marked "RTI ZERO F" on the Ectron R687 marked "Pressure XDCR." Adjust the "RTI ZERO F" trim-pot until you get the following output on the Mac II screen:

p_xdcr = 0 (bits)

Zero The External Load Cell

CHECK HERE

☐ With the lower grip lowered, zero the external load cell using the ten-turn-pot marked "XDCR 2" "ZERO" on the MTS 406 Controller. Adjust the "ZERO" pot until you get the following output on the Mac II screen:

Ext_LC = 0 (bits)

Complete Test Set-Up Procedure

CHECK HERE

☐ Using the Macintosh Mac II, push "Q" to end execution of the program "Zero Inputs".

Run Test Simulation

CHECK HERE

☐ Using the Macintosh Mac II, open the folder labeled "Development". Then open the folder labeled "Current 16 bit Programs". Then open the folder labeled "Shoulder Stress Simulation". Open the Think C project labeled "Shoulder Stress Simulation". Save the old file "Output.dat" under a new name, if you have not already done this. Open the file "Initialize.c". Enter all necessary info into the subroutine "Calibrations" including the Yield Strength of the specimen in psi. Set:

cycle_num	=	1
samples per ramp	=	100
samples_per_cycle	=	100

Save the file "Initialize.c". From THINK C, run the program "Shoulder Stress Simulation". This program calculates ideal elastic stress and strain data, and stores it.

☐ Using the Macintosh Mac II, push "B" to begin the command generation.

☐ Using the Macintosh Mac II, push "Q" and then "Y" to save the data and end execution of the program "Load Control".

☐ Using the Macintosh Mac II, rename the file "Output.dat" and then examine it using IGOR.

☐ To see the specimen shoulder yield boundaries on a plot of axial stress vs pressure, plot int_sho_yield_1 vs Press_Bound_1, and append ext_sho_yield_1 vs Press_Bound_1, int_sho_yield_2 vs Press_Bound_2, and ext_sho_yield_2 vs Press_Bound_2. To see the specimen shoulder stress simulation, append Int_sho_stress_X vs Pressure_X, or Ext_sho_stress_X vs Pressure_X.

The strain amplifier gains must now be found. First set the gain for the axial strain gage. Use experience or elasto-plastic simulations to estimate the maximum axial strain. Then use the expression:

$$\varepsilon'_{zz\ active} = \frac{4\Delta E}{Sg_{\ zz\ active}\ (Amp\ Gain)\ V_{excit}} + p\frac{Sg_{\ zz\ dummy}}{Sg_{\ zz\ active}}\frac{(2\nu - 1)}{E}\left(\frac{1 + K_{tz\ dummy}}{1 - \nu_o\ K_{tz\ dummy}}\right)$$

Set $\varepsilon'_{zz\ active}$ equal to the maximum axial strain expected and solve for $\frac{\Delta E}{Amp\ Gain}$:

$$\frac{\Delta E}{Amp\ Gain} = \left(\varepsilon'_{zz\ active} - p\frac{Sg_{\ zz\ dummy}}{Sg_{\ zz\ active}}\frac{(2\nu - 1)}{E}\left(\frac{1 + K_{tz\ dummy}}{1 - \nu_o\ K_{tz\ dummy}}\right)\right)\left(\frac{Sg_{\ zz\ active}\ V_{excit}}{4}\right)$$

In the equation $\frac{\Delta E}{Amp\ Gain} = X$, substitute Amp Gains of 10, 20, 50, 100, 200, 500 and 1000, and solve for ΔE Choose the Amp Gain that provides a ΔE between 5 and 10 volts so you will have good resolution. If the amplifier output exceeds ±10.0 volts, your data will be lost. For the best resolution possible, choose an Amp Gain that provides a $|\Delta E|$ between 10 and 20 volts. Then use the ZERO adjustments to bias the amplifier output in the direction opposite to the direction of the voltage change during the test.

Example: for a compression test the axial strain will be compressive, so the ΔE will be negative. Choose a gain that will give a ΔE of -15V, and then adjust the ZERO so that the amplifier is putting out +7.5V before the test starts. Then calculate the number of bits corresponding to +7.5V as follows:

$$+7.5V \frac{32767 \text{ bits}}{10V} = +24575 \text{ bits}$$

and enter 24575 as the "e_gage_1_offset" in the Calibrations() subroutine of Initialize.c in either "Mono Load Control" or "Cyclic Load Control."

Next set the gain for the circumferential strain gage. Use experience or elasto-plastic simulations to estimate the maximum circumferential strain. Then use the expression:

$$\varepsilon'_{\theta\theta \text{ active}} = \frac{4\Delta E}{Sg_{\theta\theta \text{ active}} (\text{Amp Gain}) V_{excit}} + p \frac{Sg_{\theta\theta \text{ dummy}}}{Sg_{\theta\theta \text{ active}}} \frac{(2\nu - 1)}{E} \left(\frac{1 + K_{t\theta \text{ dummy}}}{1 - \nu_o K_{t\theta \text{ dummy}}} \right)$$

Set $\varepsilon'_{\theta\theta \text{ active}}$ equal to the maximum axial strain expected and solve for $\frac{\Delta E}{\text{Amp Gain}}$:

$$\frac{\Delta E}{\text{Amp Gain}} = \left(\varepsilon'_{\theta\theta \text{ active}} - p \frac{Sg_{\theta\theta \text{ dummy}}}{Sg_{\theta\theta \text{ active}}} \frac{(2\nu - 1)}{E} \left(\frac{1 + K_{t\theta \text{ dummy}}}{1 - \nu_o K_{t\theta \text{ dummy}}} \right) \right) \left(\frac{Sg_{\theta\theta \text{ active}} V_{excit}}{4} \right)$$

In the equation $\frac{\Delta E}{\text{Amp Gain}} = X$, substitute Amp Gains of 10, 20, 50, 100, 200, 500 and 1000, and solve for ΔE Choose the Amp Gain that provides a ΔE between 5 and 10 volts so you will have good resolution. If the amplifier output exceeds $\pm$10.0 volts, your data will be lost.

For the best resolution possible, choose an Amp Gain that provides a $|\Delta E|$ between 10 and 20 volts. Then use the ZERO adjustments to bias the amplifier output in the direction opposite to the direction of the voltage change during the test.

Example: for a compression test the circumferential strain will be tensile, so the ΔE will be positive. Choose a gain that will give a ΔE of +15V, and then adjust the ZERO so that the amplifier is putting out -7.5V before the test starts. Then calculate the number of bits corresponding to -7.5V as follows:

$$-7.5V \frac{32767 \text{ bits}}{10V} = -24575 \text{ bits}$$

and enter -24575 as the "e_gage_2_offset" in the Calibrations() subroutine of Initialize.c in either "Mono Load Control" or "Cyclic Load Control."

Adjust Internal Load Cell Gain

When testing under high loads you must use a reduced internal load cell gain or the internal load cell output will exceed 10 volts and data will be lost.

Check the second column in the "Shoulder Stress Simulation" program to see if the internal load cell output exceeds 9 volts. If it does, you should use a reduced gain to avoid problems.

I use two different internal load cell gain settings:

Standard Gain
- int_l_c_gain_factor = 1.0 in the "Calibrations()" subroutine in Initialize.c

approximately 70% Gain
- int_l_c_gain_factor = approx 0.70 in the "Calibrations()" subroutine in Initialize.c

If the test machine is set for Standard Gain, it may be reset to approximately 70% Gain as follows:

☐ **Without turning on the Harwood Pressure Intensifier or the MTS HPU,** run any program ("Zero Inputs," "Mono Load Control," or "Cyclic Load Control") from THINK C so that the transducer outputs are printed to the screen.

☐ Zero the internal load cell output using the trim-pots marked "RTI ZERO" on the Ectron Model 687 internal load cell amplifier. Adjust the "RTI ZERO" trim-pots until you get the following output on the Mac II screen:

Int_LC = 0 (bits)

☐ Place a shunt resistor across the internal load cell arm of the strain gage bridge to cause the bridge to produce a large output (Int_LC = -31047).

☐ On the Ectron Model 687 internal load cell amplifier, turn the trim-pot marked "GAIN VERN" until the "Int_LC" reading equals approximately 70% of -31047 (69.94% Int_LC = -21715).

☐ In any control programs that you plan to use, set:

int_l_c_gain_factor = 0.6994

in the "Calibrations()" subroutine in Initialize.c

If the test machine is set for approximately 70% Gain, it may be reset to Standard Gain as follows:

☐ **Without turning on the Harwood Pressure Intensifier or the MTS HPU,** run any program ("Zero Inputs," "Mono Load Control," or "Cyclic Load Control") from THINK C so that the transducer outputs are printed to the screen.

☐ On the Ectron Model 687 internal load cell amplifier, turn the trim-pot marked "RTI ZERO" until the "Int_LC" reading equals zero.

☐ Place a shunt resistor across the internal load cell arm of the strain gage bridge to cause the bridge to produce a large output (Int_LC = -21715).

☐ On the Ectron Model 687 internal load cell amplifier, turn the trim-pot marked "GAIN VERN" until the "Int_LC" reading equals 143% of -21715 (Int_LC = -31047).

☐ In any control programs that you plan to use, set:

int_l_c_gain_factor = 1.0

in the "Calibrations()" subroutine in Initialize.c

Raise The Lower Grip

CHECK HERE

☐ Open the cooling water valves for the Harwood Engineering pressure intensifier and the MTS HPU.

☐ On the Harwood Engineering pressure intensifier front panel, unscrew the knob marked "AR" until it stops.

☐ Behind the Harwood Engineering pressure intensifier front panel, open the needle valve marked "X-2". The gage marked "G-3" will then read zero.

☐ **Monotonic test instructions** - Using the Macintosh Mac II, open the folder labeled "Development". Then open the folder labeled "Current 16 bit Programs". Open the folder labeled "Mono Load Control". Save the old file "Output.dat" under a new name, if you have not already done this. Open the file "Initialize.c". Enter all necessary info into the subroutine "Calibrations()". Save the file "Initialize.c". From THINK C, run the program "Mono Load Control". This program displays the transducer outputs on the screen for zeroing, provides ramp up, & ramp down command signals for load & pressure during the test, and stores the test data.

☐ **Cyclic test instructions** - Using the Macintosh Mac II, open the folder labeled "Development". Then open the folder labeled "Current 16 bit Programs". Open the folder labeled "Cyclic Load Control". Save the old file "Output.dat" under a new name, if you have not already done this. Open the file "Initialize.c". Enter all necessary info into the subroutine "Calibrations()". Save the file "Initialize.c". From THINK C, run the program "Cyclic Load Control". This program displays the transducer outputs on the screen for zeroing, displays the current cycle number on a counter, provides ramp up, cyclic, & ramp down command signals for load & pressure during the test, and stores the test data.

☐ Open the release valve on the Enerpac P18 hand pump.

☐ Check that at least 5 threads are visible on each of the collet releasing screws on the lower collet adapter. If not, unscrew them.

☐ On the MTS 406 Controller, turn the switch marked "FDBK SELECT" to the position marked "EXT." Then adjust the knob marked "GAIN" to 5.8 and the knob marked "RATE" to 10.0.

☐ On the MTS 406 Controller, turn the switch under the panel meter to the position marked "ERROR".

☐ On the panel located above the MTS 406 Controller, turn the switch to the position marked "XDCR 2" "DC" to display the external load cell output on the Digital Read Out (DRO).

☐ On the MTS 406 Controller, turn the knob marked "SET POINT" so that the panel meter on the MTS 406 reads a negative value.

☐ On the MTS 413 Master Control Panel, push the blue button marked "RESET." Then push the white button marked "HYDRAULIC PRESSURE""HIGH LOW"" once to turn the HPU on. Then push the white button marked "HYDRAULIC PRESSURE""HIGH LOW" a second time. Increase the hydraulic pump pressure to 3000 psi by turning the knob marked "PRESSURE CONTROL" on the MTS HPU cw. If the lower grip is not in its lowest position, it will move downward.

☐ Check the MTS HPU pressure and if necessary, adjust the regulator (the knob marked "PRESSURE CONTROL") so that the gage reads 3000psi. Tighten the locknut.

☐ On the MTS 406 Controller, turn the knob marked "SET POINT" counterclockwise until the lower grip begins to rise. The panel meter on the MTS 406 Controller will read a positive value. Let the grip slowly rise until the specimen bottoms against the collet stop. **Keep the compressive load on the specimen small or you may yield the specimen!**

☐ When the specimen bottoms against the collet stop, close the release valve on the Enerpac P18 hand pump.

☐ Slowly pump the Enerpac P18 hand pump to 2000psi. The lower grip should move downward slightly as the lower collet protrudes out of its opening, signifying that the specimen is indeed bottomed against the collet stop.

☐ **Do not turn off the MTS HPU while the specimen is gripped in the lower grip.**

"Zero" The Transducers

CHECK HERE

☐ The internal and external load cells must now be synchronized with each other and to the command signal from the MAC II. During this process you must make small, simultaneous adjustments to the knob marked "SET POINT" on the MTS 406 Controller and to the trim-pot marked "RTI ZERO F" on the Ectron Model 687 internal load cell amplifier, **while keeping the compressive load on the specimen small, so as not to yield the specimen!** When using the Standard Gain (int_l_c_gain_factor = 1.0 in the "Calibrations()" subroutine in Initialize.c), adjust the knobs until you get these simultaneous readings on the Mac II screen:

Ext_LC = -492 (bits) Int_LC = -862 (bits)

These numbers are derived as follows:

- "zero_offset_load" is the value of the user-specified compressive load in subroutine "Calibrations()" in file "Initialize.c". This is typically set to -300.0 pounds force.
- The external load cell calibration is 20,000 lbf per 10VDC.
- "ten_volt_load" is the value of this calibration (modified by the NIDAQ board gain) in subroutine "Calibrations()" in file "Initialize.c".
- There are 32,767 bits per 10 volts

$$\frac{\text{zero\_offset\_load}}{\text{ten\_volt\_load}} * 32{;}767 = \frac{-300}{20000} * 32{,}767 = -492 \text{ (bits)}$$

The internal load cell calibration is given by a curve fit in file "Modify Commands.c" (A is the area of the specimen shoulders, 0.15 in^2).

$$\text{stress\_in\_shoulder} = \frac{\text{zero\_offset\_load}}{A * 10000.0}$$

int_l_c_no_pressure = 1.31456 * stress_in_shoulder

For a zero_offset_load = -300#, stress_in_shoulder = -0.2
int_l_c_no_pressure = -0.263

here, $\frac{\text{int\_l\_c\_no\_pressure} * 32767}{10 \text{ V}} = \frac{-0.263 \text{ V} * 32767}{10 \text{ V}} = -862 \text{ (bits)}$

When testing under high loads which call for using a reduced gain, ("int_l_c_gain_factor" less than unity), adjust the knobs until you get these simultaneous readings:

Ext_LC = -492 (bits) Int_LC = int_l_c_gain_factor * -862 (bits)

☐ Zero the strain gage amplifiers using the trim-pots marked "ZERO" on the Ectron R687's. The "GAIN VERN" switches should be in the "OUT" position. Turn the knobs marked "GAIN" to "1K". Adjust the "RTI ZERO" trim-pots until you get the following output on the Mac II screen:

e_gage_1 = 0 (bits) e_gage_2 = 0 (bits)

Turn the knobs marked "GAIN" to "10". Adjust the "RTO ZERO" trim-pot until you get the following output on the Mac II screen:

e_gage_1 = 0 (bits) e_gage_2 = 0 (bits)

☐ Set the strain gage amplifier gains to the values determined in "Run Test Simulation" using the knobs marked "GAIN" on the Ectron R687's.

☐ Adjust the strain gage amplifier outputs using the trim-pots marked "RTI ZERO C" and "RTI ZERO F".

Note: the "zero_offset_load" strains the specimen, so the gage outputs cannot simply be set to the "e_gage_1_offset" and "e_gage_2_offset" values calculated in the simulation section. The correction for the strains due to the zero_offset_load are calculated as follows:

"a" is the area of the specimen gage section.
"E" is the elastic modulus of the specimen.
"ν" is the Poisson's Ratio of the specimen.

σ_{zz} = zero_offset_load / a

$\varepsilon_{zz} = \sigma_{zz} / E$

ten_volt_e_gage_1A = 10.0/(amp_gain_1 * excitation voltage/4.0 * gage_factor_1A)

$\varepsilon_{zz} = \sigma_{zz} / E$ = zero_offset_load_correction_1 * ten_volt_e_gage_1A / 32,768

zero_offset_load_correction_1 (in bits) = σ_{zz} * 32,768 / (E * ten_volt_e_gage_1A)

Adjust the "RTI ZERO" trim-pots until you get the following output on the Mac II screen:

e_gage_1 = [e_gage_1_offset + zero_offset_load_correction_1] (bits)

$\varepsilon_{\theta\theta} = - \nu * \sigma_{zz} / E$

ten_volt_e_gage_2A = 10.0/(amp_gain_2 * excitation_voltage/4.0 * gage_factor_2A)

$\varepsilon_{\theta\theta} = - \nu * \sigma_{zz} / E$ = zero_offset_load_correction_2 * ten_volt_e_gage_1A / 32,768

zero_offset_load_correction_2 (in bits) = - ν * σ_{zz} * 32,768 / (E * ten_volt_e_gage_1A)

Adjust the "RTI ZERO" trim-pots until you get the following output on the Mac II screen:

e_gage_2 = [e_gage_2_offset + zero_offset_load_correction_2] (bits)

☐ In case the axial strain gage fails, the extensometer provides a secondary signal from which gage section axial strain may be determined. The algorithm that calculates strain from the extensometer output requires that the extensometer have an output **exactly** equal to "extensometer_offset" when the specimen is under zero axial load and zero pressure. It must be set with the specimen clamped in the lower grip.

Note: the "zero_offset_load" strains the specimen, so the extensometer output cannot simply be set to "extensometer_offset". The correction for the deflection due to the zero_offset_load is determined as follows (this assumes "zero_offset_load" is set to the recommended -300 lbf value):

Adjust the trim-pot marked "RTI ZERO F" on the Ectron Model 687 internal load cell Amplifier until you get this reading on the Mac II screen corresponding to -150 pounds force:

Ext_LC = -246 (bits)

Write down the extensometer reading that appears on the Mac II screen.
Call this reading "A" bits.

Adjust the trim-pot marked "RTI ZERO F" on the Ectron Model 687 internal load cell Amplifier until you get this reading on the Mac II screen corresponding to -300 pounds force:

Ext_LC = -492 (bits)

Write down the extensometer reading that appears on the Mac II screen.
Call this reading "B" bits.

Adjust the extensometer amplifier outputs using the trim-pots marked "RTI ZERO C" and "RTI ZERO F" until you get the following output on the Mac II screen:

exten = extensometer_offset + 2.0 x (B - A) (bits)

Pre-Pressurizing

Initial pressurization may induce a zero shift on the strain gages. You should guard against this effect by pressurizing the experimental set-up several times before running the actual test. This is usually done with the specimen under a hydrostatic stress state, maintaining the axial stress equal to (-1) * pressure.

CHECK HERE

☐ Ensure that all safety guards are in place.

☐ Ensure that the cooling water valves for the Harwood Engineering pressure intensifier and the MTS HPU are both open.

☐ Verify that the Enerpac P18 hand pump is pressurized. If it is not, then slowly pump it up, being careful not to place a large load on the specimen, or you can yield it.

☐ Using the Macintosh Mac II, open the file "Initialize.c". Enter all necessary info into the subroutine "Calibrations()", and set

ramp_pressure_to	= XXXXX.0
cycle_pressure_from	= XXXXX.0
cycle_pressure_to	= XXXXX.0
ramp_stress_to	= - XXXXX.0
cycle_stress_from	= - XXXXX.0
cycle_stress_to	= - XXXXX.0

Save the file "Initialize.c". From THINK C, run the program.

☐ Check the transducer readings on all channels, and readjust if necessary.

☐ On the Harwood Engineering pressure intensifier front panel, push the green button marked "CONTROL POWER ON". The red indicator light labeled "CONTROL POWER ON" and the yellow indicator light labeled "BOTTOM LIMIT SWITCH ACTIVATED" will light up. Then push the green button marked "SYSTEM START" to start the hydraulic pumps. The green indicator lights labeled "DRIVE PUMP RUN" and "RETRACTING PUMP RUN" will light up. The gage marked "G-2" should read 500 psi.

Protect your hearing; put on the sound suppressors!

☐ Behind the Harwood Engineering pressure intensifier front panel, close the needle valve marked "X-2".

☐ On the Harwood Engineering pressure intensifier front panel, open the valve marked "XA". Then adjust the knob marked "AR" until the gage marked "G-3" reads 1000 psi.

☐ On the Harwood Engineering pressure intensifier front panel, adjust the regulator marked "R-1" until the gage marked "G-1" reads (peak pressure required / 32.25 + 1000) psi.
Do not exceed 5000 psi!

☐ Using the Macintosh Mac II, push "T" to bring up the Test command menu. Then push "B" to begin the command generation.

☐ On the Harwood Engineering pressure intensifier front panel, the yellow indicator light labeled "BOTTOM LIMIT SWITCH ACTIVATED" will go out, and the reading on the DRO will change. When the test is complete, the pressure command will be zero and the load command will be "zero_offset_load". This event will be evidenced by the lighting of the yellow indicator light labeled "BOTTOM LIMIT SWITCH ACTIVATED" on the Harwood Engineering pressure intensifier front panel, and a steady reading on the DRO.

☐ On the Harwood Engineering pressure intensifier front panel, adjust the regulator marked "R-1" until the gage marked "G-1" reads zero psi.

☐ On the Harwood Engineering pressure intensifier front panel, adjust the knob marked "AR" until the gage marked "GA" reads zero psi. Then close the valve marked "XA".

☐ Behind the Harwood Engineering pressure intensifier front panel, open the needle valve marked "X-2".

☐ On the Harwood Engineering pressure intensifier front panel, push the red button marked "STOP". The green indicator lights labeled "DRIVE PUMP RUN" and "RETRACTING PUMP RUN" will go out, but the red indicator light labeled "CONTROL POWER ON" and the yellow indicator light labeled "BOTTOM LIMIT SWITCH ACTIVATED" will remain lit. Then push the red button labeled"OFF" to extinguish these remaining indicator lights.

☐ Using the Macintosh Mac II, push "Q" and then "Y" to save the data and end execution of the program "Load Control".

☐ Using the Macintosh Mac II, rename the file "Output.dat" and then examine it using IGOR. At the start of this run;

pressure = p = 1000 psi, and

$$\sigma_{zz} = \frac{\text{zero\_offset\_load}}{a} \quad \text{psi.}$$

$$\varepsilon_{zz} = \frac{\frac{\text{zero\_offset\_load}}{a} + 2\,\nu\,p}{E}, \quad \varepsilon_{\theta\theta} = \frac{-p + \nu p - \frac{\nu * \text{zero\_offset\_load}}{a}}{E}$$

For a steel specimen with a 0.200" diameter gage section and -300 lbf load, typical starting values are:

$$\sigma_{zz} = \frac{-300}{0.0314} = -9550 \text{ psi.}$$

$$\varepsilon_{zz} = \frac{-9550 + 2*0.3*1000}{29000000} = -0.000309$$

$$\varepsilon_{\theta\theta} = \frac{-1000 - 0.3(-1000 - 9550)}{29000000} = 0.000074$$

As soon as the pressure command exceeds zero_offset_load/a psi during the run, we have:

$$\sigma_{zz} = -1 * \text{pressure} = -p \text{ psi}$$

$$\varepsilon_{zz} = \varepsilon_{\theta\theta} = \frac{-p\,(1 - 2\,\nu)}{E}$$

For a steel specimen with a 0.200" diameter gage section, typical strain values when p = 10,000 psi are:

$$\varepsilon_{zz} = \varepsilon_{\theta\theta} = \frac{-10000\,(1 - 2 * 0.3)}{29000000} = -0.000138$$

Finding The Strain Calibration Factors:

You will find variables named "strain_cal_X" in the Calibrations() subroutine of Initialize.c in either "Mono Load Control" or "Cyclic Load Control." If you wish to use non-unity strain calibration factors, repeat the instructions found in the Pre-Pressurizing section with the following modifications:

Make a copy of "Cyclic Load Control". In Initialize(), set:

```
cycle_num                =      1;
last_cycle_num           =      1;
ramp_pressure_to         =      0.0;
cycle_pressure_from      =      0.0;
cycle_pressure_to        =      0.0;
ramp_stress_to           = -20000.0;
cycle_stress_from        = -20000.0;
cycle_stress_to          = -20000.0;
samples_per_ramp_1       =      400;
samples_per_ramp_2       =      1;
samples_per_cycle        =      400;
extra_samples_at_peaks   =      100;
load_cell_gain      =    8;
strain_cal_1             =      1.0;
strain_cal_2             =      1.0;
```

Use this program and the instructions from the Pre-Pressurizing section to do a strain calibration run. However, **do not turn on the Harwood Pressure Intensifier: do not put any pressure into the vessel at all.**

During the strain calibration run:

Gage Section Axial Stress = - 20000 psi.

$$\text{Calculated Gage Section Axial Strain} = \frac{-20000}{E}$$

$$\text{Calculated Gage Section Circumferential Strain} = \frac{\nu * 20000}{E}$$

After the strain calibration run with strain_cal_1 and strain_cal_2 both equal to 1.0, find the actual values of strain_cal_1 and strain_cal_2 from the following equations:

$$\text{strain\_cal\_1} = \frac{\text{Calculated Gage Section Axial Strain}}{\text{Gage Section Axial Strain displayed in output.dat}}$$

$$\text{strain\_cal\_2} = \frac{\text{Calculated Gage Section Circumferential Strain}}{\text{Gage Section Circumferential Strain displayed in output.dat}}$$

Finding The Pressure Calibration Factors:

You will find variables named "pressure_cal_X" in the Calibrations() subroutine of Initialize.c in either "Mono Load Control" or "Cyclic Load Control." If you wish to use non-unity pressure calibration factors, repeat the instructions found in the Pre-Pressurizing section with the following modifications:

Make a copy of "Cyclic Load Control."

In Initialize(), set:

cycle_num	=	1;
last_cycle_num	=	64;
ramp_pressure_to	=	P;
cycle_pressure_from	=	P;
cycle_pressure_to	=	P;
ramp_stress_to	=	- P;
cycle_stress_from	=	- P;
cycle_stress_to	=	- P;
samples_per_ramp_1	=	400;
samples_per_ramp_2	=	1;
samples_per_cycle	=	400;
pressure_cal_1	=	1.0;
pressure_cal_2	=	1.0;

Use this program and the instructions from the Pre-Pressurizing section to do a pressure calibration run.

At the start of the pressure calibration run,

pressure P = 1000 psi, and

gage section axial stress $\sigma = \frac{\text{zero\_offset\_load} + P * (A - a)}{a}$ psi, where

A = cross sectional area of specimen shoulder, and

a = cross sectional area of specimen gage section.

Then;

$$\text{Calculated Gage Section Axial Strain} = \frac{\sigma + 2 * \nu * P}{E}$$

$$\text{Calculated Gage Section Circumferential Strain} = \frac{-P - \nu * (\sigma - P)}{E}$$

During the actual run, pressure = Gage Section Axial Stress = - P psi.

Calculated Gage Section Axial Strain = Calculated Gage Section Circumferential Strain (for steel, this equals $\frac{-P * (1 - 2 * \nu)}{E}$ = -498 microstrain when P = 40,000 psi)

After the pressure calibration run with pressure_cal_1 and pressure_cal_2 both equal to 1.0, find the actual values of pressure_cal_1 and pressure_cal_2 from the following equations:

$$\text{pressure\_cal\_1} = 1.0 - \frac{(\text{Calculated Axial Strain}) - (\text{Axial Strain displayed in output.dat}) * E}{2.0 * \nu * \text{pressure\_psi}}$$

$$\text{pressure\_cal\_2} = 1.0 - \frac{(\text{Calc'd Circum Strain}) - (\text{Circum Strain displayed in output.dat}) * E}{2.0 * \nu * \text{pressure\_psi}}$$

Run Test

CHECK HERE

☐ Ensure that all safety guards are in place.

☐ Ensure that the cooling water valves for the Harwood Engineering pressure intensifier and the MTS HPU are both open.

☐ Verify that the Enerpac P18 hand pump is pressurized. If it is not, then slowly pump it up, being careful not to place a large load on the specimen, or you can yield it.

☐ Using the Macintosh Mac II, open the file "Initialize.c". Enter all necessary info into the subroutine "Calibrations()". Here are typical values to use in the programs, based upon the gage diameter:

Gage Diameter d	Short-Shoulder Length L_1	Gage Length L_2	Int Long-Shoulder Length L_3	Ext Long Shoulder Length L_4	L_4 For Stroke Xdcr S_4	Tweak Fillet Length fillet_fudge	Tweak Shoulder Length seal_fudge
0.200	0.340	1.003	0.275	0.88	1.00	0.	0.
0.220	0.346	1.004	0.274	0.88	1.00	0.	0.
0.250	0.356	0.993	0.280	0.88	1.00	0.	0.
0.290	0.370	0.984	0.284	0.88	1.00	0.	0.

Save the file "Initialize.c". From THINK C, run the program.

☐ Check the transducer readings on all channels, and readjust if necessary.

☐ On the Harwood Engineering pressure intensifier front panel, push the green button marked "CONTROL POWER ON". The red indicator light labeled "CONTROL POWER ON" and the yellow indicator light labeled "BOTTOM LIMIT SWITCH ACTIVATED" will light up. Then push the green button marked "SYSTEM START" to start the hydraulic pumps. The green indicator lights labeled "DRIVE PUMP RUN" and "RETRACTING PUMP RUN" will light up. The gage marked "G-2" should read 500 psi.

Protect your hearing; put on the sound suppressors!

☐ Behind the Harwood Engineering pressure intensifier front panel, close the valve marked "X-2"

☐ On the Harwood Engineering pressure intensifier front panel, open the valve marked "XA". Then adjust the knob marked "AR" until the gage marked "G-3" reads 1000 psi.

☐ On the Harwood Engineering pressure intensifier front panel, adjust the regulator marked "R-1" until the gage marked "G-1" reads (peak pressure required / 32.25 + 1000) psi.
Do not exceed 5000 psi!

☐ Using the Macintosh Mac II, push "T" to bring up the Test command menu. Then push "B" to begin the command generation.

☐ On the Harwood Engineering pressure intensifier front panel, the yellow indicator light labeled "BOTTOM LIMIT SWITCH ACTIVATED" will go out, and the reading on the DRO will change. When the test is complete, the pressure command will be zero and the load command will be "zero_offset_load". This event will be evidenced by the lighting of the yellow indicator light labeled "BOTTOM LIMIT SWITCH ACTIVATED" on the Harwood Engineering pressure intensifier front panel, and a steady reading on the DRO.

Emergency shut down procedure if specimen breaks

Leaking Fluid: The test program is designed to recharge the intensifier (pressure ramps to zero, load ramps to zero_offset_load / a. Then after a few seconds, pressure and load ramp back up and test continues.) whenever the intensifier hits the upper limit switch. If the leak is very bad, the test machine will try to do continuous recharge cycles. In this case, it is best to stop the test by pushing "S" and then continue with the standard instructions.

Broken Specimen: When a specimen breaks, the ram may retract or extend. The test program is designed to go into "Stop" mode (pressure ramps to zero, load ramps to "zero_offset_load" whenever the stroke transducer in the hydraulic ram measures a displacement greater than "stroke_xdcr_limit" inches. Fluid is usually pumped out by the charge pump in the intensifier.

1. Push the emergency stop button (red button marked "OFF") on the Harwood Engineering pressure intensifier front panel.

2. On the Harwood Engineering pressure intensifier front panel, unscrew the knob marked "AR" until it stops.

3. Push "S" to stop the program in case the automatic system has not been triggered.

4. On the MTS 413 Master Control Panel, push the red button marked "HYDRAULIC OFF" to stop the hydraulic pump. The blue button marked "RESET" will light up.

5. If the extensometer moves, its spring-loaded mount will try to push it between the vessel and the ram. Do not let the extensometer get crushed by the ram! On the MTS 406 Controller, turn the knob marked "SET POINT" so that the panel meter on the MTS 406 reads a negative value. The lower grip will move downward.

☐ On the Harwood Engineering pressure intensifier front panel, adjust the regulator marked "R-1" until the gage marked "G-1" reads zero psi.

☐ On the Harwood Engineering pressure intensifier front panel, adjust the knob marked "AR" until the gage marked "GA" reads zero psi. Then close the valve marked "XA".

☐ Behind the Harwood Engineering pressure intensifier front panel, open the valve marked "X-2"

☐ On the Harwood Engineering pressure intensifier front panel, push the red button marked "STOP". The green indicator lights labeled "DRIVE PUMP RUN" and "RETRACTING PUMP RUN" will go out, but the red indicator light labeled "CONTROL POWER ON" and the yellow indicator light labeled "BOTTOM LIMIT SWITCH ACTIVATED" will remain lit. Then push the red button labeled"OFF" to extinguish these remaining indicator lights.

☐ Using the Macintosh Mac II, push "Q" and then "Y" to save the data and end execution of the program "Load Control".

☐ Record the number of cycles listed on the cycle counter.

☐ Using the Macintosh Mac II, rename the file "Output.dat" and then examine it using IGOR.

Lower The Lower Grip

CHECK HERE

☐ Open the release valve on the Enerpac P18 hand pump.

☐ Simultaneously screw in each of the two collet releasing screws on the lower collet adapter. This will free the specimen from the self-holding action of the collet.

☐ On the MTS 406 Controller, turn the switch under the panel meter to the position marked "ERROR".

☐ On the MTS 406 Controller, turn the knob marked "SET POINT" so that the panel meter on the MTS 406 reads a negative value. The lower grip will move downward.

☐ On the MTS 413 Master Control Panel, push the red button marked "HYDRAULIC OFF" to stop the hydraulic pump. The blue button marked "RESET" will light up.

☐ Close the cooling water valves for the Harwood Engineering pressure intensifier and the MTS HPU.

Specimen Removal

CHECK HERE

- [ ] Remove the extensometer.

- [ ] Loosen and unscrew the nut which retains the electrical feedthru plug. Be careful not to let the weight of the nut hang on the wire.

- [ ] Loosen and unscrew the nut for the high pressure tubing connection to the intensifier.

- [ ] Loosen the SHCS's which mount the vessel. Unscrew them, lowering the vessel onto the support arm, and freeing the lower endcap.

- [ ] Rotate the support arm out from underneath the upper grip, ensuring that the high pressure tubing exits the port on the left side of the vessel. Remove the SHCS's and the lower endcap by sliding it down and off of the specimen. The anti-extrusion rings and the spacer will now be unsupported and may drop out of the vessel bore.

- [ ] Using a torque wrench and the reaction-torque tool to prevent the vessel from rotating, loosen the 4 SHCS in the upper adapter. Be careful not to knock the vessel off the support arm! Remove the SHCS and then carefully lift the upper adapter straight up by 1 inch. Carefully reach underneath and hold the load cell wire to prevent it from being tugged while you place the upper adapter on the support arm, to the left of the vessel.

- [ ] Thread the puller provided into the tapped holes in the plug in the feedthru bore

- [ ] Taking extreme care not to move the specimen axially, remove the feedthru from its bore as you simultaneously rotate the specimen counter clockwise to unwind the strain gage leads from around the gage section of the specimen. If you re-install the extensometer extension, it can be used as a handle to help rotate the specimen.

- [ ] Slide the white plastic bushing back over the leads. Cut or unsolder the leads from their respective connections and dummy (pressure compensating) gages.

- [ ] Rotate the specimen clockwise to wind the leads around the gage section. Remove the extensometer extension if you re-installed it to use as a handle.

- [ ] Carefully push the specimen and Load Cell Housing upward, until they come out of the vessel bore. The lower seal will remain in the vessel.

- [ ] Remove the lower anti-extrusion rings and seal from the vessel bore by tapping them out with a plastic drift punch inserted down the vessel bore.

Reduce The Test Data

These are the IGOR commands used to reduce monotonic test data:

Load waves

•Display Int_LC_Stress vs e_gage_1
•Append Int_LC_Stress vs e_gage_2
•Append Pressure vs e_gage_1
•Modify lstyle(Pressure)=2
•Modify mirror=1,minor=1,highTrip=1e+06,lowTrip=1e-05,zero(bottom)=1
•Modify zero=1
•Append Int_LC_Stress_1 vs e_gage_1_1
•Append Int_LC_Stress_1 vs e_gage_2_1
•Display Int_LC_Stress vs Pressure
•Modify grid=1,mirror=1
•Label bottom "Pressure, psi";DelayUpdate
•Label left "Axial Stress, psi"
•Duplicate Pressure MPA_Pressure
•Duplicate Pressure_1 MPA_Pressure_1
•MPA_Pressure = Pressure * .00689476
•MPA_Pressure_1 = Pressure_1 * .00689476
•Duplicate e_gage_1 True_e_gage_1
•Duplicate e_gage_1_1 True_e_gage_1_1
•Duplicate e_gage_2 True_e_gage_2
•Duplicate e_gage_2_1 True_e_gage_2_1
•True_e_gage_1 = ln(e_gage_1 + 1)
•True_e_gage_1_1 = ln(e_gage_1_1 + 1)
•True_e_gage_2 = ln(e_gage_2 + 1)
•True_e_gage_2_1 = ln(e_gage_2_1 + 1)
•Duplicate e_gage_1 True_trans_strain
•Duplicate e_gage_1_1 True_trans_strain1
•Duplicate Int_LC_Stress T_MPA_Int_LC_Stress
•Duplicate Int_LC_Stress_1 T_MPA_Int_LC_Stress_1
•T_MPA_Int_LC_Stress = (Int_LC_Stress * .00689476 + MPA_Pressure) / (1 + 2*e_gage_2 + e_gage_2*e_gage_2) - MPA_Pressure
•T_MPA_Int_LC_Stress_1 = (Int_LC_Stress_1 * .00689476 + MPA_Pressure_1) / (1 + 2*e_gage_2_1 + e_gage_2_1*e_gage_2_1) - MPA_Pressure_1
•Display T_MPA_Int_LC_Stress vs True_e_gage_1
•Append T_MPA_Int_LC_Stress vs True_e_gage_2
•Append T_MPA_Int_LC_Stress_1 vs True_e_gage_1_1
•Append T_MPA_Int_LC_Stress_1 vs True_e_gage_2_1
•Modify mirror=1,minor=1,zero(left)=1,lowTrip(bottom)=0.0001
•Label bottom "True Strain";DelayUpdate
•Label left "True Axial Stress or Pressure, MPa"
•Duplicate T_MPA_Int_LC_Stress Eff_True_Stress,Eff_True_Strain,e1_minus_el,e2_minus_el
•Duplicate T_MPA_Int_LC_Stress_1 Eff_True_Stress_1,Eff_True_Strain_1,e1_minus_el_1,e2_minus_el_1
•Eff_True_Stress = sqrt((T_MPA_Int_LC_Stress + MPa_Pressure) * (T_MPA_Int_LC_Stress + MPa_Pressure))
•Eff_True_Stress_1 = sqrt((T_MPA_Int_LC_Stress_1 + MPa_Pressure_1) * (T_MPA_Int_LC_Stress_1 + MPa_Pressure_1))
•Eff_True_Strain = sqrt(2) * sqrt((True_e_gage_1 - True_e_gage_2)*(True_e_gage_1 - True_e_gage_2) + (True_e_gage_2 - True_e_gage_1)*(True_e_gage_2 - True_e_gage_1))/3
•Eff_True_Strain_1 = sqrt(2) * sqrt((True_e_gage_1_1 - True_e_gage_2_1)*(True_e_gage_1_1 - True_e_gage_2_1) + (True_e_gage_2_1 - True_e_gage_1_1)*(True_e_gage_2_1 - True_e_gage_1_1))/3

•Display Eff_True_Stress vs Eff_True_Strain
•Duplicate Eff_True_Strain elastic_cf,elastic_cf_offset
•ShowInfo
•CurveFit line Eff_True_Stress(xcsr(A),xcsr(B)) /X=Eff_True_Strain /D=elastic_cf
elastic_cf= K0+K1*Eff_True_Strain
K0= -10.6247;K1= 238911;V_chisq= 580.088; V_npnts= 401;
V_numNaNs= 0; V_numINFs= 0; V_siga= 0.171106; V_sigb= 63.645;
V_q= 1; V_Rab= -2.12464; V_Pr= 0.999986;
•elastic_cf= -10.6247+238911*Eff_True_Strain
•Append elastic_cf vs Eff_True_Strain
•elastic_cf_offset = -10.6247 +238911 * (Eff_True_Strain -.000250)
•Append elastic_cf_offset vs Eff_True_Strain
•Modify grid=1,mirror=1,minor=1
•Display MPA_Pressure vs True_e_gage_2
•ShowInfo
•Modify grid=1,mirror=1,minor=1
•CurveFit line MPA_Pressure(xcsr(A),xcsr(B)) /X=True_e_gage_2
y= K0+K1*x
K0= -1.64646;K1= -157978;V_chisq= 610.369; V_npnts= 493;
V_numNaNs= 0; V_numINFs= 0; V_siga= 0.129669; V_sigb= 86.2047;
V_q= 1; V_Rab= 2.47965; V_Pr= -0.999947;
•Append MPA_Pressure vs True_e_gage_1
•CurveFit line MPA_Pressure(xcsr(A),xcsr(B)) /X=True_e_gage_1
y= K0+K1*x
K0= -5.22246;K1= 78073.4;V_chisq= 741.479; V_npnts= 493;
V_numNaNs= 0; V_numINFs= 0; V_siga= 0.144896; V_sigb= 46.953;
V_q= 1; V_Rab= -1.59624; V_Pr= 0.999912;
•True_trans_strain = True_e_gage_1 + 2*True_e_gage_2 - (T_MPA_Int_LC_Stress - 2*MPA_Pressure) * .4/ 204100
•True_trans_strain1 = True_e_gage_1_1 + 2*True_e_gage_2_1 - (T_MPA_Int_LC_Stress_1 - 2*MPA_Pressure_1) *.4/ 204100
•Display True_trans_strain vs Eff_True_Stress
•Modify grid=1,mirror=1,minor=1,zero(left)=1
•Modify grid=1,mirror=1,minor=1
•Append True_trans_strain1 vs Eff_True_Stress_1
•Display Eff_True_Stress vs Eff_True_Strain
•Append/T Eff_True_Stress vs True_trans_strain
•Append/T Eff_True_Stress_1 vs True_trans_strain1
•Append Eff_True_Stress_1 vs Eff_True_Strain_1
•Duplicate Eff_True_Strain Elastic_limit
•Elastic_limit = 980
•Append Elastic_limit vs Eff_True_Strain
•Modify zero=1,minor=1,mirror(left)=1
•Label bottom "Effective Strain";DelayUpdate
•Label left "Effective Stress, MPa";DelayUpdate
•Label top "Volumetric Transformation Strain"

APPENDIX B - COMPUTER CODE FOR MONOTONIC TESTING

PROGRAM MAIN.C

```
#include "main.h"

/* * * * * * * * * * * * * * * * * * * * * * * * * * * *
 *
 *    Load Control.c
 *
 *              11/15/92
 *
 *    Programmer: MAB
 *
 *
 * * * * * * * * * * * * * * * * * * * * * * * * * * * */

main()
{
        limit_switch_state      =       &var_limit_switch_state;
        stroke_xdcr             =       &var_stroke_xdcr;
        int_load_cell           =       &var_int_load_cell;
        ext_load_cell           =       &var_ext_load_cell;
        extensometer            =       &var_extensometer;
        pressure_xdcr           =       &var_pressure_xdcr;
        e_gage_ch_1             =       &var_e_gage_ch_1;
        e_gage_ch_2             =       &var_e_gage_ch_2;
        e_gage_ch_3             =       &var_e_gage_ch_3;

        Set_Up_DAQ();
        Calibrations();
        Set_Up_Counter();
        Init_Linked_List();

        /* Write a one to the solenoid valve's relay,
           to open the solenoid valve on the air line                          */
        DIG_Out_Line(5,1,0,1);

        /* Print the instructions for zeroing                                  */
        printf("          Running intensifier and load control program\n\n");
        printf("    ****    Be sure to set the FDBK SELECT switch to EXT    ****\n\n\n");
        printf("                Zero all transducers now\n\n\n");
        printf("               To enter TEST mode, press <T>\n\n\n");

        /* zero inputs routine                                                 */

                /*  Check the keyboard for keystrokes                          */
                GetKeys ((long *)KeyMaps);

                /*  If the test is running then proceed with the program       */
                while (quit_zero_inputs == 0)
                {
                        Read_Inputs();

                        /* commands remain zero while operator checks zeros
                           zeroing ends when <T> is pressed.                    */
```

```
            if (n<5)
            {
                    n++;
            }
            else
            {
                    n = 0;
            }
            old_pressure_xdcr[n]        = *pressure_xdcr;
            old_ext_load_cell[n]        = *ext_load_cell;
            old_int_load_cell[n]        = *int_load_cell;
            old_extensometer[n]         = *extensometer;
            old_e_gage_ch_1[n]          = *e_gage_ch_1;
            old_e_gage_ch_2[n]          = *e_gage_ch_2;
            old_e_gage_ch_3[n]          = *e_gage_ch_3;
            sum_old_pressure_xdcr       = 0;
            sum_old_ext_load_cell       = 0;
            sum_old_int_load_cell       = 0;
            sum_old_extensometer        = 0;
            sum_old_e_gage_ch_1         = 0;
            sum_old_e_gage_ch_2         = 0;
            sum_old_e_gage_ch_3         = 0;
            for (m = 0; m < 6; m++)
            {
                    sum_old_pressure_xdcr += old_pressure_xdcr[m];
                    sum_old_ext_load_cell  += old_ext_load_cell[m];
                    sum_old_int_load_cell   += old_int_load_cell[m];
                    sum_old_extensometer  += old_extensometer[m];
                    sum_old_e_gage_ch_1   += old_e_gage_ch_1[m];
                    sum_old_e_gage_ch_2   += old_e_gage_ch_2[m];
                    sum_old_e_gage_ch_3   += old_e_gage_ch_3[m];
            }
            printf("p_xdcr=%5.0f ext_LC=%5.0f int_LC=%5.0f exten=%5.0f
                    gage_1=%5.0f gage_2=%5.0f\n",
            sum_old_pressure_xdcr / 6,
            sum_old_ext_load_cell / 6,
            sum_old_int_load_cell / 6,
            sum_old_extensometer  / 6,
            sum_old_e_gage_ch_1   / 6,
            sum_old_e_gage_ch_2   / 6);
/*          sum_old_e_gage_ch_3   / 6    */

            Calculate_Zero_Commands();

            Calculate_Modified_Commands();

            Write_Analog_Outputs();

            /*  Check the keyboard for keystrokes                                   */
            GetKeys ((long *)KeyMaps);
            if (KeyMaps[2] == 2) quit_zero_inputs = 1;  /* <T> has been pressed*/
    }

/*  Set the initial stroke xdcr value                                               */
AI_Read(5,1,1,stroke_xdcr);
initial_stroke_xdcr = *stroke_xdcr;
```

```
/* Print the instructions                                                    */
printf("\n\n\n          Running intensifier and load control program\n\n");
printf("    ****    Be sure to set the FDBK SELECT switch to EXT    ****\n\n\n");
printf("To BEGIN a new test, press \t\t\t\t<B>\n\n\n");
printf("To PAUSE a running test, press \t\t\t\t<P>\n\n\n");
printf("To RESUME a running test, press \t\t\t<R>\n\n\n");
printf("To STOP a running test prematurely, press \t\t<S>\n");
printf("  THEN turn off all hydraulics, THEN QUIT\n\n");
printf("To QUIT the control program after running a test,\n");
printf("  FIRST turn off all hydraulics, THEN press \t\t<Q>.\n");
printf("  This step saves all data.\n\n");

/*  Check the keyboard for keystrokes                                        */
GetKeys ((long *)KeyMaps);

/*  If the test is running then proceed with the program                     */
while (quit_test == 0)
{
        Read_Inputs();

        /*  commands remain zero until <B> is pressed.
                commands then ramp to initial values
                commands then cycle
                commands then ramp to zero and remain zero.

                commands are held constant if <P> is pressed.
                commands continue when <R> is pressed.

                commands ramp to zero and remain zero when <S> is pressed.

                data is written to output.dat and program ends when <Q> is pressed.

                decisions as to store data or not to store data
                are made in the command subroutines.  the ramps
                and cycle #'s 1-10, 2**4-2**15 are stored by default.        */

        Decide_Command_Based_On_Keyboard();

        Calculate_Modified_Commands();

        Write_Analog_Outputs();

        /*      if              the intensifier has tripped the upper limit switch
                                and stop has not yet been commanded,
                then    stop the test
        if (*limit_switch_state == 1)
        {
                stop_test       = 1;
                stop_ramp       = 1;
                printf("limit switch tripped\n");
                stop_pressure_at = pressure_command;
                stop_load_at    = load_command;
        }                                                                    */

        /*  Check the keyboard for keystrokes                                */
```

```
        GetKeys ((long *)KeyMaps);
    }

    /* Write a zero to the solenoid valve's relay,
        to close the solenoid valve on the air line                    */
    DIG_Out_Line(5,1,0,0);

    Write_Data_File();
    printf("Intensifier and load control program has finished");
}
```

FUNCTION SUBPROGRAM INITIALIZE.C

```
#include "mainExt.h"

/* * * * * * * * * * * * * * * * * * * * * * * * * * * *
 * Calibrations
 *
 *                11/15/92
 *
 * Programmer: MAB
 *
 *
 * * * * * * * * * * * * * * * * * * * * * * * * * * * */

Calibrations()
{
/*      date                    = 11/22/96;             date of test                                    */
/*      specimen number         = Carb#19;              number of specimen                              */
/*      test letter             =         A;            A = test 1, B = test 2, etc.                    */
/*      specimen status         =         ;             OK, Failed, Controller Problem...               */
/*      gage section gage       =                       EA-06-125TA-120                                 */
/*      gage lot number         =                       R-A56AD95                                       */
/*      general notes           =                       4320, Carb, Q @ 1550 F (845C)                   */

d                       =       0.2010;         /* diameter of specimen gage section                    */
D                       =       0.4365;         /* diameter of specimen shoulders                       */
fillet_fudge            =       0.000;          /* fudge factor for increasing effective gage length    */
seal_fudge              =       0.000;          /* factor for increasing eff internal long-sho length   */
L1                      =       0.308 - fillet_fudge;           /* effective short-shoulder length      */
L2                      =       1.003 + 2. * fillet_fudge;      /* effective gage length                */
L3                      =       0.275 - fillet_fudge + seal_fudge; /* eff internal long-sho len         */
L4                      =       0.880 - seal_fudge;     /* effective external long-shoulder length      */
S4                      =       1.000;          /* effective external long-shoulder length
                                                   used for stroke xdcr calibration                     */
E                       = 29000000.0;           /* Young's modulus for specimen + dummy                 */
nu                      =       0.3;            /* Poisson's ratio for specimen + dummy                 */

cycle_num               =       1;              /* test begins at this cycle number                     */
last_cycle_num          =       1;              /* test ends at this cycle number                       */
ramp_pressure_to        =   94276.0;            /* peak pressure in a command ramp                      */
ramp_stress_to          =  188552.0;            /* peak stress in a command ramp                        */
samples_per_ramp_up     = 8044.;                /* even number of samples in a command ramp             */
samples_per_ramp_down   = 3000.;                /* even number of samples in a command ramp             */
store_Nth_sample        =       2;              /* store only every Nth sample                          */
bits_of_dither          =       0;              /* bits of dither applied to MTS command                */
                                                /* a 1 bit dither amplitude = .05% of the
                                                   full scale (10 volt) MTS command signal              */

amp_gain_1              =     200.0;            /* amplifier gain for strain gage 1                     */
amp_gain_2              =     500.0;            /* amplifier gain for strain gage 2                     */
amp_gain_3              =    1000.0;            /* amplifier gain for strain gage 3                     */
excitation_voltage      =      5.00;            /* excitation voltage for strain gages                  */
gage_factor_1A          =     2.035;            /* gage factor of active gage 1                         */
Kt_1A                   =     0.020;            /* transverse sensitivity of active gage 1              */
gage_factor_2A          =     2.055;            /* gage factor of active gage 2                         */
```

```
Kt_2A                   =          0.014;          /* transverse sensitivity of active gage 2          */
gage_factor_3A          =          1.000;          /* gage factor of active gage 3                     */
Kt_3A                   =          0.000;          /* transverse sensitivity of active gage 3          */
gage_factor_1D          =          2.035;          /* gage factor of dummy gage 1                      */
Kt_1D                   =          0.020;          /* transverse sensitivity of dummy gage 1           */
gage_factor_2D          =          2.055;          /* gage factor of dummy gage 2                      */
Kt_2D                   =          0.014;          /* transverse sensitivity of dummy gage 2           */
gage_factor_3D          =          1.000;          /* gage factor of dummy gage 3                      */
Kt_3D                   =          0.000;          /* transverse sensitivity of dummy gage 3           */
extensometer_offset     =   -14000.;               /* zero offset on extensometer channel, bits        */
e_gage_1_offset         =   -25000.;               /* zero offset on e_gage_1 channel in bits          */
e_gage_2_offset         =    25000.;               /* zero offset on e_gage_2 channel in bits          */

strain_cal_1            =  1.0000;                 /* strain calibration for gage 1                    */
pressure_cal_1          =  1.0000;                 /* pressure calibration for gage 1                  */
strain_cal_2            =  1.0000;                 /* strain calibration for gage 2                    */
pressure_cal_2          =  1.0000;                 /* pressure calibration for gage 2                  */
strain_cal_3            =  1.0000;                 /* strain (load) calibration for gage 3             */
pressure_cal_3          =  1.0000;                 /* pressure calibration for gage 3                  */

int_load_cell_gain      =  1;                      /* gain setting for NIDAQ board: 1,2,4 or 8 */
int_l_c_gain_factor     =  1.0;                    /* when running high compressive load tests,
                                                   set this to 0.7 and adjust the amp gain accordingly */
ten_volt_pressure       = 125000.0;                /* pressure (psi) calibration for 10 volts          */
ext_load_cell_gain      =       1;                 /* gain setting for NIDAQ board: 1,2,4 or 8         */
ten_volt_load           = 20000.0 / ext_load_cell_gain;    /* load (lbf) calibration (for 10V)         */
ten_volt_deflection     =          0.080;          /* deflection (in) calibration for 10 volts         */
stroke_xdcr_gain        =          1;              /* gain setting for NIDAQ board: 1,2,4 or 8 */
ten_volt_stroke         =          1.416/ stroke_xdcr_gain;
                                                   /* stroke (in) calibration for 10 volts             */
                                                   /* 0.7166 @ CAL FACTOR = 0,   TOGGLE = fine         */
                                                   /* 1.416  @ CAL FACTOR = 100, TOGGLE = fine         */
                                                   /* 2.2727 @ CAL FACTOR = 420, TOGGLE = coarse*/
stroke_xdcr_limit       = 0.20 * (32768.0 / ten_volt_stroke);
                                                   /* allowable stroke limit for monotonic tests       */
zero_offset_load        = -300.;                   /* small negative load (lbf); keeps setup together  */
samples_per_stop_ramp   = 300.;                    /* number of samples in stop ramp                   */
                                                   /*    must be >= 1.                                 */

/*****************************************************************************************/

A  = 3.1415927*(pow(D,2))/4.0;                     /* area of specimen shoulders                       */
a  = 3.1415927*(pow(d,2))/4.0;                     /* area of specimen gage section                    */
EA = E * A;                                        /* elastic constant                                 */

ramp_load_to    =    ramp_stress_to * a;           /* peak load in a command ramp                      */

stop_ramp_sample        =       samples_per_stop_ramp;
ramp_down_sample        =       samples_per_ramp_down;

nuo                     =  0.285;                  /* Poisson's ratio for e gage calibration beam      */
ten_volt_e_gage_1A      = 10.0/(amp_gain_1 * excitation_voltage/4.0 * gage_factor_1A);
                                                   /* strain gage 1 calibration for 10 volts           */
ten_volt_e_gage_2A      = 10.0/(amp_gain_2 * excitation_voltage/4.0 * gage_factor_2A);
                                                   /* strain gage 2 calibration for 10 volts           */
ten_volt_e_gage_3A      = 10.0/(amp_gain_3 * excitation_voltage/4.0 * gage_factor_3A);
```

```
                                        /* strain gage 2 calibration for 10 volts                */
dummy_gage_1        =   gage_factor_1D * (2.0 * nu - 1.0) *   (1.0 + Kt_1D)        /
                                (gage_factor_1A *      E      * (1.0 - nuo * Kt_1D));
                                        /* correction for dummy gage 1 effects                   */
dummy_gage_2        =   gage_factor_2D * (2.0 * nu - 1.0) *   (1.0 + Kt_2D)        /
                                (gage_factor_2A *      E      * (1.0 - nuo * Kt_2D));
                                        /* correction for dummy gage 2 effects                   */
dummy_gage_3        =   gage_factor_3D * (2.0 * nu - 1.0) *   (1.0 + Kt_3D)        /
                                (gage_factor_3A *      E      * (1.0 - nuo * Kt_3D));
                                        /* correction for dummy gage 3 effects                   */
corr_1          =   1.0 - nuo * Kt_1A;      /* correction for transverse sensitivity effects */
corr_2          =   1.0 - nuo * Kt_2A;      /* correction for transverse sensitivity effects */
corr_3          =   1.0 - nuo * Kt_3A;      /* correction for transverse sensitivity effects */
corr_4          =   1.0 - Kt_1A * Kt_2A;    /* correction for transverse sensitivity effects */

C1              =   1.0 / L2;               /* constants for extensometer to strain conversion   */
C2              =   3.198E-7 / L2 + (L1 + L3) / (EA * L2);
C3              =   L4 / (EA * L2);
C4              =   3.198E-8 / L2 + 2.0 * (L1 + L3) * nu / (E * L2);

CS3             =   S4 / (EA * L2);         /* constant for stroke xdcr to strain conversion     */
}


/* * * * * * * * * * * * * * * * * * * * * * * * * * * *
 * Set_Up_DAQ
 *
 *              11/15/92
 *
 * Programmer: MAB
 *
 *
 * * * * * * * * * * * * * * * * * * * * * * * * * * * */

Set_Up_DAQ()
{
        /*   Setup the I/O Board   */

        Board_Reset(5);                         /* Reset the DAQ board                   */
        AI_Config(5,0,10,0);                    /* Configure the analog input channels   */
        AO_Setup(5,0,0,10,0,0,0);               /* Configure analog output channel 0     */
        AO_Setup(5,1,0,10,0,0,0);               /* Configure analog output channel 1     */
        DIG_Prt_Config(5,0,0,0);                /* Configure digital port 0 for input    */
        DIG_Prt_Config(5,1,1,0);                /* Configure digital port 1 for output   */

        /*  Initialize Analog Outputs to Zero   */

        /*  Use the DAC to output a 0 (zero) volt signal on channel 0
        AO_Write(5,0,0);   */

        /*  Use the DAC to output a 0 (zero) volt signal on channel 1
        AO_Write(5,1,0);*/

        /*  Write a zero to the cycle counter                                   */
        DIG_Out_Line(5,1,3,0);
        /*  Reset the cycle counter to 0                                        */
```

```
        DIG_Out_Line(5,1,2,0);
        DIG_Out_Line(5,1,2,1);
        for (index=1;index<15000;index++);
        DIG_Out_Line(5,1,2,0);
}


/* * * * * * * * * * * * * * * * * * * * * * * * * * * *
 * Set_Up_Counter  used when not starting from cycle 1
 *
 *              11/15/92
 *
 * Programmer: MAB
 *
 *
 * * * * * * * * * * * * * * * * * * * * * * * * * * * */

Set_Up_Counter()
{
        int loop1;

        for (loop1=1;loop1<(cycle_num);loop1++)
        {
                /*  Write a zero to the cycle counter                   */
                DIG_Out_Line(5,1,3,0);
                for (index=1;index<15000;index++);
                /*  Write a one to the cycle counter                    */
                DIG_Out_Line(5,1,3,1);
                for (index=1;index<15000;index++);
                /*  Write a zero to the cycle counter                   */
                DIG_Out_Line(5,1,3,0);
        }
}


/* * * * * * * * * * * * * * * * * * * * * * * * * * * *
 * Initialize Linked List
 *
 *              11/15/92
 *
 * Programmer: MAB
 *
 *
 * * * * * * * * * * * * * * * * * * * * * * * * * * * */

Init_Linked_List()
{
        /*  Initialize Linked List for data storage    */
        first_data = (struct data *)malloc((unsigned)sizeof(struct data));
        first_data->length = 0;
        first_data->next = NULL;
        last_data = first_data;
        ext_l_c_load_ptr = last_data->ext_l_c_load;
        int_l_c_load_ptr = last_data->int_l_c_load;
        pressure_ptr = last_data->pressure;
        extensometer_ptr = last_data->extensometer;
```

```
        stroke_xdcr_ptr = last_data->stroke_xdcr;
        e_gage_1_ptr = last_data->e_gage_1;
        e_gage_2_ptr = last_data->e_gage_2;
        e_gage_3_ptr = last_data->e_gage_3;
        len = 0;
}
```

FUNCTION SUBPROGRAM DECIDE_WHICH_COMMAND.C

```
#include "mainExt.h"

/* * * * * * * * * * * * * * * * * * * * * * * * * * * *
 * Decide Which Command Based On Keyboard
 *
 *              12/15/92
 *
 * Programmer: MAB
 *
* * * * * * * * * * * * * * * * * * * * * * * * * * * */

Decide_Command_Based_On_Keyboard()
{
        if (KeyMaps[4] == 8)    pause_test = 1;         /* pause has been commanded     */

        if (KeyMaps[1] == 128)  pause_test = 0;         /* resume has been commanded    */

/*      if ((abs(*e_gage_ch_1) > 31050) && (stop_test == 0))
        {       command a stop when axial strain is at 95% 'cuz specimen is probably buckled
                stop_test       = 1;
                stop_ramp       = 1;
                printf("Strain limit exceeded\n");
                stop_pressure_at = pressure_command;
                stop_load_at    = load_command;
        }       */
        if ((abs(*stroke_xdcr - initial_stroke_xdcr) > stroke_xdcr_limit) && (stop_test == 0))
        {                       /* command a stop when stroke xdcr limit has been exceeded  */
                stop_test       = 1;
                stop_ramp       = 1;
                printf("Stroke limit exceeded\n");
                stop_pressure_at = pressure_command;
                stop_load_at    = load_command;
        }

        if (end_test == 1)                              /* test over, specimen didn't break */
        {
                Calculate_Zero_Commands();
                /*  Write a zero to the solenoid valve's relay,
                  to close the solenoid valve on the air line                           */
                DIG_Out_Line(5,1,0,0);
                if (KeyMaps[1] == 16)                           /* <Q> has been pressed */
                {
                        printf("\nAre you sure that you want to QUIT?\t\t\t<Y> or <N>\n\n");
                        unsure_quit_test = 1;
                }
                if ((KeyMaps[2] == 1) && (unsure_quit_test == 1))  quit_test = 1;
                                                        /* <Y> has been pressed         */
        }
        else if (begin_test == 0)                       /* <B> has not been pressed yet */
        {
                Calculate_Zero_Commands();
                if (KeyMaps[1] == 16)                   /*      <Q> has been pressed    */
                {
```

```
                printf("\nAre you sure that you want to QUIT?\t\t\t<Y> or <N>\n\n");
                unsure_quit_test = 1;
            }
            if ((KeyMaps[2] == 1) && (unsure_quit_test == 1)) quit_test = 1;
                                                    /* <Y> has been pressed          */
            if (KeyMaps[1] == 8)    /* Upon pressing <B>, command generation will begin */
            {
                begin_test      = 1;
                begin_ramp      = 1;
                /*  Clock the cycle counter         once                            */
                DIG_Out_Line(5,1,3,1);
                DIG_Out_Line(5,1,3,0);
            }
        }
        else if (pause_test == 1)           /* don't change commands - check for <S>    */
        {
            if (KeyMaps[0] == 2)        /* Upon pressing <S> the stop routine will begin    */
            {
                pause_test      = 0;
                stop_test       = 1;
                stop_ramp       = 1;
                stop_pressure_at = pressure_command;
                stop_load_at    = load_command;
            }
        }
        else if ( stop_test == 0)           /*      <S> has not been pressed yet        */
        {
            if (begin_ramp) Calculate_Ramp_Up_Commands();
            else if (begin_ramp == 0) Calculate_Ramp_Down_Commands();
            if (KeyMaps[0] == 2)        /* Upon pressing <S>the stop routine will begin */
            {
                stop_test       = 1;
                stop_ramp       = 1;
                stop_pressure_at = pressure_command;
                stop_load_at    = load_command;
            }
        }
        else                                /*      <S> has been pressed            */
        {
            if (stop_ramp == 1) Calculate_Stop_Ramp_Commands();
            else
            {
                Calculate_Zero_Commands();
                /*  Write a zero to the solenoid valve's relay,
                        to close the solenoid valve on the air line                 */
                DIG_Out_Line(5,1,0,0);
                if (KeyMaps[1] == 16)           /*      <Q> has been pressed        */
                {
                    printf("\nAre you sure that you want to QUIT?\t\t\t<Y> or <N>\n\n");
                    unsure_quit_test = 1;
                }
                if ((KeyMaps[2] == 1) && (unsure_quit_test == 1))   quit_test = 1;
                                                    /*      <Y> has been pressed    */
            }
        }
}
```

FUNCTION SUBPROGRAM CALCULATE_COMMANDS.C

```
#include "mainExt.h"

/* * * * * * * * * * * * * * * * * * * * * * * * * * * *
 * Calculate Zero Commands
 *
 *                  11/15/92
 *
 * Programmer: MAB
 *
 *
 * * * * * * * * * * * * * * * * * * * * * * * * * * * */

Calculate_Zero_Commands()
{
        pressure_command = 0;
        load_command    = 0;
}

/* * * * * * * * * * * * * * * * * * * * * * * * * * * *
 * Calculate Ramp Up Commands
 *
 *                  11/15/92
 *
 * Programmer: MAB
 *
 *
 * * * * * * * * * * * * * * * * * * * * * * * * * * * */

Calculate_Ramp_Up_Commands()
{
        /*  Ramp data is always to be stored  */
        Store_Data();

        /*          calculate pressure and load command for next sample                 */
        ramp_up_sample++;
        pressure_command = ramp_up_sample / samples_per_ramp_up * ramp_pressure_to;
        load_command    = ramp_up_sample / samples_per_ramp_up * ramp_load_to;
        if (ramp_up_sample >= samples_per_ramp_up) begin_ramp = 0;
}

/* * * * * * * * * * * * * * * * * * * * * * * * * * * *
 * Calculate Ramp Down Commands
 *
 *                  11/15/92
 *
 * Programmer: MAB
 *
 *
 * * * * * * * * * * * * * * * * * * * * * * * * * * * */

Calculate_Ramp_Down_Commands()
{
        if (ramp_down_sample >= samples_per_ramp_down) /* store cycle number in encoded data line     */
```

```
        {
                store_cycle_num_data = 1;
                Store_Data();
        }

        /*  Ramp data is always to be stored  */
        Store_Data();

        /*          calculate pressure and load command for next sample                 */
        ramp_down_sample--;
        pressure_command = ramp_down_sample / samples_per_ramp_down * ramp_pressure_to;
        load_command    = ramp_down_sample / samples_per_ramp_down * ramp_load_to;
        if (ramp_down_sample <= 0)
        {
                begin_ramp = 1;
                end_test = 1;
        }
}

/* * * * * * * * * * * * * * * * * * * * * * * * * * * *
 * Calculate Stop Ramp Commands
 *
 *              11/15/92
 *
 * Programmer: MAB
 *
 *
 * * * * * * * * * * * * * * * * * * * * * * * * * * * */

Calculate_Stop_Ramp_Commands()
{
        if (stop_ramp_sample >= samples_per_stop_ramp) /* store cycle number in encoded data line      */
        {
                store_cycle_num_data = 1;
                Store_Data();
        }

        /*  Ramp data is always to be stored  */
        Store_Data();

        /*          calculate pressure and load command for next sample                 */
        stop_ramp_sample--;
        pressure_command = stop_ramp_sample / samples_per_stop_ramp * stop_pressure_at;
        load_command    = stop_ramp_sample / samples_per_stop_ramp * stop_load_at;
        if (stop_ramp_sample <= 0) stop_ramp = 0;
}
```

FUNCTION SUBPROGRAM MODIFY_COMMANDS.C

```
#include "mainExt.h"

/* * * * * * * * * * * * * * * * * * * * * * * * * * * *
 * Calculate Modified Commands
 *
 *              11/15/92
 *
 * Programmer: MAB
 *
 *
 * * * * * * * * * * * * * * * * * * * * * * * * * * * */

Calculate_Modified_Commands()
{
        /*  Scale the 16 bit pressure to proper units                                   */

        pressure_psi  = *pressure_xdcr / 32768.0 * ten_volt_pressure;

        /*  Overdrive pressure if it is lagging behind                                  */

        if (pressure_command > 2000.0)
        {
                scaled_pressure_command = pressure_command *
                (1.0 + (last_pressure_command - pressure_psi) / last_pressure_command);
                if ((last_pressure_command - pressure_psi) / last_pressure_command > 0.15)
                        scaled_pressure_command = 1.15 * pressure_command;
        }
        else
        {
                scaled_pressure_command = pressure_command;
        }

        last_pressure_command = pressure_command;

        /*      Determine the load command in terms of Internal Load Cell voltage output (pressure decreases
                output)                                                                 */

                load_from_geom  = (A - a) * pressure_psi;
                stress_in_shoulder = (load_command - load_from_geom) / (A * 10000.0);
        /*      Prevent load command from ever going positive by keeping it below zero_offset_load      */

                if ((load_command - load_from_geom) >= zero_offset_load) stress_in_shoulder = zero_offset_load /
                (A * 10000.0);

        /*      First calculate the axial load contribution to internal load cell output    */

                if (stress_in_shoulder < -7.5209)
                {
                        int_l_c_no_pressure = 1.28025 * stress_in_shoulder - 0.176308;
                }
                else if (stress_in_shoulder < -3.3550)
                {
                        int_l_c_no_pressure = 1.29494 * stress_in_shoulder - 0.065825;
```

```
        }
        else /*   (stress_in_shoulder > -3.3550)       */
        {
                int_l_c_no_pressure = 1.31456 * stress_in_shoulder;
        }


/*      Now calculate the pressure contribution to internal load cell output:
        the internal load cell pressure effect = (output under pressure from plug cal) -
        (output w/o pressure from solid bar cal, evaluated at a shoulder stress = -pressure)          */

        if (pressure_psi > 75209.0)
        {
                pressure_psi = - pressure_psi / 10000.0;
                int_l_c_pressure_effect = (.565514 * pressure_psi - 0.0200375) - (1.28025 * pressure_psi
                - 0.176308);
        }
        else if (pressure_psi > 33550.0)
        {
                pressure_psi = - pressure_psi / 10000.0;
                int_l_c_pressure_effect = (.565514 * pressure_psi - 0.0200375)   (1.29494 * pressure_psi
                - 0.065825);
        }
        else if (pressure_psi > 16889.0)
        {
                pressure_psi = - pressure_psi / 10000.0;
                int_l_c_pressure_effect = (.565514 * pressure_psi - 0.0200375) - (1.31456 *
                pressure_psi);
        }
        else /*   (pressure_psi < 16889)     */
        {
                pressure_psi = - pressure_psi / 10000.0;
                int_l_c_pressure_effect = (.577378 * pressure_psi) - (1.31456 * pressure_psi);
        }

/*      The overall internal load cell output is the sum of the
        axial load contribution and the pressure effect                                 */

        int_l_c_load_command = int_l_c_no_pressure + int_l_c_pressure_effect;
        pressure_psi = - pressure_psi * 10000.0;
}
```

FUNCTION SUBPROGRAM READ_INPUTS.C

```
#include "mainExt.h"

/* * * * * * * * * * * * * * * * * * * * * * * * * * * * *
 * Read_Inputs
 *
 *                  11/15/92
 *
 * Programmer: MAB
 *
 *
 * * * * * * * * * * * * * * * * * * * * * * * * * * * * */

Read_Inputs()
{
        /*  Use the ADC to store 16 bit representations of these signals  */
        AI_Read(5,0,int_load_cell_gain,int_load_cell);
        AI_Read(5,1,stroke_xdcr_gain,stroke_xdcr);
        AI_Read(5,2,1,pressure_xdcr);
        AI_Read(5,3,1,extensometer);
        AI_Read(5,4,ext_load_cell_gain,ext_load_cell);
        AI_Read(5,5,1,e_gage_ch_1);
        AI_Read(5,6,1,e_gage_ch_2);

/*      AI_Read(5,7,1,e_gage_ch_3);       */
        *e_gage_ch_3 = 0;

        DIG_In_Line(5,0,0,limit_switch_state);
}
```

FUNCTION SUBPROGRAM WRITE_ANALOG_OUTPUTS.C

```
#include "mainExt.h"

/* * * * * * * * * * * * * * * * * * * * * * * * * * * *
 * Write_Analog_Outputs
 *
 *                11/15/92
 *
 * Programmer: MAB
 *
 *
 * * * * * * * * * * * * * * * * * * * * * * * * * * * */

Write_Analog_Outputs()
{
        /*  Use the DAC to output a -10 to +10 volt signal on channel 0                */
        AO_Write(5,0,-2048.0 * scaled_pressure_command / ten_volt_pressure);

        if (dither < 0)
        {
                /*  Use the DAC to output a -10 to +10 volt signal on channel 1                */
                AO_Write(5,1,2048.0 * int_l_c_gain_factor * int_l_c_load_command / 10.0 - bits_of_dither );
                dither = 1;
        }
        else
        {
                /*  Use the DAC to output a -10 to +10 volt signal on channel 1                */
                AO_Write(5,1,2048.0 * int_l_c_gain_factor * int_l_c_load_command / 10.0 + bits_of_dither );
                dither = -1;
        }

}
```

FUNCTION SUBPROGRAM STORE_DATA.C

```
#include "mainExt.h"

/* * * * * * * * * * * * * * * * * * * * * * * * * * * *
 * Store Data
 *
 *              11/15/92
 *
 * Programmer: MAB
 *
 *
 * * * * * * * * * * * * * * * * * * * * * * * * * * * */

Store_Data()
{
        /*  store every store_Nth_sample sample to limit size of data file      */

        sample_counter ++;
        if (sample_counter == store_Nth_sample)
        {
                store_sample_flag = 1;
                sample_counter    = 0;
        }
        else
        {
                store_sample_flag = 0;
        }

        if ((store_cycle_num_data == 0) && (store_sample_flag == 0)) return;

        *ext_l_c_load_ptr = *ext_load_cell;          /* corrected for pressure in Write_Data_File()      */
        *int_l_c_load_ptr = *int_load_cell;          /* corrected for pressure in Write_Data_File()      */

        if (store_cycle_num_data == 1)
        {
                *e_gage_3_ptr = 9999;
                if (recharge_test == 1)      /* to distinguish recharge ramps from the cycle afterwards      */
                {
                        *pressure_ptr = -cycle_num;
                }
                else
                {
                        *pressure_ptr = cycle_num;
                }
                store_cycle_num_data = 0;
        }
        else
        {
                *e_gage_3_ptr = *e_gage_ch_3;
                *pressure_ptr = *pressure_xdcr;
        }

        *extensometer_ptr = *extensometer;
        *stroke_xdcr_ptr = *stroke_xdcr;
```

```
        *e_gage_1_ptr = *e_gage_ch_1;
        *e_gage_2_ptr = *e_gage_ch_2;

        ext_l_c_load_ptr++;
        int_l_c_load_ptr++;
        pressure_ptr++;
        extensometer_ptr++;
        stroke_xdcr_ptr++;
        e_gage_1_ptr++;
        e_gage_2_ptr++;
        e_gage_3_ptr++;

        len++;
        if (len >= LISTLEN)
        {
                last_data->length = len;
                last_data->next = (struct data *)malloc((unsigned)sizeof(struct data));
                last_data=last_data->next;
                last_data->length = 0;
                last_data->next = NULL;
                ext_l_c_load_ptr    = last_data->ext_l_c_load;
                int_l_c_load_ptr    = last_data->int_l_c_load;
                pressure_ptr = last_data->pressure;
                extensometer_ptr = last_data->extensometer;
                stroke_xdcr_ptr = last_data->stroke_xdcr;
                e_gage_1_ptr = last_data->e_gage_1;
                e_gage_2_ptr = last_data->e_gage_2;
                e_gage_3_ptr = last_data->e_gage_3;
                len = 0;
                /*              printf("1 block filled\n");             */
        }
}
```

FUNCTION SUBPROGRAM WRITE_DATA_FILE.C

```
#include "mainExt.h"

/* * * * * * * * * * * * * * * * * * * * * * * * * * * *
 * Write Data File
 *
 *       11/15/92
 *
 * Programmer: MAB
 *
 *
 * * * * * * * * * * * * * * * * * * * * * * * * * * * */

Write_Data_File()
{
    printf("Please be patient Huseyin, I am writing the data now\n\n");
    /*      Add 1 block of zero data because the last incomplete
            block of data will not be printed to the file                    */
    for (index = 0; index <= LISTLEN + 5; index++)
    {
    *ext_l_c_load_ptr = 0;
    ext_l_c_load_ptr++;
    *int_l_c_load_ptr = 0;
    int_l_c_load_ptr++;
    *pressure_ptr = 0;
    pressure_ptr++;
    *extensometer_ptr = 0;
    extensometer_ptr++;
    *stroke_xdcr_ptr = 0;
    stroke_xdcr_ptr++;
    *e_gage_1_ptr = 0;
    e_gage_1_ptr++;
    *e_gage_2_ptr = 0;
    e_gage_2_ptr++;
    *e_gage_3_ptr = 8888;
        e_gage_3_ptr++;
        len++;
        if (len >= LISTLEN)
        {
            last_data->length = len;
            last_data->next = (struct data *)malloc((unsigned)sizeof(struct data));
            last_data=last_data->next;
            last_data->length = 0;
            last_data->next = NULL;
            ext_l_c_load_ptr = last_data->ext_l_c_load;
            int_l_c_load_ptr = last_data->int_l_c_load;
            pressure_ptr = last_data->pressure;
            extensometer_ptr = last_data->extensometer;
            stroke_xdcr_ptr = last_data->stroke_xdcr;
            e_gage_1_ptr = last_data->e_gage_1;
            e_gage_2_ptr = last_data->e_gage_2;
            e_gage_3_ptr = last_data->e_gage_3;
            len = 0;
        }
```

```
    }

    /*    Write all the linked list data to file output.dat                    */

    fp = fopen(" output.dat", "w");
    if (fp == NULL)
    {
        fprintf(stderr, "Error:  can't open file output.dat\n");
        exit(-1);
    }
    fprintf(fp, "IGOR\n");
    fprintf(fp, "WAVES Int_LC_Stress, Ext_LC_Stress, Pressure, Extensometer, Ex_gage_1, Stroke_xdcr,
St_gage_1, e_gage_1, e_gage_2\n");
  fprintf(fp, "BEGIN\n");
    while (first_data != NULL)
    {
        len = first_data->length;
        if (len > 0)
        {
            for (index = 0; index < len; index++)
            {
                if (first_data->e_gage_3[index] == 9999)      /* code for cycle number line */
                {
                    cycle_num = first_data->pressure[index];
                    fprintf(fp, "END\n");
                    fprintf(fp,"\nWAVES Int_LC_Stress_%d, Ext_LC_Stress_%d, Pressure_%d,
Extensometer_%d, Ex_gage_1_%d, Stroke_xdcr_%d, St_gage_1_%d, e_gage_1_%d, e_gage_2_%d\n",
cycle_num,cycle_num,cycle_num,cycle_num,cycle_num,cycle_num,cycle_num,cycle_num,cycle_num);
                fprintf(fp, "BEGIN\n");
                }
                else if (first_data->e_gage_3[index] == 8888) ;                    /* do nothing          */
                else                                                               /* data line           */
                {
                    /* calculate apparent, then actual strains, correcting for
                        a) hydrostatic strains picked up by the dummy gages,
                        b) transverse sensitivity of all the gages                                        */

                pressure_psi =     first_data->pressure[index]          * ten_volt_pressure   / 32768.0;
                ext_l_c_load_lbf = first_data->ext_l_c_load[index]      * ten_volt_load      / 32768.0;

                deflection_in=     (first_data->extensometer[index] - extensometer_offset) * ten_volt_deflection /
                                   32768.0;

                stroke_in      =   (first_data->stroke_xdcr[index] - initial_stroke_xdcr) * ten_volt_stroke / 32768.0;

                apparent_e_1 =     (first_data->e_gage_1[index] - e_gage_1_offset) * ten_volt_e_gage_1A / 32768.0
                                   +       pressure_psi * dummy_gage_1;
                apparent_e_2 =     (first_data->e_gage_2[index] - e_gage_2_offset) * ten_volt_e_gage_2A / 32768.0
                                   +       pressure_psi * dummy_gage_2;

                actual_e_1     =   (apparent_e_1 * corr_1 - apparent_e_2 * Kt_1A * corr_2) / corr_4;
                actual_e_2     =   (apparent_e_2 * corr_2 - apparent_e_1 * Kt_2A * corr_1) / corr_4;

                int_l_c_output = first_data->int_l_c_load[index] * 10.0 / 32768.0 / int_l_c_gain_factor;

                if (pressure_psi > 75209.0)
```

```
{
    pressure_psi = - pressure_psi / 10000.0;
    int_l_c_pressure_effect = (.565514 * pressure_psi - 0.0200375) - (1.28025 * pressure_psi -
                                        0.176308);
}
else if (pressure_psi > 33550.0)
{
    pressure_psi = - pressure_psi / 10000.0;
    int_l_c_pressure_effect = (.565514 * pressure_psi - 0.0200375) - (1.29494 * pressure_psi -
                                        0.065825);
}
else if (pressure_psi > 16889.0)
{
    pressure_psi = - pressure_psi / 10000.0;
    int_l_c_pressure_effect = (.565514 * pressure_psi - 0.0200375) - (1.31456 * pressure_psi);
}
else /*   (pressure_psi < 16889)     */
{
    pressure_psi = - pressure_psi / 10000.0;
    int_l_c_pressure_effect = (.577378 * pressure_psi) - (1.31456 * pressure_psi);
}
pressure_psi = -pressure_psi * 10000.0;
int_l_c_no_pressure = int_l_c_output - int_l_c_pressure_effect;


if (int_l_c_no_pressure < -9.8049)
{
    stress_in_shoulder = 7810.97 * int_l_c_no_pressure + 1377.14;
}
else if (int_l_c_no_pressure < -4.4103)
{
    stress_in_shoulder = 7722.36 * int_l_c_no_pressure + 508.33;
}
else /*   (int_l_c_no_pressure > -4.4103)     */
{
    stress_in_shoulder = 7607.11 * int_l_c_no_pressure;
}


load_from_geom = (A - a) * pressure_psi;
int_l_c_load_lbf = stress_in_shoulder * A;

fprintf(fp, "%9.0f\t%9.0f\t%6.0f\t%6.0f\t%9.6f\t%6d\t%9.6f\t%9.6f\t%9.6f\n",
    (stress_in_shoulder * A + load_from_geom) / a,
    (ext_l_c_load_lbf + load_from_geom) / a,
    pressure_psi,
    first_data->extensometer[index] - extensometer_offset,
    C1 * deflection_in - C2 * int_l_c_load_lbf - C3 * ext_l_c_load_lbf - C4 * pressure_psi,
    first_data->stroke_xdcr[index] - initial_stroke_xdcr,
    C1 *  stroke_in  -  C2 * int_l_c_load_lbf - CS3 * ext_l_c_load_lbf - C4 * pressure_psi,
    strain_cal_1 * actual_e_1 + (1.0 - pressure_cal_1) * 2.0 * nu * pressure_psi / E,
    strain_cal_2 * actual_e_2 + (1.0 - pressure_cal_2) * 2.0 * nu * pressure_psi / E);

/*  fprintf(fp, "%9.0f\t%9.0f\t%6.0f\t%6.0f\t%9.6f\t%9.6f\t%9.6f\t%9.4f\n",
    (stress_in_shoulder * A + load_from_geom) / a,
    (ext_l_c_load_lbf + load_from_geom) / a,
```

```
                    pressure_psi,
                    first_data->extensometer[index] - extensometer_offset,
                    C1 * deflection_in - C2 * int_l_c_load_lbf - C3 * ext_l_c_load_lbf - C4 * pressure_psi,
                    strain_cal_1 * actual_e_1 + (1.0 - pressure_cal_1) * 2.0 * nu * pressure_psi / E,
                    strain_cal_2 * actual_e_2 + (1.0 - pressure_cal_2) * 2.0 * nu * pressure_psi / E,
                    first_data->e_gage_3[index] * 10.0 / 32768 * 50);
*/
                }
            }
        }
        first_data = first_data->next;
    }
    fprintf(fp, "END\n");
    if (fclose(fp) != 0)
    {
        fprintf(stderr, "Error:  can't close file output.dat\n");
        exit(-1);
    }
}
```

HEADER MAIN.H

```
/* * * * * * * * * * * * * * * * * * * * * * * * * * * * * * * * * * * * * * * *
 *
 * 11/15/92
 *
 * Programmer:MAB
 *
 * * * * * * * * * * * * * * * * * * * * * * * * * * * * * * * * * * * * * * * */

#include <stdio.h>
#include <stdlib.h>
#include <math.h>
#include "NI_DAQ_MAC.h"
#define LISTLEN (1<<10)

                                /* GLOBAL VARIABLES */

FILE            *fp;                    /* file pointer for out.dat                  */
Boolean         KeyMaps[16];            /* packed array of 0/1's from keyboard       */

int16           var_limit_switch_state; /* var storing intensifier upper limit switch read by DAQ*/
int16           var_stroke_xdcr;        /* variable storing stroke xdcr read by DAQ  */
int16           var_ext_load_cell;      /* variable storing external load cell read by DAQ  */
int16           var_int_load_cell;      /* variable storing internal load cell read by DAQ  */
int16           var_pressure_xdcr;      /* variable storing pressure xdcr read by DAQ  */
int16           var_extensometer;       /* variable storing extensometer read by DAQ  */
int16           var_e_gage_ch_1;        /* variable storing strain gage 1 read by DAQ  */
int16           var_e_gage_ch_2;        /* variable storing strain gage 2 read by DAQ  */
int16           var_e_gage_ch_3;        /* variable storing strain gage 3 read by DAQ  */

int16           *limit_switch_state;    /* intensifier upper limit switch read by DAQ
                                           = 0 when ok, and = 1 (5 vdc) when at the limit  */
int16           *stroke_xdcr;           /* stroke xdcr read by DAQ                   */
int16           *ext_load_cell;         /* external load cell read by DAQ            */
int16           *int_load_cell;         /* internal load cell read by DAQ            */
int16           *pressure_xdcr;         /* pressure xdcr read by DAQ                 */
int16           *extensometer;          /* extensometer read by DAQ                  */
int16           *e_gage_ch_1;           /* strain gage 1 read by DAQ                 */
int16           *e_gage_ch_2;           /* strain gage 2 read by DAQ                 */
int16           *e_gage_ch_3;           /* strain gage 3 read by DAQ                 */

short int       n = 0;                  /* array index used while zeroing            */
short int       m;                      /* loop counter used while zeroing           */
int16           old_pressure_xdcr[6];   /* last 5 transducer readings                */
int16           old_ext_load_cell[6];   /* last 5 transducer readings                */
int16           old_int_load_cell[6];   /* last 5 transducer readings                */
int16           old_extensometer[6];    /* last 5 transducer readings                */
int16           old_e_gage_ch_1[6];     /* last 5 transducer readings                */
int16           old_e_gage_ch_2[6];     /* last 5 transducer readings                */
int16           old_e_gage_ch_3[6];     /* last 5 transducer readings                */
long double     sum_old_pressure_xdcr = 0;  /* sum of last 5 transducer readings     */
long double     sum_old_ext_load_cell = 0;  /* sum of last 5 transducer readings     */
long double     sum_old_int_load_cell = 0;  /* sum of last 5 transducer readings     */
long double     sum_old_extensometer = 0;   /* sum of last 5 transducer readings     */
```

```
long double     sum_old_e_gage_ch_1 = 0;    /* sum of last 5 transducer readings                    */
long double     sum_old_e_gage_ch_2 = 0;    /* sum of last 5 transducer readings                    */
long double     sum_old_e_gage_ch_3 = 0;    /* sum of last 5 transducer readings                    */

short int       index;                      /* loop counter                                         */
short int       store_cycle_num_data = 0;   /* set to 1 when storing cycle num                      */
short int       quit_zero_inputs = 0;       /* set to 1 after <T> is pressed                        */
short int       begin_test       = 0;       /* set to 1 after <B> is pressed                        */
short int       pause_test       = 0;       /* set to 1 after <P> is pressed                        */
short int       stop_test        = 0;       /* set to 1 after <S> is pressed                        */
short int       unsure_quit_test = 0;       /* set to 1 after <Q> is pressed                        */
short int       quit_test = 0;              /* set to 1 after <Q> and <Y> are pressed               */
short int       recharge_test = 0;          /* set to 1 when top limit switch is activated          */
short int       begin_ramp = 0;             /* changed when begin/end ramps running                 */
short int       stop_ramp        = 0;       /* set to 1 when stop ramp is running                   */
short int       recharge_ramp    = 0;       /* set to 1 when recharge ramp is running               */
short int       dither           = 0;       /* set to +/-1 to add dither to MTS command             */
short int       broken_specimen= 0;         /* set to 1 after *e_gage_ch_3 jumps                    */
short int       end_test         = 0;       /* set to 1 after Calc_Ramp_Down_Command run            */
short int       store_sample_flag = 0;      /* used to store every Nth sample's data                */
short int       sample_counter = 0;         /* used to count samples                                */
short int       store_Nth_sample;           /* store only every Nth sample's data                   */
long double     cycle_sample     = 0;       /* sample number in a command cycle                     */
long double     ramp_1_sample  = 0;         /* sample number in cyclic command ramp  1              */
long double     ramp_2_sample  = 0;         /* sample number in cyclic command ramp 2               */
long double     ramp_up_sample= 0;          /* sample number in a mono command ramp up              */
long double     ramp_down_sample  = 0;      /* sample number in a mono command ramp down            */
long double     stop_ramp_sample;           /* sample number in a mono stop command ramp            */
long double     stop_ramp_1_sample;         /* sample number in cyclic stop command ramp 1          */
long double     stop_ramp_2_sample;         /* sample number in cyclic stop command ramp 2          */
long double     recharge_ramp_1_sample;     /* sample number in cyclic recharge command ramp        */
long double     recharge_ramp_2_sample;     /* sample number in cyclic recharge command ramp        */
long double     samples_per_cycle;          /* number of samples in a command cycle                 */
long double     samples_per_ramp_1;         /* number of samples in cyclic command ramp 1           */
long double     samples_per_ramp_2;         /* number of samples in cyclic command ramp 2           */
long double     samples_per_ramp_up;        /* number of samples in a mono command rampup           */
long double     samples_per_ramp_down;      /* number of samples in a mono command ramp down        */
long double     samples_per_stop_ramp;      /* number of samples in mono stop command ramp 1        */
long double     samples_per_stop_ramp_1;    /* number of samples in cyclic stop command ramp 1      */
long double     samples_per_stop_ramp_2;    /* number of samples in cyclic stop command ramp 2      */
long double     samples_per_recharge_ramp_1; /* number of samples in cyclic recharge command ramp 1 */
long double     samples_per_recharge_ramp_2; /* number of samples in cyclic recharge command ramp 2 */
long double     extra_samples_at_peaks;     /* number of samples at wave tip values                 */
int             cycle_num;                  /* cycle number                                         */
int             recharge_cycle_num  = 0;    /* cycle number of a recharge cycle                     */
int             recharge_num     = 0;       /* number of recharge cycles                            */
int             last_cycle_num;             /* test ends at this cycle number                       */
int             recharge_stage;             /* stage of recharge process; 1, 2 or 3                 */
int             initial_stroke_xdcr;        /* initial stroke xdcr reading                          */
int             stroke_xdcr_limit;          /* allowable stroke limit                               */
int             bits_of_dither;             /* bits of dither applied to MTS command                */

long double     load_command;               /* load command                                         */
long double     pressure_command;           /* pressure command                                     */
long double     last_pressure_command;      /* previous pressure command                            */
long double     scaled_pressure_command;    /* pressure command        corrected for phase lag      */
```

```
long double     int_l_c_output;             /* internal load cell output recalled in write_data_file */
long double     int_l_c_load_command;       /* internal load cell command                            */
long double     int_l_c_no_pressure;        /* internal load cell output with no pressure effect     */
long double     int_l_c_pressure_effect;    /* pressure effect on internal load cell output          */
long double     ext_l_c_load_command;       /* external load cell command                            */
long double     ramp_pressure_to;           /* peak pressure in a command ramp                       */
long double     cycle_pressure_from;        /* peak pressure in a command cycle                      */
long double     cycle_pressure_to;          /* peak pressure in a command cycle                      */
long double     stop_pressure_at;           /* peak pressure in a stop command ramp                  */
long double     recharge_pressure_at;       /* peak pressure in a recharge command ramp              */
long double     ramp_stress_to;             /* peak stress in a command ramp                         */
long double     cycle_stress_from;          /* peak stress in a command cycle                        */
long double     cycle_stress_to;            /* peak stress in a command cycle                        */
long double     ramp_load_to;               /* peak load in a command ramp                           */
long double     cycle_load_from;            /* peak load in a command cycle                          */
long double     cycle_load_to;              /* peak load in a command cycle                          */
long double     stop_load_at;               /* peak load in a stop command ramp                      */
long double     recharge_load_at;           /* peak load in a recharge command ramp                  */

long double     load_from_geom;             /* component of calculated load                          */
long double     stress_in_shoulder;         /* calculated stress in specimen shoulder                */
long double     zero_offset_load;           /* small negative load; keeps setup together             */
long double     pressure_psi;               /* pressure transducer reading in psi                    */
long double     deflection_in;              /* extensometer reading in inches                        */
long double     stroke_in;                  /* stroke xdcr reading in inches                         */
long double     ext_l_c_load_lbf;           /* external load cell reading in pounds force            */
long double     int_l_c_load_lbf;           /* internal load cell reading in pounds force            */
long double     int_l_c_gain_factor;        /* allows amp gain adjustment for high load tests        */
int             ext_load_cell_gain;         /* gain setting for NIDAQ board: 1,2,4 or 8              */
int             int_load_cell_gain;         /* gain setting for NIDAQ board: 1,2,4 or 8              */
int             stroke_xdcr_gain;           /* gain setting for NIDAQ board: 1,2,4 or 8              */

int             *ext_l_c_load_ptr;          /* pointer to external load cell derived load in linked list */
int             *int_l_c_load_ptr;          /* pointer to internal load cell derived load in linked list */
int             *pressure_ptr;              /* pointer to pressure in linked list                    */
int             *extensometer_ptr;          /* pointer to extensometer in linked list                */
int             *stroke_xdcr_ptr;           /* pointer to stroke xdcr in linked list                 */
int             *e_gage_1_ptr;              /* pointer to strain gage 1 in linked list               */
int             *e_gage_2_ptr;              /* pointer to strain gage 2 in linked list               */
int             *e_gage_3_ptr;              /* pointer to strain gage 3 in linked list               */
int             len;                        /* number of full records in current block     */

long double     E;                          /* Young's modulus                                       */
long double     nu;                         /* Poisson's ratio                                       */
long double     D;                          /* diameter of specimen shoulders                        */
long double     d;                          /* diameter of specimen gage section                     */
long double     A;                          /* area of specimen shoulders
        */
long double     a;                          /* area of specimen gage section                         */
long double     EA;                         /* elastic constant                                      */
long double     L1, L2, L3, L4, S4;         /* lengths of specimen segments                          */
long double     C1, C2, C3, C4, CS3;        /* constant for deflection to strain calculation         */
long double     fillet_fudge;               /* fudge factor for gage length equivalence              */
long double     seal_fudge;                 /* fudge factor for sho length equivalence               */
long double     ten_volt_pressure;          /* pressure (psi) calibration for 10 volts               */
long double     ten_volt_load;              /* load (lbf) calibration for 10 volts                   */
```

```
long double     ten_volt_deflection;    /* deflection (in) calibration for 10 volts     */
long double     ten_volt_stroke;        /* stroke (in) calibration for 10 volts         */
long double     amp_gain_1;             /* amplifier gain for strain gage 1             */
long double     amp_gain_2;             /* amplifier gain for strain gage 2             */
long double     amp_gain_3;             /* amplifier gain for strain gage 3             */
long double     excitation_voltage;     /* excitation voltage for strain gages          */
long double     gage_factor_1A;         /* gage factor of active gage 1                 */
long double     Kt_1A;                  /* transverse sensitivity of active gage 1      */
long double     gage_factor_2A;         /* gage factor of active gage 2                 */
long double     Kt_2A;                  /* transverse sensitivity of active gage 3      */
long double     gage_factor_3A;         /* gage factor of active gage 3                 */
long double     Kt_3A;                  /* transverse sensitivity of active gage 2      */
long double     gage_factor_1D;         /* gage factor of dummy gage 1                  */
long double     Kt_1D;                  /* transverse sensitivity of dummy gage 1       */
long double     gage_factor_2D;         /* gage factor of dummy gage 2                  */
long double     Kt_2D;                  /* transverse sensitivity of dummy gage 2       */
long double     gage_factor_3D;         /* gage factor of dummy gage 3                  */
long double     Kt_3D;                  /* transverse sensitivity of dummy gage 3       */
long double     extensometer_offset;    /* zero offset on extensometer channel in bits  */
long double     e_gage_1_offset;        /* zero offset on e_gage_1 channel in bits      */
long double     e_gage_2_offset;        /* zero offset on e_gage_2 channel in bits      */
long double     nuo;                    /* Poisson's Ratio for calibration beam         */
long double     ten_volt_e_gage_1A;     /* strain gage 1 calibration for 10 volts       */
long double     ten_volt_e_gage_2A;     /* strain gage 2 calibration for 10 volts       */
long double     ten_volt_e_gage_3A;     /* strain gage 3 calibration for 10 volts       */
long double     dummy_gage_1;           /* correction for dummy gage 1 effects          */
long double     dummy_gage_2;           /* correction for dummy gage 2 effects          */
long double     dummy_gage_3;           /* correction for dummy gage 3 effects          */
long double     apparent_e_1;           /* apparent strain from active gage 1           */
long double     apparent_e_2;           /* apparent strain from active gage 2           */
long double     apparent_e_3;           /* apparent strain from active gage 3           */
long double     actual_e_1;             /* actual strain from active gage 1             */
long double     actual_e_2;             /* actual strain from active gage 2             */
long double     actual_e_3;             /* actual strain from active gage 3             */
long double     corr_1;                 /* correction for transverse sensitivity effects */
long double     corr_2;                 /* correction for transverse sensitivity effects */
long double     corr_3;                 /* correction for transverse sensitivity effects */
long double     corr_4;                 /* correction for transverse sensitivity effects */
long double     strain_cal_1;           /* strain calibration for gage 1                */
long double     pressure_cal_1;         /* pressure calibration for gage 1              */
long double     strain_cal_2;           /* strain calibration for gage 2                */
long double     pressure_cal_2;         /* pressure calibration for gage 2              */
long double     strain_cal_3;           /* strain (load) calibration for gage 3         */
long double     pressure_cal_3;         /* pressure calibration for gage 3              */

struct data {
        int             ext_l_c_load[LISTLEN];
        int             int_l_c_load[LISTLEN];
        int             pressure[LISTLEN];
        int             extensometer[LISTLEN];
/*      int             stroke_xdcr[LISTLEN];   */
        int             e_gage_1[LISTLEN];
        int             e_gage_2[LISTLEN];
        int             e_gage_3[LISTLEN];
        int             length;
struct data *next;} *first_data, *last_data;    /* linked list for data storage         */
```

APPENDIX C - COMPUTER CODE FOR CYCLIC TESTING

PROGRAM MAIN.C

```
#include "main.h"

/* * * * * * * * * * * * * * * * * * * * * * * * * * * *
 *
 *    Load Control.c
 *
 *              11/15/92
 *
 *    Programmer: MAB
 *
 *
 * * * * * * * * * * * * * * * * * * * * * * * * * * * */

main()
{
        limit_switch_state      =       &var_limit_switch_state;
        stroke_xdcr                     =       &var_stroke_xdcr;
        int_load_cell           =       &var_int_load_cell;
        ext_load_cell           =       &var_ext_load_cell;
        extensometer            =       &var_extensometer;
        pressure_xdcr           =       &var_pressure_xdcr;
        e_gage_ch_1                     =       &var_e_gage_ch_1;
        e_gage_ch_2                     =       &var_e_gage_ch_2;
        e_gage_ch_3                     =       &var_e_gage_ch_3;

        Set_Up_DAQ();
        Calibrations();
        Set_Up_Counter();
        Init_Linked_List();

        /* Write a one to the solenoid valve's relay,
           to open the solenoid valve on the air line                   */
        DIG_Out_Line(5,1,0,1);

        /* Print the instructions for zeroing                           */
        printf("            Running intensifier and load control program\n\n");
        printf("    ****    Be sure to set the FDBK SELECT switch to EXT    ****\n\n\n");
        printf("                Zero all transducers now\n\n\n");
        printf("                To enter TEST mode, press <T>\n\n\n");

        /* zero inputs routine                                          */

                /*  Check the keyboard for keystrokes                   */
                GetKeys ((long *)KeyMaps);

                /*  If the test is running then proceed with the program */
                while (quit_zero_inputs == 0)
                {
                        Read_Inputs();

                        /* commands remain zero while operator checks zeros
                           zeroing ends when <T> is pressed.            */
```

```
                if (n<5)
                {
                        n++;
                }
                else
                {
                        n = 0;
                }
                old_pressure_xdcr[n]  = *pressure_xdcr;
                old_ext_load_cell[n]  = *ext_load_cell;
                old_int_load_cell[n]  = *int_load_cell;
                old_extensometer[n]           = *extensometer;
                old_e_gage_ch_1[n]            = *e_gage_ch_1;
                old_e_gage_ch_2[n]            = *e_gage_ch_2;
                old_e_gage_ch_3[n]            = *e_gage_ch_3;
                sum_old_pressure_xdcr         = 0;
                sum_old_ext_load_cell         = 0;
                sum_old_int_load_cell= 0;
                sum_old_extensometer          = 0;
                sum_old_e_gage_ch_1                   = 0;
                sum_old_e_gage_ch_2                   = 0;
                sum_old_e_gage_ch_3                   = 0;
                for (m = 0; m < 6; m++)
                {
                        sum_old_pressure_xdcr += old_pressure_xdcr[m];
                        sum_old_ext_load_cell += old_ext_load_cell[m];
                        sum_old_int_load_cell += old_int_load_cell[m];
                        sum_old_extensometer  += old_extensometer[m];
                        sum_old_e_gage_ch_1   += old_e_gage_ch_1[m];
                        sum_old_e_gage_ch_2   += old_e_gage_ch_2[m];
                        sum_old_e_gage_ch_3   += old_e_gage_ch_3[m];
                }
                printf("p_xdcr=%5.0f Ext_LC=%5.0f Int_LC=%5.0f exten=%5.0f
                        gage_1=%5.0f gage_2=%5.0f\n",
                sum_old_pressure_xdcr / 6,
                sum_old_ext_load_cell / 6,
                sum_old_int_load_cell / 6,
                sum_old_extensometer  / 6,
                sum_old_e_gage_ch_1   / 6,
                sum_old_e_gage_ch_2   / 6);
        /*      sum_old_e_gage_ch_3   / 6    */

                Calculate_Zero_Commands();

                Calculate_Modified_Commands();

                Write_Analog_Outputs();

                /*   Check the keyboard for keystrokes                          */
                GetKeys ((long *)KeyMaps);
                if (KeyMaps[2] == 2) quit_zero_inputs = 1;  /* <T> has been pressed */
        }

/* Set the initial stroke xdcr value                                           */
AI_Read(5,1,1,stroke_xdcr);
initial_stroke_xdcr = *stroke_xdcr;
```

```
/* Print the instructions                                                    */
printf("\n\n\n          Running intensifier and load control program\n\n");
printf("    ****    Be sure to set the FDBK SELECT switch to EXT    ****\n\n\n");
printf("To BEGIN a new test, press \t\t\t\t<B>\n\n\n");
printf("To PAUSE a running test, press \t\t\t\t<P>\n\n\n");
printf("To RESUME a running test, press \t\t\t<R>\n\n\n");
printf("To STOP a running test prematurely, press \t\t<S>\n");
printf("  THEN turn off all hydraulics, THEN QUIT\n\n");
printf("To QUIT the control program after running a test,\n");
printf("  FIRST turn off all hydraulics, THEN press \t\t<Q>.\n");
printf("  This step saves all data.\n\n");

/*  Check the keyboard for keystrokes                                        */
GetKeys ((long *)KeyMaps);

/*  If the test is running then proceed with the program                     */
while (quit_test == 0)
{
        Read_Inputs();

        /*  commands remain zero until <B> is pressed.
                commands then ramp to initial values
                commands then cycle
                commands then ramp to zero and remain zero.

                commands are held constant if <P> is pressed.
                commands continue when <R> is pressed.

                commands ramp to zero and remain zero when <S> is pressed.

                data is written to output.dat and program ends when <Q> is pressed.

                decisions as to store data or not to store data
                are made in the command subroutines.  the ramps
                and cycle #'s 1-10, 2**4-2**15 are stored by default.        */

        Decide_Command_Based_On_Keyboard();

        Calculate_Modified_Commands();

        Write_Analog_Outputs();

        /*      if              the intensifier has tripped the upper limit switch
                                and stop has not yet been commanded,
                then    recharge the intensifier,
                                storing all data during the recharge
                                and the cycle immediately following the recharge  */
        if (*limit_switch_state == 1) recharge_test = 1;
        if ((recharge_test == 1) && (stop_test == 0))
                Recharge_Intensifier();

        /*  Check the keyboard for keystrokes                                */
        GetKeys ((long *)KeyMaps);
}
```

```
        /* Write a zero to the solenoid valve's relay,
                to close the solenoid valve on the air line                    */
        DIG_Out_Line(5,1,0,0);

        Write_Data_File();
        printf("Intensifier and load control program has finished");
}
```

FUNCTION SUBPROGRAM INITIALIZE.C

```
#include "mainExt.h"

/* * * * * * * * * * * * * * * * * * * * * * * * * * * *
 * Calibrations
 *
 *                11/15/92
 *
 * Programmer: MAB
 *
 *
 * * * * * * * * * * * * * * * * * * * * * * * * * * * */

Calibrations()
{
/*      date                    =  5/8/97;          date of test                                    */
/*      specimen number         =     22;           number of specimen                              */
/*  test letter                 =      A;           A = test 1, B = test 2, etc.                    */
/*  specimen status             =                   Failed at cycles                                */
/*      gage section gage =                         EA-06-125TM-120                                 */
/*      gage lot number         =                   R-A56AD84                                       */
/*      general notes           =                   1070    Steel                                   */

D                       =       0.4375;             /* diameter of specimen shoulders              */
d                       =       0.290;              /* diameter of specimen gage section           */
fillet_fudge            =       0.000;          /* fudge factor for increasing effective gage length */
seal_fudge              =       0.000;/* factor for increasing eff internal long-sho length */
L1                      =       0.340 - fillet_fudge;       /* effective short-shoulder length */
L2                      =       1.003 + 2. * fillet_fudge;  /* effective gage length           */
L3                      =       0.275 - fillet_fudge + seal_fudge; /* eff internal long-sho len */
L4                      =       0.880 - seal_fudge;     /* effective external long-shoulder length */
S4                      =       1.000;                  /* effective external long-shoulder length
                                                           used for stroke xdcr calibration        */
E                       = 29000000.0;       /* Young's modulus for specimen + dummy            */
nu                      =       0.3;        /* Poisson's ratio for specimen + dummy            */

cycle_num               =     1;            /* test begins at this cycle number                */
last_cycle_num          =  32750;           /* test ends at this cycle number 32766 max        */
ramp_pressure_to        =  50000.0;         /* peak pressure in command ramp 1                 */
cycle_pressure_from     =  50000.0;         /* peak pressure in command ramp 2 and             */
cycle_pressure_to       =  50000.0;         /* other peak pressure in a command cycle          */
ramp_stress_to          = -50000.0;         /* peak stress in command ramp 1                   */
cycle_stress_from       =  10000.0;         /* peak stress in command ramp 2 and               */
                                            /*  one peak stress in a command cycle             */
cycle_stress_to         = -110000.0;        /* other peak stress in a command cycle            */
samples_per_ramp_1      = 1000.;            /* number of samples in command ramp 1             */
                                            /*    must be >= 1.                                */
samples_per_ramp_2      = 1000.;            /* number of samples in command ramp 2             */
                                            /*    must be >= 1.                                */
samples_per_cycle       =  400.;            /* number of samples in a command cycle            */
                                            /*    must be even number >= 2.                    */
extra_samples_at_peaks  =   15.;            /* number of samples at wave tip values            */
store_Nth_sample        =      2;           /* store only every Nth sample                     */
bits_of_dither          =      0;           /* bits of dither applied to MTS command           */
```

```
                                        /* a 1 bit dither amplitude = .05% of the
                                        full scale (10 volt) MTS command signal          */

amp_gain_1              =     100.0;    /* amplifier gain for strain gage 1                 */
amp_gain_2              =     200.0;    /* amplifier gain for strain gage 2                 */
amp_gain_3              =    1000.0;    /* amplifier gain for strain gage 3                 */
excitation_voltage      =      5.00;    /* excitation voltage for strain gages              */
gage_factor_1A          =     2.050;    /* gage factor of active gage 1                     */
Kt_1A                   =     0.019;    /* transverse sensitivity of active gage 1          */
gage_factor_2A          =     2.080;    /* gage factor of active gage 2                     */
Kt_2A                   =     0.011;    /* transverse sensitivity of active gage 2          */
gage_factor_3A          =     1.000;    /* gage factor of active gage 3                     */
Kt_3A                   =     0.000;    /* transverse sensitivity of active gage 3          */
gage_factor_1D          =     2.050;    /* gage factor of dummy gage 1                      */
Kt_1D                   =     0.019;    /* transverse sensitivity of dummy gage 1           */
gage_factor_2D          =     2.080;    /* gage factor of dummy gage 2
        */
Kt_2D                   =     0.011;    /* transverse sensitivity of dummy gage 2   */
gage_factor_3D          =     1.000;    /* gage factor of dummy gage 3
        */
Kt_3D                   =     0.000;    /* transverse sensitivity of dummy gage 3   */
extensometer_offset     =     0.;       /* zero offset on extensometer channel, bits*/
e_gage_1_offset         =     0.;       /* zero offset on e_gage_1 channel in bits  */
e_gage_2_offset         =     0.;       /* zero offset on e_gage_2 channel in bits  */

strain_cal_1            =     1.0000;   /* strain calibration for gage 1                    */
pressure_cal_1          =     1.0000;   /* pressure calibration for gage 1                  */
strain_cal_2            =     1.0000;   /* strain calibration for gage 2                    */
pressure_cal_2          =     1.0000;   /* pressure calibration for gage 2                  */
strain_cal_3            =     1.0000;   /* strain (load) calibration for gage 3             */
pressure_cal_3          =     1.0000;   /* pressure calibration for gage 3                  */

int_load_cell_gain      =          1;   /* gain setting for NIDAQ board: 1,2,4 or 8 */
int_l_c_gain_factor     =        1.0;   /* when running high compressive load tests,
                                        set this to 0.7 and adjust the amp gain accordingly   */
ten_volt_pressure       = 125000.0;     /* pressure (psi) calibration for 10 volts          */
ext_load_cell_gain      =     1;        /* gain setting for NIDAQ board: 1,2,4 or 8         */
ten_volt_load           = 20000.0 / ext_load_cell_gain; /* load (lbf) calibration (for 10V) */
ten_volt_deflection     =     0.0666;   /* deflection (in) calibration for 10 volts         */
                                        /*       checked 1/16/97                            */
stroke_xdcr_gain        =     1;        /* gain setting for NIDAQ board: 1,2,4 or 8         */
ten_volt_stroke         =     1.416/ stroke_xdcr_gain;  /* stroke (in) calibration for 10 volts  */
                                        /* 0.7166 @ CAL FACTOR = 0,   TOGGLE = fine  */
                                        /* 1.416  @ CAL FACTOR = 100, TOGGLE = fine  */
                                        /* 2.2727 @ CAL FACTOR = 420, TOGGLE = coarse*/
stroke_xdcr_limit       = 0.20 * (32768.0 / ten_volt_stroke);
                                        /* allowable stroke limit for cyclic tests   */
zero_offset_load        = -600.;        /* small negative load (lbf); keeps setup together  */
samples_per_stop_ramp_1 = 500.;         /* number of samples in stop ramp 1                 */
                                        /*    must be >= 1.                                 */
samples_per_stop_ramp_2 = 500.;         /* number of samples in stop ramp 2                 */
                                        /*    must be >= 1.                                 */
samples_per_recharge_ramp_1 = 1000.;    /* number of samples in recharge ramp 1             */
                                        /*    must be >= 1.                                 */
samples_per_recharge_ramp_2 = 1000.;    /* number of samples in recharge ramp 2             */
                                        /*    must be >= 1.                                 */
```

```
/*****************************************************************************************/

A  = 3.1415927*(pow(D,2))/4.0;                  /* area of specimen shoulders                  */
a  = 3.1415927*(pow(d,2))/4.0;                  /* area of specimen gage section               */
EA = E * A;                                     /* elastic constant                            */

ramp_load_to    =    ramp_stress_to * a;        /* peak load in command ramp 1                 */
cycle_load_from =    cycle_stress_from * a;     /* peak load in command ramp 2 and             */
                                                /*  one peak load in a command cycle           */
cycle_load_to   =    cycle_stress  to * a;      /* peak load in a command cycle                */

stop_ramp_1_sample          = samples_per_stop_ramp_1;
stop_ramp_2_sample          = samples_per_stop_ramp_2;
recharge_ramp_1_sample      = samples_per_recharge_ramp_1;
recharge_ramp_2_sample      = samples_per_recharge_ramp_2;

nuo                         =  0.285;           /* Poisson's ratio for e gage calibration beam */
ten_volt_e_gage_1A          = 10.0/(amp_gain_1 * excitation_voltage/4.0 * gage_factor_1A);
                                                /* strain gage 1 calibration for 10 volts      */
ten_volt_e_gage_2A          = 10.0/(amp_gain_2 * excitation_voltage/4.0 * gage_factor_2A);
                                                /* strain gage 2 calibration for 10 volts      */
ten_volt_e_gage_3A          = 10.0/(amp_gain_3 * excitation_voltage/4.0 * gage_factor_3A);
                                                /* strain gage 2 calibration for 10 volts      */
dummy_gage_1                = gage_factor_1D * (2.0 * nu - 1.0) *    (1.0 + Kt_1D)       /
                              (gage_factor_1A *       E       * (1.0 - nuo * Kt_1D));
                                                /* correction for dummy gage 1 effects         */
dummy_gage_2                = gage_factor_2D * (2.0 * nu - 1.0) *    (1.0 + Kt_2D)       /
                              (gage_factor_2A *       E       * (1.0 - nuo * Kt_2D));
                                                /* correction for dummy gage 2 effects         */
dummy_gage_3                = gage_factor_3D * (2.0 * nu - 1.0) *    (1.0 + Kt_3D)       /
                              (gage_factor_3A *       E       * (1.0 - nuo * Kt_3D));
                                                /* correction for dummy gage 3 effects         */
corr_1          =    1.0 -  nuo  * Kt_1A;       /* correction for transverse sensitivity effects */
corr_2          =    1.0 -  nuo  * Kt_2A;       /* correction for transverse sensitivity effects */
corr_3          =    1.0 -  nuo  * Kt_3A;       /* correction for transverse sensitivity effects */
corr_4          =    1.0 - Kt_1A * Kt_2A;       /* correction for transverse sensitivity effects */

C1              =    1.0 / L2;                  /* constants for extensometer to strain conversion */
C2              =    3.198E-7 / L2 + (L1 + L3) / (EA * L2);
C3              =    L4 / (EA * L2);
C4              =    3.198E-8 / L2 + 2.0 * (L1 + L3) * nu / (E * L2);

CS3             =    S4 / (EA * L2); /* constant for stroke xdcr to strain conversion      */
}


/* * * * * * * * * * * * * * * * * * * * * * * * * * * * *
 * Set_Up_DAQ
 *
 *              11/15/92
 *
 * Programmer: MAB
 *
 *
 * * * * * * * * * * * * * * * * * * * * * * * * * * * * */
```

```
Set_Up_DAQ()
{
        /*   Setup the I/O Board   */

        Board_Reset(5);                                  /* Reset the DAQ board                    */
        AI_Config(5,0,10,0);                             /* Configure the analog input channels    */
        AO_Setup(5,0,0,10,0,0,0);                        /* Configure analog output channel 0      */
        AO_Setup(5,1,0,10,0,0,0);                        /* Configure analog output channel 1      */
        DIG_Prt_Config(5,0,0,0);                 /* Configure digital port 0 for input*/
        DIG_Prt_Config(5,1,1,0);                 /* Configure digital port 1 for output      */

        /*  Initialize Analog Outputs to Zero   */

        /*  Use the DAC to output a 0 (zero) volt signal on channel 0
        AO_Write(5,0,0);   */

        /*  Use the DAC to output a 0 (zero) volt signal on channel 1
        AO_Write(5,1,0);*/

        /*  Write a zero to the cycle counter                                    */
        DIG_Out_Line(5,1,3,0);
        /*  Reset the cycle counter to 0                                         */
        DIG_Out_Line(5,1,2,0);
        DIG_Out_Line(5,1,2,1);
        for (index=1;index<15000;index++);
        DIG_Out_Line(5,1,2,0);
}

/* * * * * * * * * * * * * * * * * * * * * * * * * * * * * * * *
 * Set_Up_Counter  used when not starting from cycle 1
 *
 *                11/15/92
 *
 * Programmer: MAB
 *
 *
 * * * * * * * * * * * * * * * * * * * * * * * * * * * * * * * */

Set_Up_Counter()
{
        int loop1;

        for (loop1=1;loop1<(cycle_num);loop1++)
        {
                /*  Write a zero to the cycle counter                            */
                DIG_Out_Line(5,1,3,0);
                for (index=1;index<15000;index++);
                /*  Write a one to the cycle counter                             */
                DIG_Out_Line(5,1,3,1);
                for (index=1;index<15000;index++);
                /*  Write a zero to the cycle counter                            */
                DIG_Out_Line(5,1,3,0);
        }
}
/* * * * * * * * * * * * * * * * * * * * * * * * * * * * * * * *
```

```
* Initialize Linked List
*
*                   11/15/92
*
* Programmer: MAB
*
*
* * * * * * * * * * * * * * * * * * * * * * * * * * * * * * * * * */

Init_Linked_List()
{
        /*  Initialize Linked List for data storage    */
        first_data = (struct data *)malloc((unsigned)sizeof(struct data));
        first_data->length = 0;
        first_data->next = NULL;
        last_data = first_data;
        ext_l_c_load_ptr = last_data->ext_l_c_load;
        int_l_c_load_ptr = last_data->int_l_c_load;
        pressure_ptr = last_data->pressure;
        extensometer_ptr = last_data->extensometer;
        e_gage_1_ptr = last_data->e_gage_1;
        e_gage_2_ptr = last_data->e_gage_2;
        e_gage_3_ptr = last_data->e_gage_3;
        len = 0;
}
```

FUNCTION SUBPROGRAM DECIDE_WHICH_COMMAND.C

```
#include "mainExt.h"

/* * * * * * * * * * * * * * * * * * * * * * * * * * * * * * * *
 * Decide Which Command Based On Keyboard
 *
 *              12/15/92
 *
 * Programmer: MAB
 *
 *
 * * * * * * * * * * * * * * * * * * * * * * * * * * * * * * * */

Decide_Command_Based_On_Keyboard()
{
        if (KeyMaps[4] == 8)    pause_test = 1;         /*      pause has been commanded        */

        if (KeyMaps[1] == 128)  pause_test = 0;         /*      resume has been commanded       */

/*      if ((abs(*e_gage_ch_1) > 31050) && (stop_test == 0))
        {       command a stop when axial strain is at 95% 'cuz specimen is probably buckled
                stop_test       = 1;
                stop_ramp       = 1;
                printf("Strain limit exceeded\n");
                stop_pressure_at = pressure_command;
                stop_load_at    = load_command;
        }       */

        if ((abs(*stroke_xdcr - initial_stroke_xdcr) > stroke_xdcr_limit) && (stop_test == 0))
        {                               /* command a stop when stroke xdcr limit has been exceeded  */
                stop_test       = 1;
                stop_ramp       = 1;
                printf("Stroke limit exceeded\n");
                stop_pressure_at = pressure_command;
                stop_load_at    = load_command;
        }

        if (cycle_num > last_cycle_num)                 /*      last cycle has finished     */
        {
                if (begin_ramp == 0)    Calculate_Ramp_Down_Commands();
                else
                {
                        Calculate_Zero_Commands();
                        /*  Write a zero to the solenoid valve's relay,
                         to close the solenoid valve on the air line                            */
                        DIG_Out_Line(5,1,0,0);
                        if (KeyMaps[1] == 16)           /*      <Q> has been pressed       */
                        {
                                printf("\nAre you sure that you want to QUIT?\t\t\t<Y> or <N>\n\n");
                                unsure_quit_test = 1;
                        }
                        if ((KeyMaps[2] == 1) && (unsure_quit_test == 1))   quit_test = 1;
                                                        /* <Y> has been pressed             */
                }
```

```
}
else if (begin_test == 0)                                   /* <B> has not been pressed yet     */
{
        Calculate_Zero_Commands();
        if (KeyMaps[1] == 16)                               /*      <Q> has been pressed        */
        {
                printf("\nAre you sure that you want to QUIT?\t\t\t<Y> or <N>\n\n");
                unsure_quit_test = 1;
        }
        if ((KeyMaps[2] == 1) && (unsure_quit_test == 1))   quit_test = 1;
                                                            /*      <Y> has been pressed        */
        if (KeyMaps[1] == 8)    /*      Upon pressing <B>, command generation will begin */
        {
                begin_test      = 1;
                begin_ramp      = 1;
                /* Clock the cycle counter once                                             */
                DIG_Out_Line(5,1,3,1);
                DIG_Out_Line(5,1,3,0);
        }
}
else if (pause_test == 1)       /*      don't change commands - check for <S>               */
{
        if (KeyMaps[0] == 2)    /*      Upon pressing <S> the stop routine will begin       */
        {
                pause_test      = 0;
                stop_test       = 1;
                stop_ramp       = 1;
                stop_pressure_at = pressure_command;
                stop_load_at     = load_command;
        }
}
else if ( stop_test == 0)       /*      <S> has not been pressed yet                        */
{
        if (begin_ramp) Calculate_Ramp_Up_Commands();
        else Calculate_Cycle_Commands();
        if (KeyMaps[0] == 2)    /* Upon pressing <S>the stop routine will begin */
        {
                stop_test       = 1;
                stop_ramp       = 1;
                stop_pressure_at = pressure_command;
                stop_load_at     = load_command;
        }
}
else                                                        /*      <S> has been pressed        */
{
        if (stop_ramp == 1) Calculate_Stop_Ramp_Commands();
        else
        {
                Calculate_Zero_Commands();
                /* Write a zero to the solenoid valve's relay,
                   to close the solenoid valve on the air line                              */
                DIG_Out_Line(5,1,0,0);
                if (KeyMaps[1] == 16)                       /*      <Q> has been pressed        */
                {
                        printf("\nAre you sure that you want to QUIT?\t\t\t<Y> or <N>\n\n");
                        unsure_quit_test = 1;
```

```
                    }
                    if ((KeyMaps[2] == 1) && (unsure_quit_test == 1))    quit_test = 1;
                                                                /*       <Y> has been pressed      */
                }
            }
        }
```

FUNCTION SUBPROGRAM CALCULATE_COMMANDS.C

```
#include "mainExt.h"

/* * * * * * * * * * * * * * * * * * * * * * * * * * * *
 * Calculate Zero Commands
 *
 *              11/15/92
 *
 * Programmer: MAB
 *
 *
 * * * * * * * * * * * * * * * * * * * * * * * * * * * */

Calculate_Zero_Commands()
{
        pressure_command = 0;
        load_command    = 0;
}

/* * * * * * * * * * * * * * * * * * * * * * * * * * * *
 * Calculate Ramp Up Commands
 *
 *              11/15/92
 *
 * Programmer: MAB
 *
 *
 * * * * * * * * * * * * * * * * * * * * * * * * * * * */

Calculate_Ramp_Up_Commands()
{
        /*  Ramp data is always to be stored  */
        Store_Data();

        /*          calculate pressure and load command for next sample                     */
        if (ramp_1_sample < samples_per_ramp_1)                 /*      ramp 1          */
        {
                ramp_1_sample++;
                pressure_command = ramp_1_sample / samples_per_ramp_1 * ramp_pressure_to;
                load_command    = ramp_1_sample / samples_per_ramp_1 * ramp_load_to;
        }
        else                                                    /*      ramp 2          */
        {
                ramp_2_sample++;
                pressure_command = ramp_pressure_to + ramp_2_sample / samples_per_ramp_2 *
                                        (cycle_pressure_from - ramp_pressure_to);
                load_command    = ramp_load_to + ramp_2_sample / samples_per_ramp_2 *
                                        (cycle_load_from    - ramp_load_to);
                if (ramp_2_sample >= samples_per_ramp_2) begin_ramp = 0;
        }
}

/* * * * * * * * * * * * * * * * * * * * * * * * * * * *
 * Calculate Ramp Down Commands
```

```
*
*                11/15/92
*
* Programmer: MAB
*
*
* * * * * * * * * * * * * * * * * * * * * * * * * * * * * */

Calculate_Ramp_Down_Commands()
{
        if (ramp_2_sample >= samples_per_ramp_2)        /* store cycle number in encoded data line    */
        {
                Store_Data();
                store_cycle_num_data = 1;
                Store_Data();
        }

        /*  Ramp data is always to be stored  */
        Store_Data();

        /*          calculate pressure and load command for next sample                    */
        if (ramp_2_sample > 0)                                                  /*          ramp 2          */
        {
                ramp_2_sample--;
                pressure_command = ramp_pressure_to + ramp_2_sample / samples_per_ramp_2 *
                                        (cycle_pressure_from - ramp_pressure_to);
                load_command     = ramp_load_to + ramp_2_sample / samples_per_ramp_2 *
                                        (cycle_load_from    - ramp_load_to);
        }
        else                                                                    /*          ramp 1          */
        {
                ramp_1_sample--;
                pressure_command = ramp_1_sample / samples_per_ramp_1 * ramp_pressure_to;
                load_command     = ramp_1_sample / samples_per_ramp_1 * ramp_load_to;
                if (ramp_1_sample <= 0) begin_ramp = 1;
        }
}

/* * * * * * * * * * * * * * * * * * * * * * * * * * * * *
 * Calculate Stop Ramp Commands
 *
 *                11/15/92
 *
 * Programmer: MAB
 *
 *
 * * * * * * * * * * * * * * * * * * * * * * * * * * * * * */

Calculate_Stop_Ramp_Commands()
{
        if (stop_ramp_2_sample >= samples_per_stop_ramp_2) /* store cycle number in encoded data line */
        {
                store_cycle_num_data = 1;
                Store_Data();
        }
```

```
        /*  Ramp data is always to be stored  */
        Store_Data();

        /*          calculate pressure and load command for next sample                    */
        if (stop_ramp_2_sample > 0)                                     /*          ramp 2          */
        {
                stop_ramp_2_sample--;
                pressure_command = ramp_pressure_to + stop_ramp_2_sample / samples_per_stop_ramp_2 *
                        (stop_pressure_at - ramp_pressure_to);
                load_command    = ramp_load_to    + stop_ramp_2_sample / samples_per_stop_ramp_2 *
                        (stop_load_at    - ramp_load_to);
        }
        else                                                                    /*          ramp 1 */
        {
                stop_ramp_1_sample--;
                pressure_command = stop_ramp_1_sample / samples_per_stop_ramp_1 * ramp_pressure_to;
                load_command    = stop_ramp_1_sample / samples_per_stop_ramp_1 * ramp_load_to;
                if (stop_ramp_1_sample <= 0) stop_ramp = 0;
        }
}

/* * * * * * * * * * * * * * * * * * * * * * * * * * * *
 * Calculate Recharge Down Commands
 *
 *              11/15/92
 *
 * Programmer: MAB
 *
 *
 * * * * * * * * * * * * * * * * * * * * * * * * * * * */

Calculate_Recharge_Down_Commands()
{
        if (recharge_ramp_2_sample >= samples_per_recharge_ramp_2) /* store cycle number in encoded data line*/
        {
                store_cycle_num_data = 1;
                Store_Data();
        }

        /*  Ramp data is always to be stored  */
        Store_Data();

        /*          calculate pressure and load command for next sample                    */
        if (recharge_ramp_2_sample > 0)                                 /*          ramp 2          */
        {
                recharge_ramp_2_sample--;
                pressure_command = ramp_pressure_to + recharge_ramp_2_sample /
                                samples_per_recharge_ramp_2 * (recharge_pressure_at - ramp_pressure_to);
                load_command = ramp_load_to + recharge_ramp_2_sample / samples_per_recharge_ramp_2 *
                                (recharge_load_at    - ramp_load_to);
        }
        else                                                                    /*          ramp 1          */
        {
                recharge_ramp_1_sample--;
                pressure_command = recharge_ramp_1_sample / samples_per_recharge_ramp_1 *
                                        ramp_pressure_to;
```

```
                load_command = recharge_ramp_1_sample / samples_per_recharge_ramp_1 * ramp_load_to;
                if (recharge_ramp_1_sample <= 0) recharge_ramp = 0;
        }
}

/* * * * * * * * * * * * * * * * * * * * * * * * * * * *
 * Calculate Recharge Up Commands
 *
 *              11/15/92
 *
 * Programmer: MAB
 *
 *
 * * * * * * * * * * * * * * * * * * * * * * * * * * * */

Calculate_Recharge_Up_Commands()
{
        /*  Ramp data is always to be stored  */
        Store_Data();

        /*          calculate pressure and load command for next sample                 */
        if (recharge_ramp_1_sample < samples_per_recharge_ramp_1) /*        ramp 1  */
        {
                recharge_ramp_1_sample++;
                pressure_command = recharge_ramp_1_sample / samples_per_recharge_ramp_1 *
                                        ramp_pressure_to;
                load_command    = recharge_ramp_1_sample / samples_per_recharge_ramp_1 * ramp_load_to;
        }
        else                                                                    /*          ramp 2          */
        {
                recharge_ramp_2_sample++;
                pressure_command = ramp_pressure_to + recharge_ramp_2_sample /
                                samples_per_recharge_ramp_2 * (recharge_pressure_at - ramp_pressure_to);
                load_command = ramp_load_to + recharge_ramp_2_sample / samples_per_recharge_ramp_2 *
                                (recharge_load_at    - ramp_load_to);
                if (recharge_ramp_2_sample >= samples_per_recharge_ramp_2) recharge_ramp = 1;
        }
}

/* * * * * * * * * * * * * * * * * * * * * * * * * * * *
 * Calculate Cycle Commands
 *
 *              11/15/92
 *
 * Programmer: MAB
 *
 *
 * * * * * * * * * * * * * * * * * * * * * * * * * * * */

Calculate_Cycle_Commands()
{
        if (cycle_sample == 0)
        {

/* if the last cycle (ramp) was stored, store one more sample to complete the data set      */
```

```
if (cycle_num == (recharge_cycle_num + 1))
{
        Store_Data();                   /*      store sample after recharge     */
}
else
{
        if (cycle_num <= 11) Store_Data();      /*      store cycles 1-10       */
        switch (cycle_num)              /*      store cycles 2^n, and X 200's   */
        {
                case 17: Store_Data();  break;
                case 33: Store_Data();  break;
                case 65: Store_Data();  break;
                case 101:       Store_Data();   break;
                case 129:       Store_Data();   break;
                case 201:       Store_Data();   break;
                case 257:       Store_Data();   break;
                case 401:       Store_Data();   break;
                case 513:       Store_Data();   break;
                case 601:       Store_Data();   break;
                case 801:       Store_Data();   break;
                case 1001:      Store_Data();   break;
                case 1025:      Store_Data();   break;
                case 1201:      Store_Data();   break;
                case 1401:      Store_Data();   break;
                case 1601:      Store_Data();   break;
                case 1801:      Store_Data();   break;
                case 2001:      Store_Data();   break;
                case 2049:      Store_Data();   break;
                case 2201:      Store_Data();   break;
                case 2401:      Store_Data();   break;
                case 2601:      Store_Data();   break;
                case 2801:      Store_Data();   break;
                case 3001:      Store_Data();   break;
                case 3201:      Store_Data();   break;
                case 3401:      Store_Data();   break;
                case 3601:      Store_Data();   break;
                case 3801:      Store_Data();   break;
                case 4001:      Store_Data();   break;
                case 4097:      Store_Data();   break;
                case 8193:      Store_Data();   break;
                case 12289:     Store_Data();   break;
                case 16385:     Store_Data();   break;
                case 24577:     Store_Data();   break;
                case 32001:     Store_Data();   break;
                case 32766:     Store_Data();   break;
        }
}

/* if current cycle is to be stored, store cycle number in encoded data line       */

        if (cycle_num == recharge_cycle_num)    /* for cycle after recharge  */
        {
                store_cycle_num_data = 1;
                Store_Data();
        }
        else
```

```
{
        switch (cycle_num)      /* and for cycles 1-10, 2^n, and X 200's      */
        {
                case 1:         store_cycle_num_data = 1; Store_Data();     break;
                case 2:         store_cycle_num_data = 1; Store_Data();     break;
                case 3:         store_cycle_num_data = 1; Store_Data();     break;
                case 4:         store_cycle_num_data = 1; Store_Data();     break;
                case 5:         store_cycle_num_data = 1; Store_Data();     break;
                case 6:         store_cycle_num_data = 1; Store_Data();     break;
                case 7:         store_cycle_num_data = 1; Store_Data();     break;
                case 8:         store_cycle_num_data = 1; Store_Data();     break;
                case 9:         store_cycle_num_data = 1; Store_Data();     break;
                case 10: store_cycle_num_data = 1; Store_Data();     break;
                case 16: store_cycle_num_data = 1; Store_Data();     break;
                case 32: store_cycle_num_data = 1; Store_Data();     break;
                case 64: store_cycle_num_data = 1; Store_Data();     break;
                case 100:       store_cycle_num_data = 1; Store_Data();     break;
                case 128:       store_cycle_num_data = 1; Store_Data();     break;
                case 200:       store_cycle_num_data = 1; Store_Data();     break;
                case 256:       store_cycle_num_data = 1; Store_Data();     break;
                case 400:       store_cycle_num_data = 1; Store_Data();     break;
                case 512:       store_cycle_num_data = 1; Store_Data();     break;
                case 600:       store_cycle_num_data = 1; Store_Data();     break;
                case 800:       store_cycle_num_data = 1; Store_Data();     break;
                case 1000:      store_cycle_num_data = 1; Store_Data();     break;
                case 1024:      store_cycle_num_data = 1; Store_Data();     break;
                case 1200:      store_cycle_num_data = 1; Store_Data();     break;
                case 1400:      store_cycle_num_data = 1; Store_Data();     break;
                case 1600:      store_cycle_num_data = 1; Store_Data();     break;
                case 1800:      store_cycle_num_data = 1; Store_Data();     break;
                case 2000:      store_cycle_num_data = 1; Store_Data();     break;
                case 2048:      store_cycle_num_data = 1; Store_Data();     break;
                case 2200:      store_cycle_num_data = 1; Store_Data();     break;
                case 2400:      store_cycle_num_data = 1; Store_Data();     break;
                case 2600:      store_cycle_num_data = 1; Store_Data();     break;
                case 2800:      store_cycle_num_data = 1; Store_Data();     break;
                case 3000:      store_cycle_num_data = 1; Store_Data();     break;
                case 3200:      store_cycle_num_data = 1; Store_Data();     break;
                case 3400:      store_cycle_num_data = 1; Store_Data();     break;
                case 3600:      store_cycle_num_data = 1; Store_Data();     break;
                case 3800:      store_cycle_num_data = 1; Store_Data();     break;
                case 4000:      store_cycle_num_data = 1; Store_Data();     break;
                case 4096:      store_cycle_num_data = 1; Store_Data();     break;
                case 8192:      store_cycle_num_data = 1; Store_Data();     break;
                case 12288:     store_cycle_num_data = 1; Store_Data();     break;
                case 16384:     store_cycle_num_data = 1; Store_Data();     break;
                case 24576:     store_cycle_num_data = 1; Store_Data();     break;
                case 32000:     store_cycle_num_data = 1; Store_Data();     break;
                case 32765:     store_cycle_num_data = 1; Store_Data();     break;
        }
    }
}

/*  Check if data is to be stored, and store it if it should be stored                */
if (cycle_num == recharge_cycle_num)
{
```

```
        Store_Data();                                   /*      store cycle after recharge      */
}
else
{
        if (cycle_num <= 10) Store_Data(); /*                   store cycles 1-10               */
        switch (cycle_num)                              /*      store cycles 2^n, and X 200's   */
        {
                case 16: Store_Data();      break;
                case 32: Store_Data();      break;
                case 64: Store_Data();      break;
                case 100:       Store_Data();       break;
                case 128:       Store_Data();       break;
                case 200:       Store_Data();       break;
                case 256:       Store_Data();       break;
                case 400:       Store_Data();       break;
                case 512:       Store_Data();       break;
                case 600:       Store_Data();       break;
                case 800:       Store_Data();       break;
                case 1000:      Store_Data();       break;
                case 1024:      Store_Data();       break;
                case 1200:      Store_Data();       break;
                case 1400:      Store_Data();       break;
                case 1600:      Store_Data();       break;
                case 1800:      Store_Data();       break;
                case 2000:      Store_Data();       break;
                case 2048:      Store_Data();       break;
                case 2200:      Store_Data();       break;
                case 2400:      Store_Data();       break;
                case 2600:      Store_Data();       break;
                case 2800:      Store_Data();       break;
                case 3000:      Store_Data();       break;
                case 3200:      Store_Data();       break;
                case 3400:      Store_Data();       break;
                case 3600:      Store_Data();       break;
                case 3800:      Store_Data();       break;
                case 4000:      Store_Data();       break;
                case 4096:      Store_Data();       break;
                case 8192:      Store_Data();       break;
                case 12288:     Store_Data();       break;
                case 16384:     Store_Data();       break;
                case 24576:     Store_Data();       break;
                case 32000:     Store_Data();       break;
                case 32765:     Store_Data();       break;
        }
}

/*          calculate pressure and load command for next sample                 */
if (cycle_sample < extra_samples_at_peaks)
{
        pressure_command = cycle_pressure_from;
        load_command    = cycle_load_from;
        cycle_sample++;
}
else if (cycle_sample < (samples_per_cycle/2. + extra_samples_at_peaks))
{
        pressure_command = cycle_pressure_from + (cycle_sample - extra_samples_at_peaks) /
```

```
                                        (samples_per_cycle/2.) * (cycle_pressure_to - cycle_pressure_from);
                load_command = cycle_load_from + (cycle_sample - extra_samples_at_peaks) /
                                        (samples_per_cycle/2.) * (cycle_load_to - cycle_load_from);
                cycle_sample++;
        }
        else if (cycle_sample < (samples_per_cycle/2. + 2.0 * extra_samples_at_peaks))
        {
                pressure_command = cycle_pressure_to;
                load_command     = cycle_load_to;
                cycle_sample++;
        }
        else /* if (cycle_sample <= (samples_per_cycle + 2.0 * extra_samples_at_peaks))          */
        {
                pressure_command = cycle_pressure_to - ((cycle_sample - 2.0 * extra_samples_at_peaks) /
                                (samples_per_cycle/2.) - 1.) * (cycle_pressure_to - cycle_pressure_from);
                load_command = cycle_load_to - ((cycle_sample - 2.0 * extra_samples_at_peaks) /
                                (samples_per_cycle/2.) -1.) * (cycle_load_to - cycle_load_from);
                cycle_sample++;
                if (cycle_sample > (samples_per_cycle + 2.0 * extra_samples_at_peaks))
                {
                        /*  Increment the cycle number counter                                  */
                        cycle_num++;
                        /*  Increment the external cycle counter                                */
                        DIG_Out_Line(5,1,3,1);
                        DIG_Out_Line(5,1,3,0);
                        /*  Initialize the cycle sample counter                                 */
                        cycle_sample = 0;
                }
        }
}
```

FUNCTION SUBPROGRAM MODIFY_COMMANDS.C

```
#include "mainExt.h"

/* * * * * * * * * * * * * * * * * * * * * * * * * * * *
 * Calculate Modified Commands
 *
 *              11/15/92
 *
 * Programmer: MAB
 *
 *
 * * * * * * * * * * * * * * * * * * * * * * * * * * * */

Calculate_Modified_Commands()
{
        /*  Scale the 16 bit pressure to proper units                                   */

        pressure_psi  = *pressure_xdcr / 32768.0 * ten_volt_pressure;

        /*  Overdrive pressure if it is lagging behind                                  */

        if (pressure_command > 2000.0)
        {
                scaled_pressure_command = pressure_command *
                (1.0 + (last_pressure_command - pressure_psi) / last_pressure_command);
                if ((last_pressure_command - pressure_psi) / last_pressure_command > 0.15)
                        scaled_pressure_command = 1.15 * pressure_command;
        }
        else
        {
                scaled_pressure_command = pressure_command;
        }

        last_pressure_command = pressure_command;

        /*      Determine the load command in terms of Internal Load Cell voltage output (pressure decreases
output)  */

                load_from_geom   = (A - a) * pressure_psi;
                stress_in_shoulder = (load_command - load_from_geom) / (A * 10000.0);
        /*      Prevent load command from ever going positive by keeping it below zero_offset_load      */
                        if ((load_command - load_from_gcom) >= zero_offset_load) stress_in_shoulder =
                                zero_offset_load / (A * 10000.0);

        /*      First calculate the axial load contribution to internal load cell output     */

                if (stress_in_shoulder < -7.5209)
                {
                        int_l_c_no_pressure = 1.28025 * stress_in_shoulder - 0.176308;
                }
                else if (stress_in_shoulder < -3.3550)
                {
                        int_l_c_no_pressure = 1.29494 * stress_in_shoulder - 0.065825;
                }
```

```
        else /*   (stress_in_shoulder > -3.3550)       */
        {
                int_l_c_no_pressure = 1.31456 * stress_in_shoulder;
        }


/*      Now calculate the pressure contribution to internal load cell output:
        the internal load cell pressure effect = (output under pressure from plug cal) -
        (output w/o pressure from solid bar cal, evaluated at a shoulder stress = -pressure)          */

        if (pressure_psi > 75209.0)
        {
                pressure_psi = - pressure_psi / 10000.0;
                int_l_c_pressure_effect = (.565514 * pressure_psi - 0.0200375) -
                                          (1.28025 * pressure_psi - 0.176308);
        }
        else if (pressure_psi > 33550.0)
        {
                pressure_psi = - pressure_psi / 10000.0;
                int_l_c_pressure_effect = (.565514 * pressure_psi - 0.0200375) -
                                          (1.29494 * pressure_psi - 0.065825);
        }
        else if (pressure_psi > 16889.0)
        {
                pressure_psi = - pressure_psi / 10000.0;
                int_l_c_pressure_effect = (.565514 * pressure_psi - 0.0200375) -
                                          (1.31456 * pressure_psi);
        }
        else /*   (pressure_psi < 16889)      */
        {
                pressure_psi = - pressure_psi / 10000.0;
                int_l_c_pressure_effect = (.577378 * pressure_psi) - (1.31456 * pressure_psi);
        }

/*      The overall internal load cell output is the sum of the
        axial load contribution and the pressure effect                                 */

        int_l_c_load_command = int_l_c_no_pressure + int_l_c_pressure_effect;
        pressure_psi = - pressure_psi * 10000.0;
}
```

FUNCTION SUBPROGRAM READ_INPUTS.C

```
#include "mainExt.h"

/* * * * * * * * * * * * * * * * * * * * * * * * * * * *
 * Read_Inputs
 *
 *                  11/15/92
 *
 * Programmer: MAB
 *
 *
 * * * * * * * * * * * * * * * * * * * * * * * * * * * */

Read_Inputs()
{
        /*  Use the ADC to store 16 bit representations of these signals  */
        AI_Read(5,0,int_load_cell_gain,int_load_cell);
        AI_Read(5,1,stroke_xdcr_gain,stroke_xdcr);
        AI_Read(5,2,1,pressure_xdcr);
        AI_Read(5,3,1,extensometer);
        AI_Read(5,4,ext_load_cell_gain,ext_load_cell);
        AI_Read(5,5,1,e_gage_ch_1);
        AI_Read(5,6,1,e_gage_ch_2);

/*      AI_Read(5,7,1,e_gage_ch_3);                 */
        *e_gage_ch_3 = 0;

        DIG_In_Line(5,0,0,limit_switch_state);
}
```

FUNCTION SUBPROGRAM WRITE_ANALOG_OUTPUTS.C

```
#include "mainExt.h"

/* * * * * * * * * * * * * * * * * * * * * * * * * * * * * * * *
 * Write_Analog_Outputs
 *
 *                11/15/92
 *
 * Programmer: MAB
 *
 *
 * * * * * * * * * * * * * * * * * * * * * * * * * * * * * * * */

Write_Analog_Outputs()
{
        /*  Use the DAC to output a -10 to +10 volt signal on channel 0                */
        AO_Write(5,0,-2048.0 * scaled_pressure_command / ten_volt_pressure);

        if (dither < 0)
        {
                /*  Use the DAC to output a -10 to +10 volt signal on channel 1                */
                AO_Write(5,1,2048.0 * int_l_c_gain_factor * int_l_c_load_command / 10.0 - bits_of_dither );
                dither = 1;
        }
        else
        {
                /*  Use the DAC to output a -10 to +10 volt signal on channel 1                */
                AO_Write(5,1,2048.0 * int_l_c_gain_factor * int_l_c_load_command / 10.0 + bits_of_dither );
                dither = -1;
        }

}
```

FUNCTION SUBPROGRAM RECHARGE_INTENSIFIER.C

```
#include "mainExt.h"

/* * * * * * * * * * * * * * * * * * * * * * * * * * * *
 * Recharge Intensifier
 *
 *              11/15/92
 *
 * Programmer: MAB
 *
 *
 * * * * * * * * * * * * * * * * * * * * * * * * * * * */

Recharge_Intensifier()
{
        recharge_num++;
        /*  stop test if intensifier has recharged more than 4 times
        if (recharge_num > 4) stop_test = 1;                                    */
        recharge_ramp           = 1;
        recharge_cycle_num      = cycle_num;
        recharge_pressure_at = pressure_command;
        recharge_load_at   = load_command;

        /*  Ramp the pressure command down to zero  */
        while (recharge_ramp == 1)
        {
                recharge_stage = 1;

                Read_Inputs();

                Decide_Command_While_Recharging();

                if (stop_test == 1) return;

                Calculate_Modified_Commands();

                Write_Analog_Outputs();

                GetKeys ((long *)KeyMaps);
        }

        /*  Hold the pressure command at zero while the intensifier recharges  */
        for (index = 0;index<=1000;index++)
        {
                recharge_stage = 2;

                Read_Inputs();

                Decide_Command_While_Recharging();

                if (stop_test == 1) return;

                Calculate_Modified_Commands();
```

```
            Write_Analog_Outputs();

            GetKeys ((long *)KeyMaps);
        }

        /*  Ramp the pressure command back up  */
        while (recharge_ramp == 0)
        {
            recharge_stage = 3;

            Read_Inputs();

            Decide_Command_While_Recharging();

            if (stop_test == 1) return;

            Calculate_Modified_Commands();

            Write_Analog_Outputs();

            GetKeys ((long *)KeyMaps);
        }
}
```

FUNCTION SUBPROGRAM DECIDE_WHILE_RECHARGING.C

```
#include "mainExt.h"

/* * * * * * * * * * * * * * * * * * * * * * * * * * * *
 * Decide Command Based On Keyboard While Recharging
 *
 *              12/15/92
 *
 * Programmer: MAB
 *
 *
 * * * * * * * * * * * * * * * * * * * * * * * * * * * */

Decide_Command_While_Recharging()
{
        if (KeyMaps[4] == 8)    pause_test = 1;         /* pause has been commanded             */

        if (KeyMaps[1] == 128)  pause_test = 0;         /* resume has been commanded            */

/*      if ((abs(*e_gage_ch_1) > 31050) && (stop_test == 0))
        {       command a stop when axial strain is at 95% 'cuz specimen is probably buckled
                stop_test       = 1;
                stop_ramp       = 1;
                printf("Strain limit exceeded\n");
                stop_pressure_at = pressure_command;
                stop_load_at    = load_command;
                return;
        }       */

        if ((abs(*stroke_xdcr - initial_stroke_xdcr) > stroke_xdcr_limit) && (stop_test == 0))
        {                                               /* stroke xdcr limit has been exceeded  */
                stop_test       = 1;
                stop_ramp       = 1;
                printf("Stroke limit exceeded\n");
                stop_pressure_at = pressure_command;
                stop_load_at    = load_command;
                return;
        }

        if (pause_test == 1)            /* don't change commands - check for <S>   */
        {
                if (KeyMaps[0] == 2)/* Upon pressing <S>,the stop routine will begin */
                {
                        pause_test      = 0;
                        stop_test       = 1;
                        stop_ramp       = 1;
                        stop_pressure_at = pressure_command;
                        stop_load_at    = load_command;
                        return;
                }
        }
        else                                            /* <S> has not been pressed yet         */
        {
                if (KeyMaps[0] == 2)/* Upon pressing <S>,the stop routine will begin */
```

```
                {
                        stop_test           = 1;
                        stop_ramp           = 1;
                        stop_pressure_at = pressure_command;
                        stop_load_at        = load_command;
                        return;
                }
                switch (recharge_stage)
                {
                        case 1:  Calculate_Recharge_Down_Commands();     break;
                        case 2:  Calculate_Zero_Commands(); recharge_test = 0; break;
                        case 3:  Calculate_Recharge_Up_Commands();       break;
                }
        }
}
```

FUNCTION SUBPROGRAM STORE_DATA.C

```
#include "mainExt.h"

/* * * * * * * * * * * * * * * * * * * * * * * * * * * *
 * Store Data
 *
 *              11/15/92
 *
 * Programmer: MAB
 *
 *
 * * * * * * * * * * * * * * * * * * * * * * * * * * * */

Store_Data()
{
        /*  store every store_Nth_sample sample to limit size of data file      */

        sample_counter ++;
        if (sample_counter == store_Nth_sample)
        {
                store_sample_flag = 1;
                sample_counter    = 0;
        }
        else
        {
                store_sample_flag = 0;
        }

        if ((store_cycle_num_data == 0) && (store_sample_flag == 0)) return;

        *ext_l_c_load_ptr = *ext_load_cell;        /* corrected for pressure in Write_Data_File()      */
        *int_l_c_load_ptr = *int_load_cell;        /* corrected for pressure in Write_Data_File()      */

        if (store_cycle_num_data == 1)
        {
                *e_gage_3_ptr = 9999;
                if (recharge_test == 1)     /* to distinguish recharge ramps from the cycle afterwards      */
                {
                        *pressure_ptr = -cycle_num;
                }
                else
                {
                        *pressure_ptr = cycle_num;
                }
                store_cycle_num_data = 0;
        }
        else
        {
                *e_gage_3_ptr = *e_gage_ch_3;
                *pressure_ptr = *pressure_xdcr;
        }

        *extensometer_ptr = *extensometer;
        *e_gage_1_ptr = *e_gage_ch_1;
```

```
        *e_gage_2_ptr = *e_gage_ch_2;

        ext_l_c_load_ptr++;
        int_l_c_load_ptr++;
        pressure_ptr++;
        extensometer_ptr++;
        e_gage_1_ptr++;
        e_gage_2_ptr++;
        e_gage_3_ptr++;

        len++;
        if (len >= LISTLEN)
        {
                last_data->length = len;
                last_data->next = (struct data *)malloc((unsigned)sizeof(struct data));
                last_data=last_data->next;
                last_data->length = 0;
                last_data->next = NULL;
                ext_l_c_load_ptr = last_data->ext_l_c_load;
                int_l_c_load_ptr = last_data->int_l_c_load;
                pressure_ptr     = last_data->pressure;
                extensometer_ptr = last_data->extensometer;
                e_gage_1_ptr = last_data->e_gage_1;
                e_gage_2_ptr = last_data->e_gage_2;
                e_gage_3_ptr = last_data->e_gage_3;
                len = 0;
                /*              printf("1 block filled\n");             */
        }
}
```

FUNCTION SUBPROGRAM WRITE_DATA_FILE.C

```
#include "mainExt.h"

/* * * * * * * * * * * * * * * * * * * * * * * * * * * *
 * Write Data File
 *
 *              11/15/92
 *
 * Programmer: MAB
 *
 *
 * * * * * * * * * * * * * * * * * * * * * * * * * * * */

Write_Data_File()
{
        printf("Please be patient Huseyin, I am writing the data now\n\n");
        /*              Add 1 block of zero data because the last incomplete
                        block of data will not be printed to the file                   */
        for (index = 0; index <= LISTLEN + 5; index++)
        {
                *ext_l_c_load_ptr = 0;
                ext_l_c_load_ptr++;
                *int_l_c_load_ptr = 0;
                int_l_c_load_ptr++;
                *pressure_ptr = 0;
                pressure_ptr++;
                *extensometer_ptr = 0;
                extensometer_ptr++;
                *e_gage_1_ptr = 0;
                e_gage_1_ptr++;
                *e_gage_2_ptr = 0;
                e_gage_2_ptr++;
                *e_gage_3_ptr = 8888;
                e_gage_3_ptr++;
                len++;
                if (len >= LISTLEN)
                {
                        last_data->length = len;
                        last_data->next = (struct data *)malloc((unsigned)sizeof(struct data));
                        last_data=last_data->next;
                        last_data->length = 0;
                        last_data->next = NULL;
                        ext_l_c_load_ptr = last_data->ext_l_c_load;
                        int_l_c_load_ptr = last_data->int_l_c_load;
                        pressure_ptr = last_data->pressure;
                        extensometer_ptr = last_data->extensometer;
                        e_gage_1_ptr = last_data->e_gage_1;
                        e_gage_2_ptr = last_data->e_gage_2;
                        e_gage_3_ptr = last_data->e_gage_3;
                        len = 0;
                }
        }

        /*      Write all the linked list data to file output.dat       */
```

```
fp = fopen(" output.dat", "w");
if (fp == NULL)
{
        fprintf(stderr, "Error:  can't open file output.dat\n");
        exit(-1);
}
fprintf(fp, "IGOR\n");
fprintf(fp, "WAVES Int_LC_Stress, Ext_LC_Stress, Pressure, Extensometer, Ex_gage_1, e_gage_1,
        e_gage_2\n");
fprintf(fp, "BEGIN\n");
while (first_data != NULL)
{
        len = first_data->length;
        if (len > 0)
        {
                for (index = 0; index < len; index++)
                {
                        if (first_data->e_gage_3[index] == 9999)      /* code for cycle number line */
                        {
                                cycle_num = first_data->pressure[index];
                                fprintf(fp, "END\n");
                                fprintf(fp,"\nWAVES Int_LC_Stress_%d, Ext_LC_Stress_%d,
                                        Pressure_%d, Extensometer_%d, Ex_gage_1_%d,
                                        e_gage_1_%d, e_gage_2_%d\n", cycle_num,cycle_num,
                                        cycle_num,cycle_num,cycle_num,cycle_num,cycle_num);
                                fprintf(fp, "BEGIN\n");
                        }
                        else if (first_data->e_gage_3[index] == 8888) ;          /* do nothing      */
                        else                                                     /* data line       */
                        {
                                /* calculate apparent, then actual strains, correcting for
                                        a) hydrostatic strains picked up by the dummy gages,
                                        b) transverse sensitivity of all the gages                */

                        pressure_psi = first_data->pressure[index] * ten_volt_pressure   / 32768.0;
                        ext_l_c_load_lbf = first_data->ext_l_c_load[index] * ten_volt_load / 32768.0;

                        deflection_in= (first_data->extensometer[index] - extensometer_offset) *
                                        ten_volt_deflection / 32768.0;

                        apparent_e_1 = (first_data->e_gage_1[index] - e_gage_1_offset) *
                                        ten_volt_e_gage_1A / 32768.0 + pressure_psi *
                                        dummy_gage_1;
                        apparent_e_2 = (first_data->e_gage_2[index] - e_gage_2_offset) *
                                        ten_volt_e_gage_2A / 32768.0 + pressure_psi *
                                        dummy_gage_2;

                        actual_e_1 = (apparent_e_1 * corr_1 - apparent_e_2 * Kt_1A * corr_2) / corr_4;
                        actual_e_2 = (apparent_e_2 * corr_2 - apparent_e_1 * Kt_2A * corr_1) / corr_4;

                        int_l_c_output = first_data->int_l_c_load[index] * 10.0 / 32768.0 /
                                        int_l_c_gain_factor;

                        if (pressure_psi > 75209.0)
                        {
```

```
                pressure_psi = - pressure_psi / 10000.0;
                int_l_c_pressure_effect = (.565514 * pressure_psi - 0.0200375) -
                                        (1.28025 * pressure_psi - 0.176308);
        }
        else if (pressure_psi > 33550.0)
        {
                pressure_psi = - pressure_psi / 10000.0;
                int_l_c_pressure_effect = (.565514 * pressure_psi - 0.0200375) -
                                        (1.29494 * pressure_psi - 0.065825);
        }
        else if (pressure_psi > 16889.0)
        {
                pressure_psi = - pressure_psi / 10000.0;
                int_l_c_pressure_effect = (.565514 * pressure_psi - 0.0200375) -
                                        (1.31456 * pressure_psi);
        }
        else /*   (pressure_psi < 16889)     */
        {
                pressure_psi = - pressure_psi / 10000.0;
                int_l_c_pressure_effect = (.577378 * pressure_psi) - (1.31456 *
                                        pressure_psi);
        }
        pressure_psi = -pressure_psi * 10000.0;
        int_l_c_no_pressure = int_l_c_output - int_l_c_pressure_effect;


        if (int_l_c_no_pressure < -9.8049)
        {
                stress_in_shoulder = 7810.97 * int_l_c_no_pressure + 1377.14;
        }
        else if (int_l_c_no_pressure < -4.4103)
        {
                stress_in_shoulder = 7722.36 * int_l_c_no_pressure + 508.33;
        }
        else /*   (int_l_c_no_pressure > -4.4103)     */
        {
                stress_in_shoulder = 7607.11 * int_l_c_no_pressure;
        }

        load_from_geom = (A - a) * pressure_psi;
        int_l_c_load_lbf = stress_in_shoulder * A;

        fprintf(fp, "%9.0f\t%9.0f\t%6.0f\t%6.0f\t%9.6f\t%9.6f\t%9.6f\n",
                (stress_in_shoulder * A + load_from_geom) / a,
                (ext_l_c_load_lbf + load_from_geom) / a,
                pressure_psi,
                first_data->extensometer[index] - extensometer_offset,
                C1 * deflection_in - C2 * int_l_c_load_lbf - C3 * ext_l_c_load_lbf -
                C4 * pressure_psi, strain_cal_1 * actual_e_1 + (1.0 - pressure_cal_1) *
                2.0 * nu * pressure_psi / E, strain_cal_2 * actual_e_2 +
                (1.0 - pressure_cal_2) * 2.0 * nu * pressure_psi / E);

/*              first_data->e_gage_3[index] * 10.0 / 32768 * 50);     */

        }
}
```

```
                }
                first_data = first_data->next;
        }
        fprintf(fp, "END\n");
        if (fclose(fp) != 0)
        {
                fprintf(stderr, "Error:  can't close file output.dat\n");
                exit(-1);
        }
}
```

HEADER MAIN.H

```
/****************************************
 *
 * 11/15/92
 *
 * Programmer:MAB
 *
 ****************************************/

#include <stdio.h>
#include <stdlib.h>
#include <math.h>
#include "NI_DAQ_MAC.h"
#define LISTLEN (1<<10)

                    /* GLOBAL VARIABLES */

FILE        *fp;                        /* file pointer for out.dat                  */
Boolean     KeyMaps[16];                /* packed array of 0/1's from keyboard       */

int16       var_limit_switch_state;     /* var storing intensifier upper limit switch read by DAQ*/
int16       var_stroke_xdcr;            /* variable storing stroke xdcr read by DAQ        */
int16       var_ext_load_cell;          /* variable storing external load cell read by DAQ */
int16       var_int_load_cell;          /* variable storing internal load cell read by DAQ */
int16       var_pressure_xdcr;          /* variable storing pressure xdcr read by DAQ      */
int16       var_extensometer;           /* variable storing extensometer read by DAQ       */
int16       var_e_gage_ch_1;            /* variable storing strain gage 1 read by DAQ      */
int16       var_e_gage_ch_2;            /* variable storing strain gage 2 read by DAQ      */
int16       var_e_gage_ch_3;            /* variable storing strain gage 3 read by DAQ      */

int16       *limit_switch_state;        /* intensifier upper limit switch read by DAQ
                                           = 0 when ok, and = 1 (5 vdc) when at the limit  */
int16       *stroke_xdcr;               /* stroke xdcr read by DAQ                   */
int16       *ext_load_cell;             /* external load cell read by DAQ            */
int16       *int_load_cell;             /* internal load cell read by DAQ            */
int16       *pressure_xdcr;             /* pressure xdcr read by DAQ                 */
int16       *extensometer;              /* extensometer read by DAQ                  */
int16       *e_gage_ch_1;               /* strain gage 1 read by DAQ                 */
int16       *e_gage_ch_2;               /* strain gage 2 read by DAQ                 */
int16       *e_gage_ch_3;               /* strain gage 3 read by DAQ                 */

short int   n = 0;                      /* array index used while zeroing            */
short int   m;                          /* loop counter used while zeroing           */
int16       old_pressure_xdcr[6];       /* last 5 transducer readings                */
int16       old_ext_load_cell[6];       /* last 5 transducer readings                */
int16       old_int_load_cell[6];       /* last 5 transducer readings                */
int16       old_extensometer[6];        /* last 5 transducer readings                */
int16       old_e_gage_ch_1[6];         /* last 5 transducer readings                */
int16       old_e_gage_ch_2[6];         /* last 5 transducer readings                */
int16       old_e_gage_ch_3[6];         /* last 5 transducer readings                */
long double sum_old_pressure_xdcr = 0;  /* sum of last 5 transducer readings         */
long double sum_old_ext_load_cell = 0;  /* sum of last 5 transducer readings         */
long double sum_old_int_load_cell = 0;  /* sum of last 5 transducer readings         */
long double sum_old_extensometer = 0;   /* sum of last 5 transducer readings         */
```

```
long double     sum_old_e_gage_ch_1 = 0;    /* sum of last 5 transducer readings                    */
long double     sum_old_e_gage_ch_2 = 0;    /* sum of last 5 transducer readings                    */
long double     sum_old_e_gage_ch_3 = 0;    /* sum of last 5 transducer readings                    */

short int       index;                      /* loop counter                                         */
short int       store_cycle_num_data = 0;   /* set to 1 when storing cycle num                      */
short int       quit_zero_inputs = 0;       /* set to 1 after <T> is pressed                        */
short int       begin_test       = 0;       /* set to 1 after <B> is pressed                        */
short int       pause_test       = 0;       /* set to 1 after <P> is pressed                        */
short int       stop_test        = 0;       /* set to 1 after <S> is pressed                        */
short int       unsure_quit_test = 0;       /* set to 1 after <Q> is pressed                        */
short int       quit_test = 0;              /* set to 1 after <Q> and <Y> are pressed               */
short int       recharge_test = 0;          /* set to 1 when top limit switch is activated          */
short int       begin_ramp = 0;             /* changed when begin/end ramps running                 */
short int       stop_ramp        = 0;       /* set to 1 when stop ramp is running                   */
short int       recharge_ramp    = 0;       /* set to 1 when recharge ramp is running               */
short int       dither           = 0;       /* set to +/-1 to add dither to MTS command             */
short int       broken_specimen= 0;         /* set to 1 after *e_gage_ch_3 jumps                    */
short int       end_test         = 0;       /* set to 1 after Calc_Ramp_Down_Command run            */
short int       store_sample_flag = 0;      /* used to store every Nth sample's data                */
short int       sample_counter = 0;         /* used to count samples                                */
short int       store_Nth_sample;           /* store only every Nth sample's data                   */
long double     cycle_sample     = 0;       /* sample number in a command cycle                     */
long double     ramp_1_sample  = 0;         /* sample number in cyclic command ramp 1               */
long double     ramp_2_sample  = 0;         /* sample number in cyclic command ramp 2               */
long double     ramp_up_sample= 0;          /* sample number in a mono command ramp up              */
long double     ramp_down_sample  = 0;      /* sample number in a mono command ramp down            */
long double     stop_ramp_sample;           /* sample number in a mono stop command ramp            */
long double     stop_ramp_1_sample;         /* sample number in cyclic stop command ramp 1          */
long double     stop_ramp_2_sample;         /* sample number in cyclic stop command ramp 2          */
long double     recharge_ramp_1_sample;     /* sample number in cyclic recharge command ramp        */
long double     recharge_ramp_2_sample;     /* sample number in cyclic recharge command ramp        */
long double     samples_per_cycle;          /* number of samples in a command cycle                 */
long double     samples_per_ramp_1;         /* number of samples in cyclic command ramp 1           */
long double     samples_per_ramp_2;         /* number of samples in cyclic command ramp 2           */
long double     samples_per_ramp_up;        /* number of samples in a mono command rampup           */
long double     samples_per_ramp_down;      /* number of samples in a mono command ramp down */
long double     samples_per_stop_ramp;      /* number of samples in mono stop command ramp 1  */
long double     samples_per_stop_ramp_1;    /* number of samples in cyclic stop command ramp 1  */
long double     samples_per_stop_ramp_2;    /* number of samples in cyclic stop command ramp 2  */
long double     samples_per_recharge_ramp_1; /* number of samples in cyclic recharge command ramp 1 */
long double     samples_per_recharge_ramp_2; /* number of samples in cyclic recharge command ramp 2 */
long double     extra_samples_at_peaks;     /* number of samples at wave tip values                 */
int             cycle_num;                  /* cycle number                                         */
int             recharge_cycle_num = 0;     /* cycle number of a recharge cycle                     */
int             recharge_num     = 0;       /* number of recharge cycles                            */
int             last_cycle_num;             /* test ends at this cycle number                       */
int             recharge_stage;             /* stage of recharge process; 1, 2 or 3                 */
int             initial_stroke_xdcr;        /* initial stroke xdcr reading                          */
int             stroke_xdcr_limit;          /* allowable stroke limit                               */
int             bits_of_dither;             /* bits of dither applied to MTS command                */

long double     load_command;               /* load command                                         */
long double     pressure_command;           /* pressure command                                     */
long double     last_pressure_command;      /* previous pressure command                            */
long double     scaled_pressure_command;    /* pressure command        corrected for phase lag      */
```

```
long double     int_l_c_output;             /* internal load cell output recalled in write_data_file */
long double     int_l_c_load_command;       /* internal load cell command                            */
long double     int_l_c_no_pressure;        /* internal load cell output with no pressure effect     */
long double     int_l_c_pressure_effect;    /* pressure effect on internal load cell output          */
long double     ext_l_c_load_command;       /* external load cell command                            */
long double     ramp_pressure_to;           /* peak pressure in a command ramp                       */
long double     cycle_pressure_from;        /* peak pressure in a command cycle                      */
long double     cycle_pressure_to;          /* peak pressure in a command cycle                      */
long double     stop_pressure_at;           /* peak pressure in a stop command ramp                  */
long double     recharge_pressure_at;       /* peak pressure in a recharge command ramp              */
long double     ramp_stress_to;             /* peak stress in a command ramp                         */
long double     cycle_stress_from;          /* peak stress in a command cycle                        */
long double     cycle_stress_to;            /* peak stress in a command cycle                        */
long double     ramp_load_to;               /* peak load in a command ramp                           */
long double     cycle_load_from;            /* peak load in a command cycle                          */
long double     cycle_load_to;              /* peak load in a command cycle                          */
long double     stop_load_at;               /* peak load in a stop command ramp                      */
long double     recharge_load_at;           /* peak load in a recharge command ramp                  */

long double     load_from_geom;             /* component of calculated load                          */
long double     stress_in_shoulder;         /* calculated stress in specimen shoulder                */
long double     zero_offset_load;           /* small negative load; keeps setup together             */
long double     pressure_psi;               /* pressure transducer reading in psi                    */
long double     deflection_in;              /* extensometer reading in inches                        */
long double     stroke_in;                  /* stroke xdcr reading in inches                         */
long double     ext_l_c_load_lbf;           /* external load cell reading in pounds force            */
long double     int_l_c_load_lbf;           /* internal load cell reading in pounds force            */
long double     int_l_c_gain_factor;        /* allows amp gain adjustment for high load tests        */
int             ext_load_cell_gain;         /* gain setting for NIDAQ board: 1,2,4 or 8              */
int             int_load_cell_gain;         /* gain setting for NIDAQ board: 1,2,4 or 8              */
int             stroke_xdcr_gain;           /* gain setting for NIDAQ board: 1,2,4 or 8              */

int             *ext_l_c_load_ptr;          /* pointer to external load cell derived load in linked list */
int             *int_l_c_load_ptr;          /* pointer to internal load cell derived load in linked list */
int             *pressure_ptr;              /* pointer to pressure in linked list                    */
int             *extensometer_ptr;          /* pointer to extensometer in linked list                */
int             *stroke_xdcr_ptr;           /* pointer to stroke xdcr in linked list                 */
int             *e_gage_1_ptr;              /* pointer to strain gage 1 in linked list               */
int             *e_gage_2_ptr;              /* pointer to strain gage 2 in linked list               */
int             *e_gage_3_ptr;              /* pointer to strain gage 3 in linked list               */
int             len;                        /* number of full records in current block     */

long double     E;                          /* Young's modulus                                       */
long double     nu;                         /* Poisson's ratio                                       */
long double     D;                          /* diameter of specimen shoulders                        */
long double     d;                          /* diameter of specimen gage section                     */
long double     A;                          /* area of specimen shoulders                            */
long double     a;                          /* area of specimen gage section                         */
long double     EA;                         /* elastic constant                                      */
long double     L1, L2, L3, L4, S4;         /* lengths of specimen segments                          */
long double     C1, C2, C3, C4, CS3;        /* constant for deflection to strain calculation         */
long double     fillet_fudge;               /* fudge factor for gage length equivalence              */
long double     seal_fudge;                 /* fudge factor for sho length equivalence               */
long double     ten_volt_pressure;          /* pressure (psi) calibration for 10 volts               */
long double     ten_volt_load;              /* load (lbf) calibration for 10 volts                   */
long double     ten_volt_deflection;        /* deflection (in) calibration for 10 volts              */
```

```
long double     ten_volt_stroke;        /* stroke (in) calibration for 10 volts          */
long double     amp_gain_1;             /* amplifier gain for strain gage 1              */
long double     amp_gain_2;             /* amplifier gain for strain gage 2              */
long double     amp_gain_3;             /* amplifier gain for strain gage 3              */
long double     excitation_voltage;     /* excitation voltage for strain gages           */
long double     gage_factor_1A;         /* gage factor of active gage 1                  */
long double     Kt_1A;                  /* transverse sensitivity of active gage 1       */
long double     gage_factor_2A;         /* gage factor of active gage 2                  */
long double     Kt_2A;                  /* transverse sensitivity of active gage 3       */
long double     gage_factor_3A;         /* gage factor of active gage 3                  */
long double     Kt_3A;                  /* transverse sensitivity of active gage 2       */
long double     gage_factor_1D;         /* gage factor of dummy gage 1                   */
long double     Kt_1D;                  /* transverse sensitivity of dummy gage 1        */
long double     gage_factor_2D;         /* gage factor of dummy gage 2                   */
long double     Kt_2D;                  /* transverse sensitivity of dummy gage 2        */
long double     gage_factor_3D;         /* gage factor of dummy gage 3                   */
long double     Kt_3D;                  /* transverse sensitivity of dummy gage 3        */
long double     extensometer_offset;    /* zero offset on extensometer channel in bits   */
long double     e_gage_1_offset;        /* zero offset on e_gage_1 channel in bits       */
long double     e_gage_2_offset;        /* zero offset on e_gage_2 channel in bits       */
long double     nuo;                    /* Poisson's Ratio for calibration beam          */
long double     ten_volt_e_gage_1A;     /* strain gage 1 calibration for 10 volts        */
long double     ten_volt_e_gage_2A;     /* strain gage 2 calibration for 10 volts        */
long double     ten_volt_e_gage_3A;     /* strain gage 3 calibration for 10 volts        */
long double     dummy_gage_1;           /* correction for dummy gage 1 effects           */
long double     dummy_gage_2;           /* correction for dummy gage 2 effects           */
long double     dummy_gage_3;           /* correction for dummy gage 3 effects           */
long double     apparent_e_1;           /* apparent strain from active gage 1            */
long double     apparent_e_2;           /* apparent strain from active gage 2            */
long double     apparent_e_3;           /* apparent strain from active gage 3            */
long double     actual_e_1;             /* actual strain from active gage 1              */
long double     actual_e_2;             /* actual strain from active gage 2              */
long double     actual_e_3;             /* actual strain from active gage 3              */
long double     corr_1;                 /* correction for transverse sensitivity effects */
long double     corr_2;                 /* correction for transverse sensitivity effects */
long double     corr_3;                 /* correction for transverse sensitivity effects */
long double     corr_4;                 /* correction for transverse sensitivity effects */
long double     strain_cal_1;           /* strain calibration for gage 1                 */
long double     pressure_cal_1;         /* pressure calibration for gage 1               */
long double     strain_cal_2;           /* strain calibration for gage 2                 */
long double     pressure_cal_2;         /* pressure calibration for gage 2               */
long double     strain_cal_3;           /* strain (load) calibration for gage 3          */
long double     pressure_cal_3;         /* pressure calibration for gage 3               */

struct data {
        int             ext_l_c_load[LISTLEN];
        int             int_l_c_load[LISTLEN];
        int             pressure[LISTLEN];
        int             extensometer[LISTLEN];
/*      int             stroke_xdcr[LISTLEN];   */
        int             e_gage_1[LISTLEN];
        int             e_gage_2[LISTLEN];
        int             e_gage_3[LISTLEN];
        int             length;
struct data *next;} *first_data, *last_data;    /* linked list for data storage  */
```

APPENDIX D - ENGINEERING DRAWINGS

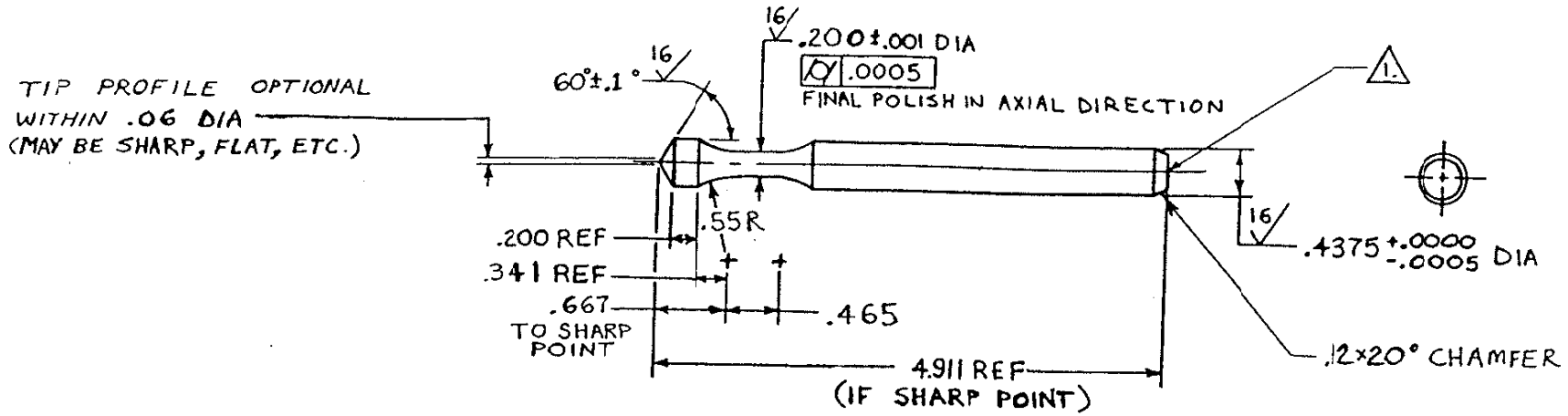

NOTES:

1. SIZE 00 TO SIZE 2 CENTER PERMISSIBLE

TOLERANCES: .XX ±.01
.XXX ±.005

FULL SCALE
DATE: 5/20/93

200 SPECIMEN

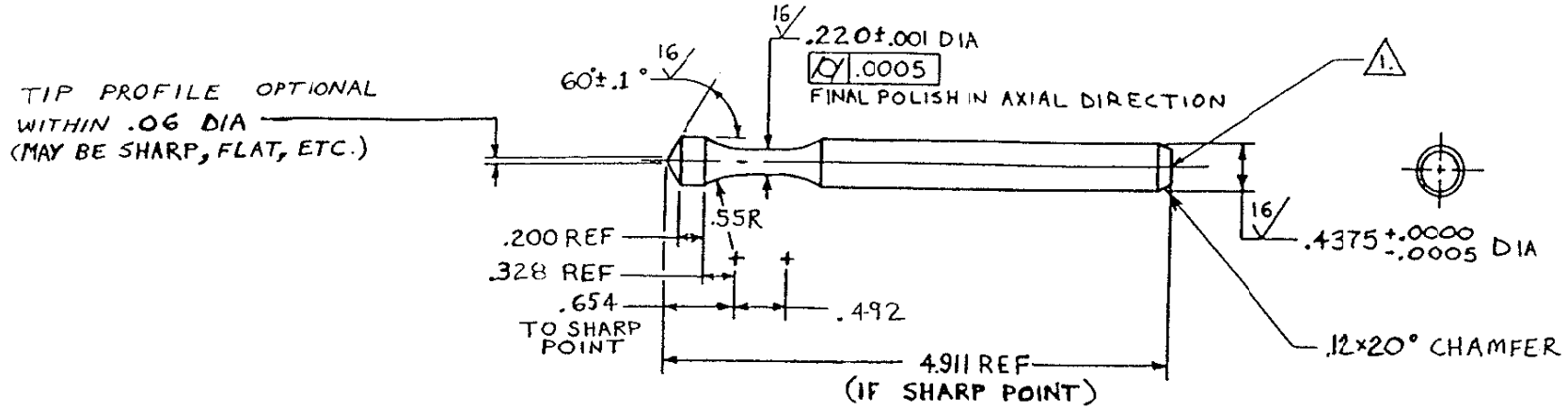

NOTES:

1. SIZE 00 TO SIZE 2 CENTER PERMISSIBLE

TOLERANCES: .XX ±.01
.XXX ±.005

FULL SCALE
DATE: 5/20/93

220 SPECIMEN

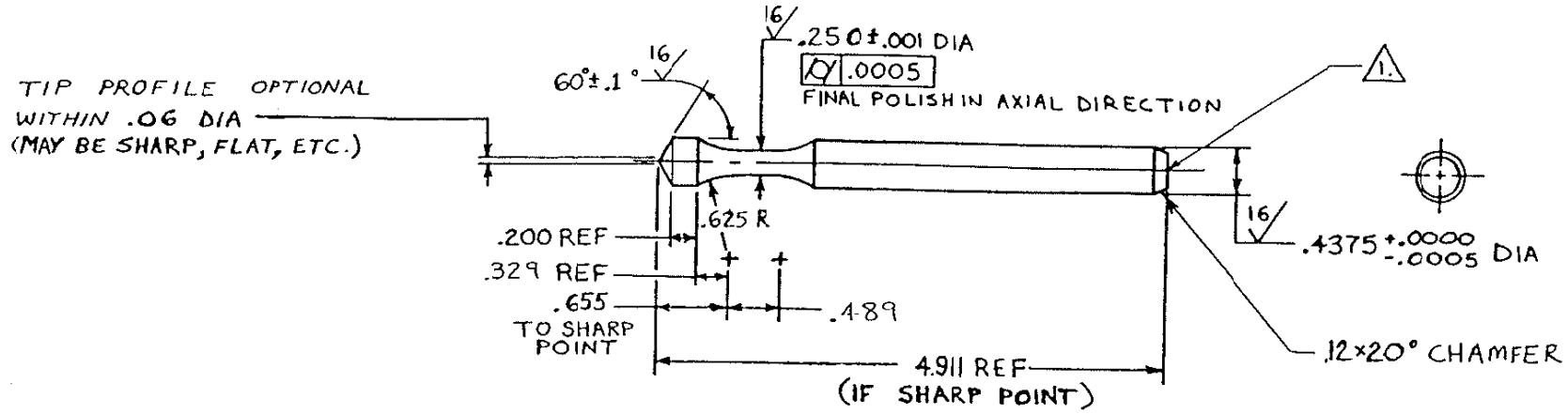

NOTES:

1. SIZE 00 TO SIZE 2 CENTER PERMISSIBLE

TOLERANCES: .XX ±.01
.XXX±.005

FULL SCALE
DATE: 5/20/93

250 SPECIMEN

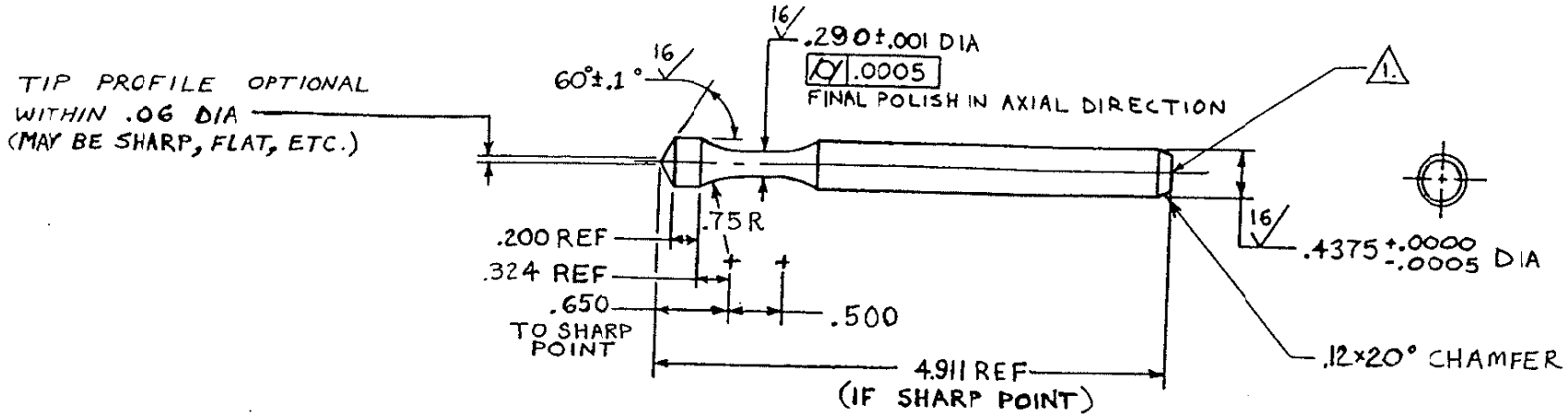

NOTES:

1. SIZE 00 TO SIZE 2 CENTER PERMISSIBLE

TOLERANCES: .XX ±.01
.XXX ±.005

FULL SCALE
DATE: 5/20/93

290 SPECIMEN

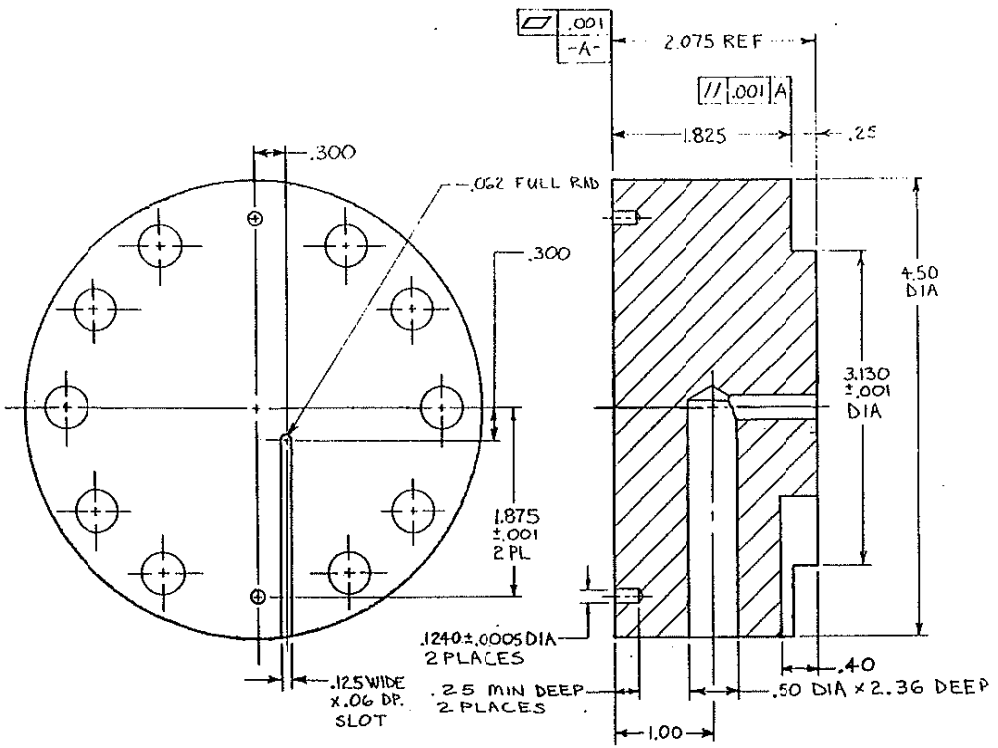

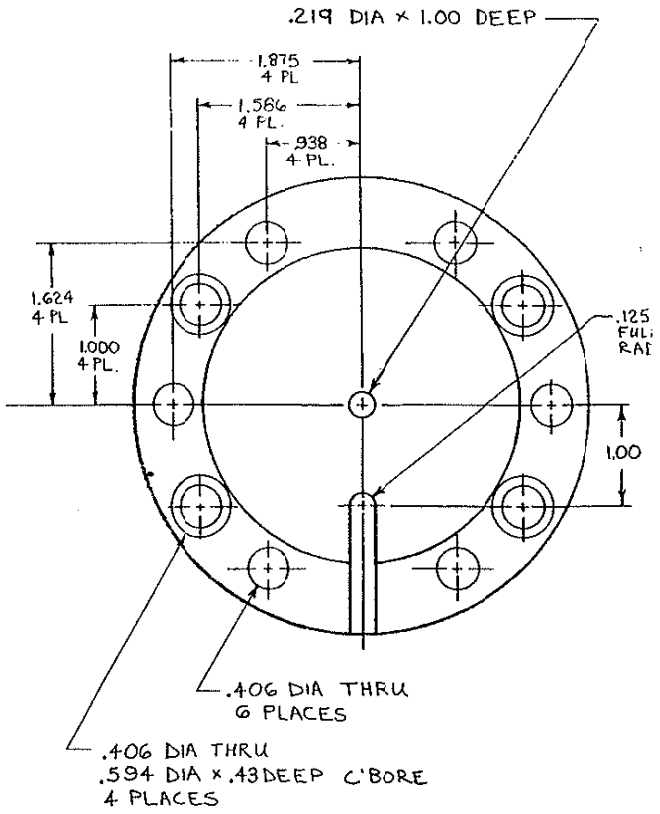

MATERIAL : 4130 STEEL
HEAT TREAT TO RC 33-40
TOLERANCES: .XX ±.01
.XXX ±.005
SURFACE FINISH: 125 μIN RMS
FULL SCALE
11/5/93 REV A: 1/8/97

ADAPTER

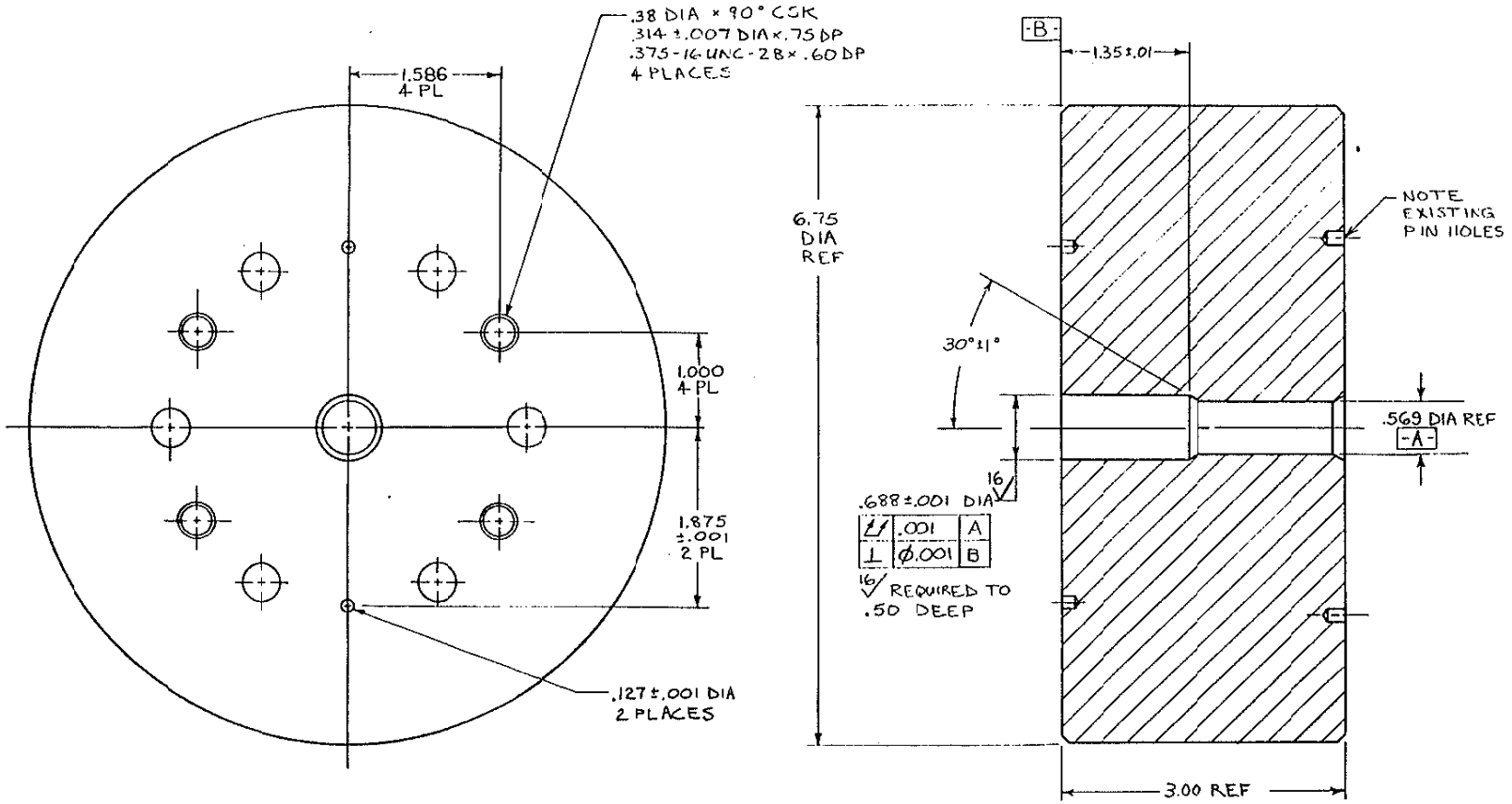

MATERIAL : 4340 STEEL, Q+T TO RC 38
FULL SCALE

PRESSURE VESSEL REWORK

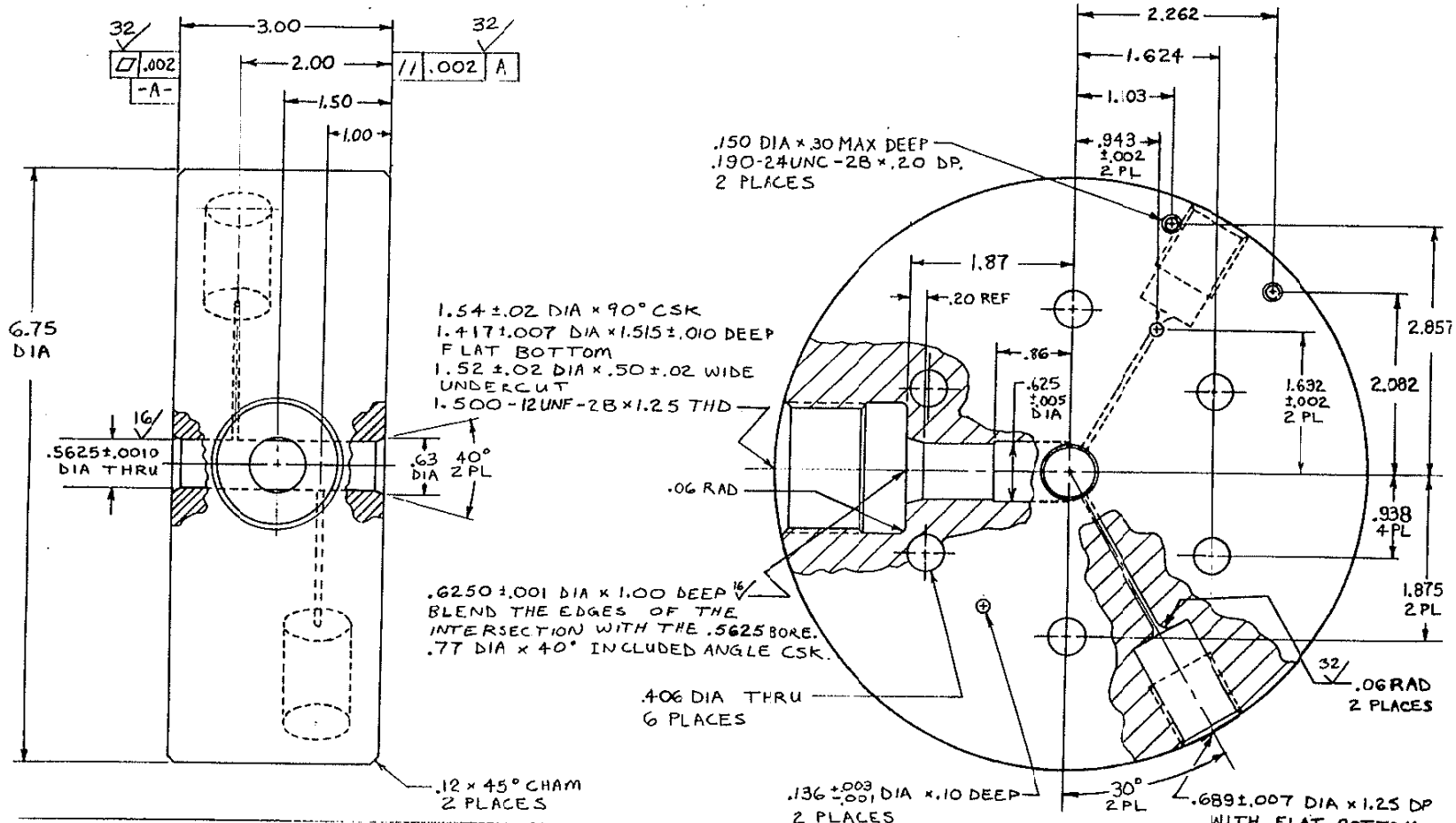

MATERIAL: E-4340 VAR (VACUUM ARC REMELTED) ALLOY STEEL PER MIL-S-8844 AND AMS 2300 HEAT TREAT TO RC 38-42

TOLERANCES: XX ± .01, XXX ± .005, ANGLES ± 2°

SCALE: 1/1

DATE: 1/8/97

125 μ INCH RMS SURFACE FINISH

PRESSURE VESSEL

SPACER DASH #	⌀D	ID	T
1	.566	.383	.125
2	.566	.446	.125
3	.566	.383	.300
4	.566	.446	.175

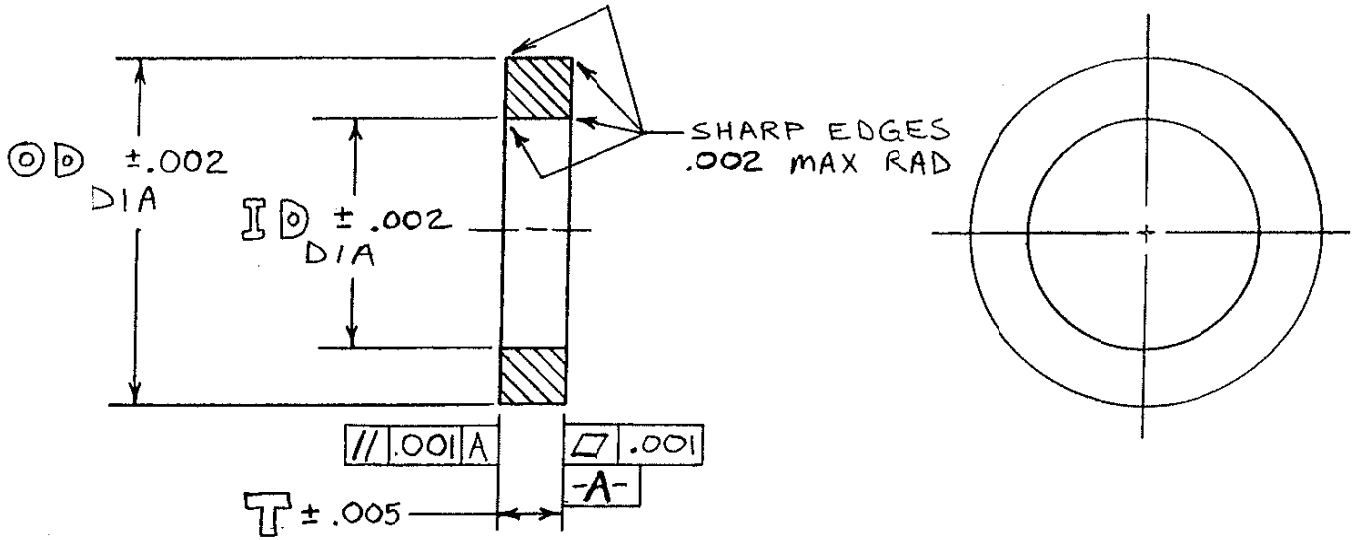

MATERIAL: ALLOY STEEL, Q+T TO HRC 36-42

SURFACE FINISH : 32 μINCH RMS

SCALE : 4/1

DATE : 5/1/93

SPACER

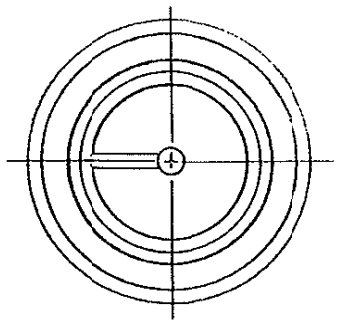

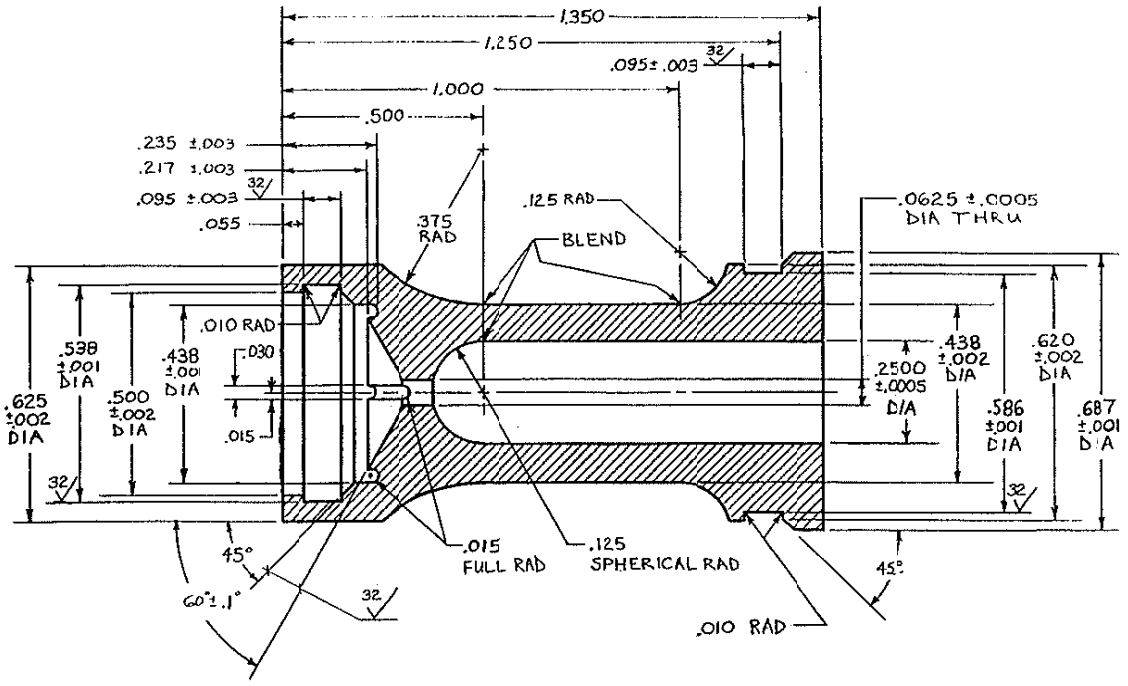

MATERIAL: O-1 TOOL STEEL
IN ANNEALED CONDITION
TOLERANCES: .XX ± .010
UNLESS NOTED: .XXX ± .005
ANGLES ± ½°
SCALE : 4/1
SURFACE FINISH: 63 μ IN RMS
DATE : 11/2/93

HEAT TREATMENT: PREHEAT AT 1200°F
AUSTENITIZE AT 1450°F, OIL QUENCH,
TEMPER AT 400°F FOR 1 HOUR.
TREAT IN VACUUM OR CONTROLLED
ATMOSPHERE FURNACE TO PREVENT
SCALING OR DECARBURIZING. LIGHT
DISCOLORATION PERMISSIBLE. HEAT
TREATED HARDNESS TO BE RC60 MIN.
HARDNESS TEST ON SAMPLE ONLY.

LOAD CELL HOUSING

DASH #	D DIA	T THICKNESS
-1	.438 ± .001	.030 ± .002

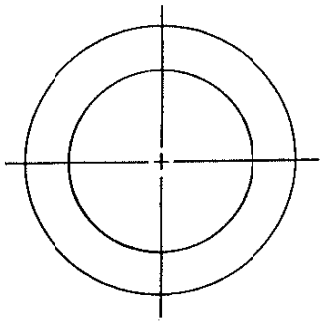

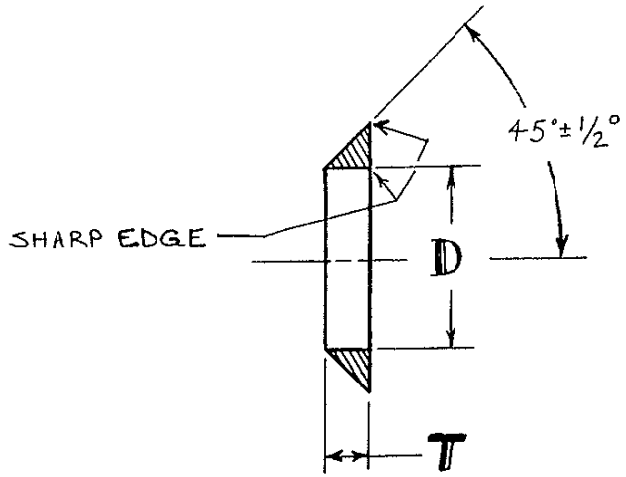

MATERIAL: BRASS
SURFACE FINISH: 32 μIN RMS
DATE: 11/3/93

INT CHAMFER RING

DASH #	D DIA	T THICKNESS
-1	.689 ±.001	.030 ±.002
-2		

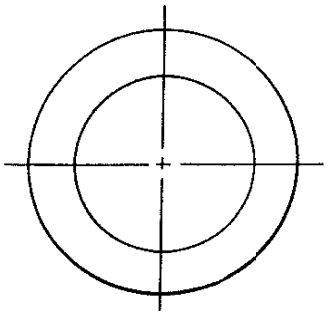

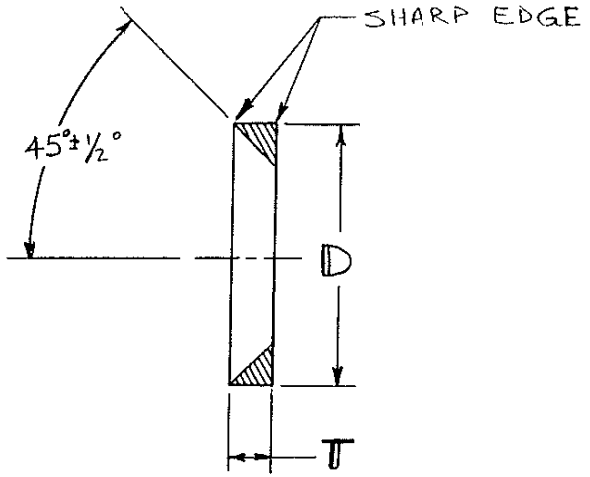

MATERIAL : BRASS
SURFACE FINISH : 32 μIN RMS
DATE : 11/3/93

EXT CHAMFER RING

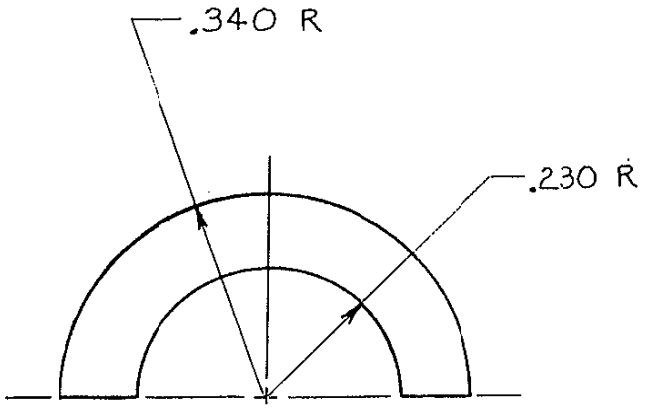

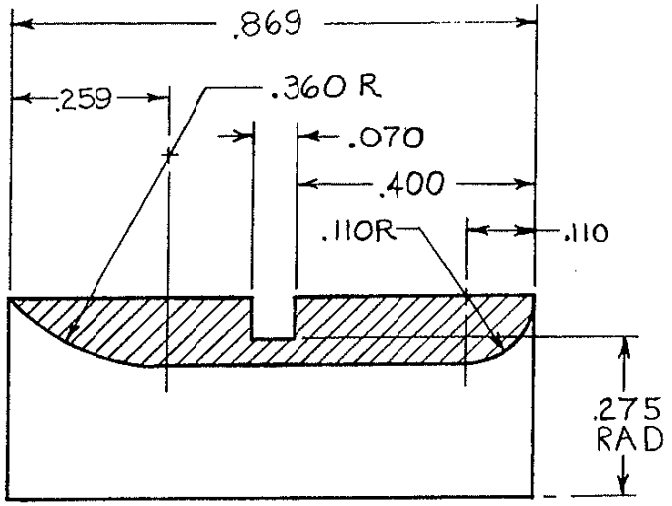

MATERIAL: STEEL
TOLERANCES: .XXX ±.005
SCALE : 4/1
DATE : 11/2/93

SPACER

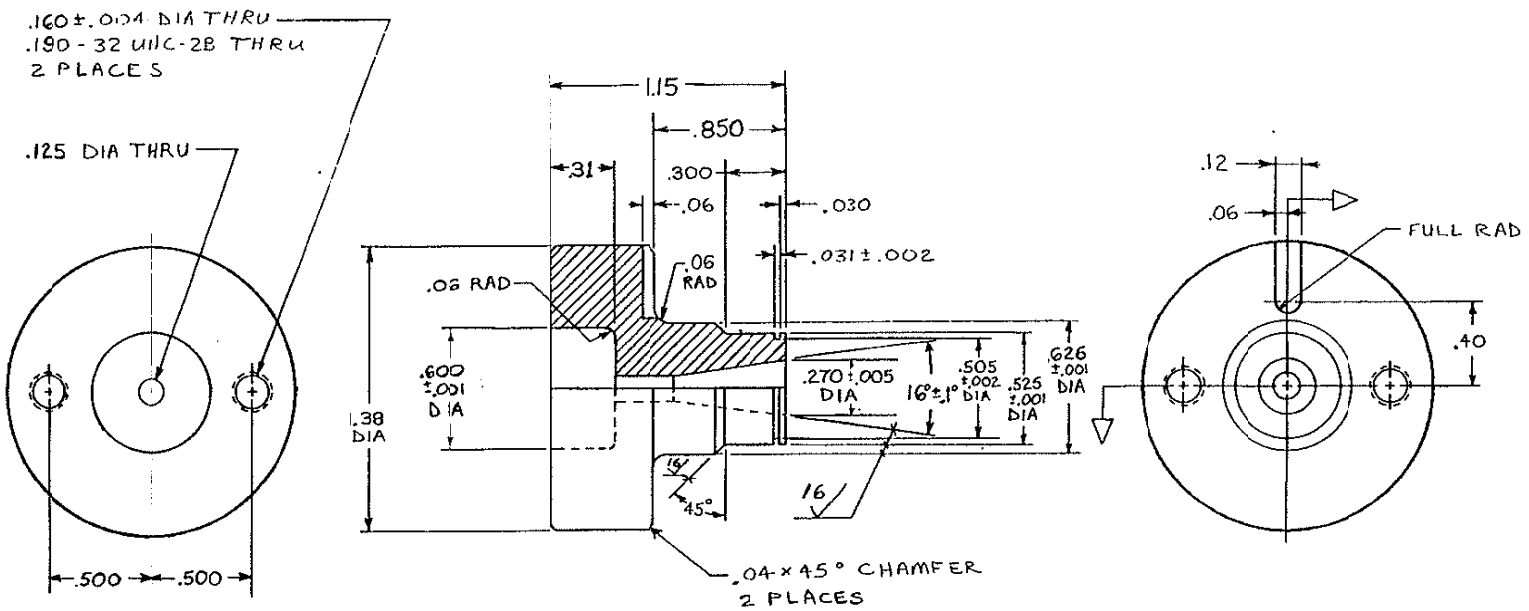

MATERIAL: DRILL ROD (O-1 TOOL STEEL)
HEAT TREAT TO R_c 35 - 40
TOLERANCES: .XX ± .01
.XXX ± .005
SURFACE FINISH: 125 MINCH RMS UNLESS SPECIFIED
SCALE: 2/1
DATE: 10/5/93
REV A: 1/8/97

FEEDTHRU BODY

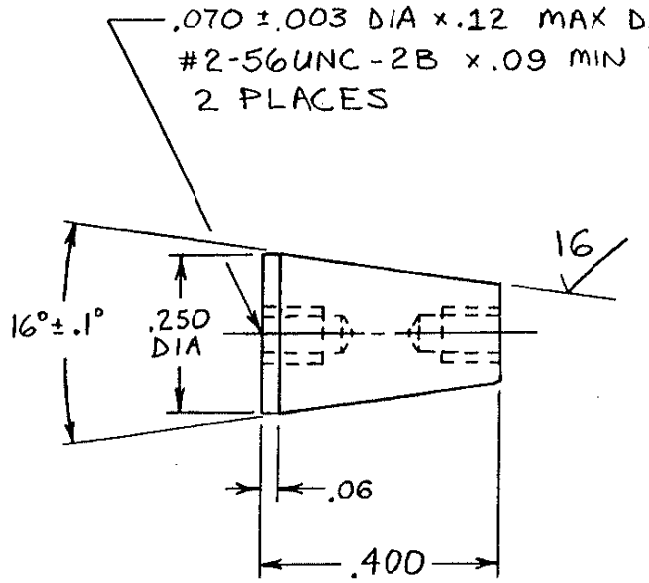

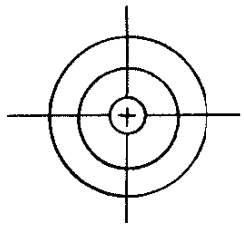

MATERIAL: 1/4 DIA DRILL ROD (O-1 TOOL STEEL)
HEAT TREAT TO R_c 35-40

TOLERANCES: .XX ± .01
.XXX ± .005

SCALE: 4 / 1

SURFACE FINISH: 63 μIN RMS

DATE: 10/5/93

CONE PLUG

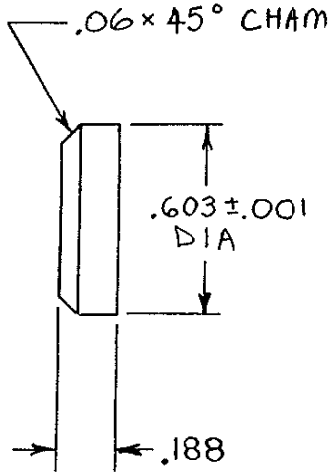

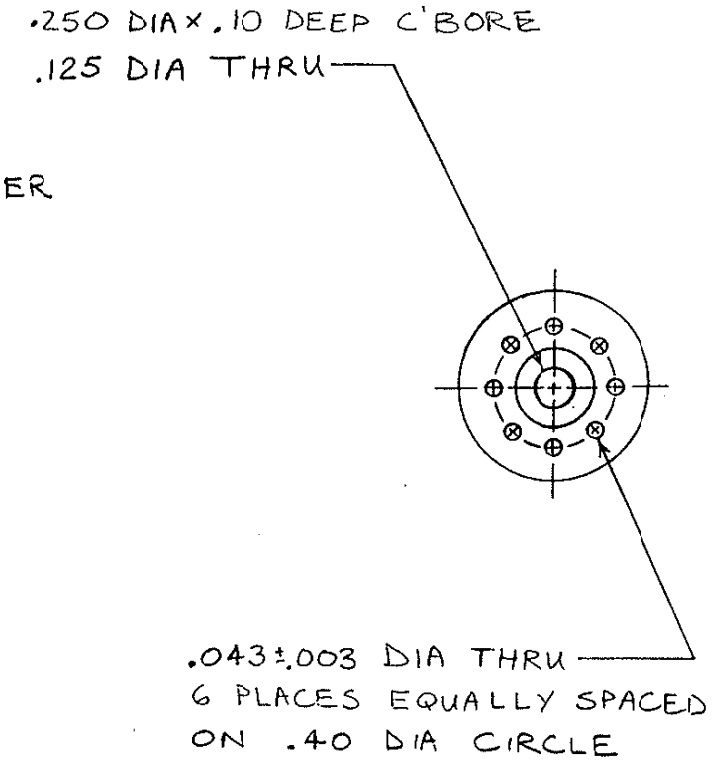

MATERIAL: TEFLON
TOLERANCES: .XX ± .01
.XXX ± .005
ANGLES ± 1°

SCALE : 2/1
SURFACE FINISH : 63 μ IN RMS
DATE : 10/5/93

INSULATOR

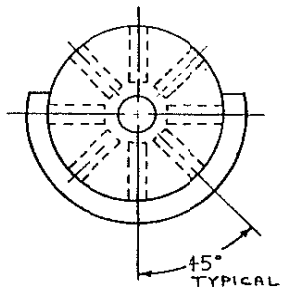

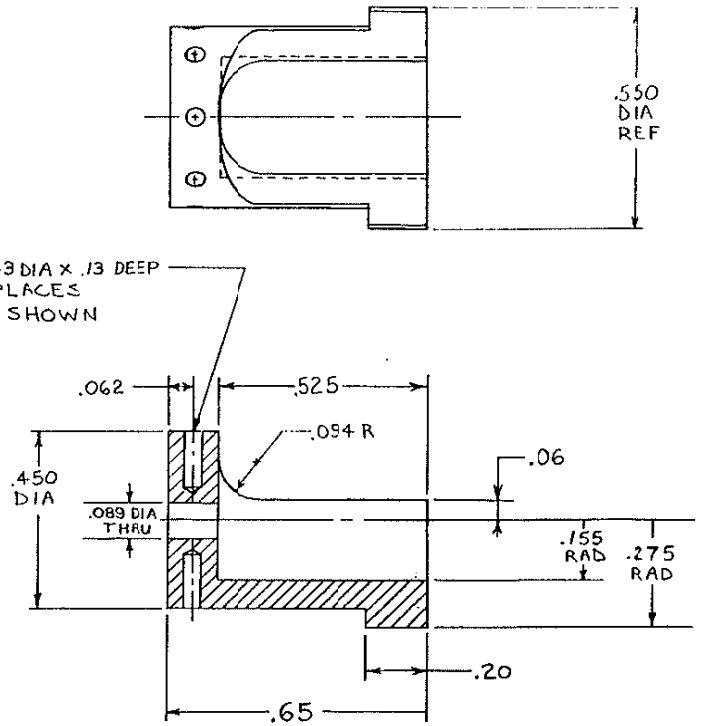

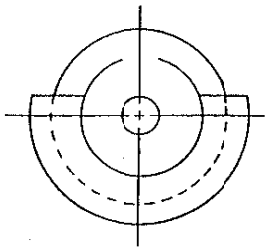

MATERIAL : TEFLON
TOLERANCES : .XX ± .01
.XXX ± .005
ANGLES ± ½°
SCALE : 4/1
SURFACE FINISH: 125 μ IN RMS
DATE : 10/8/93
REV A: 1/8/97

GAGE CARRIER

DASH #	MATERIAL
-1	LEAD
-2	TEFLON

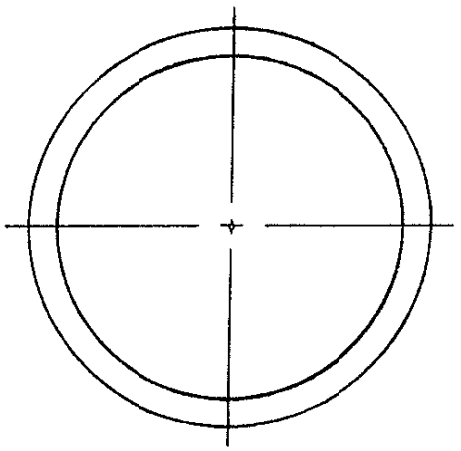

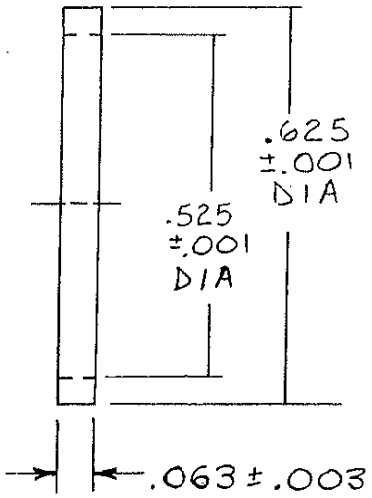

63 μin RMS SURFACE FINISH
SCALE: 4/1
DATE: 3/25/93

ANTI-EXTRUSION RING

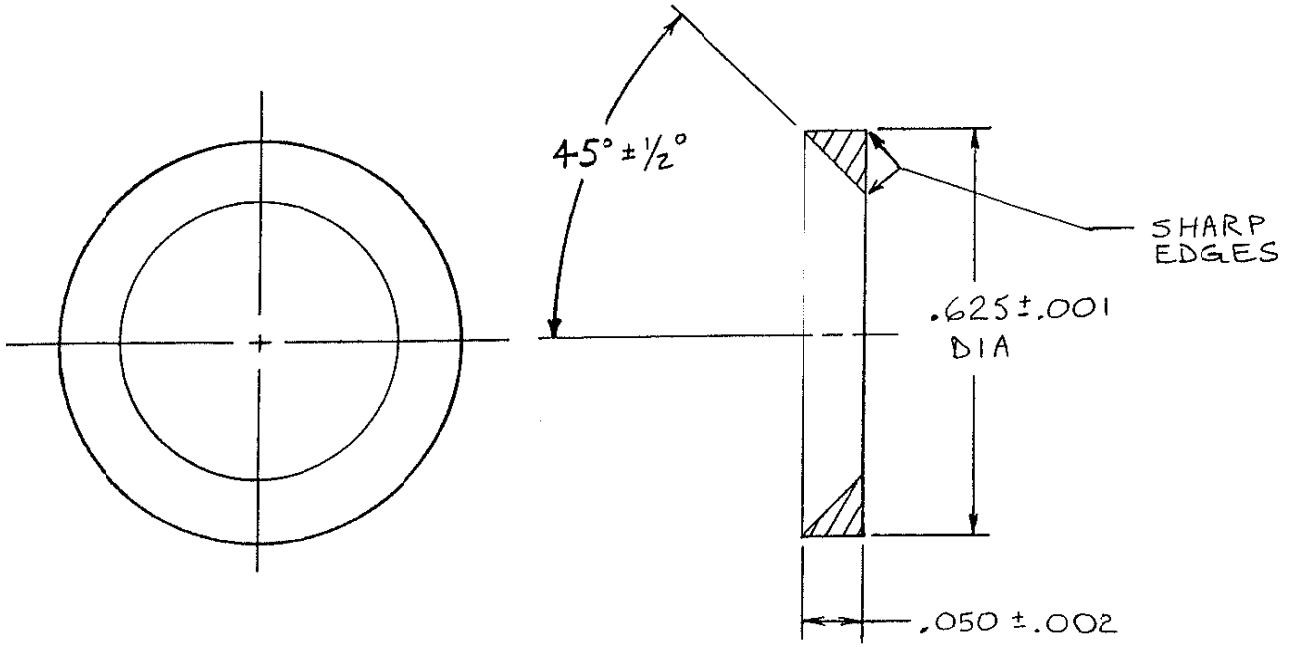

MATERIAL : BRASS
32 μin RMS SURFACE FINISH
SCALE : 4/1
DATE : 3/25/93

BEVELED RING

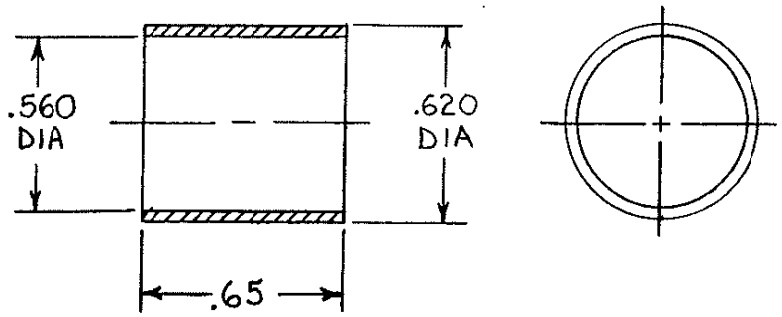

301

MATERIAL : TEFLON

TOLERANCES : .XX ±.01
.XXX ± .005

125 μin RMS SURFACE FINISH

SCALE 2/1

DATE 1/8/97

INSULATOR
TUBE

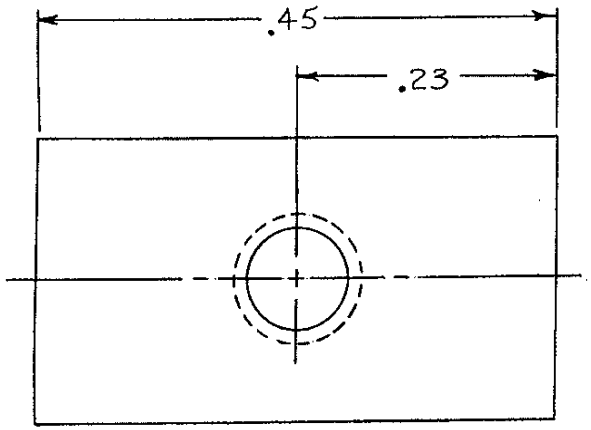

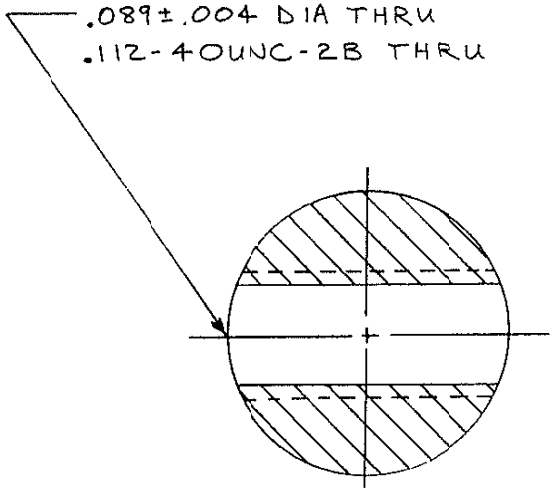

MATERIAL : 1/4 DIA DRILL ROD
TOLERANCES : .XX ±.01
.XXX ±.005

SCALE : 8/1
125 μin RMS SURFACE FINISH

CLAMP NUT

DASH #	A
-1	.125
-2	.188

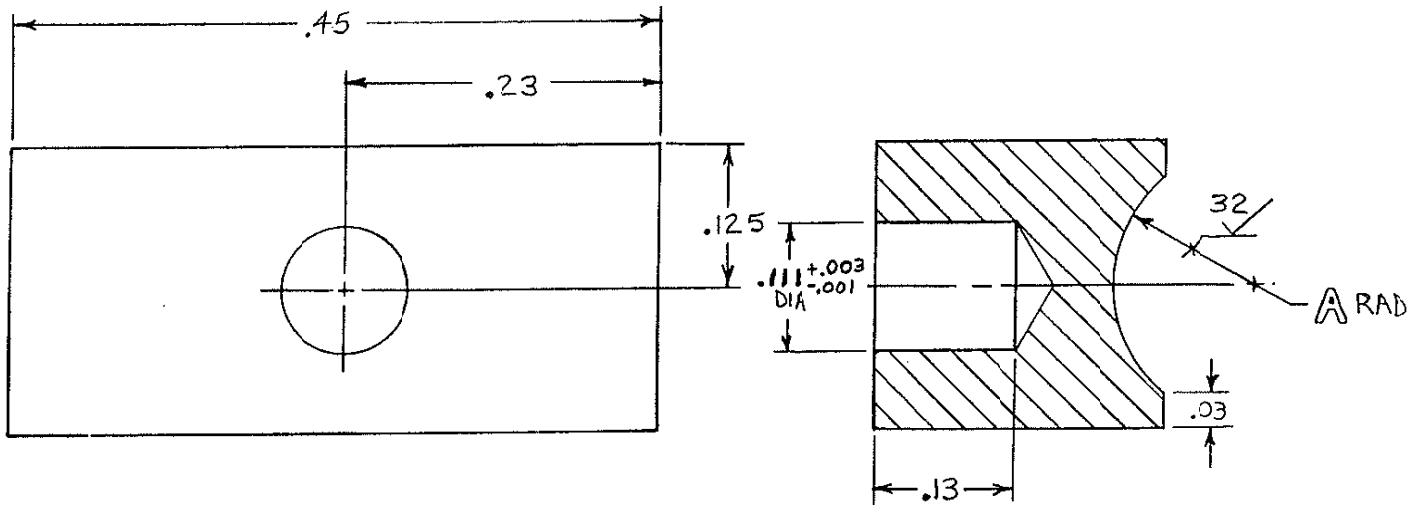

MATERIAL: 1/4 x 1/4 COLD ROLLED
STAINLESS STEEL KEYSTOCK

TOLERANCES: .XX ± .01
.XXX ± .005

SCALE: 8/1 125 min RMS SURFACE FINISH

CLAMP BLOCK

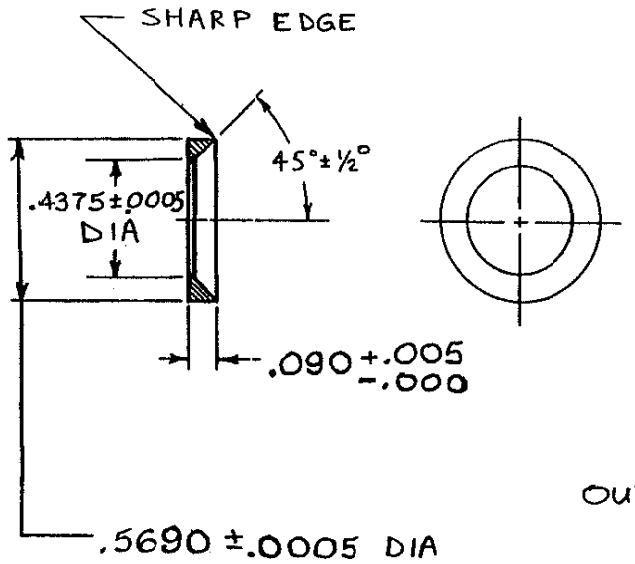

OUTER RING

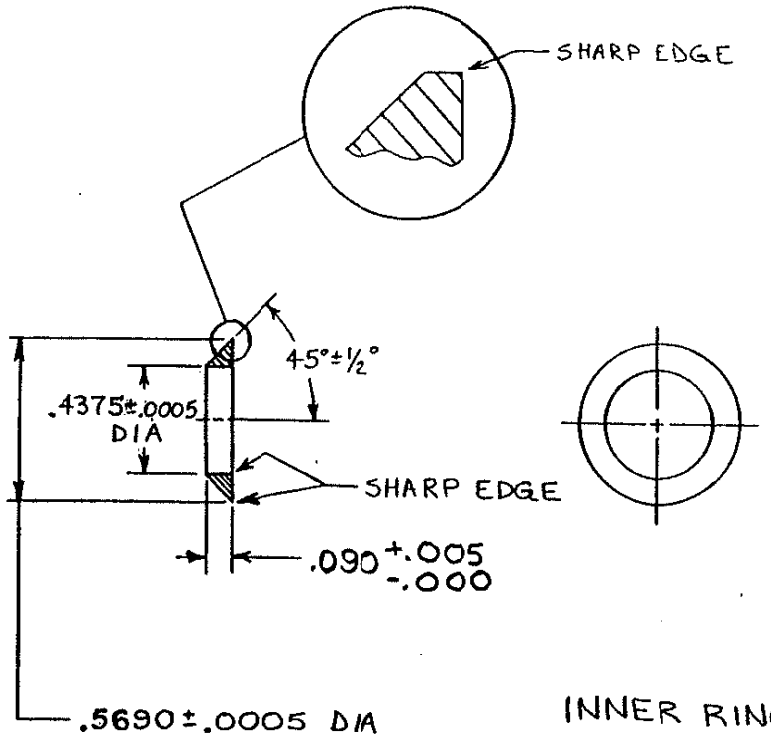

INNER RING

MATERIAL: BRASS
SURFACE FINISH: 32 μin RMS

ANTI-EXTRUSION RING

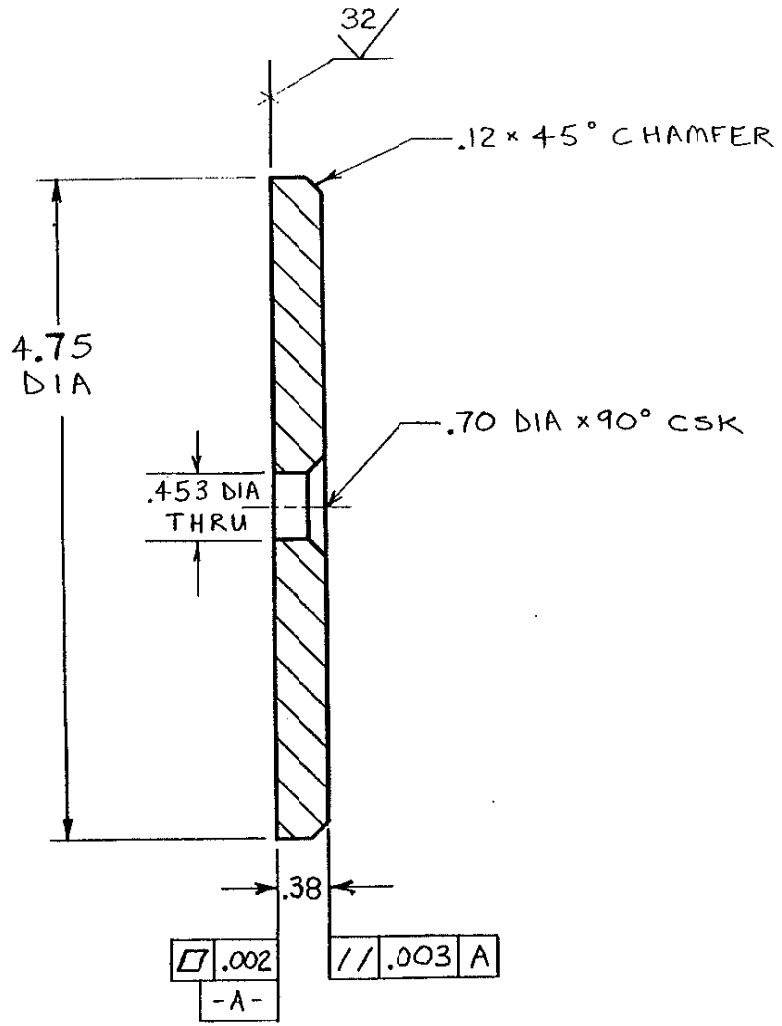

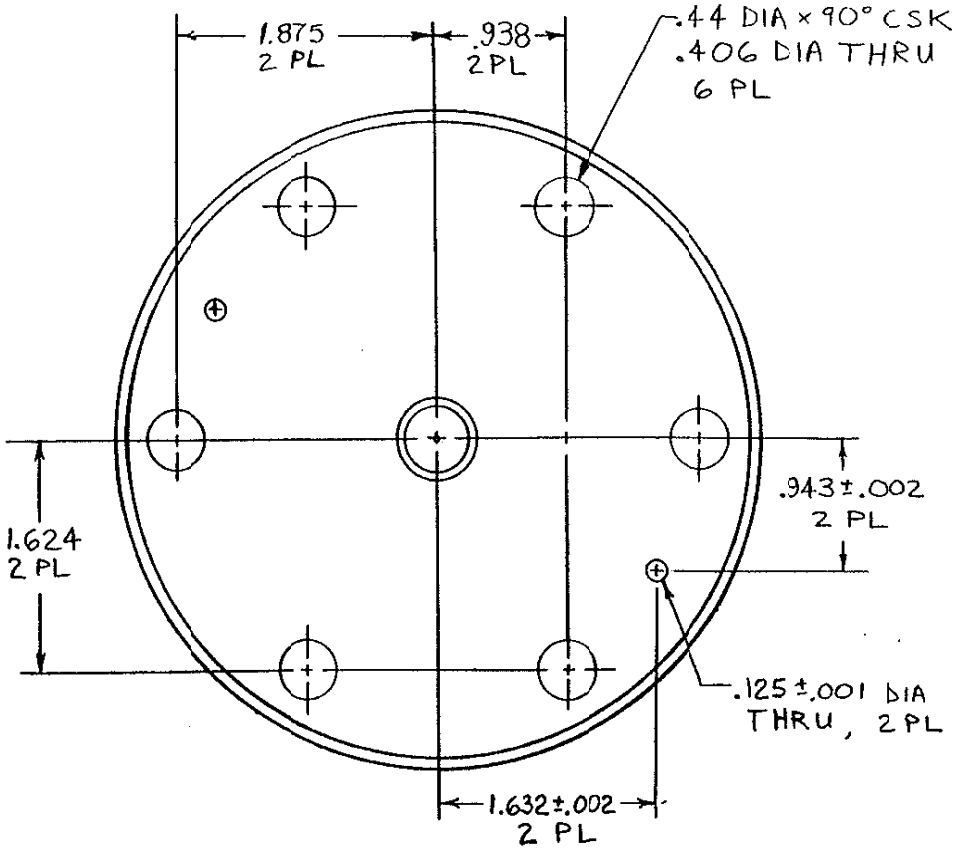

MATERIAL: 4340 STEEL,
Q+T TO HRC 36-42

TOLERANCES: .XX ± .01
.XXX ± .005

SURFACE FINISH: 125μ IN RMS

END CAP

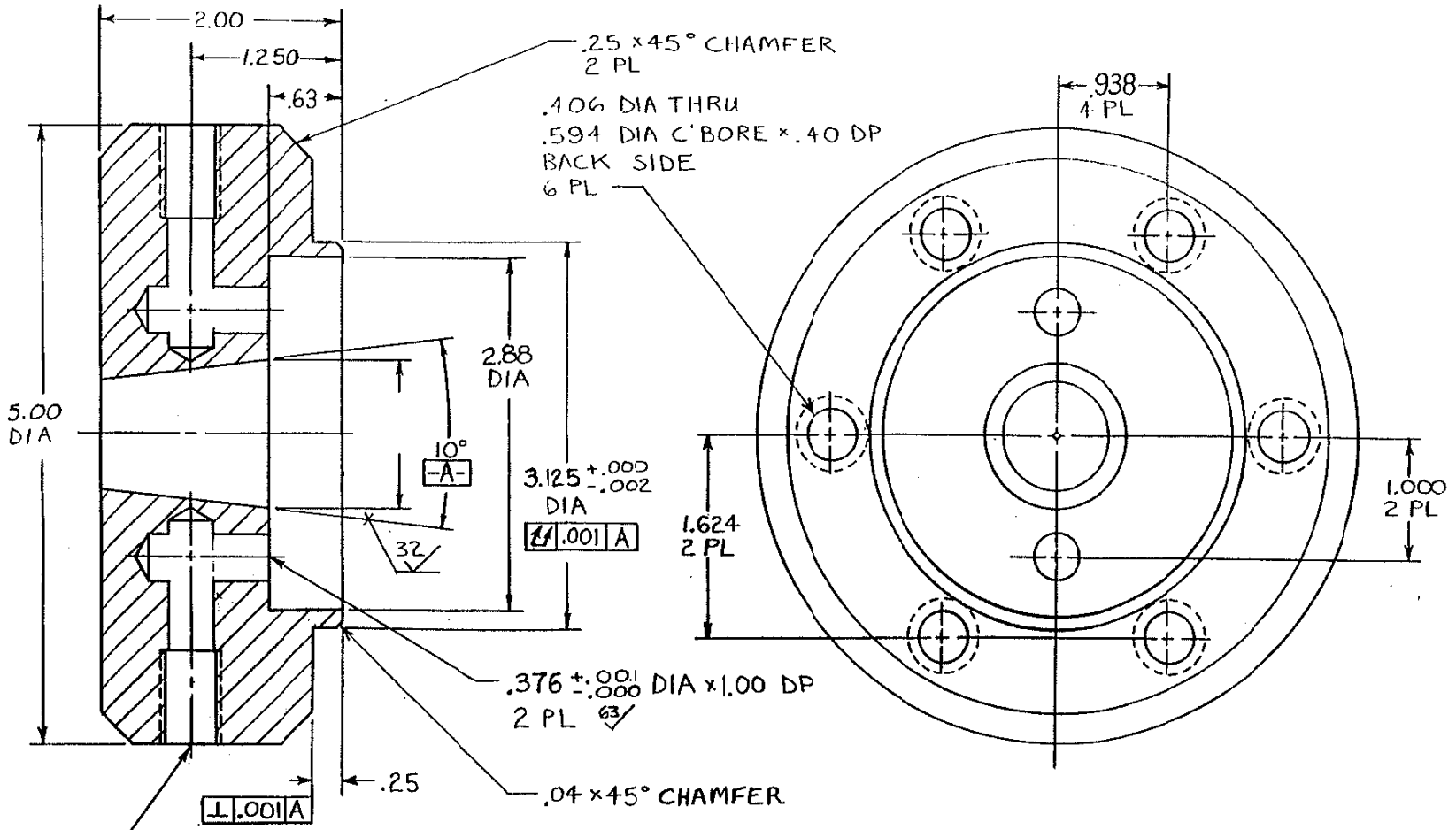

MATERIAL:

TOLERANCES .XX ± .02
.XXX ± .005
ANGLES ± 3°

SURFACE FINISH 125 μin RMS

COLLET HOLDER 1

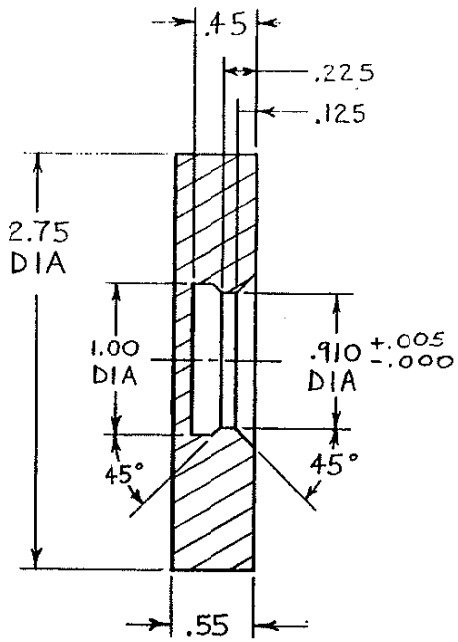

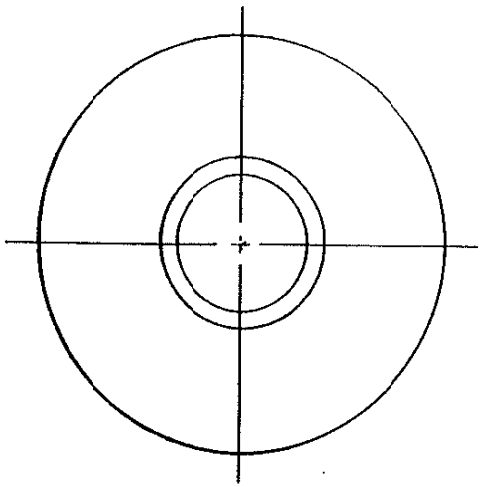

MATERIAL :

TOLERANCES: .XX ± .02
.XXX ± .005
ANGLES ± .1°

125 μin RMS SURFACE FINISH

SCALE 1/1

COLLET BASE

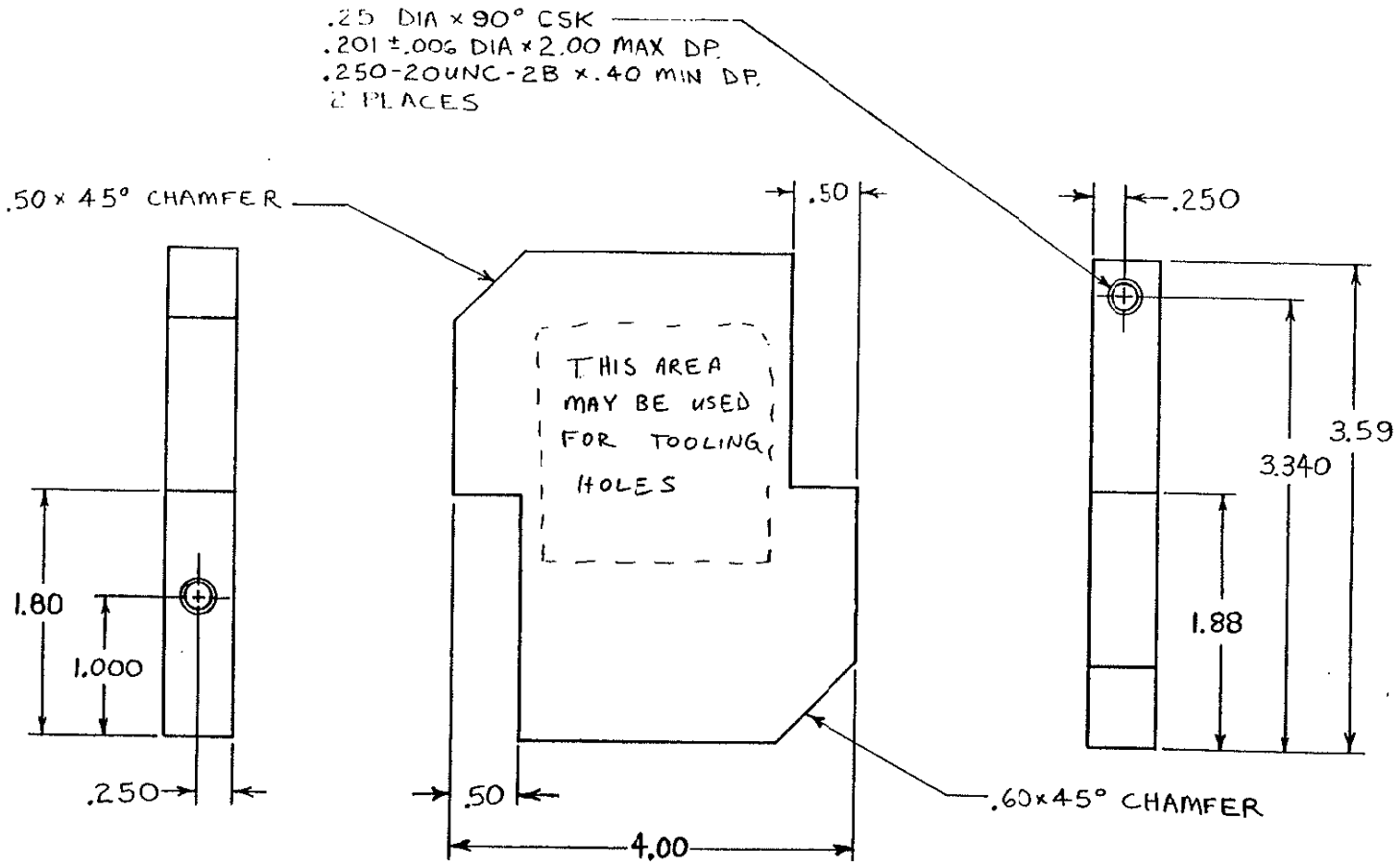

308

MATERIAL: 1/2 INCH THICK 6061 ALUMINUM PLATE

TOLERANCES: .XX ± .02
.XXX ± .005
ANGLES ± 2°

SURFACE FINISH: 250 μIN RMS

SCALE: 1/1

BRACKET

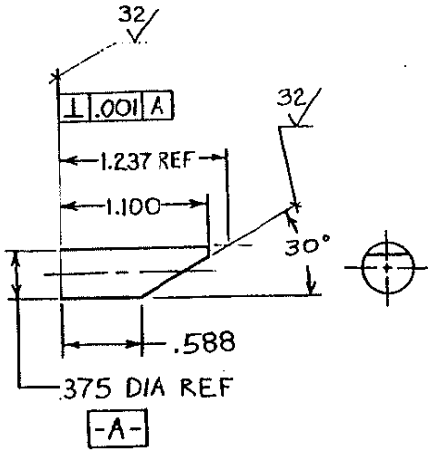

MATERIAL: .375 DIA HARDENED STEEL DOWEL PIN

TOLERANCES: .XXX ±.005
ANGLES ± .1°

FULL SCALE

PIN A

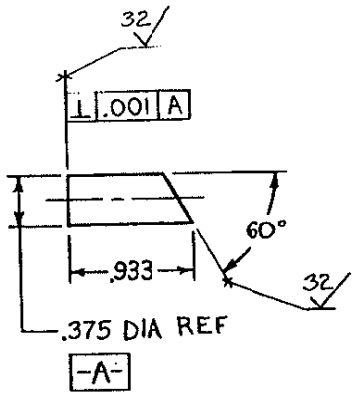

MATERIAL: .375 HARDENED STEEL DOWEL PIN

TOLERANCES: .XXX ±.005
ANGLES ±.1°

FULL SCALE

PIN B

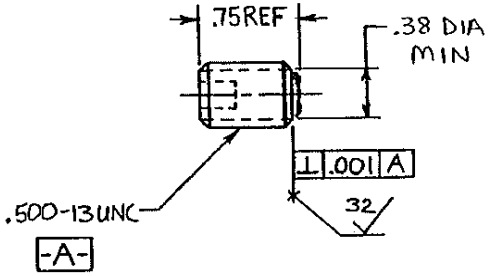

MATERIAL: .500-13UNC-3A SOCKET HEAD SETSCREW, .75 LONG

FULL SCALE

SETSCREW

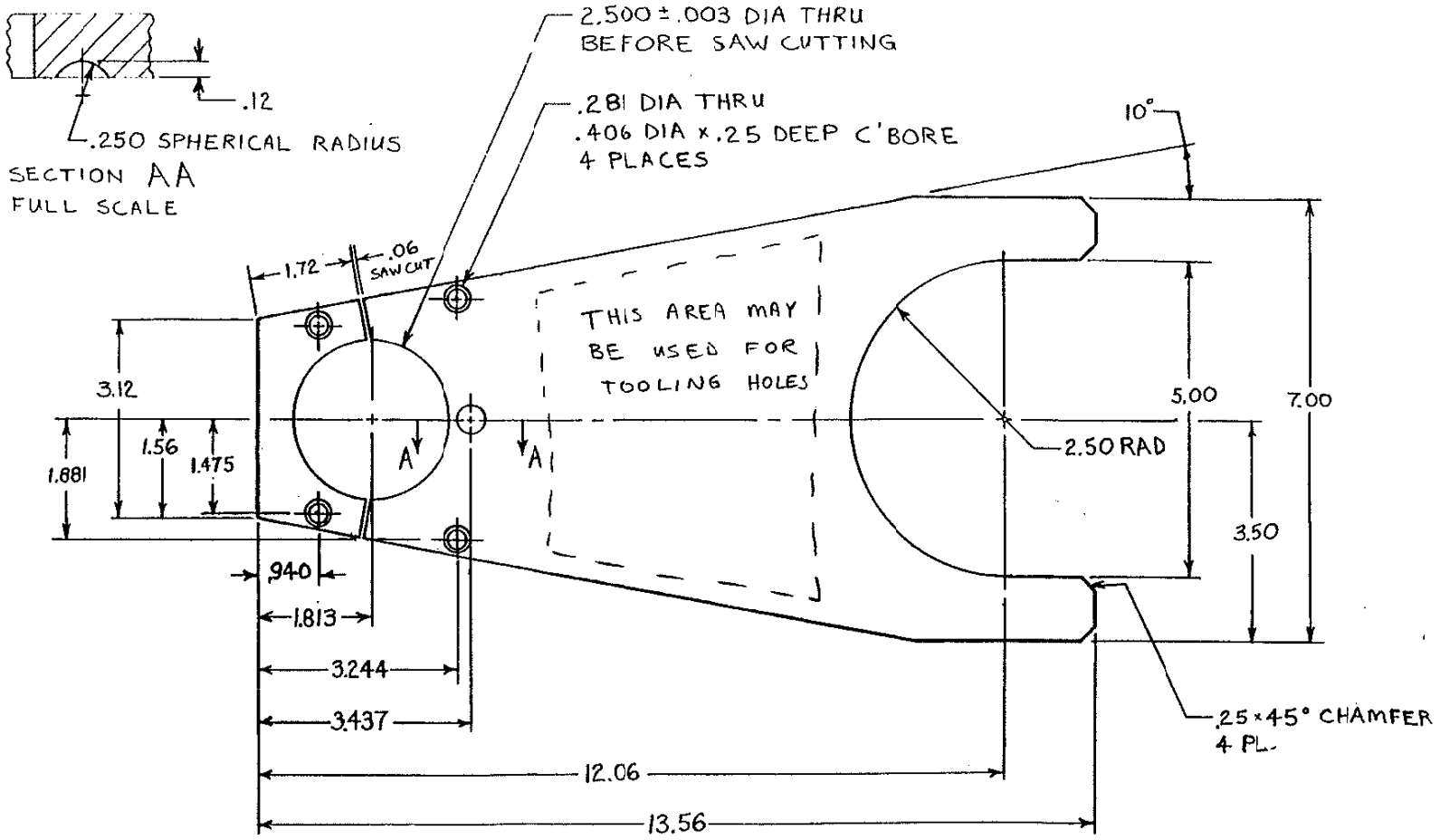

MATERIAL : 1/2 INCH THICK 6061 ALUMINUM PLATE

TOLERANCES : .XX ± .02
.XXX ± .005
ANGLES ± 1/2°

SURFACE FINISH : 250 μIN RMS

SCALE : 1/2

SUPPORT ARM

VITA

Mark Anthony Balzer was born in Montclair, New Jersey to Charles and Vittoria Balzer. He grew up in Glen Ridge, NJ, where he kept his hands dirty repairing everything from bicycles to lawnmowers to automobiles. Mark graduated in the top 10% of his Glen Ridge High School class in May of 1983, and spent his next four years at Stevens Institute of Technology, while also working part-time as a mechanic and machinist. In May of 1987, Mark graduated from Stevens with a Bachelor of Engineering with High Honor, and began working as a design engineer at Moog Inc. in East Aurora, NY. In December of that year he was admitted to the Masters program at the State University of New York at Buffalo as a part-time student. Upon completing the requirements for his Masters Degree in June, 1990, Mark left Moog and came to the University of Illinois at Urbana-Champaign to study materials and design. In Urbana, Mark was awarded two fellowships, held both research and teaching assistantships, plus taught ME 231. He challenged himself technically by taking twice the number of units required for the PhD degree. In his free time Mark became a talented balloon artist and co-founded an Internet web site and mailing list for balloon professionals, which was incorporated in early 1998 as: *Balloon HQ, LLC*. Balloon HQ's industry-sponsored, award winning web site and mailing list has become *the* Internet forum for balloon professionals worldwide. Mark also joined the Dancing Illini and became an accomplished dancer. Later, as its president, Mark turned that club into a first-class student organization with 250 members and an annual budget of over $20,000. While at a national dance convention in Chicago in 1995, Mark met Suzanne Smith; they were married on June 27, 1998. Upon graduation, Mark will work in the Mechanical Systems Engineering & Research Division at NASA's Jet Propulsion Laboratory in Pasadena, CA.